Copper-Sulfur, Copper-Oxygen, and Copper-Alkyl Complexes Relevant to Copper Protein Active Site Intermediates and Catalysis

A Dissertation
SUBMITTED TO THE FACULTY OF
UNIVERSITY OF MINNESOTA
BY

Jacqui Lynn Tehranchi

IN PARTIAL FULFILLMENT OF THE REQUIREMENTS
FOR THE DEGREE OF
DOCTOR OF PHILOSOPHY

William Baker Tolman

September 2013

Acknowledgements

"I *am among those who think that science has great beauty. A scientist in his laboratory is not only a technician: he is also a child placed before natural phenomena which impress him like a fairy tale*."
- Marie Curie

When I first applied for graduate school, I placed the above quote at the beginning of my personal statement to begin to explain why I wanted to pursue a PhD in chemistry. I still feel this describes accurately that feeling of wonder and excitement that arises when a scientist is confronted with a puzzling outcome. Since I was a child, I have always been fascinated by the "natural phenomena" in constant motion around me. I remember in 7th grade, I dissolved the shell of an egg in vinegar while keeping the membranes intact, and took the remaining egg in a container to school to show people. I have always had a passion for performing experiments and I would like to thank both of my parents for encouraging my curiosity and giving me time to just sit, think, and do whatever I found interesting.

There are many people who have significantly contributed to helping me in my graduate career. I would like to thank Dr. Delia Popescu who mentored me when I was an undergraduate student at Carnegie Mellon University in Terrence J. Collins' laboratory and encouraged me to attend graduate school. My graduate research advisor, Professor William B. Tolman has always held high standards and maintained a healthy skepticism of our science. To Dr. Lei Yang, thank you for teaching me nearly everything I know about air-sensitive synthetic inorganic chemistry and allowing me to learn a great deal

about crystallography with your samples. I am also grateful to Dr. Patrick Donoghue, with whom I have countless fruitful conversations- you became not only a collaborator but a friend. Debanjan Dhar was a first year student that has worked with me on the pK_a measurements presented in Chapter 3 and will continue this work as part of his thesis work. Thank you for your hard work, Debanjan and good luck! I would like to thank all of the members of the Tolman group, past and present, for your contributions to the field of inorganic (and polymer) chemistry as they have provided a solid foundation to build upon. In particular, I would like to thank David Boyce, Dr. Agostino Pietrangelo, Dr. Keying Ding, and Gereon Yee for countless invaluable conversations.

I have had to opportunity of working closely with Dr. Letitia Yao, who has helped me with NMR experiments and served as the WISE (Women in Science and Engineering) faculty sponsor. I would also like to thank Dr. Victor G. Young, Jr., who was so generous with his time in teaching me about crystallography. Thank you both for all of the great advice and invaluable conversations throughout the years.

To my fellow members of Tit for Tat Brewery, Deanna Miller, Emily Pelton and Maria Miranda: Thank you for creating excellent craft beer with me for over a year. I appreciated our time together, because even if we talked about research or science- we always had fun. I will truly miss our brewing sessions that gave me a good excuse to get together with my good friends and eat great food.

Thank you to members of the Lawrence Que Jr.'s group and Connie Lu's group; you have been extremely helpful for sharing ideas, chemicals, instrumentation, and beers. I would also like to thank fellow classmates, Christopher (Kit) Zall and Bess Vlaisavljevich, for great conversations on many topics including brewing and books. I must also thank Raymond De Hont for being supportive and understanding of the demands of graduate school. To all of my family and friends that I have not listed by name, thank you for your love and support throughout my life. Lastly, I would like to thank Kurt Vonnegut, Jr. for inspiring me to strive to truly understand the work I have done and any work I do in the future:

"*Any scientist who couldn't explain to an eight-year-old what he was doing was a charlatan*."
-Dr. Asa Breed (Cat's Cradle, Kurt Vonnegut, Jr.)

Dedication

This thesis is dedicated to my parents, Emilia Tehranchi and Kamyar Tehranchi, who I am forever indebted for their love, support, and belief in my abilities. Thank you for always encouraging me to do whatever I wanted and for never telling me anything was out of my reach.

Table of Contents

List of Figures

List of Schemes

List of Tables

Chapter 1: Introduction

1.1 Bioinorganic Chemistry: Using Nature as Inspiration

Biological systems provide the chemist with an abundance of examples of chemical transformations and processes that are difficult to achieve by other means. We aim to understand how enzymes perform their catalytic functions rapidly with a high degree of selectivity by creating synthetic small molecules that have related reactivity.[1] These small molecules are amenable to in-depth study due to their relatively facile synthesis and ease of alteration, especially when compared to isolation and purification of enzymes. In addition, the effect of pH and temperature can be readily studied on small molecules, whereas most proteins are rendered inactive outside of a narrow pH and temperature range. Also, some spectroscopic techniques require the use of high energy radiation that can degrade sensitive biological compounds. A great advantage to using synthetic compounds is they tend to have higher solubility in organic solvents, which is desirable because this enables the complexes to be studied at lower temperatures. Monitoring reactions at lower temperatures increases the likelihood that we can observe reactive intermediates important for understanding the mechanisms of these reactions. Understanding the mechanism of the reaction aides in designing complexes that will be more proficient at the desired transformation, either as catalytic or stoichiometric reagents. The process of developing a new copper complex is important as the synthetic compound could be potentially used as a catalyst that is capable of performing the same reactions as enzymes.

We are particularly interested in preparing complexes that mimic the reactivity of copper containing proteins as they are ubiquitous in nature and catalyze numerous

important organic transformations.[2–10] Our goal, as bioinorganic chemists, is to model the reactivity of metal-containing proteins (metalloproteins) with synthetic small molecules. Although the enzymes are high molecular weight molecules, the reactivity of the enzymes is generally confined to an area immediately around the metal site (active site). Most of the protein serves as scaffolding to support the correct geometry of the active site, facilitate electron transport, and handle substrate delivery/product release. We aim to create copper-containing small molecules to perform similar functions to the copper-containing enzymes, such as C-H bond activation. Currently, most industrial catalysts focus on the use of rare 4th (Ru, Rh, Pd) and 5th row (Ir, Pt) transition for C-H bond activation (**Figure 1-1**). Utilizing copper as a catalyst is particularly attractive due to its high natural abundance, low toxicity, and its cost-effectiveness.

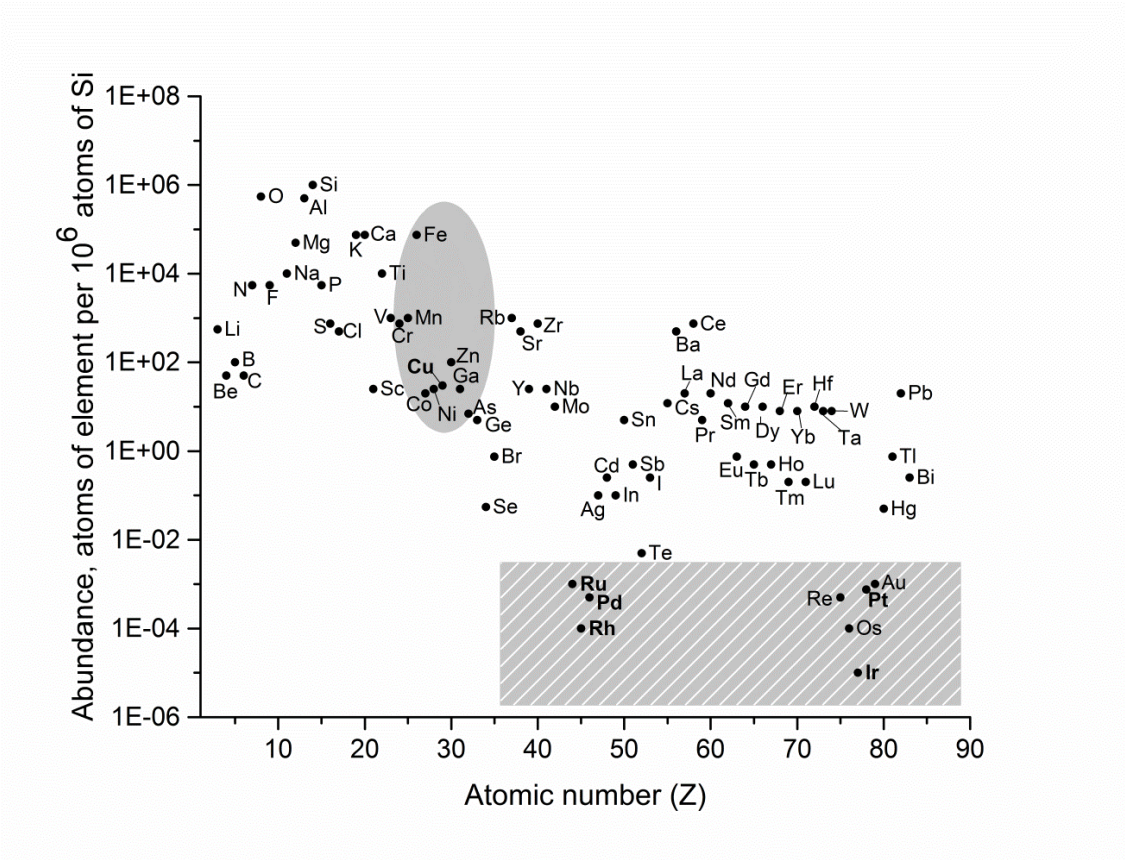

Figure 1-1: Abundance of elements found in the Earth's upper continental crust relative to the abundance of silicon (Si). Elements in the grey oval are 3d metals prevalent in biological systems. Elements in the grey and white striped rectangle are considered extremely rare. Elements of interest are bolded. Figure adapted from ref.1.

1.1.1 Copper-Containing Biosites in Biological Systems

There are a multitude of copper containing enzymes that activate oxygen in order to perform important organic transformations and functions as oxygen transport proteins in biological systems (**Figure 1-2**).

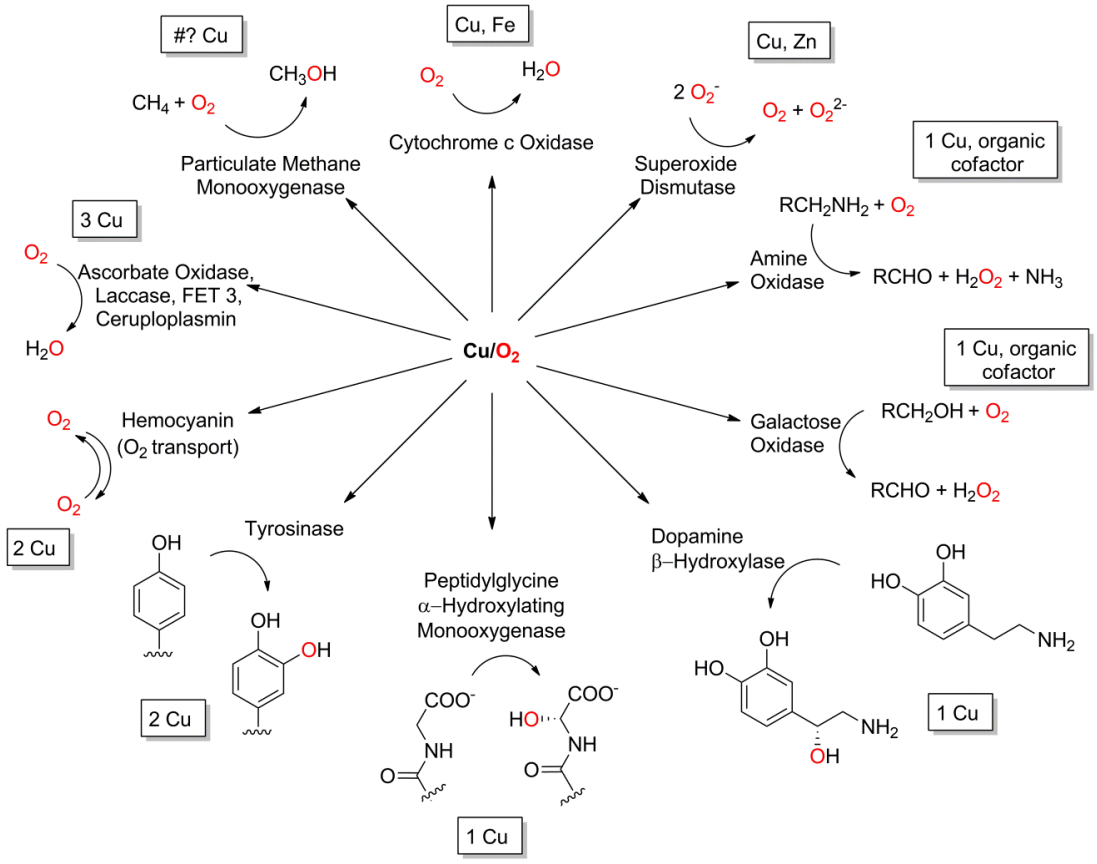

Figure 1-2: Illustration exhibiting the multitude of copper containing enzymes that use oxygen to perform a variety of important organic reactions. Figure adapted from ref.8.

Despite the wide range of functions performed by copper-containing proteins, they have a number of common structural elements. For example, the copper centers are predominately ligated by histidine residues with either trigonal or tetragonal coordination environments.[8] Traditionally, copper proteins have been categorized into different classes or "types" depending on their nuclearity and spectroscopic properties (**Table 1-1**).[10]

Table 1-1: Properties of the different types of copper containing active sites.

	Type 1	**Type 2**	**Type 3**
Class	blue (green, red)	normal	dinuclear
Function	electron transfer	reduction/oxidation	O_2 transport/activation
Proteins (i.e)	azurin	galactose oxidase	hemocyanin
	plastocyanin	phenylalanine hydroxylase	tyrosinase
	stellacyanin	amine oxidase	catechol oxidase
Cu Geometry	trigonal	tetragonal	trigonal
	tetrahedral		

Type 1 active sites, also known as blue copper proteins, are monocopper proteins that serve as electron transfer sites. They were among the first proteins to be thoroughly characterized using a variety of spectroscopic techniques.[10] The type 3 proteins contain dinuclear copper centers that transport oxygen (hemocyanin) or activate oxygen for subsequent oxidation of organic substrates (tyrosinase, catechol oxidase).[3,11] We are particularly interested in understanding the reactivity of normal "type 2" monocopper enzymes, which include enzymes capable of dioxygenase,[12] monooxygenase,[13–15] and oxidase[16–21] functions. These enzymes oxidize substrates by activating C-H bonds, a process that we would like to understand from a fundamental viewpoint in order to apply this knowledge to modern synthetic challenges.

This initial categorization of copper proteins into three major types has been expanded to include trinuclear copper clusters (one type 2 and one type 3 center), the Cu-Zn superoxide dismutase (SOD) center, and a Cu_B-$heme_a$ center (Cu_B is a type 2 center). In addition, a family of active sites that have sulfur ligated copper centers have been

chategorized: a mixed-valent binuclear Cu_A site, a ($CuSMoO_2$) site, and the tetracopper Cu_Z site (**Figure 1-3**).

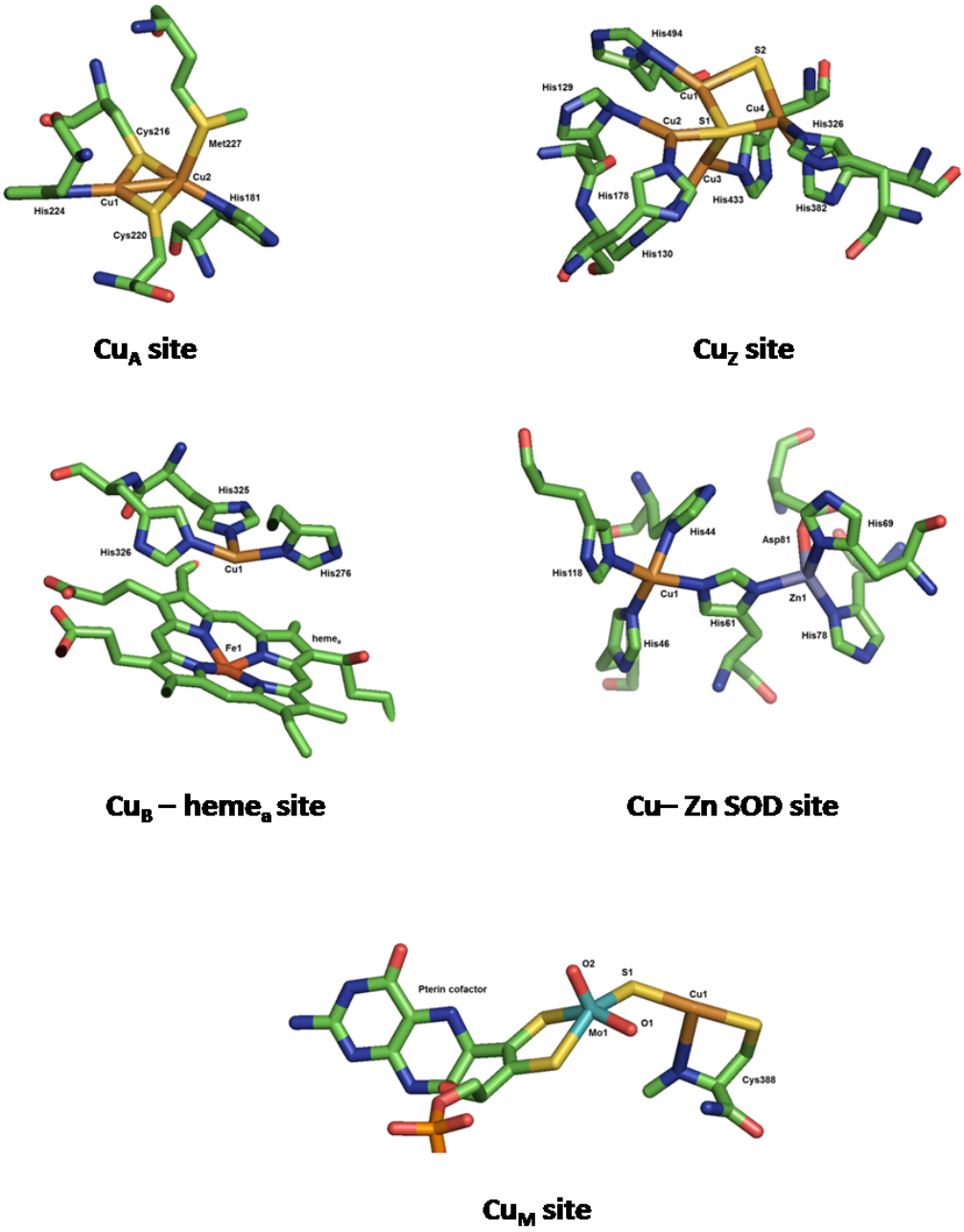

Figure 1-3: Representations of X-ray crystal structures of the more recent copper sites found in biological systems: Cu_A site and Cu_B-$heme_a$ site from cycthochrome c. oxidase (PDB ID: 1QLE),[22] Cu_Z site of nitrous oxide reductase (PDB ID:3SBP),[23]Cu-Zn SOD site (PDB ID: 2SOD),[24] and Cu_M site from CO dehydrogenase (PDB ID: 1ZXI).[25]

1.1.2 Copper-Sulfur Biosites in Biological Systems

The copper-sulfur sites have unusual binding motifs and electronic properties.[11,24–30] We are particularly interested in gaining an understanding of nitrous oxide reductase (N_2OR), an enzyme found in bacteria, fungi, and archae, because it performs the two-electron reduction of nitrous oxide (N_2O) to dinitrogen (N_2) and water as the final step of the denitrification process in the global nitrogen cycle.[31] The reduction of nitrous oxide is thermodynamically favorable ($\Delta G \approx$ -25 kcal/mol), however, the large kinetic barrier ($\Delta G^{\ddagger} \approx$ 59 kcal/mol) makes this reaction difficult to achieve under ambient conditions without the use of a catalyst.[32] Reduction of N_2O is a vital process for microorganisms that utilize this enzyme in order to maintain a proton gradient across the mitochondrial membrane, which is necessary for the production of adenosine triphosphate (ATP) during anaerobic respiration.[33] In addition, nitrous oxide is a potent environmental pollutant that has increased in concentration in the atmosphere due to anthropogenic activities.[34] By discerning the mechanism N_2OR uses to reduce N_2O, we can apply that knowledge to develop small molecular catalysts capable of remediating N_2O pollution from the atmosphere.

In order to mimic the reactivity of N_2OR, we look to the structure of its active site to garner information about the components that may be necessary for N_2O activation. The X-ray structure of N_2OR reveals two copper centers: a Cu_A site (electron transfer) and a Cu_Z site (catalytic site) (**Figure 1-3**).[23] The Cu_Z site, a $[Cu_4(\mu_4\text{-}S)(\mu_2\text{-}S)]$ cluster ligated by seven histidine residues, is the catalytic site that performs the reduction of nitrous oxide in nitrous oxide reductase.[23] The Cu_Z site of N_2OR is catalytically active under ambient conditions, which has inspired us to model its structure in an attempt to

mimic its reactivity. In order to explore copper-inorganic sulfur motifs, as well as to further understand how such an energy intensive transformation readily occurs in these enzymes, a synthetic approach to the development of small molecules that mimic the activity of the Cu_Z site is crucial. Over nearly the past two decades, many copper-sulfur motifs have been characterized, including: $[Cu(II)_2(\mu\text{-}S_2^{2-})]^{n+}$, $[Cu(II)_2(\mu\text{-}S_2^{\cdot-})]^{n+}$, and $[Cu(II)_2(\mu\text{-}1,2\text{-}S_2)^{2-})]^{n+}$ cores, among others (see Chapter 2 for more details).[35–38]

Previous work from our laboratory has reported the only copper-sulfur complex to reduce N_2O to N_2, and evidence suggests that a dicopper complex is the active species in that system.[39] This led us to aim to synthesize a $[Cu_2(\mu_2\text{-}S)]$ complex to test the hypothesis that it is the minimal unit needed to reduce N_2O. Using nature as inspiration, we aim to make a small molecule model of the Cu_Z site using nitrogen donor (N-donor) ligands as analogs for the histidine residues present in the enzyme. These N-donor ligands must also maintain a low denticity coordination environment to maintain biological relevance to the Cu_Z site of N_2OR, in which each copper is tridentate prior to binding N_2O. We are particularly interested in developing a modular synthetic route for building more complex molecules, such as the tetranuclear Cu_Z site. This approach could also be extended towards the creation of heterobimetallic (Cu-Zn SOD and the $CuSMoO_2$ site) species (see Chapter 2 for more details).

1.2 Copper(III) as an Important Intermediate for C-H Bond Activation

Although some consider the copper(III) oxidation state to be inaccessible in biological systems,[8] high-valent copper sites have been suggested as potential intermediates during the catalytic cycle of various oxidase and oxygenase enzymes.[8,40,41] The identity of the copper-oxygen species responsible for C-H bond activation in

monocopper enzymes has been widely debated.[42–47] Peptidylglycine α-hydroxylating monoxygenase (PHM) and dopamine β-monooxygenase (DβM) are two monocopper proteins that perform stereoselective hydroxylations using a reactive copper-oxygen species.[46–49] Both enzymes contain a monocopper Cu_A (electron transfer) site and a monocopper Cu_B (catalytic) site. DβM catalyzes the conversion of dopamine to norepinephrine, both of which are neurotransmitters that regulate blood pressure.[50,51] PHM performs selective hydroxylation of C-terminal glycine-extended peptides to create α-hydroxylated products, which are precursors for the synthesis of hormones (i.e. oxytocin).[46] Although kinetic studies suggest the two enzymes abide by the same mechanism,[42,43,47] density functional theory (DFT) calculations indicate different active species for the two enzymes.[47,52] Klinman and coworkers believe that the $Cu(II)_B$-$O_2^{\cdot-}$ species performs H-atom abstraction in PHM,[47] while Yoshisawa and coworkers suggest a copper(III)-oxo/copper(II)-oxyl species performs H-atom abstraction in DβM (**Scheme 1-1**).[52]

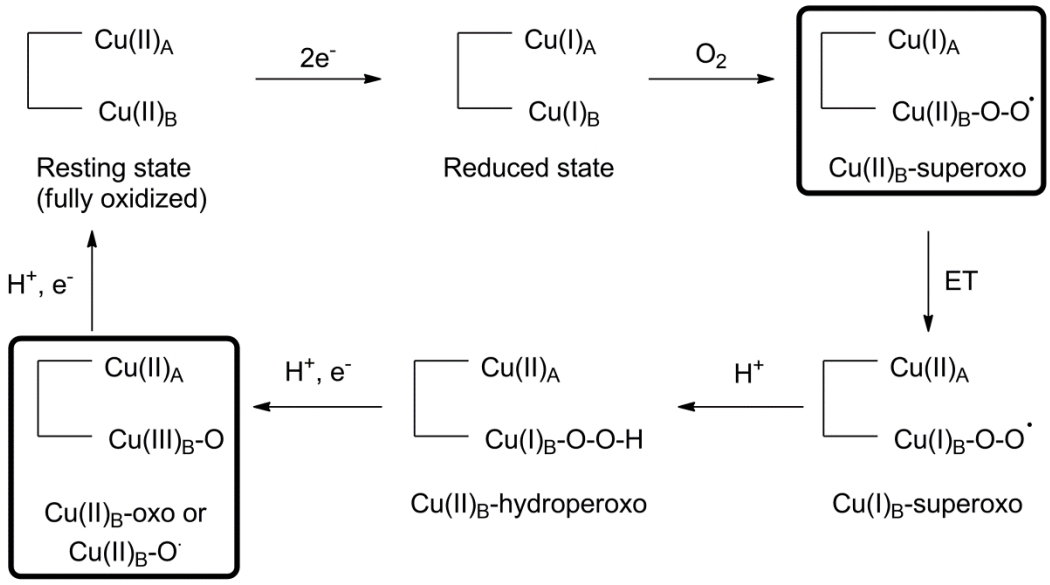

Scheme 1-1: Proposed enzymatic steps for PHM and DβM, with the compounds suggested as C-H bond activating intermediates framed in a bolded rectangle. Adapted from ref.52.

The uncertainty of the C-H activating species in the enzymes has led us to pursue the synthesis of copper(III)-oxo/copper(II)-oxyl species in order to study their reactivity towards substrates with weak C-H bonds. Preparing a copper(III) complex is not an easy feat, as copper(III) species are rare. Well characterized examples of copper(III) complexes are supported by strongly electron-donating ligands that enforce a square planar geometry as discussed in the following sections.[53–66,66–69]

1.2.1 Stable Copper(III) Complexes in the Literature

The stabilization of copper(III) complexes has been achieved through the use of polyanionic ligands with nitrogen and oxygen donors that enforce a square planar geometry to give a variety of copper(III) complexes of variable overall charge (**Figure 1-4**). Copper(III) complexes supported solely by sulfur ligands have also been reported, but have been excluded from this discussion as they are less relevant to our goal of creating enzymatic models.[61,70,71]

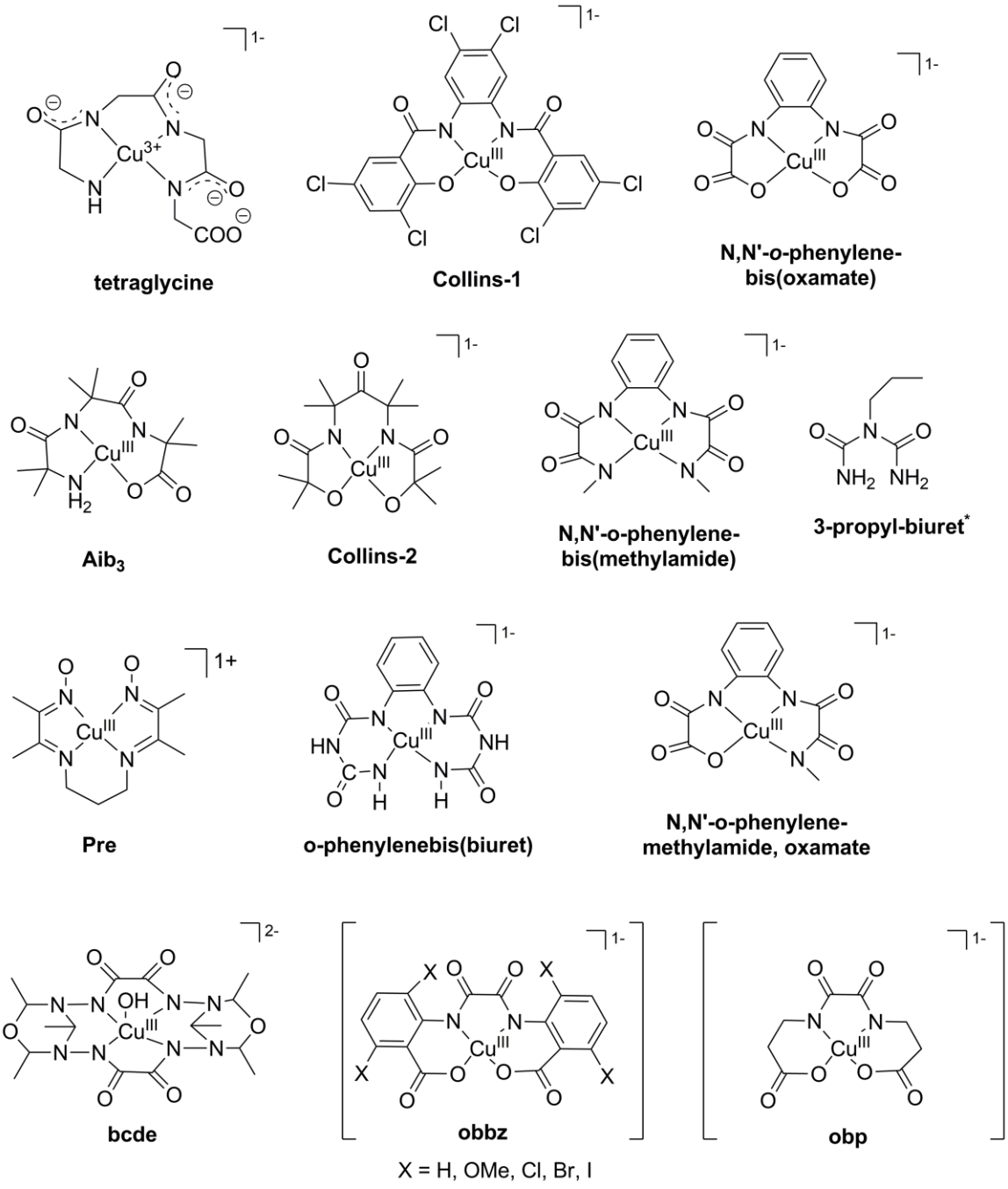

Figure 1-4: Representative selection of polyanionic ligands used to support copper(III) complexes. Copper(III) complexes that have been structurally characterized are drawn with the ligand name labeled below. The ligand denoted with * indicates it is assumed to have a square-planar structure similar to o-phenylenebis(biuret) .Complexes with brackets are proposed based on the structure of the related copper(II) complexes. See **Table 1-2** for references and characterization data.

Copper(II)/copper(III) redox couples and UV-Vis spectral features of previously reported copper(III) complexes are presented in **Table 1-2**. A wide range of potentials are observed for copper(III) complexes supported by polyanionic ligands, ranging from −1.105 V to +1.12 V vs Fc^+/Fc. Studies by Bossu[72] on polypeptides and Journaux[62] on *N,N*'-o-phenylene-bis(oxamate) ligands indicated a correlation between the visible absorption spectra and the redox couple. This correlation is attributed to the relative gain in the crystal field stabilization energy (CFSE) resulting from the change of a square planar d^9 copper(II) center to a d^8 copper(III) center. The stabilization energy of this change is ~(15/12) Δ (Δ = ligand field splitting parameter) when moving from a d^9 ((13/12) Δ) to a low-spin d^8 configuration ((28/12) Δ) for square planar complexes.[62] In addition, the change from a divalent (2^+) to a trivalent (3^+) ion further increases the ligand field splitting parameter. These factors all contribute to an increase in the crystal field stabilization energy of the copper(II) complexes, but an even larger effect on the stabilization energy of the corresponding copper(III) complex. The large stabilization energy leads to a shift of the copper(II)/copper(III) redox couple towards a more negative potential. The visible absorption spectra of the copper(II)-peptide complexes exhibit a single absorption band, which contains contributions from the three possible d-d transitions. Assuming the relative positions and intensities of the three transitions remain constant during excitation, the position of the absorbance maximum in the visible region is a measure of the equatorial bond strength (and CFSE).[72] An inverse relationship is observed for the value of λ_{max} compared to the reduction potential, and Bossu suggests this indicates the relative gain in CFSE from d^9 copper(II) to d^8 copper(III), which is of great importance to the thermodynamic stability of the copper(III) complex.

Table 1-2: Electrochemical and electron absorption features of selected copper(III) complexes. Ligands are drawn in **Figure 1-4**.NR = not reported.

Ligand	**$E_{1/2}$ vs Fc^+/Fc**	**UV-Vis** λ_{max} (nm) (ε, $M^{-1}cm^{-1}$)
Tetraglycine [b]	0.941[a]	365 (7,100)
3-propylbiuret[c]	-0.02 [a]	373(8,500)
Collins-1 [d]	0.025	NR
Collins-2 [d]	-1.105	NR
N,N′-o-phenylene-bis(oxamate)[e]	0.72 [a]	NR
N,N′-o-phenylene-methylamide,oxamate [e]	0.43 [a]	NR
N,N′-o-phenylene-bis(methylamide) [e]	0.29 [a]	460
o-phenylenebis(biuret)[f]	0.35 [a]	NR
tri-α-aminoisobutyric acid (Aib_3) [g]	0.726 [a]	395 (5,300)
Pre [h]	1.12[a]	515 (12,500)
bcde[j]	none[i]	540 (29,500)
obbz (X = Cl) [k]	0.436[a]	NR
obp [k]	0.392[a]	NR

[a] values were converted to reference vs Fc^+/Fc from reported values measured vs SCE
[b] ref.73
[c] ref.53
[d] ref.60
[e] ref.62
[f] ref.74
[g] ref.55
[h] ref.58
[i] No reduction or oxidation waves were observed
[j] ref.54
[k] ref.75

The copper(III) complexes supported by polypeptides are stable in neutral solutions ($t_{1/2}$ ~ 5.5 hours), but are sensitive to basic and acidic environments, where decomposition gives copper(II) and oxidized peptide products.[56,72,73] The [copper(III)(tetraglycine)]$^{1-}$ complex is sensitive to ambient light, and undergoes rapid decarboxylation despite its

thermodynamic stability ($E_{1/2}$ = 0.36 V vs NHE).[56] The mono-anionic copper(III) complexes prepared by Collins and coworkers, [copper(III)(Collins-1)]$^{1-}$ and [copper(III)(Collins-2)]$^{1-}$, exhibited markedly different redox potentials depending on the identity of the countercation employed.[60] When sodium was used as a counterion, the potential for a related copper(III) complex shifted by +210 mV relative to the potential measured when a tetramethylammonium counterion was used. Collins suggests that this may be due to bridging of the sodium ion between the alkoxide oxygen atoms, which would decrease the electron-donating ability of the ligand and increase the oxidation potential of the copper center. Interestingly, there was no observed effect on the redox behavior of these copper(III) complexes in non-coordinating (dichloromethane) versus coordinating (acetonitrile) solvent. Overall, the mono-anionic copper(III) complexes are thermally and aerobically stable, and no reactivity of the complexes towards C-H bonds has been reported. Similarly, the square pyramidal [copper(III)(bcde)(OH)]$^{2-}$ complex is very stable and was reported to be unreactive towards ligand exchange or decomposition.[54]

The monocationic ([copper(III)(Pre)]$^{1+}$) and neutral (copper(III)(Aib_3)) complexes have been examined for reactivity towards C-H bond activation by Mayer and coworkers.[65] Methylation of a tripeptide was performed to give α–aminoisobutyric acid (Aib_3), which was used to stabilize neutral copper(III) and nickel(III) complexes.[55] The (copper(III)(Aib_3)) complex exhibited remarkable stability towards acid decomposition and self-redox events, but underwent facile photochemical degradation. The (copper(III)(Aib_3)) complex is stable in a strongly acidic environment (30% loss, 16 days, 5 M $HClO_4$), which is in stark contrast to the corresponding non-methylated tripeptides

that undergo full decomposition in minutes.[55] In contrast to its acid stability, (copper(III)(Aib_3)) undergoes rapid decomposition when exposed to visible light (<3 min 100-W tungsten lamp) to give copper(II), carbon dioxide, acetone, unreacted Aib_3 (ligand), and what is believed to be the dipeptide (H-Aib_2-amide$^+$). This type of decarboxylation reaction has been observed with other first row transition metal-amino carboxylates (Fe[76,77] and Co[78,77]), although those reactions required the use of ultraviolet radiation. The (copper(III)(Aib_3)) complex did not react with weak C-H bonds (C-H bond strength, 78 kcal/mol), although it readily oxidizes phenols to give coupled products (O-H bond strength, 81 kcal/mol).[65] In contrast, the monocationic [copper(III)(Pre)]$^{1+}$ complex readily attacks both weak C-H bonds and O-H bonds.[65] Mayer and coworkers attribute the inactivity of (copper(III)(Aib_3)) towards C-H bonds to the observation that H-atom abstraction from O-H bonds is more rapid than for C-H bonds of the same strength.[65] The nature of the difference in reactivity of (copper(III)(Aib_3)) and [copper(III)(Pre)]$^{1+}$ is unclear, as the axial coordination of solvent to the square planar copper(III) complex complicates a comprehensive understanding of the entropic contributions to the overall driving force of the reaction. The reactivity of these two complexes suggest that future endeavors to utilize copper(III) complexes as reactive species should aim for the creation of neutral or monocationic complexes.

In conclusion, previous studies indicate that in order to stabilize a copper(III) center, the supporting ligand should: enforce a square planar geometry, be tri- or tetradentate, and have strong electron-donating capabilities. As we are interested in using a copper(III) as a reactive intermediate, our challenge is to stabilize the copper(III) state in order for it to be observed, but not to the extent that it would

prohibit the desired reactivity. We hypothesized that this goal could be reached by using a dianionic tridentate mer-coordinating ligand to stabilize a copper(III)-hydroxide moiety. The copper(III)-hydroxide species would then be studied for reactivity towards weak C-H bonds (see Chapter 3). In addition, we utilized a less sterically hindered derivative of the ligand to stabilize a copper(III)-cyanomethide complex (see Chapter 4) that has relevance to postulated intermediates in copper catalyzed carbon-carbon bond forming reactions. To place this latter work into proper context, the following section discusses copper(III)-carbon species.

1.2.2 Proposed Copper(III)-Carbon Intermediates in Organometallic Reactions

For several decades, organocuprate(III) complexes have been of interest due to their relevance as proposed intermediates in reactions employing Gilman reagents ($R_2Cu^{I}Li$, R = alkyl, aryl) to achieve carbon-carbon bond formation.[79,80] Typically, the S_N2 (or S_N2') reaction of a Gilman reagent involves the conjugate addition of a copper(I)-alkyl to an α,β-unsaturated carbonyl compound followed by cross-coupling with an organic halide to selectively form a new carbon-carbon bond.[79,81,81–86] The existence of a copper(III)-alkyl intermediate has been postulated as being critical for these reactions,[59,83,84,87,87–92] and theoretical calculations support this hypothesis.[93–98] In general, copper catalyzed carbon-carbon coupling reactions are believed to involve copper(I) starting complexes that generate a reactive copper(III) species.[68,69,99] The mechanism for either stoichiometric or catalytic systems involves three general steps: transmetallation, oxidative addition, and reductive elimination (**Figure 1-5**).[69] The reaction begins with the transmetallation of the copper(I) salt with a main-group organometallic reagent (R-M), followed by nucleophilic attack of the copper nucleus by an electrophile ([E]). The

electrophile coordinates to the copper center via oxidative addition to give the formally copper(III) intermediate, which undergoes reductive elimination to yield the desired carbon-carbon coupled product (R-E) and to regenerate the starting copper(I) complex, thus completing the catalytic cycle.

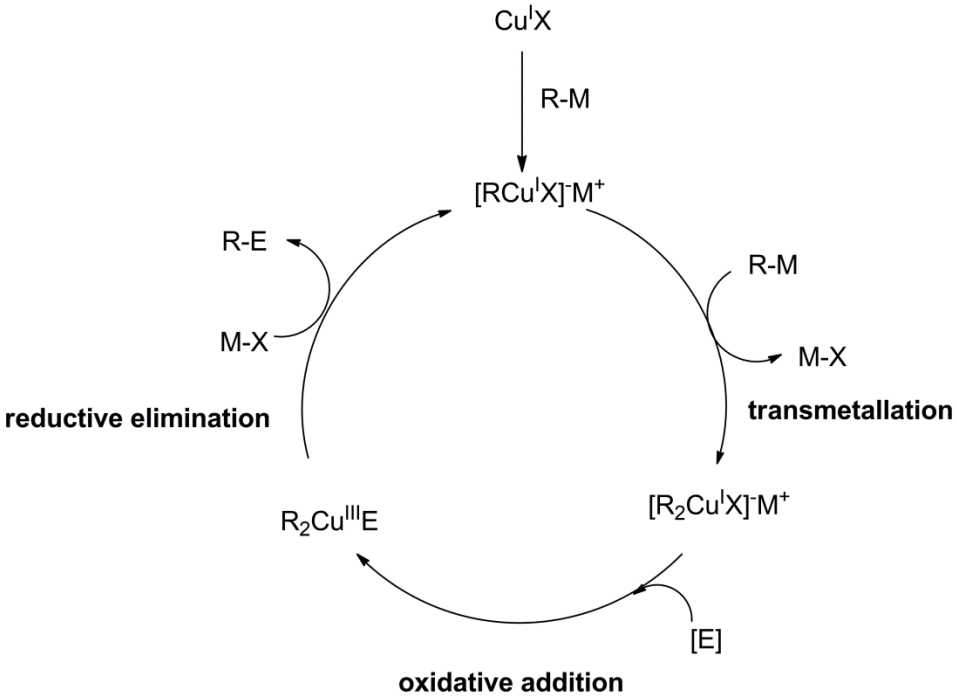

Figure 1-5: Proposed catalytic cycle for the reaction of copper(I)-alkyl complexes with a main-group organometallic reagent (M-X) and an electrophile ([E]) to give a copper(III) intermediate, followed by reductive elimination to form the desired carbon-carbon coupled product (R-E). Adapted from [69].

The copper(III) species that is postulated to perform carbon-carbon coupling had not been observed experimentally until recently. In an attempt to gain insight into the mechanism of the reaction of Gilman reagents with alkyl halides, rapid-injection NMR spectroscopy studies were performed with the goal of identifying possible reaction intermediates. In these reactions, square planar mono-anionic and neutral copper(III)-alkyl intermediates were observed at −100 °C (**Scheme 1-2**).[82,100,101]

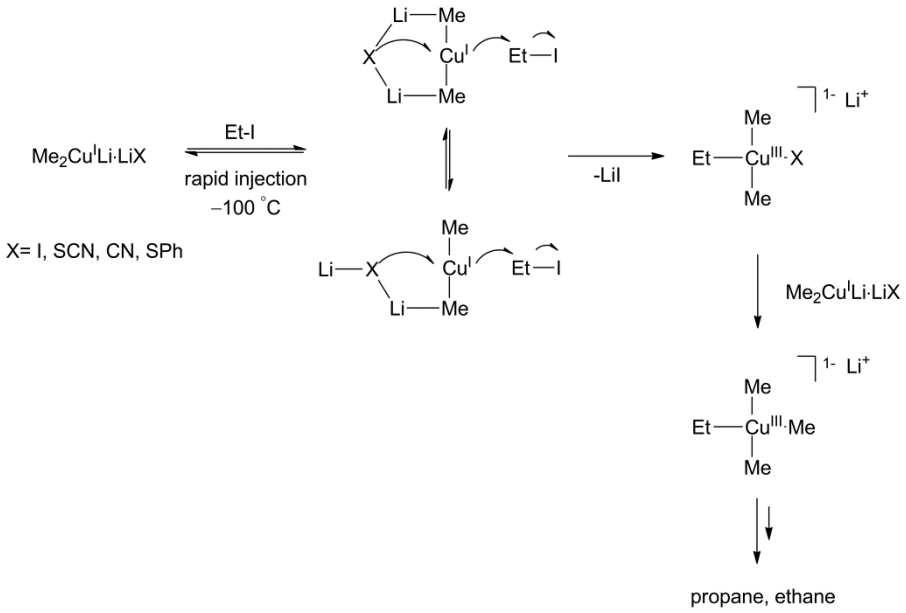

Scheme 1-2: Proposed reaction pathway for the formation of copper(III)-alkyl intermediates.

The results suggested that the oxidative addition of ethyl iodide (EtI) to the copper(I) center formed a [copper(III)Me_3Et]$^{1-}$ complex. The oxidative addition appears to occur in *trans* fashion, which Cope and coworkers acknowledge is unusual because oxidative addition typically produces *cis*-addition products.[100] Both a cyclic (both lithium atoms coordinated) and acyclic (only one lithium atom coordinated) arrangements for the oxidative attack can be imagined to give the copper(III) complex, [copper(III)Me_2EtX]$^{1-}$ (X = I, SCN, CN, SPh) (middle drawing in **Scheme 1-2**). Depending on the nature of the lithium salt used (X substituent), the stability of [copper(III)Me_2EtX]$^{1-}$ varied from a few seconds (X = SCN) to indefinitely (X = SPh) at −100 °C. At elevated temperatures (> −80 °C), all complexes exhibited some decay as evidenced by the formation of [copper(III)Me_3Et]$^{1-}$, which then undergoes further decay to produce propane and ethane.[81] The formation of multiple products is undesirable, as this indicates the active

species is following multiple pathways, which leads to a diminished yield of the desired product.

Cope and coworkers studied the reaction of halo-Gilman reagents [copper(I)Me_2]X (X = Cl, Br, I) in the presence of allyl chlorides. They were able to observe η^3-copper(III) π-complexes and η^1-copper(III) σ-complexes (**Scheme 1-3**).[82]

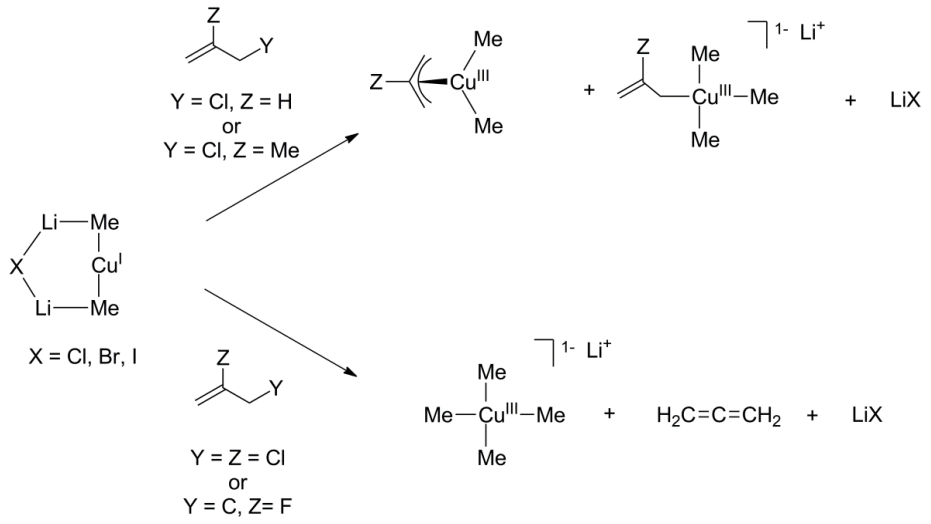

Scheme 1-3: Different pathways observed for the reaction of [copper(I)Me_2]$^{1-}$ with allyl chloride complexes depending on the nature of the substituents.

The treatment of halo-Gilman reagents with allyl chlorides containing a chloride in the position β to the unsaturation, however, led to β-chloride elimination and formation of [tetramethylcopper(III)]$^{1-}$ and allene. The observation by Cope and coworkers of [tetramethylcopper(III)]$^{1-}$ was the first report of this previously elusive compound.[82] While formation of [tetramethylcopper(III)]$^{1-}$ at −100 °C was essentially quantitative, reactions performed at higher temperatures (−100 °C and 0 °C) led to diminished yields (70% and 20% respectively) and formation of ethane as a side-product.

The choice of ligand was demonstrated to have a dramatic effect on the stability of the copper(III) intermediate, as it was also noted that the addition of dimethylsulfide or trimethylphosphine to the copper(I) starting material led to a cleaner formation of [tetramethylcopper(III)]$^{1-}$. Further studies were performed, using a range of phosphine and nitrogen donor ligands to assess the effect of ligands on the stability of neutral copper(III) complexes observed by rapid-injection NMR spectroscopy (**Figure 1-6**).[100]

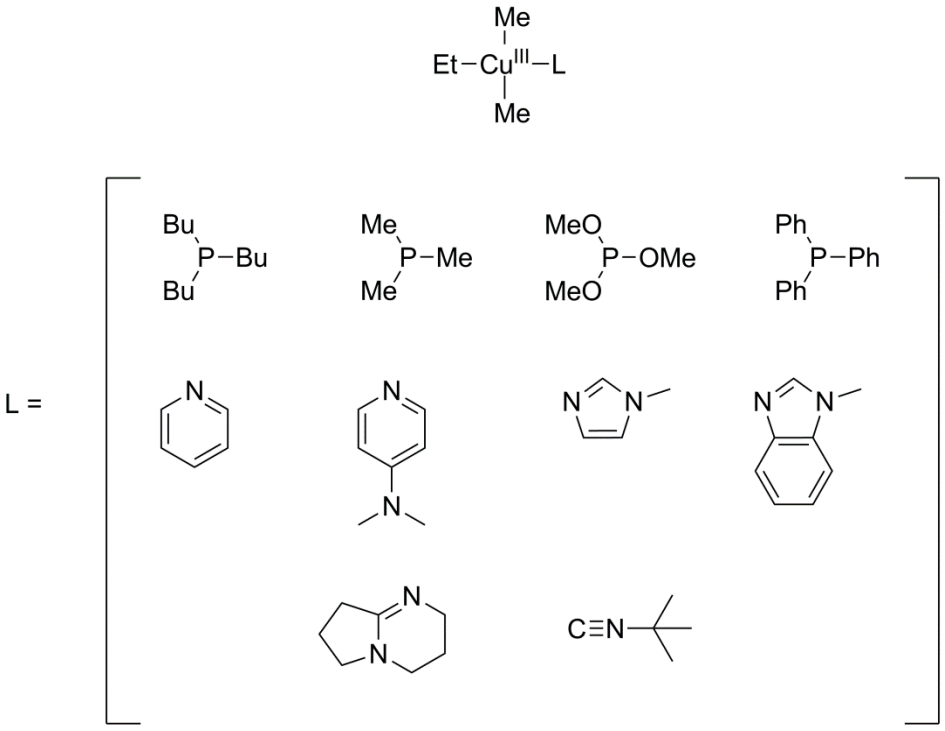

Figure 1-6: Neutral copper(III) complexes observed upon complexation with various neutral ligands.

The intermediates observed by rapid-injection NMR spectroscopy formally place copper in the +3 oxidation state, while calculations suggest the charge on the copper center is closer to +1.[94] DFT calculations and natural population analysis (NPA) by Snyder[94] of the neutral and charged "copper(III)" 3d orbitals gave population values between 9.4 and 9.7. These population values are equivalent to the population values observed for the

copper(I)-alkyl complexes. Snyder suggests the formulation of these compounds as d^{10} copper atoms (copper(I)) that have highly ionic bonds with a small degree of covalent interaction between the ligands and the Cu(d_{x2-y2}) orbital.[94] Thus, while these simple copper-alkyl complexes are formally copper(III) as is consistent with an oxidative addition mechanism,[69] DFT calculations[94] suggest they are actually in the copper(I) oxidation state.

Direct C-H bond activation has been reported where copper(III) compounds are implicated as the active species. Barton and coworkers reported the C-H bond activation of indoles in the presence of copper(I) and an aryl-bismuth(V) oxidant.[102] More recently, less toxic bis(aryl)iodium salts have shown to oxidize copper(II) salts leading to the arylation of indoles.[103] While the mechanism for the arylation is unclear, DFT calculations suggest the iodium salt directly oxidizes copper(I) to give a copper(III)-aryl intermediate.[99,104] In addition, copper(III) complexes are proposed to form when copper(I) salts in the presence of a chiral ligand are exposed to a hypervalent iodine(III) reagent, yielding asymmetric carbon-carbon coupled products.[68] The use of high valent iodine(III) has complicated the mechanistic understanding of these processes,[105,106] as it is a powerful oxidant and product formation was observed in the absence of copper (albeit with lower yields and harsher conditions) for some systems.[107,108] While these reactions may possess utility for obtaining the desired carbon-carbon coupled products, there is still much to be learned about their mechanisms. In addition, it would be desirable to use less harsh oxidants, as strong oxidants have the potential to undergo side reactions.

Macrocyclic N-confused porphyrins and doubly N-confused porphyrins ligands have also been used to stabilize copper(III) complexes.[109–116] Ribas and coworkers used a

macrocyclic ligand to affect the disproportionation of copper(II) salts to afford a copper(I) species and a stable [copper(III)-aryl]$^{2+}$ complex at room temperature (**Scheme 1-4**).

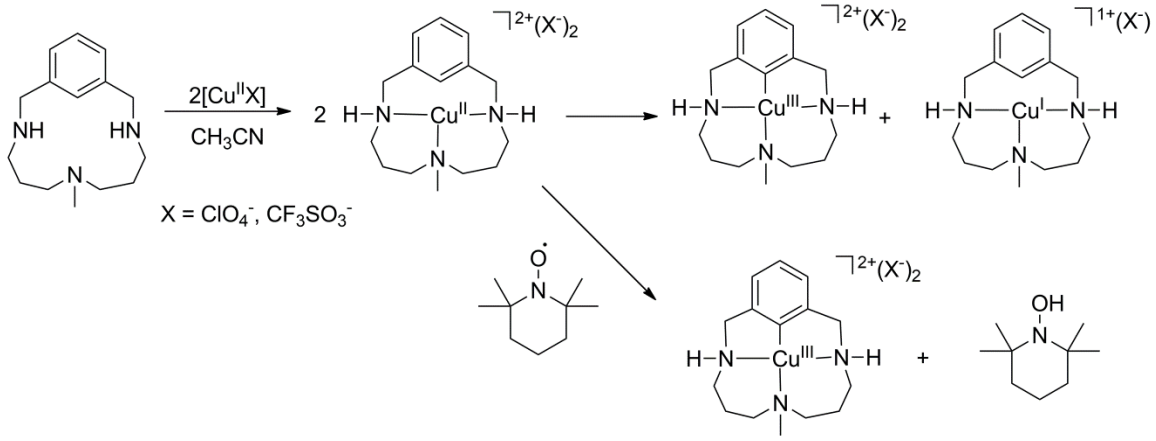

Scheme 1-4: Route for the preparation of a copper(III)-aryl complex by disproportionation (top) or addition of TEMPO (bottom).

The copper(II)-macrocyclic complex is short lived and readily undergoes disproportionation. Ribas and coworkers describe a three-center-three-electron C-H-Cu(II) interaction that is supported by evidence obtained from pulsed-EPR spectroscopy and DFT calculations.[117] A proton-coupled electron transfer (PCET) mechanism is believed to be the rate determining step in the C-H bond activation of the ligand, which is further supported by the addition of TEMPO to the copper(II) complex affording the [copper(III)-aryl]$^{2+}$ complex. In order to generate higher yields of the copper(III) complex, the reaction can be run under an oxygen atmosphere to oxidize the copper(I) product to the copper(II) starting material.[118] When copper(II) halide salts are used, a five coordinate square pyramidal [copper(III)-aryl-halide]$^{1+}$ complex is obtained that is more air stable than its corresponding [copper(III)-aryl]$^{2+}$ counterpart. This enhanced stability is evidenced by significantly lower redox potentials for the copper(II)/copper(III) couple

(250 mV).[119] While this reaction occurs without the need for harsh oxidants, it is limited in scope due the intramolecular attack of the copper(III) center on the ligand.

In order to obtain more control over the many possible mechanistic pathways and preclude unwanted side reactions that are involved with the formation of a copper(III) species, we chose to use a strongly electron-donating ligand that enforces a square planar geometry, which should aid in stabilizing a copper(III) center according to ligand field theory. In addition, we aim to develop a ligand system that will direct the reactivity of the copper center towards exogenous C-H bonds by designing a ligand without C-H bonds in close proximity to the copper center, thereby reducing the likelihood of intramolecular attack.

1.3 Brief Overview of the Following Chapters

With the goal of modeling copper-oxygen and copper-sulfur biosites, we used a dianionic ligand that would enforce a square planar geometry in order to stabilize both the copper(II) and copper(III) oxidation states. As both copper(II) and copper(III) prefer a square planar geometry, this should minimize the reorganization energy of the system when changing oxidation states. Previous reports of nickel(II)-hydroxide,[120] nickel(II)-bicarbonate,[120,121] and nickel(II)-μ-(CN)-iron(II) complexes[120] by Holm and coworkers supported by an NNN-pincer ligand led us to pursue the use of related ligands in copper chemistry.[122–124] We chose *N,N*′-bis(2,6-diisopropylphenyl)-2,6-pyridinedicarboxamide and *N,N*′-bis(2,6-dimethylphenyl)-2,6-pyridinedicarboxamide as ligands to support copper(II) complexes with various ancillary ligands (**Figure 1-7**).[123,124]

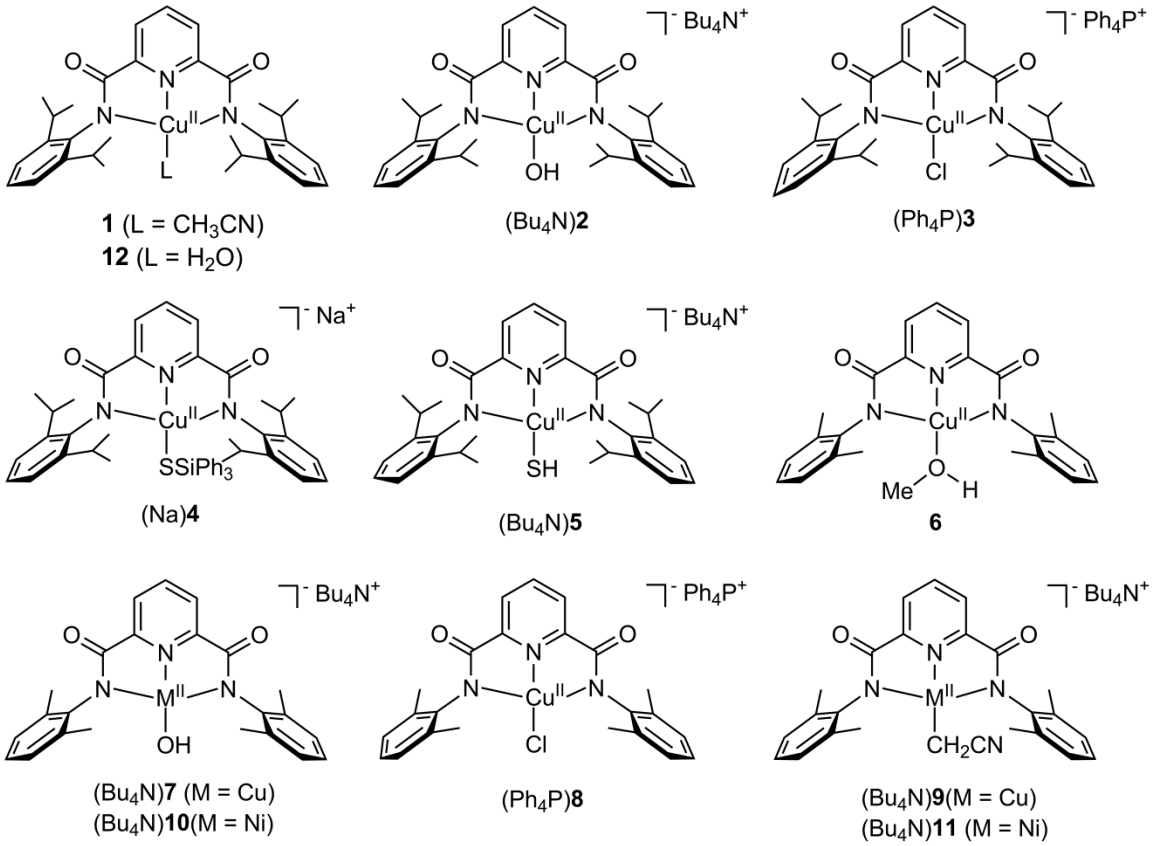

Figure 1-7: Copper and nickel complexes supported by *N,N′*-bis(2,6-dimethylphenyl)-2,6-pyridinedicarboxamide and *N,N′*-bis(2,6-diisopropylphenyl)-2,6-pyridinedicarboxamide ligands with a numbering scheme.

Chapter 2 explores the utilization of the more sterically protected use *N,N′*-bis(2,6-diisopropylphenyl)-2,6-pyridinedicarboxamide ligand to produce novel monocopper(II)-sulfur complexes (Na)**4** and (Bu_4N)**5**. These compounds were synthesized with the intent of using them as building blocks for creating homo- and heterobinuclear complexes in a controlled fashion. Both (Na)**4** and (Bu_4N)**5** were fully characterized by a variety of spectroscopic techniques, including: electron paramagnetic resonance (EPR) spectroscopy, ultraviolet-visible (UV-Vis) spectroscopy, X-ray crystallography, and electro-spray ionization mass-spectrometry (ESI-MS).

Chapter 3 investigates the effects of the steric environment provided by the NNN-pincer on the stability and reactivity of copper(III)-hydroxide complexes **2'** and **7'** towards weak C-H bonds. The copper(III)-hydroxide complexes are derived from the oxidation of their corresponding copper(II)-hydroxide complexes, (Bu_4N)**2** and (Bu_4N)**7**. The less sterically hindered **7'** exhibited increased reactivity as evidenced by rapid self-decay. Yet, while the self-decay rate of **7'** was measured to be several orders of magnitude faster than the more sterically protected **2'** in 1,2-difluorobenzene, the rates of C-H bond activation for the two complexes were essentially identical. Attempts to slow the self-decay pathway by altering the supporting cation are also discussed. In addition, the preliminary investigation assessing the thermodynamic parameters of the hydrogen atom abstraction reaction of the copper(III)-hydroxide complex is presented.

Chapter 4 reports the unprecedented reactivity of copper(II)-hydroxide, (Bu_4N)**7**, with acetonitrile to give the C-H activated copper(II)-cyanomethide complex, (Bu_4N)**9**. Also included are nickel(II) complexes, ((Bu_4N)**10** and (Bu_4N)**11**), that were prepared to compare reactivity with their related copper complexes((Bu_4N)**7** and (Bu_4N)**9**). The complexes were characterized using UV-Vis, EPR, and proton nuclear magnetic spectroscopy (^{1}H-NMR),ESI-MS, X-ray crystallography, and Fourier transform infrared spectroscopy (FT-IR). Kinetic studies were pursued to gain mechanistic information about the conversion of (Bu_4N)**7** to (Bu_4N)**9**. In addition, both metal(II)-cyanomethide complexes were examined for their ability to act as cyanomethylating reagents.

Chapter 2: Modeling Copper-Sulfur Biosites

In an attempt to model the Cu_Z site of nitrous oxide reductase, we aimed to synthesize copper-sulfur complexes with only one sulfur moiety in order to build complexity and nuclearity in a step-wise fashion. Preliminary efforts focused on the use of dinucleating ligands with the goal of obtaining 2Cu:1S complexes, however, this route was unsuccessful (see section 2.2). Efforts were then focused on the creation of 1Cu:1S complexes that have the potential to act as synthons for the controlled formation of binuclear species (2Cu:1S) (see section 2.3).This work primarily focuses on the synthesis and characterization of novel mononuclear copper(II)-sulfur complexes, with copper(II)-$SSiPh_3$ and copper(II)-SH units.

2.1.1 Properties of Nitrous Oxide Reductase (N_2OR)

Copper-sulfur containing proteins are prevalent throughout all lifeforms[5] and perform a variety of reactions under ambient conditions that are difficult to achieve synthetically due to large kinetic barriers.[125] The properties of these copper-sulfur active sites provide inspiration for synthetic inorganic chemists to develop molecules that may mimic the structure and function of these sites. Of particular interest is the enzyme nitrous oxide reductase (N_2OR), which reduces nitrous oxide (N_2O) to dinitrogen (N_2) and water, a very important step in the global denitrification cycle.[2,126–129] Nitrous oxide is an environmental pollutant and a potent greenhouse gas, making remediation of this industrial and agricultural waste product a high priority. There is also interest in using this waste product as a "green oxidant" due to its potential to behave as an oxo-transfer reagent with an appropriate catalyst, to give dinitrogen (**Scheme 2-1**). This reaction

would be of significant environmental importance as it utilizes N_2O to perform an oxidation reaction, which would ideally be used to create higher value products from hydrocarbons, while converting an environmental pollutant (N_2O) into a benign product, N_2.

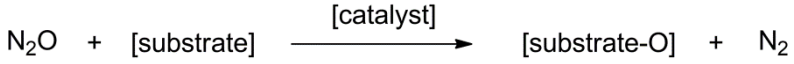

Scheme 2-1: Idealized reaction of nitrous oxide (N_2O) acting as an oxo-transfer reagent in the presence of a catalyst to give an oxidized substrate and dinitrogen (N_2).

While the reduction of nitrous oxide is thermodynamically favorable ($\Delta G \approx -25$ kcal/mol) the large activation energy for the reaction ($\Delta G^{\ddagger} \approx 59$ kcal/mol) indicates a catalyst is needed for the reduction reaction to occur under ambient conditions.[32] In addition, another challenge is activating N_2O, as it is a notoriously poor ligand for metal centers because it is both a poor π-acceptor and σ-donor.[130] Very few nitrous oxide complexes have been well characterized and only one vanadium complex with a linear nitrogen bound N_2O molecule has been structurally characterized by X-ray crystallography.[131]

2.1.1.1 Function and Structure of N_2OR

N_2OR plays a critical role in the global nitrogen cycle by performing the last step of the denitrification process, reducing nitrous oxide to molecular nitrogen (**Figure 2-1**). For denitrifying organisms, the oxidized forms of nitrogen are used in place of oxygen as terminal electron acceptors for anaerobic respiration, which is coupled to ATP synthesis.[132]

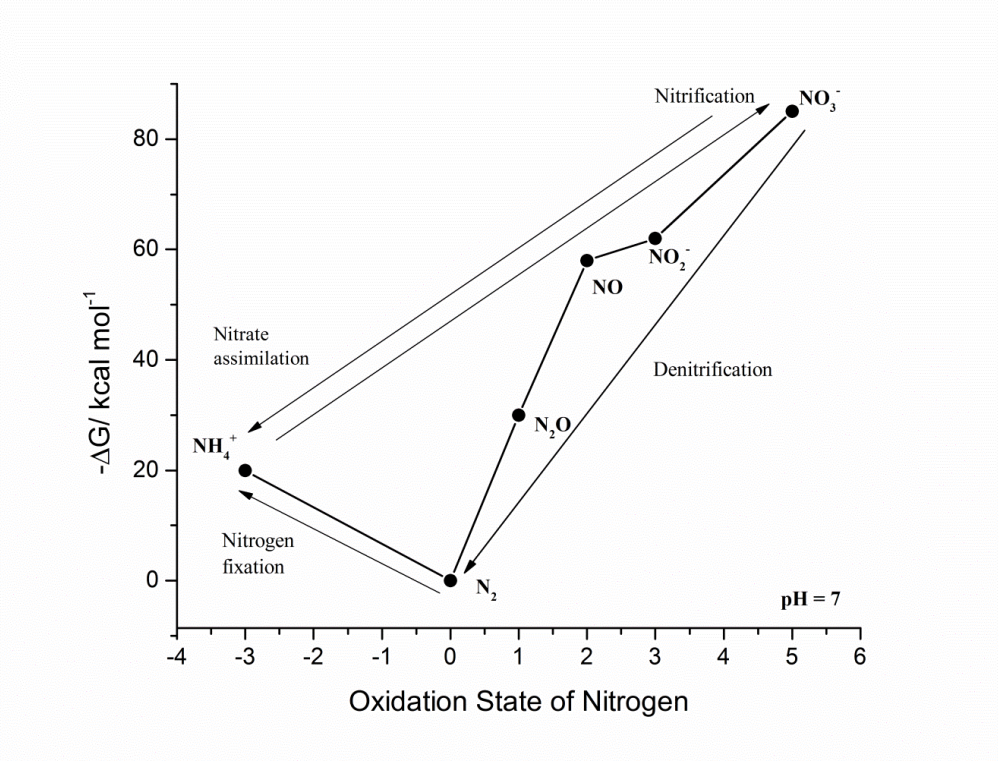

Figure 2-1: Thermochemistry of the bacterial nitrogen cycle (at pH 7). The values of ΔG are calculated per mole of nitrogen atoms and using dinitrogen (N_2) as the standard (zero). Adapted from ref.133.

In addition to serving this important function, elimination of nitrous oxide from the atmosphere is of vital environmental importance as many anthropogenic sources (artificial fertilizer and burning of fossil fuels) have led to an increase of N_2O in the atmosphere (**Figure 2-2**).[134] A very potent greenhouse gas, N_2O is third to only methane and carbon dioxide as an ozone destroying pollutant.[32,135,136]According to the United States Environmental Protection Agency, nitrous oxide has a lifetime in the atmosphere of 120 years and global warming potential of 310, meaning that one pound of nitrous oxide in the atmosphere will cause 310 times as much warming as one pound of carbon dioxide.[34]

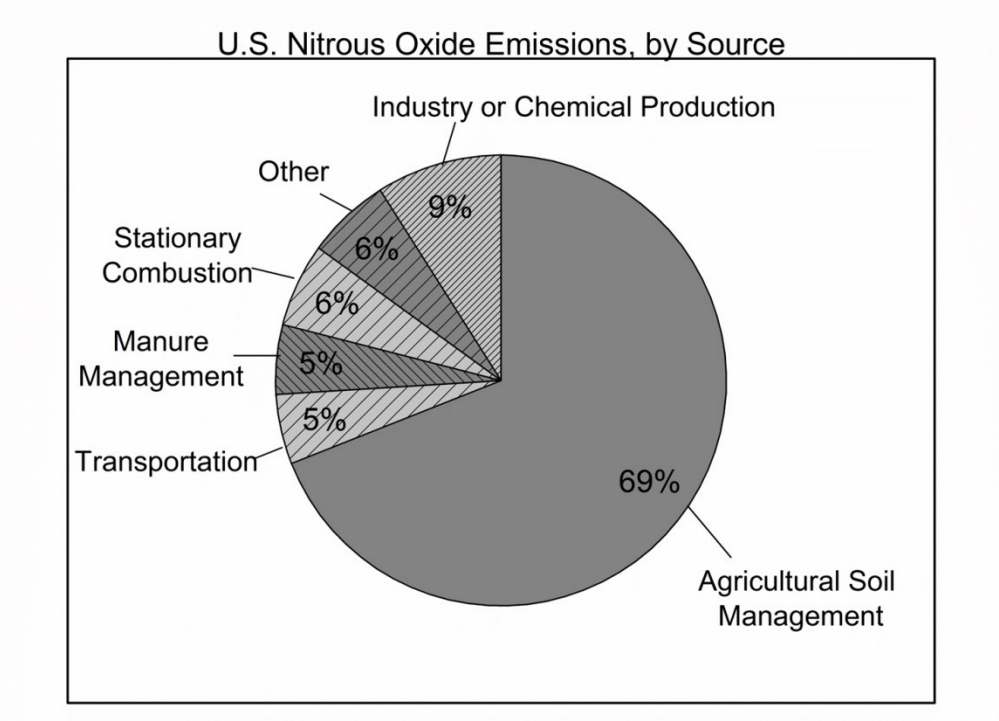

Figure 2-2: United States nitrous oxide emissions by source for 1990-2011, as reported by the United States Environmental Protection Agency, ref.134.

The isolation of N_2OR led to the identification of two copper active sites: the Cu_A and the Cu_Z site.[23,137–139] The Cu_A site was identified as a binuclear copper center with a $[Cu_2(\mu_2\text{-cysteine})_2]^{n+}$ core on the basis of the similarity of its EPR spectrum,[126,127] magnetic circular dichroism features,[140] and X-ray absorption spectrum[140–142] to the spectroscopic data of the Cu_A center in cytochrome *c* oxidase (COX). In both N_2OR and COX, the Cu_A site functions as an electron transfer center to deliver electrons to the catalytic site of the enzyme, which is typically located in a nearby subunit.[143] Structural identification of the active form of the Cu_Z site has been complicated by variations in enzyme preparations that led to the isolation of different forms of the enzyme.[23,129,139,144–147] The X -ray crystallographic data, in conjunction with resonance Raman spectroscopic data, has led to the proposal of three different structures of the Cu_Z site, with the following cores: $[Cu_4(\mu_4\text{-OH})]^n$, $[Cu_4(\mu_4\text{-S})]^n$, and $[Cu_4(\mu_4\text{-S})(\mu_2\text{-S})]^n$ (**Figure**

2-3).[23,137,138,148] At the beginning of this thesis project, the site was proposed to contain a $[Cu_4(\mu_4\text{-}S)]^{n+}$ cluster with a bridging solvent labile species (OH or H_2O).

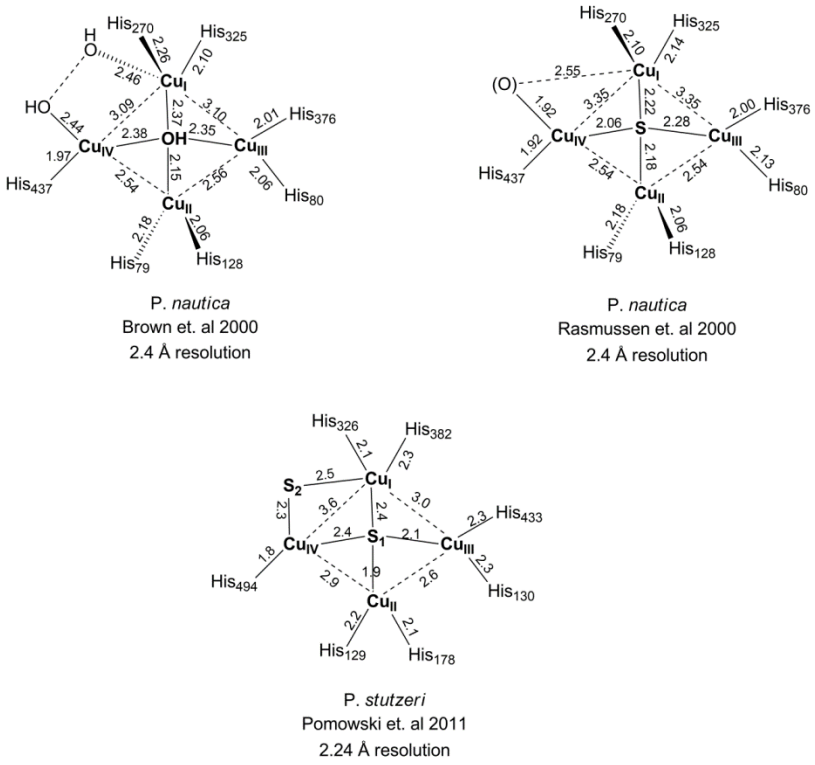

Figure 2-3: Representations of the various structures postulated for the Cu_Z site of N_2OR by X-ray crystallography. Note: (O) represents an unknown protonation state of oxygen as either OH^- or H_2O.

The Cu_Z site is located in the N -terminal domain of N_2OR, which displays a seven-blade β-propeller fold (**Figure 2-4**).[23] Within the same domain, the Cu_A site is located nearly at a distance of 40Å in the C -terminus; whereas the Cu_A site from the other domain is at a shorter distance of ~10Å.

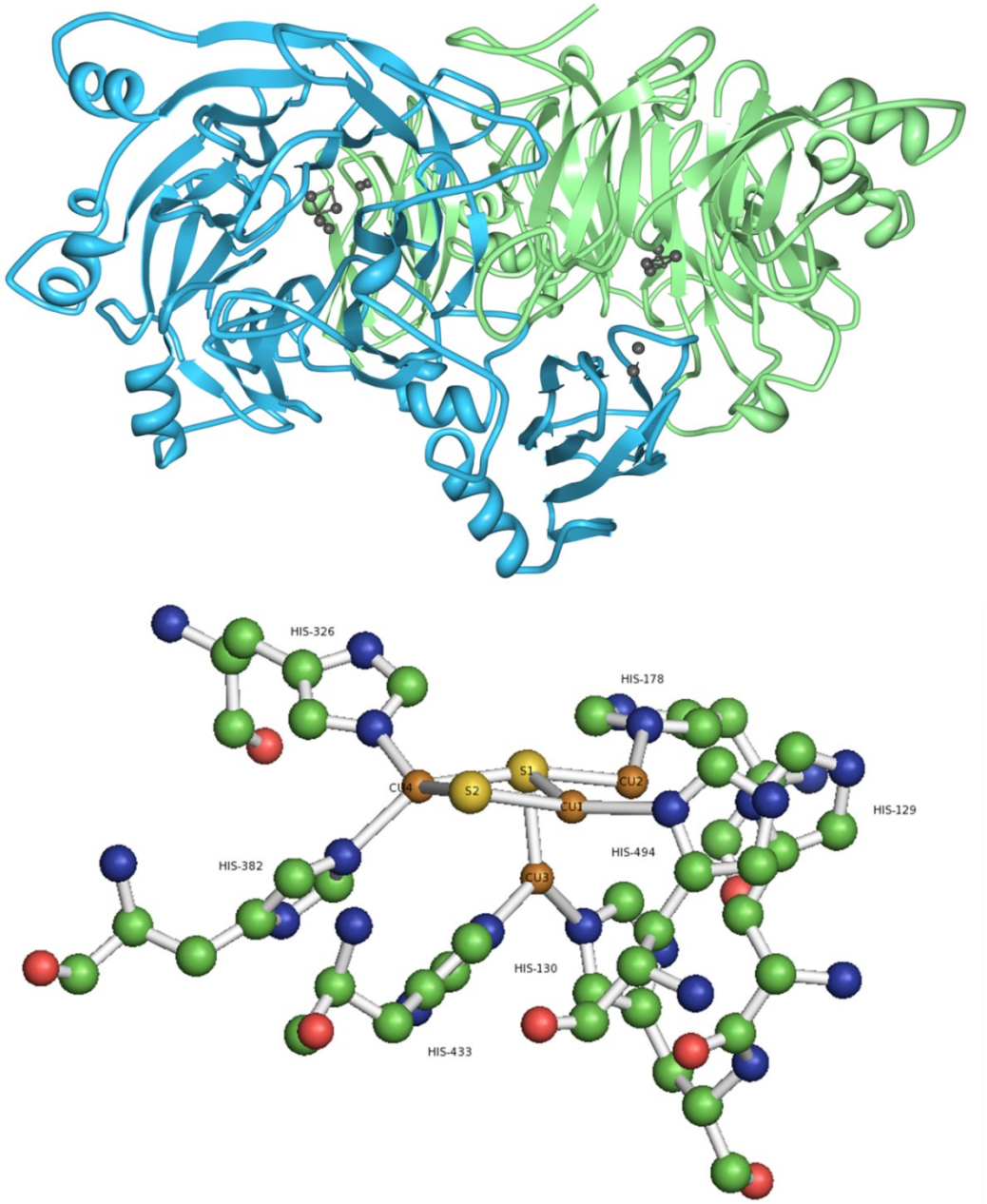

Figure 2-4: (Top): X-ray structure of the homodimeric nitrous oxide reductase isolated from P. *stutzeri* at 1.7Å resolution (PDB ID: 3SBQ).The two subunits are distinguished by different color shading of the protein backbone. Copper and sulfur atoms are represented as ball and stick models; (Bottom): Representation of the Cu_Z site indicating a [4Cu:2S] site ligand by seven histidine residues.

Isolation of N_2OR under strict anaerobic conditions provides the purple form of the enzyme with high activity.[5,128,149] When the enzyme is prepared in aerobic (or not strictly anaerobic) conditions, a pink form is obtained that only displays 20 -40% of the specific activity of the purple form.[150] Upon reduction of the pink form to the fully reduced (all copper(I)) state, a fourfold enhancement of activity (4.5 μkat mg^{-1})) is observed compared to the purple form (1.1 μkat mg^{-1})[5,145] (kat = 1 mol/ s). The reduction of the pink form requires the use of methyl viologen, which is not a physiologically relevant reduction agent and suggests that this pathway is not accessible under normal catalytic conditions. Interestingly, methyl viologen is not successful at producing a fully reduced state for the purple form of N_2OR, suggesting that substrate activation and electron transfer for the two forms are distinct.[128,145,146,151]

The differences observed in the pink and purple forms are attributed to changes observed in the crystal structures obtained by Zumft and coworkers at both the Cu_A and Cu_Z sites.[23] The Cu_A site of the pink form is a delocalized mixed-valent [$Cu_{1A}^{1.5}Cu_{2A}^{1.5}$] species, where each copper is ligated by a histidine residue, two bridging cysteine residues, and either a methionine (Cu_{1A}) or tryptophan (Cu_{2A}) residue. The delocalized state of the Cu_A site is corroborated by the narrow 7-line hyperfine splitting observed in the EPR spectrum arising from coupling of the unpaired spin to both Cu ions (I = 3/2). In the purple form, the histidine residue of Cu_{2A} is rotated and not coordinated to Cu_{2A}, yet the EPR spectrum remains similar to the spectrum obtained for the pink form. It has been suggested that the histidine rotation may have mechanistic implications pertaining to the external reduction of the Cu_A site and substrate binding (see section 2.1.1.2 for more details). The X-ray structure revealed a dramatically different structure for the Cu_Z site,

as a second sulfur atom was located in the electron density map. Further evidence for the second sulfur atom is that the bond distances from copper to sulfur (2.5 and 2.6 Å) are more consistent with copper-sulfur bonds as opposed to copper-oxygen bonds that would be expected for a solvent derived ligand as observed in the other structures of the Cu_Z site (**Figure 2-3**).[138,148] In addition, deconvolution of the complex UV-Vis spectrum indicated a sulfur→copper charge transfer band that corresponded to the Cu_A site in addition to a spectrum that was assigned to the purple form of the Cu_Z site. To reconcile the differences observed in the Cu_Z structures, Zumft and coworkers suggest that the active form of the enzyme (Cu_Z) is dominant in the purple form of the enzyme, whereas the inactive form (with only one sulfur atom), is dominant in the pink form (Cu_Z*) of the enzyme (**Figure 2-5**).[23] The second sulfur atom (S_2) is exposed to a substrate channel, making it vulnerable to attack by oxygen under aerobic preparations and leading to the irreversible formation of the Cu_Z* form. The activity observed in the pink form of the enzyme is attributed to residual Cu_Z in the enzyme, providing an explanation for why the activity of the pink form is low relative to the purple form of the enzyme.

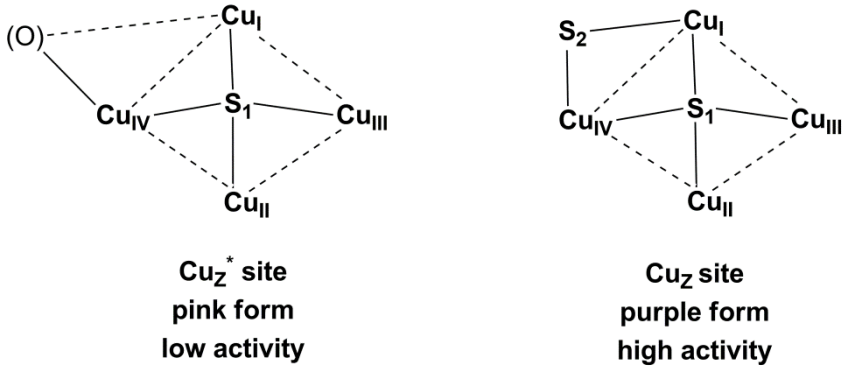

Figure 2-5: Summary of the structures that are proposed to correspond with the different observed forms of the Cu_Z site, Cu_Z and Cu_Z*.

2.1.1.2 **Proposed Mechanisms for N_2OR**

Zumft and coworkers were able to collect a crystal structure of N_2O interacting with the Cu_Z site of N_2OR by pressurizing crystals with N_2O and flash cooling with liquid nitrogen (**Figure 2-6**).[23] Their finding represents the first example of a crystal structure with copper and N_2O in close proximity. The N_2O is modeled as a linear molecule and is in a side-on configuration relative to the Cu_2-Cu_4-S_1 face of the Cu_Z site. Interestingly, the orientation of N_2O suggests that this is a pre-coordinated state, as the copper-nitrogen (2.8-3.8 Å) and copper-oxygen (3.4 Å) distances are too long to be considered true bonds. In addition, rearrangement of the N_2O ligand would be necessary for N_2 to escape via the substrate channel and for water (the other product of the reaction) to be released into the distal water cavity. Previously, N_2O was predicted to bind along the Cu_1-Cu_4 edge, but due to the discovery of a sulfur atom occupying this position, that hypothesis appears less feasible.[133,148] The weak interaction between the Cu_Z site and N_2O leads to a conformational change observed in the crystal structure about the Cu_A site, taking it from being ligated by three amino acid residues to four, where the Cu_{2A} is now fully ligated. This conformational change suggests the Cu_A site only transfers an electron after the substrate is in close proximity to the active site. While this structure of N_2OR with N_2O in the binding pocket offers some mechanistic information regarding the sequence of substrate binding and electron transfer, questions about the mechanism of N_2O activation still remain.

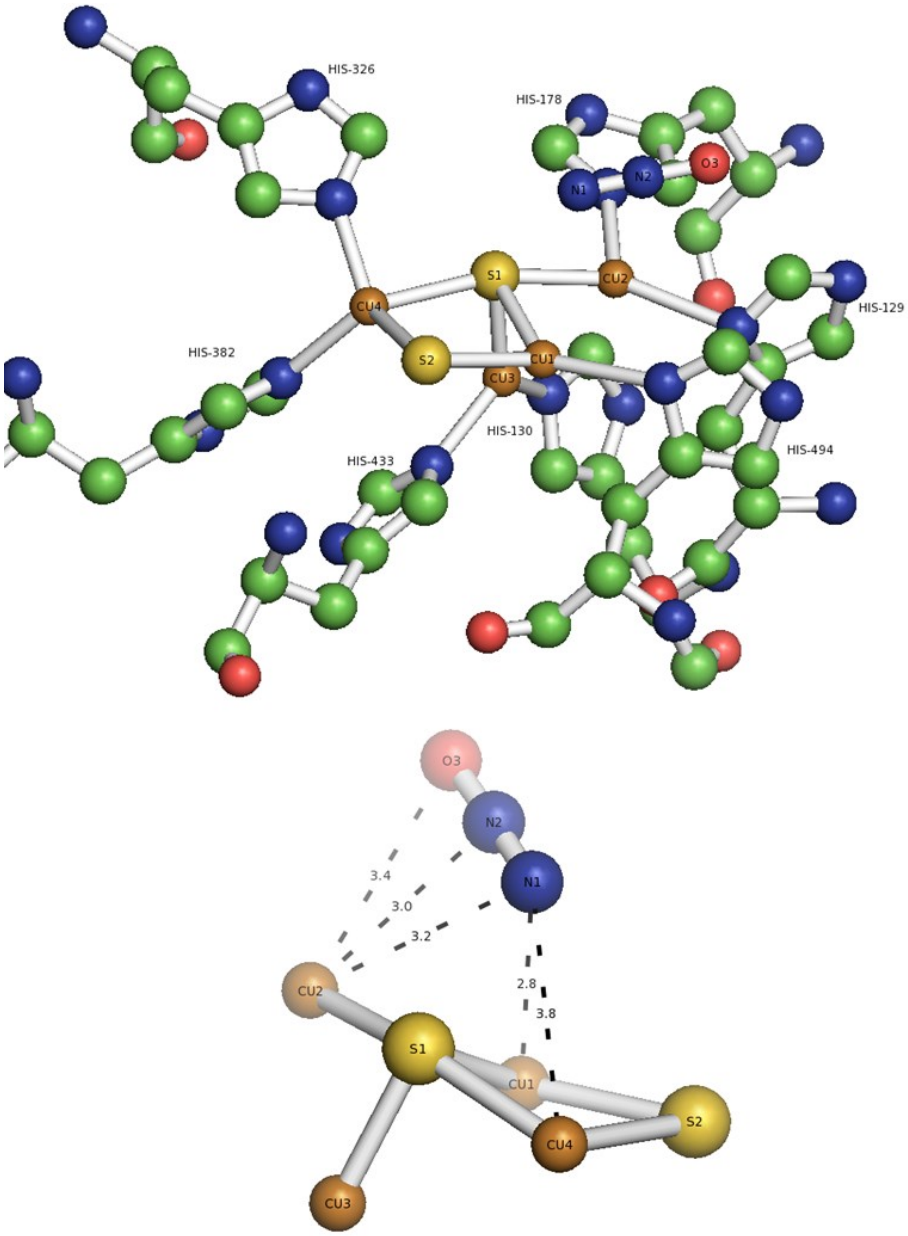

Figure 2-6: (Top) X-ray structure of N_2O in the binding pocket of N_2OR near the Cu_Z site (PDB ID: 3SBR); (Bottom): Enlarged view of the Cu_Z site and N_2O binding pocket with interatomic distances reported in Å.

2.1.1.3 **Model Complexes of N_2OR**

The novel structure of the Cu_Z site and its important biological function of reducing nitrous oxide to dinitrogen has motivated researchers to aim to prepare small molecules that mimic the structure and reactivity of the Cu_Z site. The majority of previous efforts have focused on obtaining structural models of the Cu_Z and Cu_A sites of N_2OR through the use of neutral and mono-anionic nitrogen based ligands. Nitrogen donors are used as analogues for the histidine residues that support the Cu_Z and Cu_A sites, which has led to the characterization of several copper-sulfur motifs (**Figure 2-7**).[35,37,39,152–162] It should be noted that a μ_4-sulfido cluster with phosphine donors[20] has been prepared, although these ligands are not biologically relevant nor have studies been reported that assess the reactivity of the complex towards N_2O.

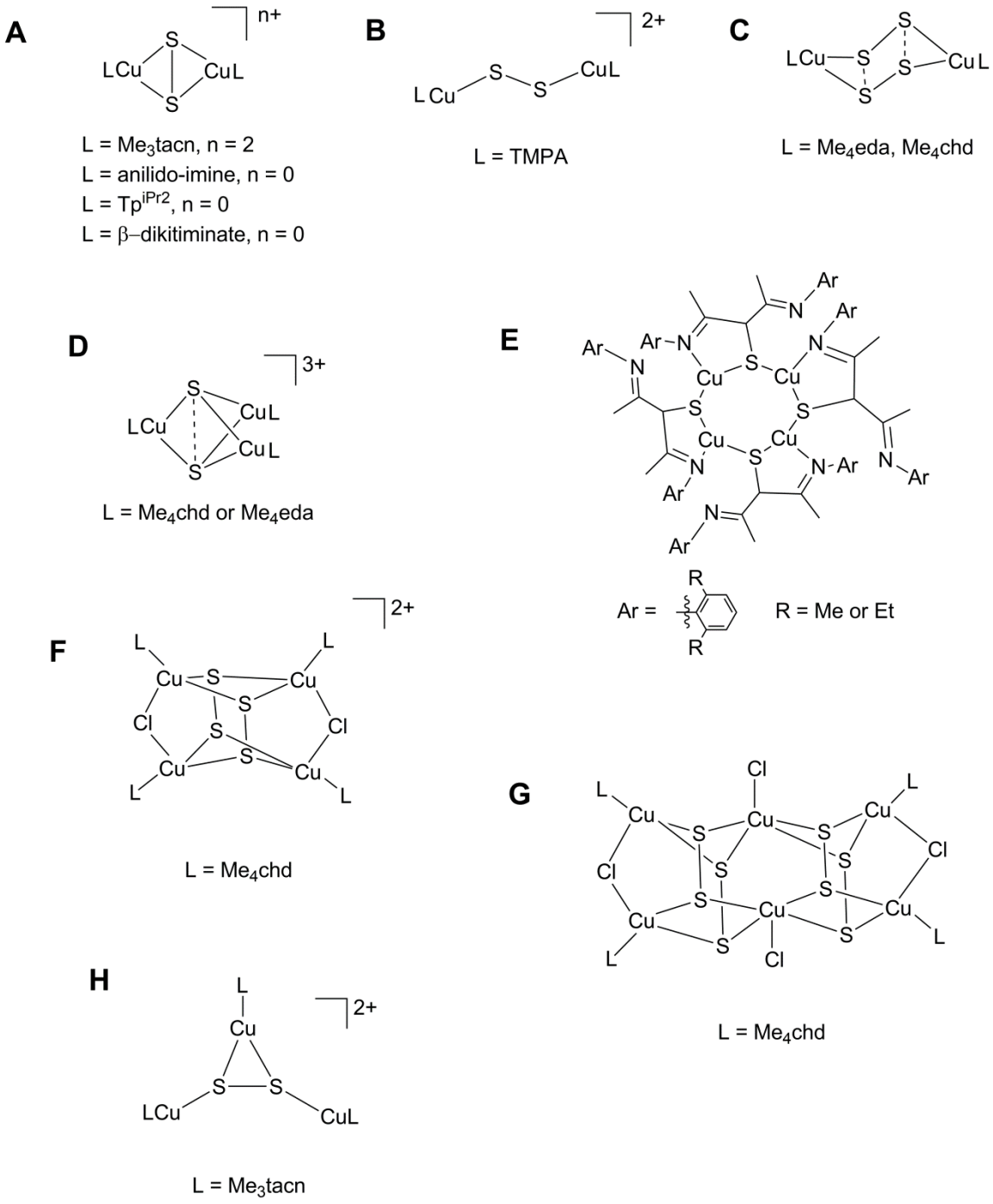

Figure 2-7: Selected synthetically obtained copper-sulfur complexes. Literature references for A,[36,152,154] B,[154] C,[35] D,[157] E,[156] F and G,[163], and H[39].

All of the copper-sulfur clusters previously obtained are multi-copper, multi-sulfur complexes, although mono-copper(II)-thiolates have been prepared in attempts to model

blue copper proteins (see section 2.3.1).[164–169] There are many factors influencing the formation of these higher nuclearity structures, including the high degree of covalency between copper and sulfur bonds.[170–172] For example, when *N,N,N',N'*-tetramethyl-*trans*-(1*R*,2*R*)-diaminocyclohexane (Me_4chd) was used as a ligand to support copper-sulfur clusters, the denticity and oxidation state of sulfur varied significantly depending on the nature of the copper source used.[35] Addition of a non-coordinating triflate copper source ($Cu(OTf)_2$) to the ligand (Me_4chd) and a sulfur source (Li_2S or Na_2S_2), led to the isolation of a tri-copper complex, core **D**. When copper(II)-chloride was used as the copper source, a hexa-copper (core **G**) and a dicopper (core **C**) were isolated. The disproportionation reaction believed to cause formation of core **G**, gives a species where the oxidation state of the sulfur species is best described as disulfide (S_2^{2-}) based on bond distances determined by crystallography. The dicopper species, core **C**, has a similar structure to previously reported trans-($S_2^{\cdot-}$) complex,[158] with short sulfur-sulfur bonds. Addition of a copper(I) source to core **G** or **C** led to the formation of core **F**, which has sulfur-sulfur bond distances consistent with the ligation of S_2^{2-} to copper(II). Although the same ligand was employed, differences in anions present led to the isolation of copper-sulfur complexes with sulfur as S_2^{2-}, $S_2^{\cdot-}$, and the more complicated oxidation state exhibited in core **D**.

The description of the electronic picture of cores **C** and **D** have raised a great deal of debate about fundamental bonding concepts.[171,173–176] There has been much discussion about whether or not a sulfur-sulfur bond is present in $[Cu_3S_2]^{3+}$, core **D**. The three-fold symmetric $[Cu_3S_2]^{3+}$ core has copper-sulfur distances of 2.25 Å , a sulfur-sulfur distance of 2.73 Å, and all three copper atoms in a square planar environment.[157] In addition, the

EPR spectrum indicates that the three copper nuclei are in electronically equivalent environments.[157] The electronic structure of $[Cu_3S_2]^{3+}$, core **D**, has been described by three different electronic structures: $[Cu^{II}_2Cu^{III}(S^{2-})_2]^{3+}$, $[Cu^{II}_3(S_2^{3-})]^{3+}$, $[Cu^{II}_2Cu^{I}(S_2)^{2-}]^{3+}$ (**Figure 2-8**).[176]

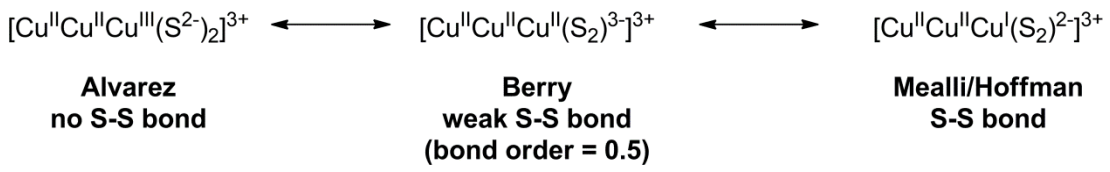

Figure 2-8: Proposed electronic configurations for the description of the $[Cu_3S_2]^{3+}$ core, **D**, adapted from ref.176.

Both the Alvarez and Mealli/Hoffman formulations assume full delocalization of the unpaired electrons among the three copper centers in order to be consistent with the EPR data, which indicates three equivalent copper nuclei.[175] The Alvarez formulation of **D** as a formally $[Cu^{II}_2Cu^{III}(S^{2-})_2]^{3+}$ core is analogous to a previously reported $[Cu_3O_2]^{3+}$ structure[177–179] that is best described as a $[Cu^{II}_2Cu^{III}(O)^{2-})_2]^{3+}$ system. Applying the same logic to core **D** is problematic, as the highly oxidizing copper(III) ion would be bound to a fully reduced S^{2-} ion; two species that should be chemically incompatible.[176] Similarly, the Mealli/Hoffman proposal of **D** as a $[Cu^{II}_2Cu^{I}(S_2)^{2-}]^{3+}$ compound requires a copper(I) ion to be in a square planar geometry, which is very unlikely due to its preference for tetrahedral coordination based on ligand field theory. The Berry description of **D** as $[Cu^{II}_3(S_2^{3-})]^{3+}$ has three equivalent copper nuclei bound to a S_2^{3-} ion, therefore eliminating the need to evoke full delocalization to explain the EPR spectrum.[176] In addition, copper(II) prefers a square planar geometry based on ligand field theory, so there is not any geometric incompatibility. A major difference of this formulation, Berry contends, is the S_2^{3-} ion is strongly antiferromagnetically coupled to the three copper(II)

nuclei, which creates four magnetic molecular orbitals. The Alvarez and Mealli/Hoffman formulations require only two magnetic molecular orbitals because they have invoked full delocalization of their copper nuclei. Berry suggests the **D** core is best described as $[Cu^{II}_3(S_2^{3-})]^{3+}$ and is the first example of a coordination compound with this S_2^{3-} ligand. Computational studies on S_2^{3-} indicated a formal bond order of 0.5 for the sulfur-sulfur, which is between Alvarez (no sulfur-sulfur bond) and Mealli/Hoffman (sulfur-sulfur bond) descriptions. Berry cautions that when delocalized bonding is in play, descriptions of the electronic configurations will always be oversimplifications. Indeed, XAS and DFT calculations indicate that **D** is best described as a configuration somewhere between the $[Cu^{II}_2Cu^{III}(S)^{2-})_2]^{3+}$ and $[Cu^{II}_3(S_2^{3-})]^{3+}$ formulations.[171]

Previous work with copper(I)-R_3TACN (TACN = 1,4,7-trialkyltriazacyclononane , R= Me, Et, iPr) and copper(I)-TMCHD (TMCHD = *N,N,N′,N′*-tetramethyl-2*R*,3*R*-cyclohexanediamine) complexes has shown that $SSbPh_3$ is a competent sulfur transfer reagent (see **Scheme 2-2**) for obtaining copper-sulfur complexes **A** and **D** with higher yields than previously reported.[180] The isolation and X-ray structural characterization of the neutral (R_3TACN)Cu-$SSbPh_3$ complex was unique in the literature as there are no reports of X-ray crystal structures of transition metals coordinated to $SSbPh_3$ despite its use as a sulfur transfer agent.[181–183]

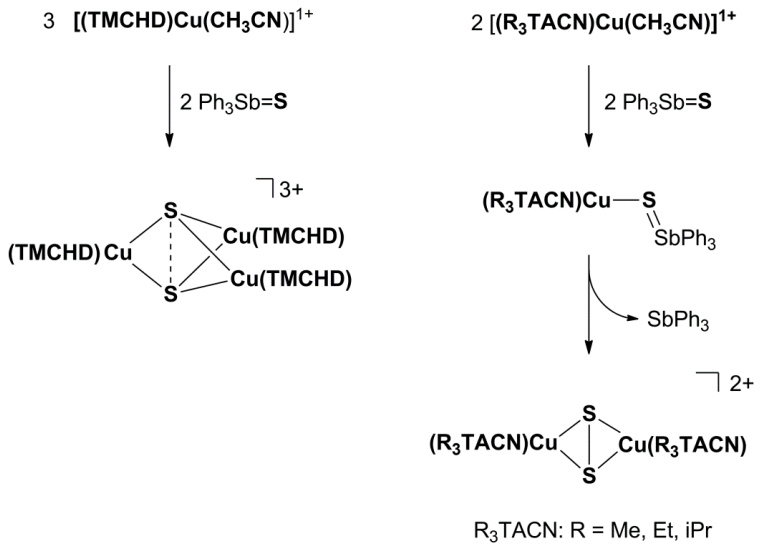

Scheme 2-2: (Left): Reaction scheme for the synthesis of **D**, $[(TMCHD)_3Cu_3(\mu^3\text{-}S)_2]^{3+}$ complex, using Ph_3SbS as a sulfur transfer reagent; (Right): Isolation of a Cu-$SSbPh_3$ species which undergoes further reaction to obtain **A**, a $[(R_3TACN)Cu_2(\mu\text{-}\eta^2\text{: }\eta^2\text{-}S_2)]^{2+}$ complex (R = Me, Et, iPr).

The $(R_3TACN)CuSSbPh_3$ complex displayed instability in solution and decomposed to the $[(R_3TACN)Cu_2S_2]^{2+}$ complex (core **A**).[180] Kinetic studies on the addition of $(Me_3TACN)Cu(CH_3CN)$ to $(Me_3TACN)CuSSbPh_3$ indicated that a rapid pre-equilibrium was likely occurring, where a postulated $[(Me_3TACN)Cu_2(\mu\text{-}SSbPh_3)]^{2+}$ species may be formed (see **Scheme 2-3**). The dicopper species is believed to undergo rapid decay to produce the $[(Me_3TACN)Cu_2(\mu\text{-}\eta^2\text{: }\eta^2\text{-}S_2)]^{2+}$ and the $[(Me_3TACN)Cu(SbPh_3)]^{+}$ complexes.

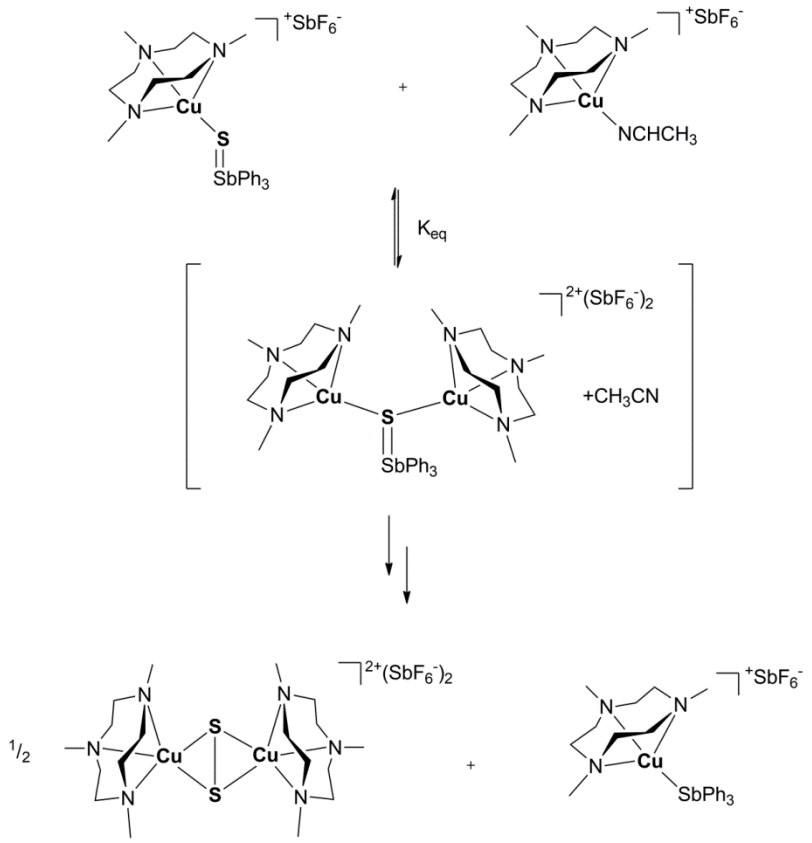

Scheme 2-3: Postulated mechanism based on kinetic studies performed by ^{1}H-NMR for the reaction of $(Me_3TACN)Cu(CH_3CN)$ with $(Me_3TACN)Cu(SSbPh_3)$ to obtain $[(Me_3TACN)Cu_2(\mu\text{-}\eta^2\text{: }\eta^2\text{-}S_2)]^{2+}$and $(Me_3TACN)Cu(SbPh_3)$.

While the use of $SSbPh_3$ afforded a discrete copper-$SSbPh_3$ complex, its propensity to form the higher nuclearity $[Cu_2(\mu\text{-}\eta^2\text{: }\eta^2\text{-}S_2]^{2+}$ structure is problematic when aiming to design a system without sulfur-sulfur bonds. In order to prevent formation of these thermodynamic products, it may be necessary to use more sterically hindered ligands that may prevent the formation of higher nuclearity clusters.

Although several copper-sulfur clusters have been obtained with N-donor ligands, currently only one system has been reported to reduce N_2O to N_2.[39] A $[(Me_3TACN)_3Cu_3S_2]^{2+}$ complex (Me_3TACN = 1,4,7-trimethyltriazacyclononane) was used to obtain a unique cluster, Core **H**, with a bridging disulfide (S_2^{2-}) moiety between

three copper ions. The electronic structure of core **H** was described as a $Cu^{II}Cu^{I}_2$ based on the metal-ligand bond distances. While the $[(Me_3TACN)_3Cu_3S_2]^{2+}$ motif differs from the μ_4-sulfido moiety in the Cu_Z site, it was successful at quantitatively reducing N_2O at −80 °C as evidenced by the release of dinitrogen.[39] As all of the copper centers in core **H** are coordinatively saturated, it was postulated that an equilibrium exists that involves the dissociation of a $[(Me_3TACN)Cu]^{1+}$ moiety, creating a $[(Me_3TACN)_2Cu_2S_2]^{2+}$ species that is responsible for N_2O attack (**Scheme 2-4**).

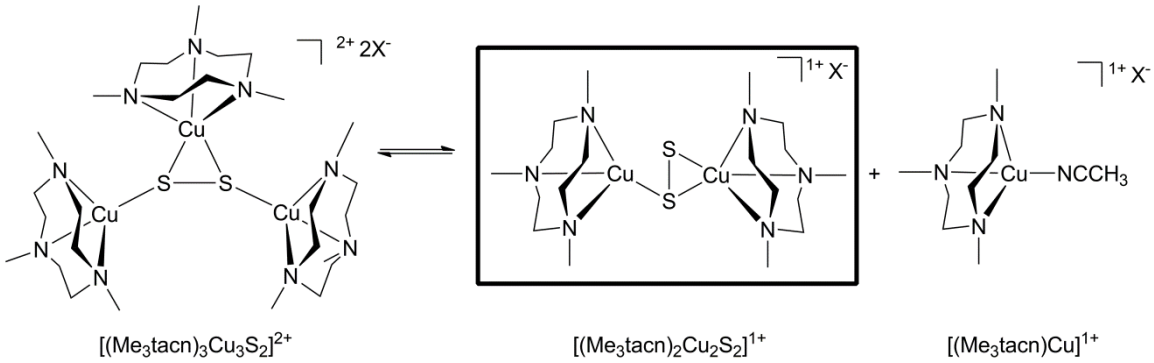

Scheme 2-4: Equilibrium between $[(Me_3TACN)_3Cu_3S_2]^{2+}$ with $[(Me_3TACN)_3Cu]^{1+}$ and $[(Me_3TACN)_2Cu_2S_2]^{1+}$, where the complex postulated to activate nitrous oxide is in a bolded frame.

This mechanistic hypothesis was corroborated by DFT calculations and mass spectrometry data indicating loss of a copper(I) fragment in solution to form the $[(Me_3TACN)_2Cu_2S_2]^{1+}$ cluster. The proposed $[(Me_3TACN)_2Cu_2S_2]^{1+}$ cluster has an open coordination site, and is proposed to bind and reduce N_2O. DFT calculations indicate the transition state for N_2O activation involves two copper centers with a bridging O-bound N_2O molecule (**Figure 2-9**).

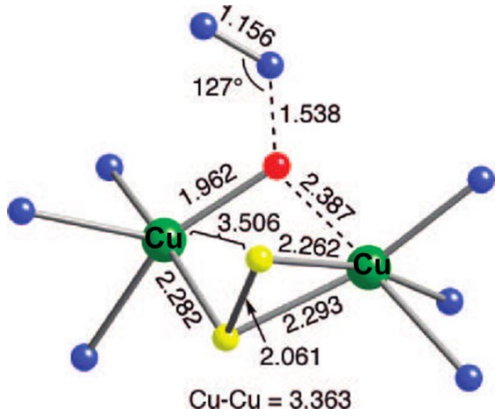

Figure 2-9: The DFT optimized transition state indicating the N_2O molecule is favored to bind to the $[(Me_3TACN)_2Cu_2S_2]^{1+}$ moiety via the oxygen atom of N_2O bridging to the two copper centers. Figure reproduced from ref.39.

Further experimental and computational studies are needed to verify if this new proposed binding mode is a viable route to N-O bond cleavage in the enzyme. In addition, this result inspired us to create a discrete $[Cu_2(\mu\text{-}S)]^n$ complex to assess if a dicopper species may be the minimal unit required for reduction of N_2O. We developed two strategies with the aim of obtaining a $[Cu_2(\mu\text{-}S)]^n$ complex to study. The first approach employed the use of dinucleating ligands (Strategy 1) and the second approach utilized a sterically hindered and strongly electron-donating ligand (Strategy 2) (**Scheme 2-5**). Strategy 1 relies on the use of a dinucleating ligand to prevent the formation of higher nuclearity clusters (see section 2.2). In contrast, strategy 2 aims to use a copper(II)-hydrosulfide complex as a synthon for the creation of a $[Cu_2(\mu\text{-}S)]^n$ compound in a stepwise fashion (see section 2.3).

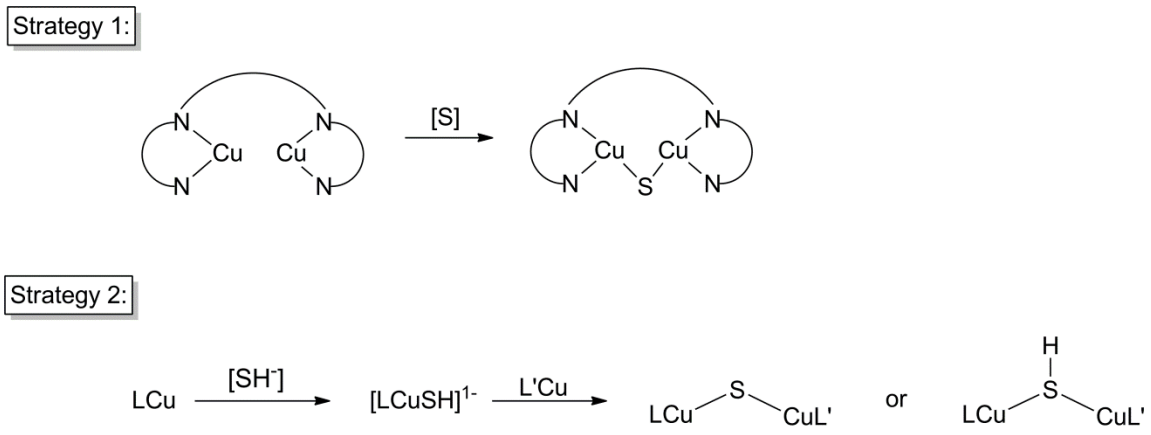

Scheme 2-5: Two strategies for the synthesis of a$[Cu_2(\mu\text{-}S)]^n$. Strategy 1 utilizes a dinuclear ligand while strategy 2 relies on a step-wise synthesis.

2.2 Strategy 1: Using Dinucleating Ligands to Form 2Cu:1S Complexes

Initial efforts at obtaining a copper-sulfur complex to mimic half the structure of the Cu_z site (2Cu:1S) focused on the use of dinucleating ligands (**Scheme 2-6**). Dinucleating ligands avoid the monomer-dimer equilibrium complications that arise when synthesizing a dinuclear complex from mononuclear complexes.[184]

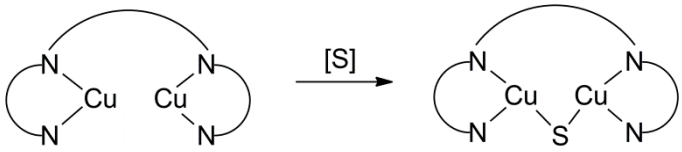

Scheme 2-6: General scheme for the addition of a sulfur source, [S], to a dicopper complex supported by a dinucleating ligand.

2.2.1 Monoanionic Phenolate Based Dinucleating Ligands

Dinucleating phenolate ligands have a rich history in bioinorganic chemistry with copper and other transition metals.[184–194] Much work has focused on species that would perform oxidative chemistry to mimic catecholase,[195–199] lactamase,[200,201] and tyrosinase[202,203] activity as well as the polymerization of cyclic esters.[204] We were

attracted to the use of dinucleating phenolate ligands due to the one-step modular synthesis via a modified Mannich reaction[205], inexpensive and commercially available starting materials, and the ability to perform the reaction on a multi-gram scale. Additionally, the monoanionic ligand may support copper(I) and copper(II) complexes or a mixed valent system via coupling through the bridging ligand(s). In general, dinucleating ligands have the advantage of holding two metal centers in close proximity, which eliminates the monomer to dimerization processes that would need to occur in order to create a dicopper complex when mononucleating ligands are used. In particular, the dinucleating phenolate ligands are attractive due to the wide array of the amines and para-substituents that may be substituted on the phenol. These alterations enable the modular synthesis of a family of electronically and sterically modified ligands, which can be advantageous when trying to gain an understanding of the mechanistic details of a reaction. In addition, the phenol ring serves as both a rigid spacer and a tether for the nitrogen donors, which prevents the formation of multiple species in solution. Another important feature is the oxygen of the phenolate ligand that bridges the two copper centers bringing them in close proximity to one another, thereby increasing the likelihood of installing an additional bridging ligand.

In order to prevent degradation of the ligand, only fully saturated amines devoid of easily reducible substituents were studied as the pendent groups. A family of mono-anionic phenolate ligands was prepared with various amines and substituents on the phenol. In addition, some imine phenolate ligands were also prepared and a representative group of the ligands is presented in **Figure 2-10**, although only the details

of reactions with L^1-phen will be discussed here due to the similarity of the chemistry observed with that of the other related ligands.

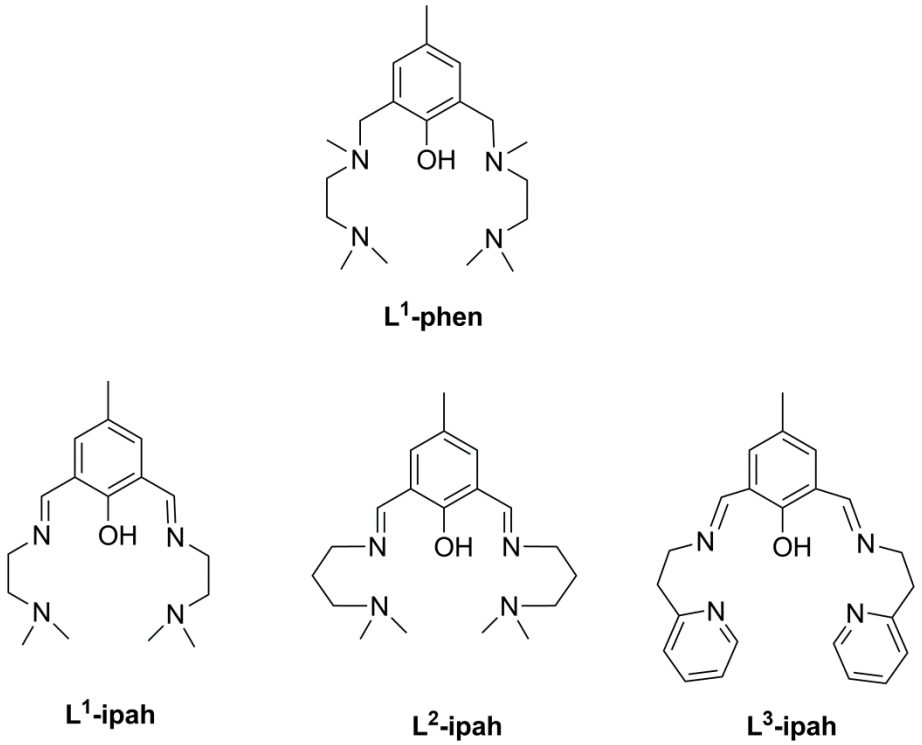

Figure 2-10: Selected structures of dinucleating phenolate ligands used for the synthesis of copper-sulfur complexes. The top row contains amine linkages coming off the phenol spacer while the bottom row has imine linkages.

Dicopper(II) phenolate complexes are well established in the literature, and typically produce symmetric di-bridged structures with the phenoxide serving as one bridge, and either a counter ion or a solvent molecule as the other bridging group.[184,191,190,185,189,205,206,199,207] When halides are used, however, asymmetric binding geometries have been obtained, as there is a low energetic barrier between four and five coordinate copper(II) complexes (**Figure 2-11**).[185] Despite the use of a symmetric ligand, Robson and coworkers reported an X-ray crystal structure where the copper ions are bound in an asymmetric fashion with each copper nuclei having a unique 5-coordinate

binding environment: one with a N_2OBr_2 ligand set in a square pyramidal geometry, and the other with a N_2O_2Br ligand set with a geometry between square pyramidal and trigonal bipyramidal.

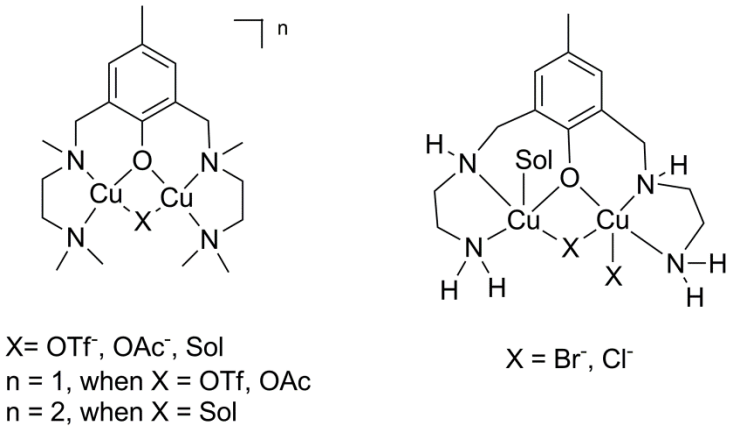

Figure 2-11: Symmetric (left) and asymmetric (right) binding modes of dicopper(II) phenolate complexes, where Sol = solvent molecule.

The different binding modes are easily distinguishable by examining their electronic spectra: symmetric or nearly symmetric binding modes are characterized by a sharp d → d transition band (λ_{max} ~ 590 nm), while asymmetric binding modes exhibit a broadened, lower energy (λ_{max} ~ 650 nm) d → d band.[185] The distorted binding mode exhibits the flexibility of this ligand to accommodate different metal binding geometries. The ability of these ligands to support different geometries when small molecules are exchanged (solvent molecules and counter anions) was encouraging to us, because it suggested there is potential for subsequent reactions to incorporate a sulfur ligand (S^{-2} or S_2^{-2}) to create a $[Cu_2S_y]^n$ core.

2.2.1.1 Attempts to Synthesize Dicopper(I)-Sulfur Complexes

The synthesis of unique copper(I) phenolate complexes was surveyed in addition to the synthesis of known dicopper(II) complexes due to the potential for reacting further

with reducible sulfur sources (e.g. elemental sulfur). Metallation reactions were attempted by using both the free ligand (L^1-phen) and the lithium salt (LiL^1-phen) with various copper(I) sources in a one ligand to two copper ratio. Both strongly (Cl−, OAc^-) and weakly (OTf^-) coordinating anions were used in the reactions, although none were successful is stabilizing a dicopper(I) species. The reactions underwent rapid disproportionation (<1 min) in both dichloromethane and tetrahydrofuran as confirmed by the plating of metallic copper(0) in the bottom of the reaction vessel. This led to the use of other copper(I) sources $[Cu(CH_3CN)_4]^+X^-$ (X = BF_4^-, OTf^-, PF_6^-, SbF_6^-) with acetonitrile as the solvent, which has previously been shown to aid in the stabilization of copper(I) complexes.[208] These reactions also resulted in rapid disproportionation.

Due to the difficulty in isolating a dicopper(I) species with all amine donors, we turned to using softer imine and pyridyl donors on the same phenolate backbone. The isolation of ($Cu_2(L^3$-ipah)(μ-Cl)) was accomplished by the reaction of $Na(L^3$-ipah) with 2 equivalents of CuCl and provided a useful dicopper(I) starting material. We explored the reactivity of ($Cu_2(L^3$-ipah)(μ-Cl)) with $(TMS)_2S$, as the formation of TMSCl is thermodynamically favorable due to the strength of the S-Cl bond. In addition, TMSCl is a liquid, which can be readily separated from the desired solid product. Similarly, we investigated the reaction of ($Cu_2(L^3$-ipah)(μ-Cl))with Ph_3SbS as it has been previously shown to react with copper(I) complexes to form isolable copper(I)-$SSbPh_3$ adducts.[180] Several reaction conditions were attempted to obtain copper sulfur clusters from the ($Cu(L^1$-phen)(μ-OH))$(X)_2$ (X = OAc^-, $CF_3SO_3^-$) starting material, but all conditions led to the formation of insoluble copper-sulfur products and recovery of the ligand (**Scheme 2-7**).

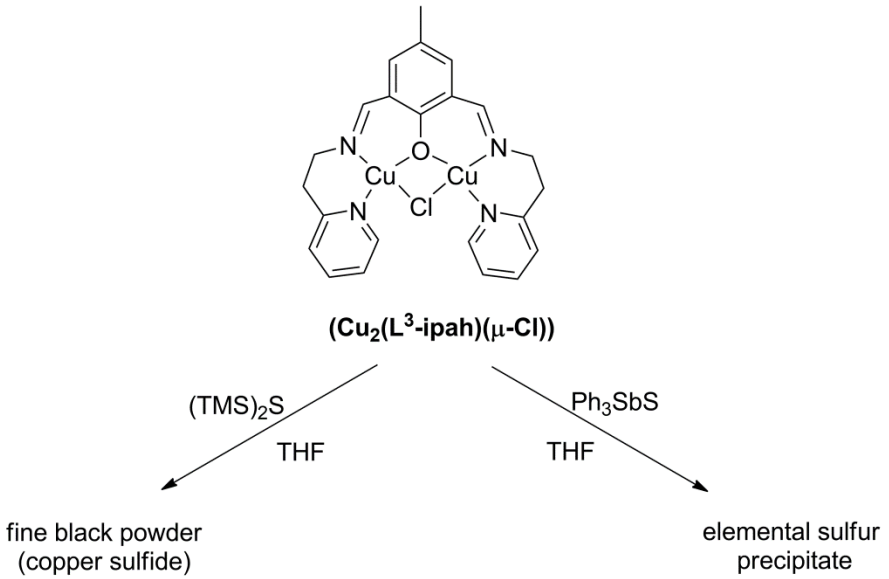

Scheme 2-7: Reaction of a ($Cu_2(L^3$-ipah)(μ-Cl)) with (TMS)S and Ph_3SbS to give undesired products.

The insoluble copper-sulfur products are believed to be copper sulfide products, $[Cu_xS_y]^{n+}$, where the ligand is no longer coordinated to the copper nuclei. We were unable to synthesize any discrete copper-sulfur complex using dinucleating phenolate ligands. We considered that the bridging phenolate moiety maybe too strongly donating, preventing the formation of our dicopper(I) complexes, and therefore turned to using a neutral dinucleating ligand without a bridging moiety.

2.2.2 Use of Neutral Dinucleating Ligands to Create 2Cu:1S Complexes

In addition to the phenolate ligand scaffold, a xylene based ligand set was also used to compare how a neutral dinucleating ligand without a bridging moiety would affect the formation of dicopper species (**Figure 2-12**).

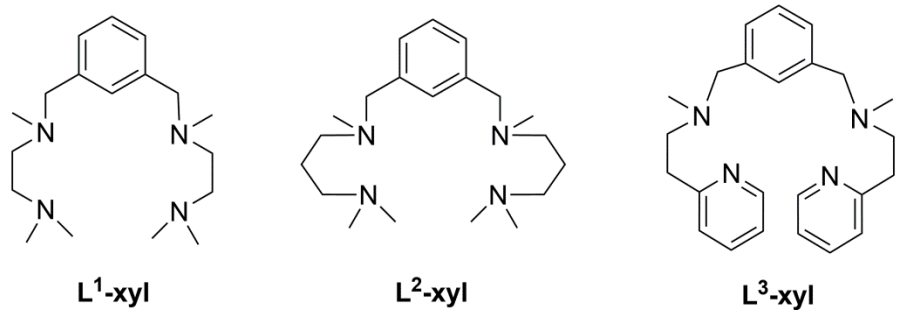

Figure 2-12: Selected xylene based dinucleating ligands prepared for the synthesis for dicopper species and copper-sulfur complexes

The synthesis of a dicopper(I) complex was achieved and produced an extremely air-sensitive product (**Scheme 2-8**). Further reaction of this dicopper(I) species with one or two equivalents of a sulfur source (Na_2S_2, S_2Cl_2, Ph_3SbS) led to the formation of intractable products. No reaction was observed in the presence of elemental sulfur.

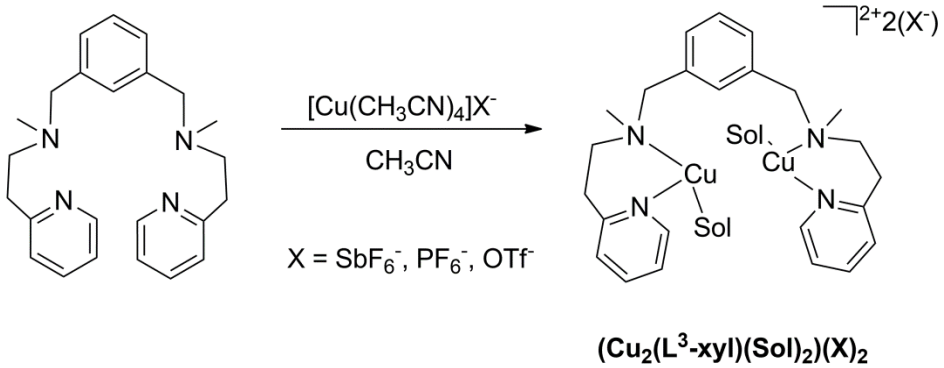

Scheme 2-8: Synthesis of $(Cu_2(L^3\text{-xyl})(Sol)_2)(X)_2$ where Sol = solvent molecule.

2.2.2.1 **Macrocyclic Dinucleating Ligands**

The previously used neutral ligands contained many degrees of freedom in solution, which we believed may have contributed to the difficulty in isolating a copper-sulfur complex. We turned to using a neutral macrocyclic ligand in order to reduce the number of possible configurations in solution and to minimize the risk of creating coordination oligomers. The dicopper(I) species supported by a $(xyl)_2(DETA)_2$ ligand (**Scheme 2-9**)

with perchlorate counterions has been previously shown to perform oxygen insertion into the aryl spacer of the macrocycle.[209,210] We chose to explore if this ligand would be suitable for obtaining copper-sulfur complexes. The synthesis of $(xyl)_2(DETA)_2$ was carried out according to the literature procedure and confirmed by comparison of ^{1}H-NMR data to the literature compound.[211] Attempts to react $[Cu(I)_2(xyl)_2(DETA)_2]X_2$ (X = SbF_6^-, PF_6^-)complexes with sulfur sources (Na_2S_2 and Ph_3SbS) were unsuccessful, as only starting material was recovered from these reactions.

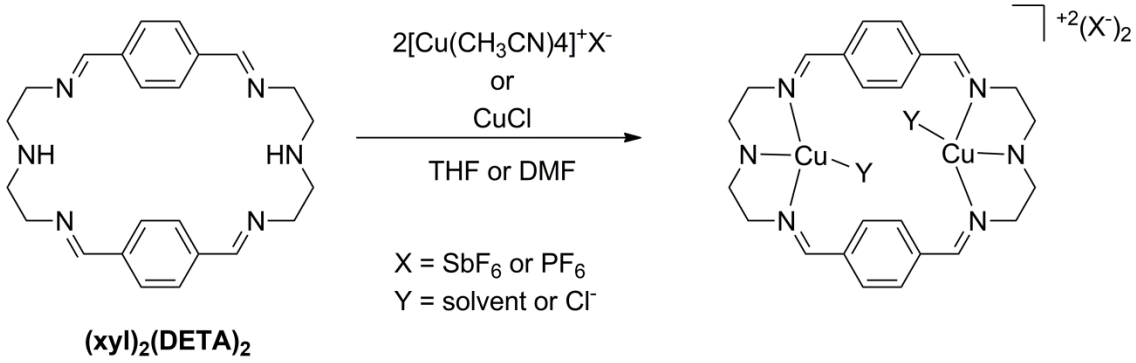

Scheme 2-9: Route for the synthesis of $[Cu(I)_2(xyl)_2(DETA)_2]^{+2}$ complexes.

The formation of these intractable products, in the case of the dinucleating phenolate and xylene based ligands, led us to investigate the effects of using a stronger electron-donating ligand with non-mineral sources of sulfur with the aim of obtaining discrete copper-sulfur complexes. By using a ligand with more electron-donating capabilities, we aimed to stabilize a copper-sulfur complex while minimizing the thermodynamically favorable formation of copper sulfide products (see section 2.3).

2.3 Strategy 2: Creating 1Cu:1S complexes

The majority of previous work in the literature has focused on modeling the Cu_A and Cu_Z site through reactions of copper(I) or copper(II) complexes with inorganic sulfur sources (Na_2S, Li_2S), elemental sulfur (S_8), or thiolates. We chose to explore the use of alternative sulfur sources, hydrosulfide (SH^-) and triphenylsilanethiol ($SSiPh_3^-$). There are many difficulties in preparing copper(II)-sulfur complexes, including: the propensity for thiolates to serve as bridging ligands and the tendency of thiolates to act as reducing agents to form disulfide (S_2^{2-}) and copper(I).[212] We sought a ligand and sulfur source that might eliminate these issues and not lead to the thermodynamic products, such as previously examined dicopper(II)-disulfide complexes. This led us to pursue the synthesis of copper(II) complexes using non-mineral sulfur sources ($-SSiPh_3^-$ and $-SH^-$) in conjunction with a tridentate, square planar geometry enforcing ligand. We selected the dianionic *N,N′*-bis(2,6-diisopropylphenyl)-2,6-pyridinedicarboxamide (L^{iPr}) as our ligand,[120] because it is tridentate and enforces a square planar geometry, which should strongly bind copper(II) on the basis of ligand field theory. With only one open coordination site on the copper, we aimed to reduce the likelihood of forming multinuclear copper-sulfur clusters.

Our interest in obtaining a copper(II)-hydrosulfide was spurred by the report of a nickel(II)-hydrosulfide complex.[120] In order to stabilize a copper(II)hydrosulfide complex, we utilized *N,N′*-bis(2,6-diisopropylphenyl)-2,6-pyridinedicarboxamide, which has been demonstrated to stabilize M(II)-hydroxide[120,123,213,124], and M(II)-bicarbonate[120,121] complexes (M = Cu or Ni), copper(II)-superoxo[122], and nickel(II)-μ-CN-iron(II)(Me_6-TREN)[120] complexes (**Figure 2-13**).

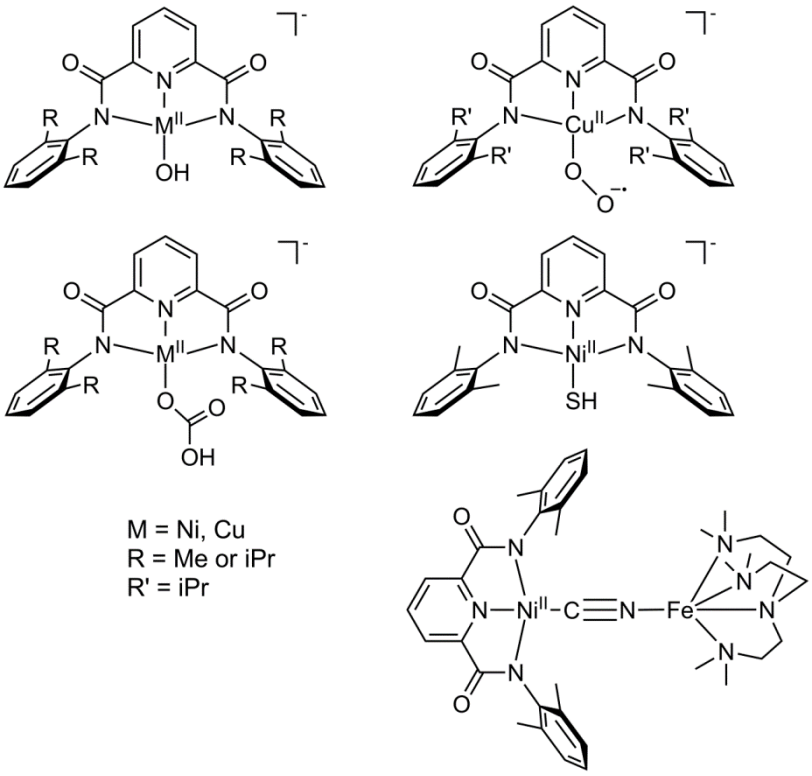

Figure 2-13: Isolated nickel and copper complexes supported by bis(2,6-disubstituted phenyl)-pyridine-2,6-dicarboxamide ligands with cations omitted for clarity.

Characterizing a copper(II)-hydrosulfide would be a novel contribution to the literature, as the only reported complex of this type was obtained by an unknown synthetic process that the authors admitted was not reproducible.[214] In addition, a copper(II)-hydrosulfide is an interesting synthetic target because it may allow for the building of higher nuclearity complexes with either a sulfide or hydrosulfide bridges (**Scheme 2-10**).

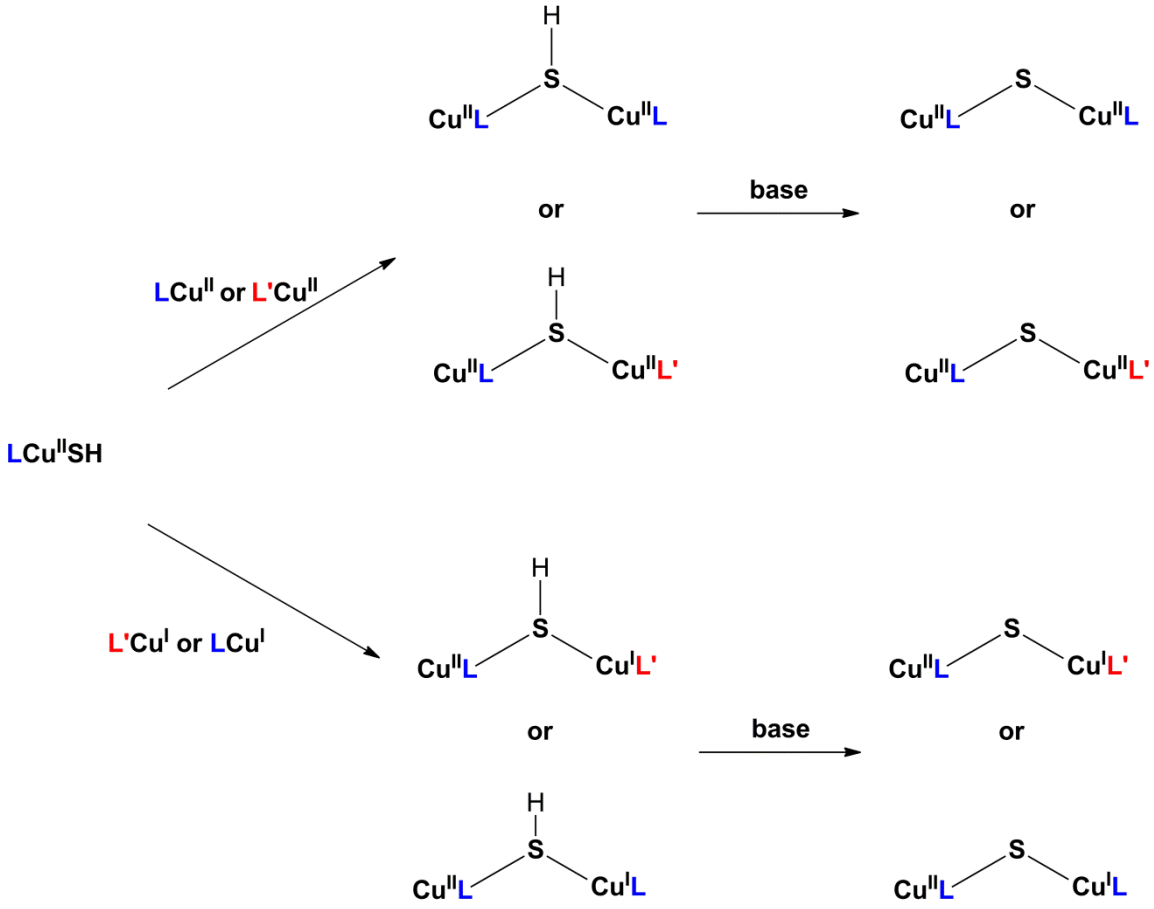

Scheme 2-10: Synthetic strategy for the synthesis of sulfur bridged homoletpetic or heteroleptic dicopper complexes using a copper(II)hydrosulfide starting complex.

By using a ligand that strongly favors the formation of square planar copper complexes, we aimed to enter a different regime of reactivity than previously observed by neutral and monoanionic complexes that favored trigonal and tetrahedral complexes (i.e. TACN,

TMCHD, β-diketiminate and anilido-imine ligands). In addition, the characterization of the nickel(II)-(μ-CN)-iron(II) complex suggested it may be possible to create bimetallic complexes with copper. The copper(II)-hydrosulfide could potential act as a synthon to create dicopper or bimetallic species in a step-wise fashion, with the goal of creating Cu-(μ-SH)-M (M= Cu, Fe, Zn) complexes (**Scheme 2-11**).

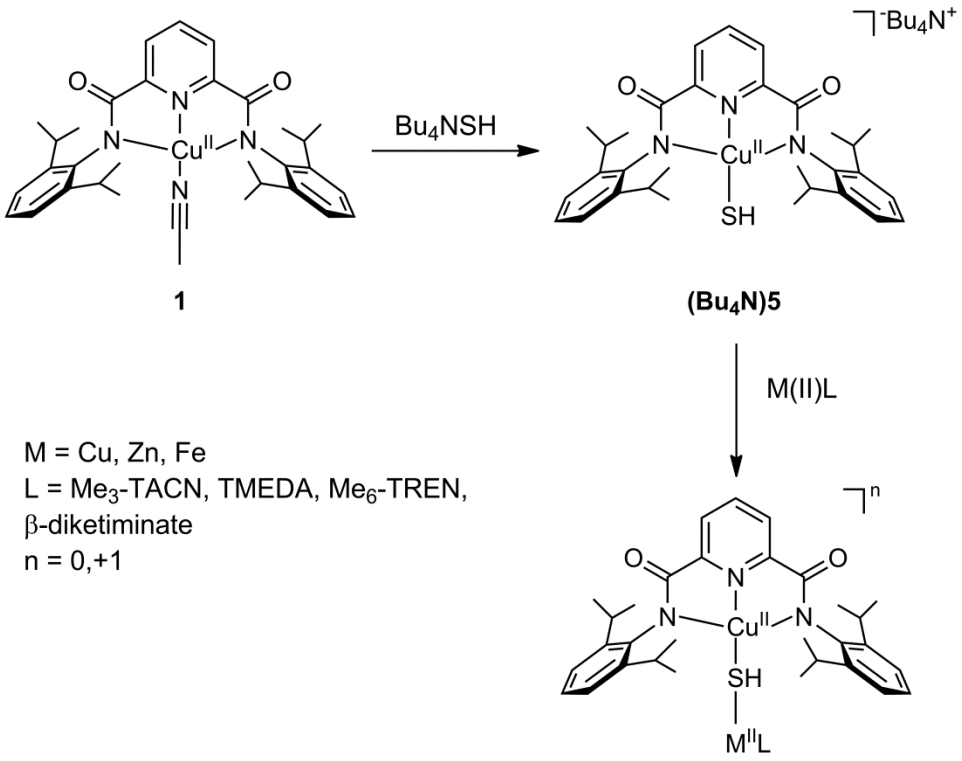

Scheme 2-11: Proposed route for the preparation of a copper(II)-hydrosulfide and further homo- or hetero-bimetallic complexes.

Hydrosulfide salts are synthesized by passing hydrogen sulfide (H_2S) through a solution of the desired hydroxide salt and must be stored under inert atmosphere to avoid rapid decomposition .[215] Due to the highly toxic nature of hydrogen sulfide, we initially chose to follow an alternative route for obtaining a copper-hydrosulfide in-situ. In this route, we would prepare a copper(II)-$SSiPh_3$ complex, which upon addition of a fluoride source and proton source should result in cleavage of the sulfur-silicon bond to give us the

desired product (**Scheme 2-12**). The silicon-fluorine bond is much stronger (142 kcal/mol) than the silicon-sulfur bond (54 kcal/mol) and should provide significant driving force for this desilylation reaction.[216] In essence, the -$SSiPh_3$ group is acting as a silyl-protected hydrosulfide and offers a less toxic synthetic route.

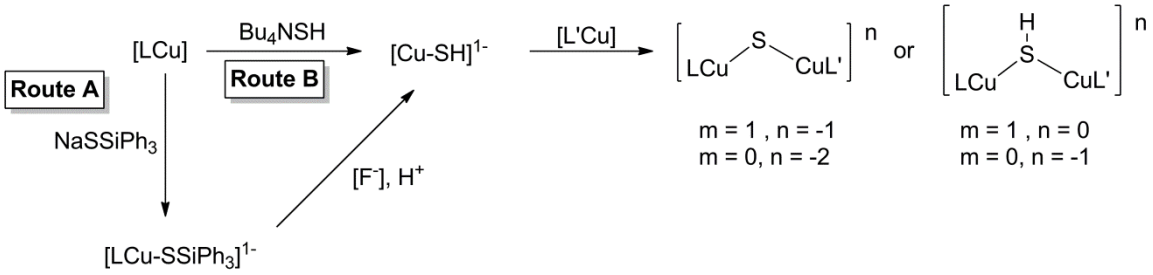

Scheme 2-12: (Route A): Proposed synthetic route for the desilylation of a copper(II)-$SSiPh_3$ complex to give the desired copper(II)-hydrosulfide complex. (Route B): Synthetic route for the direct preparation of a copper(II)-hydrosulfide. Both routes converge on the reaction of the copper(II)-hydrosulfide with another copper species. L = utilized *N,N*′-bis(2,6-diisopropylphenyl)-2,6-pyridinedicarboxamide, L' = ligand, [F^-] = fluoride source.

Previous work in our laboratory reported a (copper(II)-CH_3CN) complex (**1**), which has been characterized by a variety of spectroscopic techniques, including X-ray crystallography (**Figure 2-14**).[123]

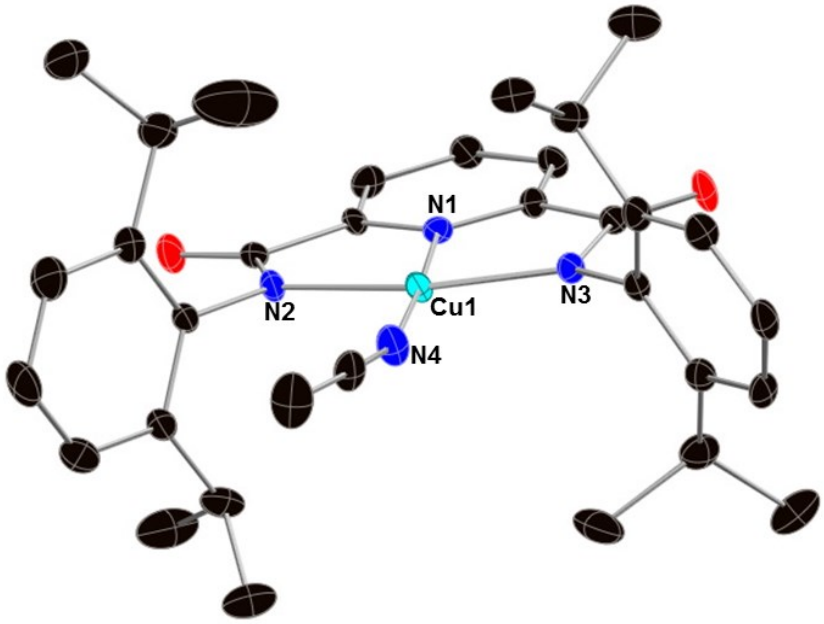

Figure 2-14: The X-ray crystal structure of the asymmetric unit of $L^{iPr}Cu(CH_3CN)$, **1**, with atoms drawn at 50% thermal ellipsoids. Only one molecule of **1** is shown for clarity. A molecule of toluene and hydrogen atoms of the ligand are omitted for clarity. Space group: P2/n, R1 = 0.0734, wR2 = 0.2043.

The structure of **1** revealed a square planar copper(II) center coordinated by the tridentate ligand and an exogenous acetonitrile molecule (selected bond distances and angles are presented in **Table 2-1**). The copper(II)-amide bonds (1.967(3) and 1.945(3) Å) are slightly lower than the range of reported distances in the International Tables for Crystallography (2.026 Å (σ = 0.056)), but this is to be expected for a dianionic ligand that forms an overall neutral complex.[217] In addition, the observed asymmetry in the bond distances for Cu1-N2 (1.967 Å) and Cu1-N3 (1.945 Å) are attributed to an artifact of crystallization; the acetonitrile moiety is coordinated in a bent fashion (Cu1-N4-C32∠ = 162.9°) to the copper, while the acetonitrile ligand itself remains relatively linear (N4-C32-C33∠ = 178.5°). The Cu1-N1 distance of 1.912(3) Å is significantly shorter than other reported four coordinate copper-pyridine complexes (2.023Å (σ = 0.019)).[217]

Table 2-1: Selected bond distances (Å) and bond angles (°) from the X-ray crystal structure of **1**.

	Bond Distance		Bond Angle
Cu1-N1	1.912(3)	N3-Cu1-N1	80.9(1)
Cu1-N2	1.967(3)	N1-Cu1-N2	80.8(1)
Cu1-N3	1.945(3)	N2-Cu1-N4	96.6(1)
Cu1-N4	1.974(3)	N3-Cu1-N4	101.7(1)
		N1-Cu1-N4	177.0(1)
		Cu1-N4-C32	162.9(1)

2.3.1 Route A: Isolation and Characterization of [Copper(II)-SSiPh$_3$]$^{1-}$

The neutral copper(II)-CH_3CN complex, **1**, provided a convenient starting material for the synthesis of copper(II)-thiolate complexes. The use of silanethiols and their salts has previously been used for the preparation of Ru(II), Fe(II), Mn(II), Co(II), Ni(II), Cu(I), Au(I), and lanthanide complexes, although two silanethiol moieties are typically bound to the metal center to form bridged complexes.[218–232] We utilized the sterically hindered sodium triphenylsilanethiol with the sterically encumbered **1** and were able to isolate a discrete copper(II)-triphenylsilanethiol complex, (Na)**4** (**Scheme 2-13**).

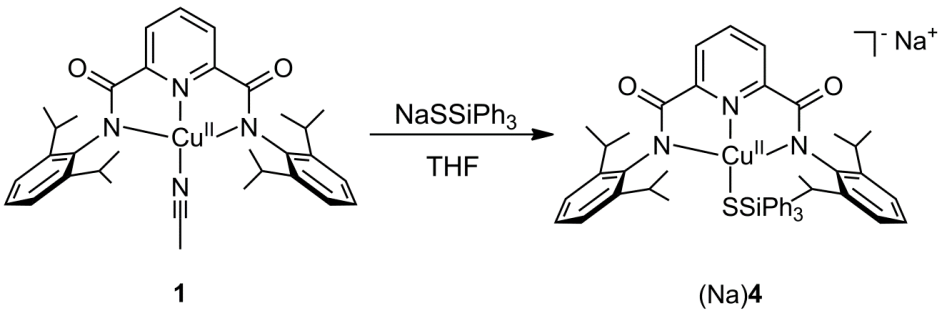

1 (Na)**4**

Scheme 2-13: Synthesis of (Na)**4** by the addition of $NaSSiPh_3$ to **1** in THF.

The complex (Na)**4** is the first copper(II)-silanethiol complex reported in the literature, and was characterized by UV-Vis spectroscopy, EPR spectroscopy and single crystal X-ray crystallography (**Figure 2-15**).

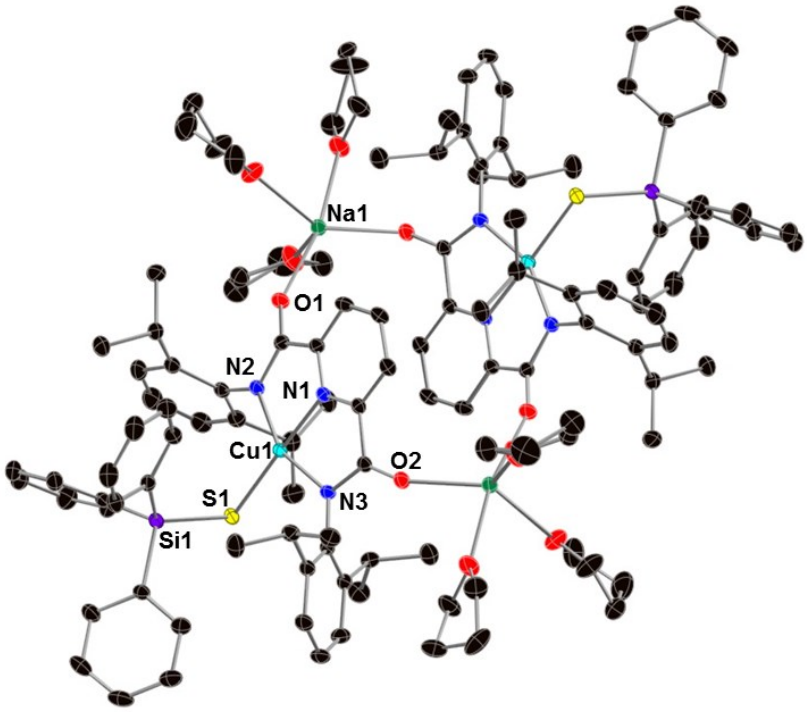

Figure 2-15: X-ray crystal structure of the dimeric Na($L^{Me}CuSSiPh_3$), (Na)**4,** with thermal ellipsoids drawn at 50% and hydrogen atoms omitted for clarity. Space group: $P2_1/n$, R1 = 0.0395, wR2 = 0.1109.

The structure of (Na)**4** in the solid state is dimeric, with sodium atoms bridging the oxygen atom of the carboxamide of two ligands and three molecules of tetrahydrofuran filling out the sodium coordination sphere. For clarity, the structure of the asymmetric unit with the cation and solvent molecules omitted is presented in **Figure 2-16**.

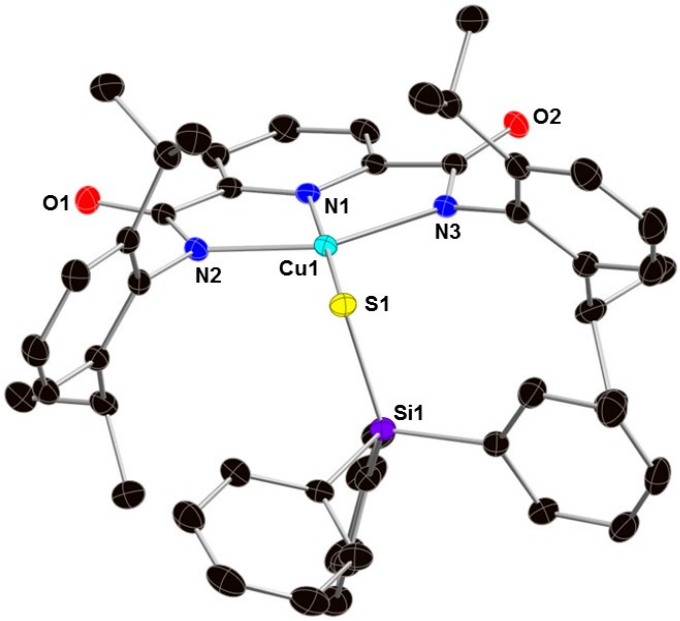

Figure 2-16: X-ray structure of a single molecule of the anionic portion of $Na(L^{Me}CuSSiPh_3)$, **4**$^-$**,** with thermal ellipsoids drawn at 50%. Hydrogen and sodium atoms are omitted for clarity.

The long copper-sulfur bond, 2.245 Å, in (Na)**4** is consistent with a copper(II)-thiolate interaction and is similar to the bond distance observed for the previously reported (tris-pyrazolyhydroborate)Cu(II)-thiolate complexes.[166] The S-Si bond distance (2.0886(7) Å) is similar to that reported distance in a $(Au(Ph_3)(SSiPh_3)$ complex (2.105(3)Å).[233] In addition, the copper-nitrogen bonds are all slightly elongated (~0.1 Å) when compared to **1**, which is to be expected when comparing a neutral species to a more electronic-rich monoanionic species.

Table 2-2: Selected bond distances (Å) and bond angles (°) from the X-ray crystal structure of (Na)**4**.

	Bond Distance		**Bond Angle**
Cu1-S1	2.2459(5)	N2-Cu1-S1	102.08(4)
Cu1-N1	1.944(1)	N2-Cu1-N3	156.79(6)
Cu1-N2	2.052(1)	N1-Cu1-N3	79.07(6)
Cu1-N3	2.050(2)	N3-Cu1-S1	99.68(4)
S1-Si1	2.0886(7)	Cu1-S1-Si1	113.01(2)

The UV-Vis spectrum of (Na)**4** in tetrahydrofuran exhibits features with λ_{max} at 378 nm ($\varepsilon \sim 4800\ M^{-1}cm^{-1}$) and 480 nm ($\varepsilon \sim 1200\ M^{-1}cm^{-1}$) at room temperature. When solutions of (Na)**4** in tetrahydrofuran are cooled below room temperature, a shift in the UV-Vis spectrum is observed that is reversible upon warming to room temperature (**Figure 2-17**). This thermochromic behavior has not been observed for any of the other copper(II) complexes supported by the *N,N*′-bis(2,6-disubstitutedpropylphenyl)-2,6-pyridinedicarboxamide ligand. One possible explanation is that a 5-coordinate copper species may be obtained reversibly upon axial coordination of a tetrahydrofuran molecule (the solvent). Copper halides and nickel halides have been reported to undergo geometric changes from tetrahedral to octahedral due to interactions with solvent molecules during heating-cooling cycles, which corresponded to changes observed in their measured d-d bands.[234–237] Another possible explanation for the thermochromic behavior could be the presence of a monomer-dimer equilibrium in solution, where temperature determines which species is more dominant. Indeed, the solid state structure of (Na)**4** is dimeric, which indicates it is possible for such an equilibrium to occur in solution.

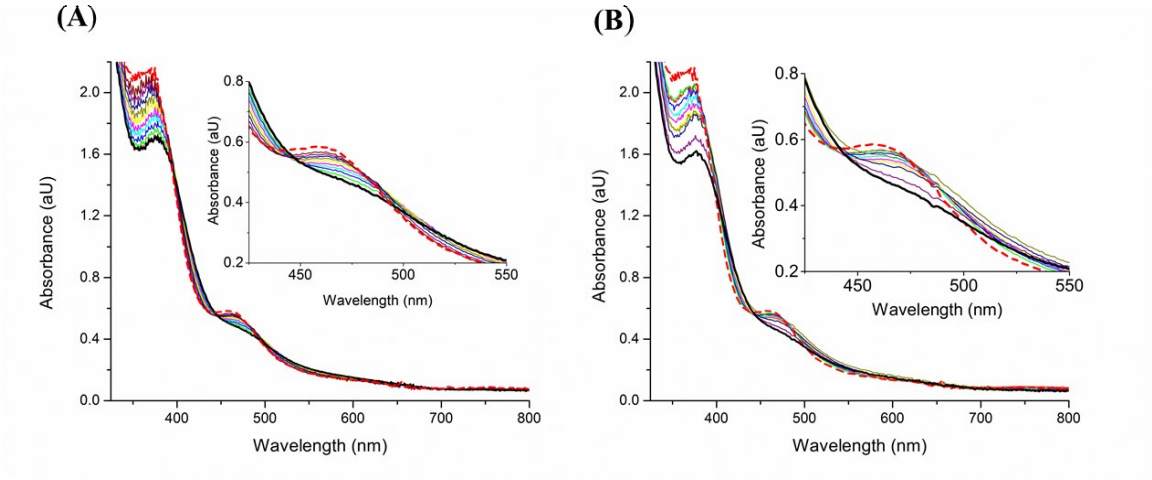

Figure 2-17: Thermochromic behavior of (Na)**4** in tetrahydrofuran upon (A) cooling a 25 °C solution of (Na)**4** (bold line) in 10 degree increments (intermediate spectra) until reaching −80 °C (dashed bold line); (B) warming a −80 °C solution of (Na)**4** (dashed bold line) in 10 degree increments (intermediate spectra) until reaching 20 °C (bold line).

Further details about the electronic structure of (Na)**4** were obtained by using EPR spectroscopy . The EPR spectrum of (Na)**4** is very broad (g_x =2.005, g_y= 2.055, g_z = 2.25), with a small copper hyperfine coupling constant (A = 80 x 10^{-4} cm^{-1}) and no observable nitrogen superhyperfine coupling (**Figure 2-18**). The broadened spectrum is in contrast to the EPR spectra of the related copper(II) complexes **1**, (Bu_4N)**2**, (Ph_4P)**3**, and (Bu_4N)**5**) that exhibit hyperfine coupling with the nitrogen atoms of the ligand. EPR measurements were collected under a variety of conditions, with different solvent mixtures and samples prepared at different concentrations, although no improvements in the sharpness of the spectra were observed. In addition, EPR collection was performed under a variety of temperatures and power settings without any improvements in the spectra. If a dimer-monomer equilibrium is occurring in solution, it may be contributing to the broadness observed in the EPR spectrum of (Na)**4**, as multiple species would lead to a more complex spectrum.

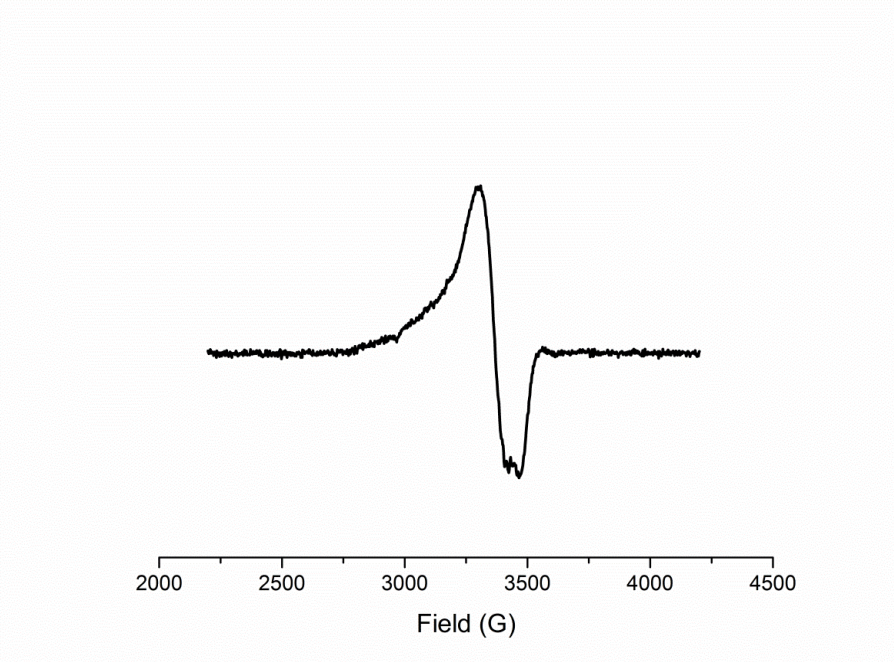

Figure 2-18: X-band EPR spectrum of (Na)**4** measured at 10K in 1:1::toluene:tetrahydrofuran.

Electrochemical oxidation of (Na)**4** by cyclic voltammetry indicates multiple redox events (**Figure 2-19**). Identification of the redox events is unclear, although the features are well separated (E_{pc} = -0.26, 0.22, 0.83 V vs Fc/Fc^{+}). The reversible redox event at 0.83 V is likely due to ligand oxidation, as it is observed in other voltammograms of (Bu_4N)**5** (see **Figure 2-26**).

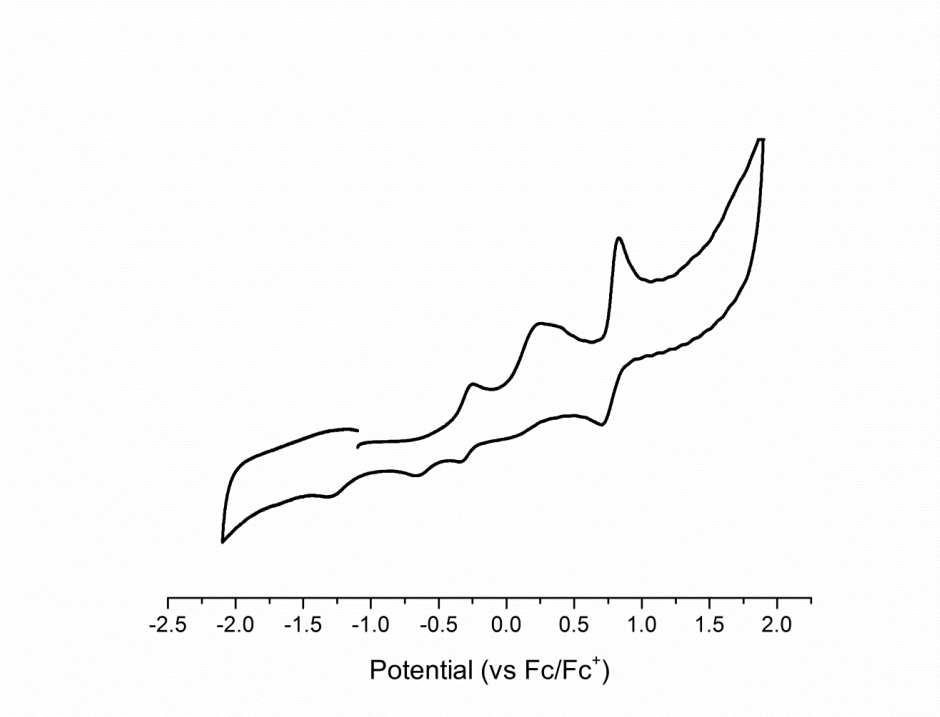

Figure 2-19: Cyclic voltammogram of (Na)**4** in 0.2 M Bu_4NPF_6 in acetonitrile at room temperature.

Attempts to cleave the sulfur-silicon bond of (Na)**4** with tetrabutylammonium fluoride (Bu_4NF) were unsuccessful. Addition of tetrabutylammonium fluoride (Bu_4NF) to (Na)**4**, led to the formation of pale green solution, which bared a strong resemblance the spectrum obtained when Bu_4NF was added to **1** (**Figure 2-20**). Although fluoride is a poor ligand for copper(II), the possibility that it may be coordinating to our copper center led us to purse the alternative route (Route B) to prepare a copper(II)-hydrosulfide directly (see section 2.3.2).

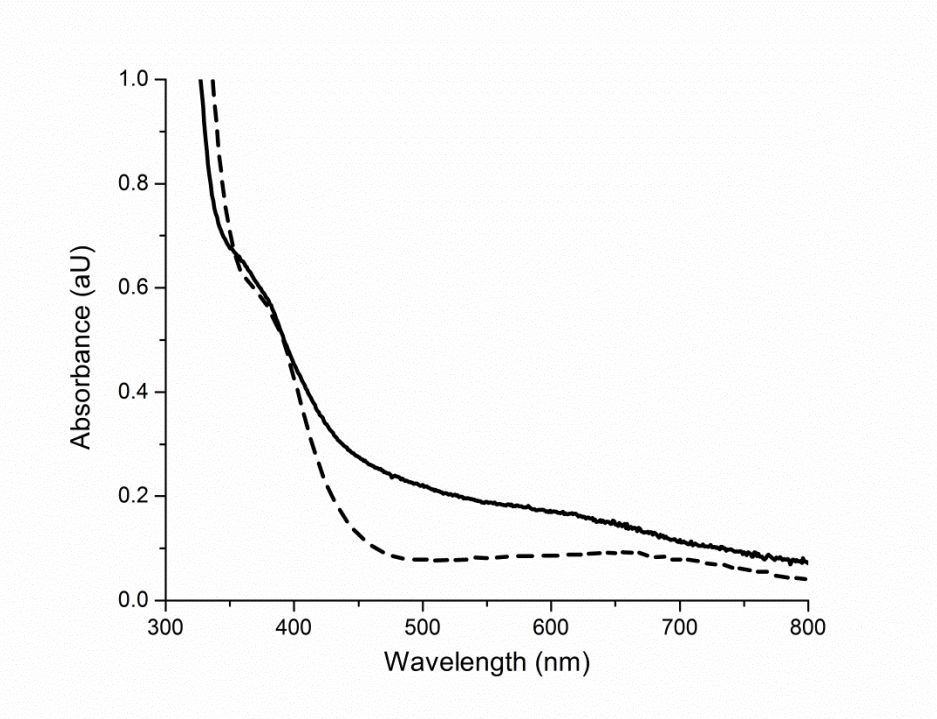

Figure 2-20: UV-Vis spectra of the reaction of the product formed after the reaction of (Na)**4** with Bu_4NF (solid) and the addition of Bu_4NF to **1** (dashed) in tetrahydrofuran.

Although (Na)**4** was not found to be useful as a synthon for creating a hydrosulfido complex, it has interesting spectroscopic properties similar to other monocopper-sulfur species in proteins, such as the type I blue copper sites and the type II red copper centers. As members of the cupredoxin family,[3,11,238] red type II copper proteins are in a special class of catalytic proteins[7,239,240] related to a larger family of electron transfer proteins.[4,6,9,241–246] The red type II copper proteins (i.e. nitrosocyanin) have weak absorbance features in the visible region ($\varepsilon \sim 40\ M^{-1}\ cm^{-1}$), low reduction potentials (+85 mV vs NHE), and large hyperfine coupling constants ($A(Cu) \sim 150 \times 10^{-4}\ cm^{-1}$).[247,248] Whereas the type I blue copper sites, are typically in a trigonal or tetrahedral array and exhibit intense visible absorption around 600 nm ($\varepsilon \sim 5000\ M^{-1}\ cm^{-1}$), high reduction potentials (150-800 mV vs NHE), and small hyperfine coupling constant ($A(Cu) \sim 100 \times 10^{-4}\ cm^{-1}$) with rhombic or axial EPR spectra.[9,242,249,250]

Previous efforts to model cupredoxins has primarily focused on obtaining structural models of the blue (type I) copper proteins, namely plastocyanin. This has led to the isolation of several monocopper-monothiolate structures supported by monoanionic or neutral nitrogen donor ligands (**Figure 2-21**).

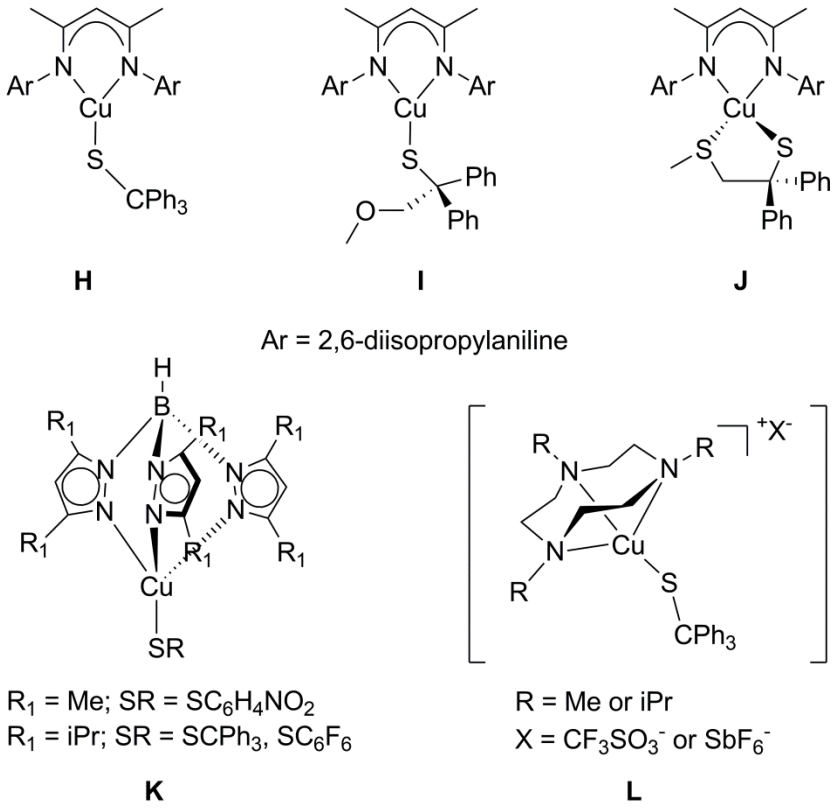

Figure 2-21: Representations of model complexes for blue copper proteins featuring copper(II)-thiolate moieties. Complex L is in brackets to indicate this structure is proposed, and not structurally characterized. References for H,[251] I and J,[168] K,[164–167] and L.[252]

Complexes supported by a tris(pyrazolyl)hydroborate ligand (**K**) and R_3TACN (**L**) are four coordinate, whereas the copper center in plastocyanin is three coordinate. The use of bidentate ligands to make a three coordinate copper center led to the isolation of complexes **H**, and **I**, and **J**. As copper proteins are typically grouped by their

spectroscopic properties, selected spectral data and redox properties of these synthetic compounds are compared to blue and red copper proteins in **Table 2-3**.

Table 2-3: Spectral and redox properties of selected type 1 and type 2 copper active sites and model complexes. Figure adapted from Yang et al., ref.252.

Complex[a] or Protein	**UV-Vis [λ_{max}, nm (ε, M^{-1} cm^{-1})]**	**$g_{\|}$**	**A (Cu) (x 10^{-4} cm^{-1})**	**Reduction Potential (mV vs NHE)[b]**
Azurin[c]	619 (5,100)	2.255	60	+276
	780 (sh)			
Stellacyanin[d]	604 (4,000)	NA[m]	NA[m]	+260[l]
	845(sh, 700)			
Nitrosocyanin[e]	390 (4,400)	2.22[f]	201[f]	+85[e]
K (R = CPh_3)[g]	625 (6,340)	2.23	66	-343
K (R = C_6F_5)[h]	670(5,960)	2.32	56	+243
H[i]	749(5,800)	2.17	111	-180
J[j]	691 (2,300)	2.15	98	-203
L (R = iPr, X =OTf)[k]	630 (1,500)	2.2	84	+317
	780 (sh)			
L (R = Me, X =OTf)[k]	609 (1,600)	2.24	94	+299[n]
	740 (sh)			
(Na)**4**	378(4800)	2.25	-	+294[n]
	480 (1200)			

[a] See **Figure 2-21** for strucures of the model complexes
[b] NHE (normal hydrogen electrode) and conversions were made using ref.253
[c] From *A.denitrificans* ref.254
[d] From *R. vernicifera* ref.255
[e] From *N. europaea* ref.7
[f] ref.240
[g] ref.256 and ref.252
[h] ref.169
[i] ref.251
[j] ref.168
[k] ref.252
[l] For cucumber stellacyanin ref.257
[m] Not available due to a rhombic EPR signal
[n] Estimated due to irreversible wave

The deep red color of (Na)**4** was a primary indicator that it may have similar spectral features to the red type II copper proteins. The high energy UV-Vis feature of (Na)**4** at 378 nm ($\varepsilon \sim 4800\ M^{-1}\ cm^{-1}$) resembles the high energy feature observed for nitrosocyanin at 390 nm ($\varepsilon \sim 4{,}400\ M^{-1}\ cm^{-1}$). In addition, similar g values (~2.2) are observed for (Na)**4** and nitrosocyanin, although the broadness of the (Na)**4** EPR spectrum prohibits a reliable comparison of their copper hyperfine coupling values. The multiple irreversible redox events observed for (Na)**4** complicate a direct comparison of its reduction potential to other complexes, although its lowest reduction potential (+294 mV vs NHE) is more similar to azurin (+274 mV vs NHE), stellacyanin (+260 mV vs NHE), and the synthetic complex **L** (+299 mV vs NHE) ,than nitrosocyanin (+85 mV vs NHE).

2.3.2 Route B: Synthesis and Characterization of [Copper(II)-SH]$^{1-}$

Due to the complications that arose from trying to generatre a copper(II)-SH from a copper(II)-$SSiPh_3$ complex (Route A), we attempted a more direct synthetic approach (Route B). The nickel(II)-SH reported by Holm and coworkers was synthesized by the addition of a hydrosulfide salt (Et_4NSH) to a nickel(II)-OH complex.[120] Inspired by this approach, the synthesis of (Bu_4N)**5** was achieved by the addition of freshly prepared Bu_4NSH to **1** in tetrahydrofuran at room temperature (**Scheme 2-14**).

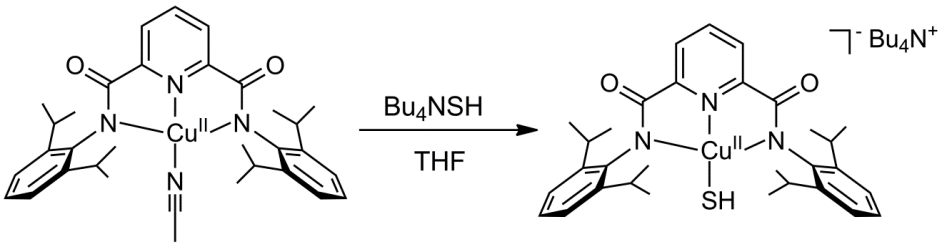

1 (Bu_4N)**5**

Scheme 2-14: Addition of Bu_4NSH to **1** to give (Bu_4N)**5** in tetrahydrofuran.

The structure of (Bu4N)**5** is a novel addition to the literature, as there is only one report of a copper(II)-hydrosulfide that was obtained in an irreproducible manner.[214] The complex was fully characterized by elemental analysis, ESI-MS, EPR spectroscopy, and X-ray crystallography.

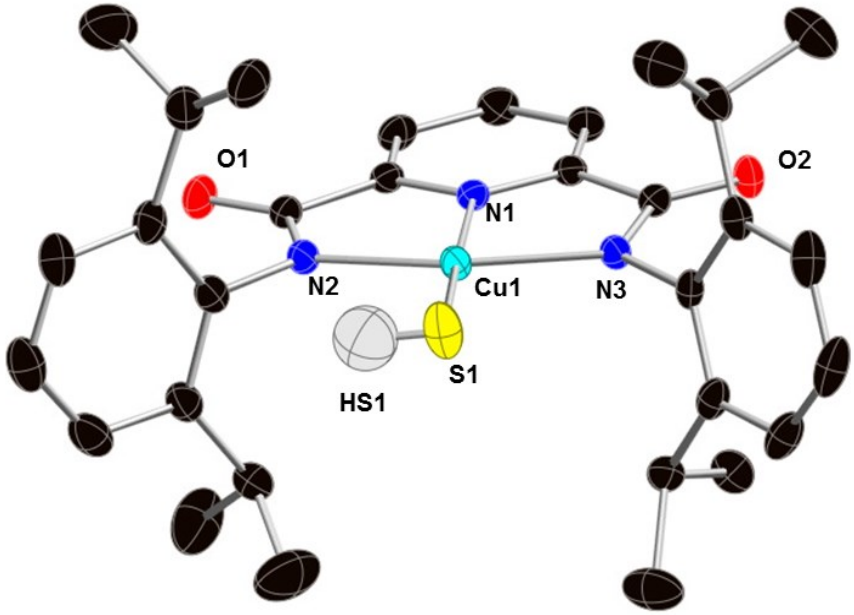

Figure 2-22: X-ray structure of the anionic portion (Bu_4N)(L^{iPr}CuSH), $\mathbf{5}^-$, with thermal ellipsoids drawn at 50%. Hydrogen atom of the supporting ligand are omitted for clarity. Space group: $P2_1/n$, R1 = 0.0472, wR2 = 0.1303.

Unlike (Na)**4**, the solid state structure of (Bu_4N)**5** is monomeric, and indicates a single hydrosulfide moiety bound to the square planar copper center. This binding mode is unusual, as typically, hydrosulfide ligands form bridged or clustered complexes.[258] The hydrogen atom on the hydrosulfide was located by using the difference Fourier map. The copper-nitrogen bond distances and angles are similar to the values obtained for Na(**4**) (**Table 2-4**). The copper-sulfur bond (2.2208(7)Å) is slightly shorter than the bond

distance observed for (Na)**4** (2.2459(5) Å) but remains within the range characteristic of copper(II)-thiolate interactions.

Table 2-4: Selected bond distances (Å) and bond angles (°) from the X-ray crystal structure of (Bu_4N)**5**.

	Bond Distance		**Bond Angle**
Cu1-S1	2.2208(7)	N2-Cu1-N3	158.39(7)
Cu1-N1	1.948(2)	N1-Cu1-N2	79.51(7)
Cu1-N2	2.021(2)	N1-Cu1-N3	79.18(7)
Cu1-N3	2.022(2)	N1-Cu1-S1	175.62(5)
S1-HS1	0.99(4)1	N3-Cu1-S1	98.35(5)
		N2-Cu1-S1	103.15(5)

To gather information about the electronic structure of (Bu_4N)**5**, it was characterized by UV-Vis and EPR spectroscopy. The UV-Vis spectrum is unremarkable for copper(II) complexes with a charge transfer band at 378 nm ($\varepsilon \sim 4800\ M^{-1}\ cm^{-1}$) and a d-d band at 480 nm ($\varepsilon \sim 1200\ M^{-1}\ cm^{-1}$) (**Figure 2-23**).

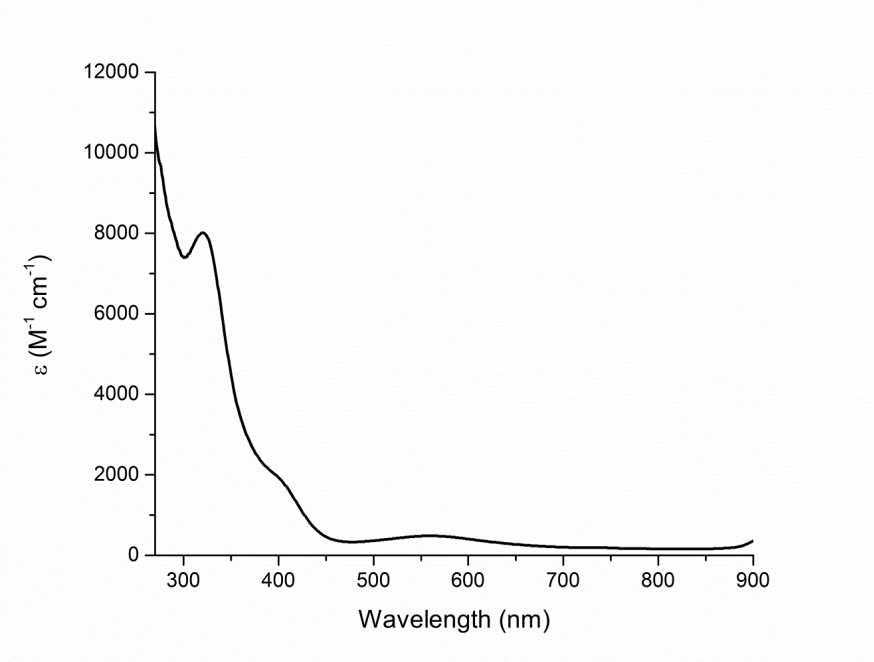

Figure 2-23: UV-Vis spectrum of (Bu_4N)**5**, 0.375 mM in tetrahydrofuran.

The EPR spectrum of (Bu_4N)**5** gave a spectrum with rich nitrogen and copper hyperfine coupling (**Figure 2-24**). The simulated spectrum overlays well with the experimental spectrum and indicates a large copper hyperfine coupling constant that is often seen in type II copper centers.[10]

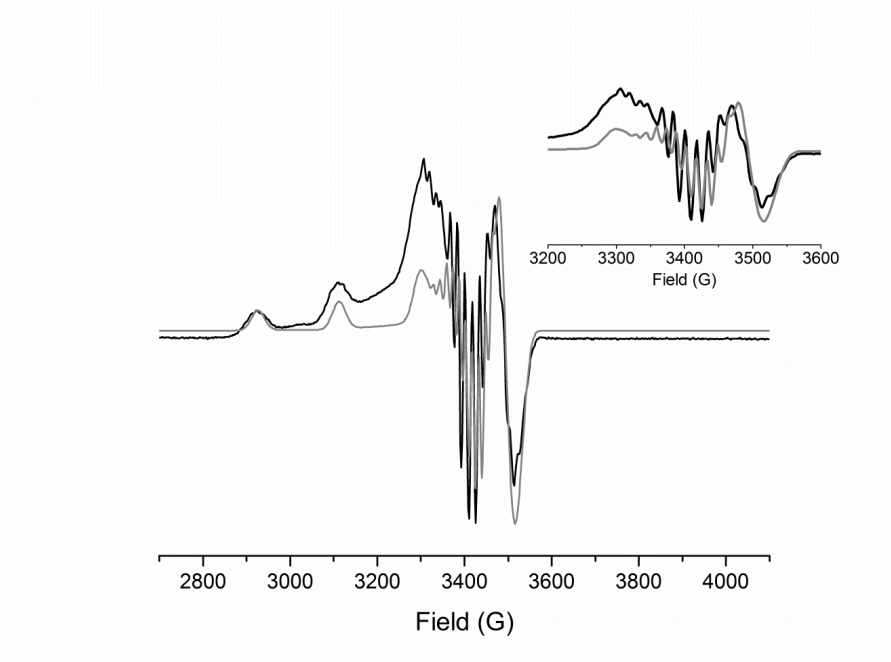

Figure 2-24: EPR spectrum of (Bu_4N)**5** (black) and simulated spectrum (grey). Sample was measured at 10 K in a 1:1::toluene:tetrahydrofuran solvent mixture.

The EPR spectral values of (Bu_4N)**5** are close to the related copper(II)-hydroxide complex (Bu_4N)**2** (**Figure 2-25**). Both have large copper hyperfine coupling values (A), 186 and 193 x 10^{-4} cm^{-1} respectively, as well as similar nitrogen coupling constants, 15 and 16.7 x 10^{-4} cm^{-1} respectively. The positioning of the g values of (Bu_4N)**5** are placed more closely together (g_x =2.012, g_y= 2.03, g_z = 2.15) and further upfield than the g values observed in (Bu_4N)**2** (g_x =2.033, g_y= 2.055, g_z = 2.19).

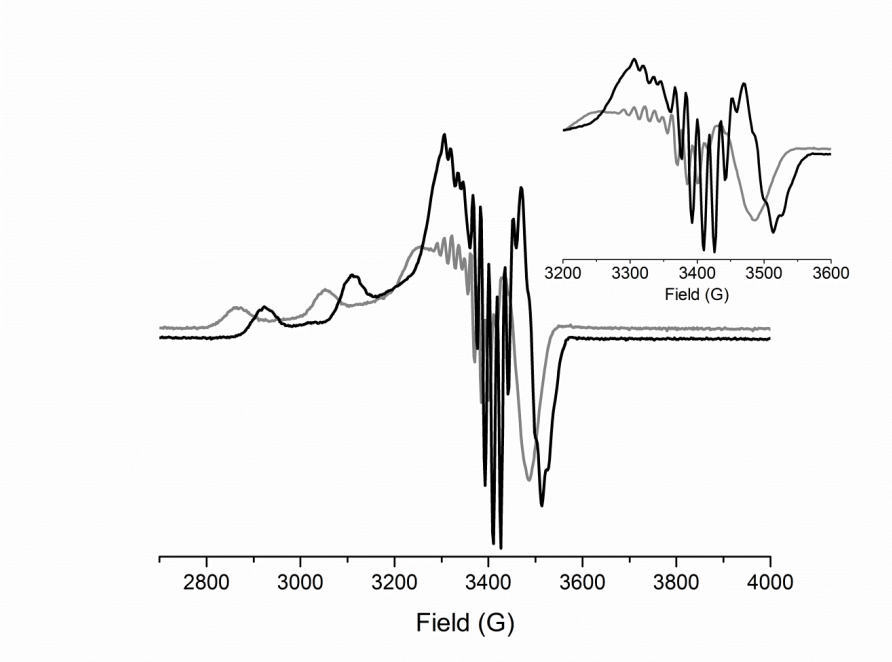

Figure 2-25: Overlay of the EPR spectra of (Bu_4N)**5** (black) and (Bu_4N)**2** (grey).

Electrochemical studies of (Bu_4N)**5** provides a rich cyclic voltammogram with multiple redox events (**Figure 2-26**). The redox events are difficult to identify due to the number of events observed and the covalent nature of the copper-sulfur bond, however, three distinct features are observed that are separated by approximately 0.4 V (E_{pa} = 0.047, 0.447, 0.872 V vs. Fc), and are at a higher potential than (Na)**4** measured in tetrahydrofuran (E_{pc} = -0.26, 0.22, 0.83 V vs Fc/Fc). Both complexes exhibit three redox events, although a direct comparison of the redox potentials cannot be made as the measurements were collected in different solvents. Attempts to measure the redox behavior of (Bu_4N)**5** in tetrahydrofuran and acetonitrile gave completely irreversible waves.

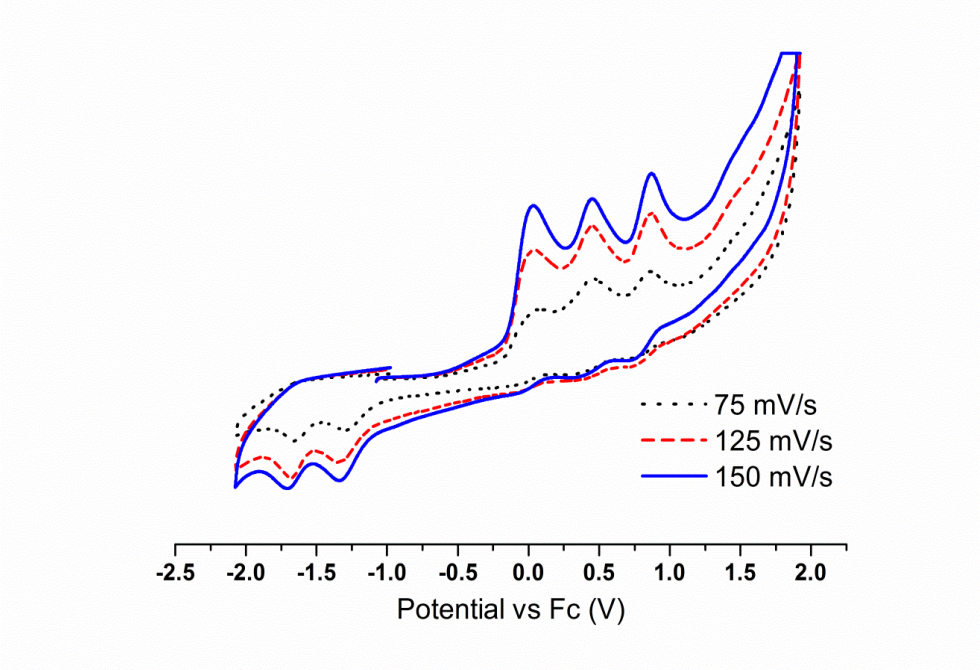

Figure 2-26: Cyclic voltammogram at multiple scan rates for (Bu_4N)**5** in 0.2 M $(Bu_4N)(PF_6)$ in acetone at room temperature.

2.3.3 Attempts to Synthesize (Cu(μ-SH)M) Bimetallic Complexes

Isolation of a discrete copper(II)-hydrosulfide complex, (Bu_4N)**5,** led us to pursue the formation of homo- and heterobimetallic complex that would have a hydrosulfide bridge with biologically relevant 3rd row transition metals. The intended $(Cu(\mu\text{-}SH)M)^n$ complexes (M = Cu(I), Cu(II), Fe(II), Zn(II)) would be expected to have interesting spectroscopic and electronic properties. For instance, a $(Cu(\mu\text{-}SH)Zn)^n$ complex would contain a hydrosulfide moeity bridging a redox-active and redox-inactive metal, which may modulate the redox activity of the copper center. Whereas a $(Cu(\mu\text{-}SH)Fe)^n$ complex has two redox-active metals that could be either ferromagnetically or anti-ferromagnetically coupled. It would be interesting to compare the electronic configurations of these singly bridged complexes to their stability and reactivity.

Reactions of (Bu_4N)**5** with various metal complexes were monitored by UV-Vis spectroscopy (**Scheme 2-15**). No new spectral features were observed upon the addition of metal complexes to (Bu_4N)**5** by UV-Vis spectroscopy. Additionally, reactions setup for crystallization did not produce any new complexes. To date, attempts to isolate dimetallic species by utilizing (Bu_4N)**5** as a synthon for a singly bridged hydrosulfide complex, have been unsuccessful. It is possible that the sterically hindered (Bu_4N)**5** is preventing the formation of dinuclear complexes. Attempts to utilize the less sterically hindered ligand derivative are currently being pursued.

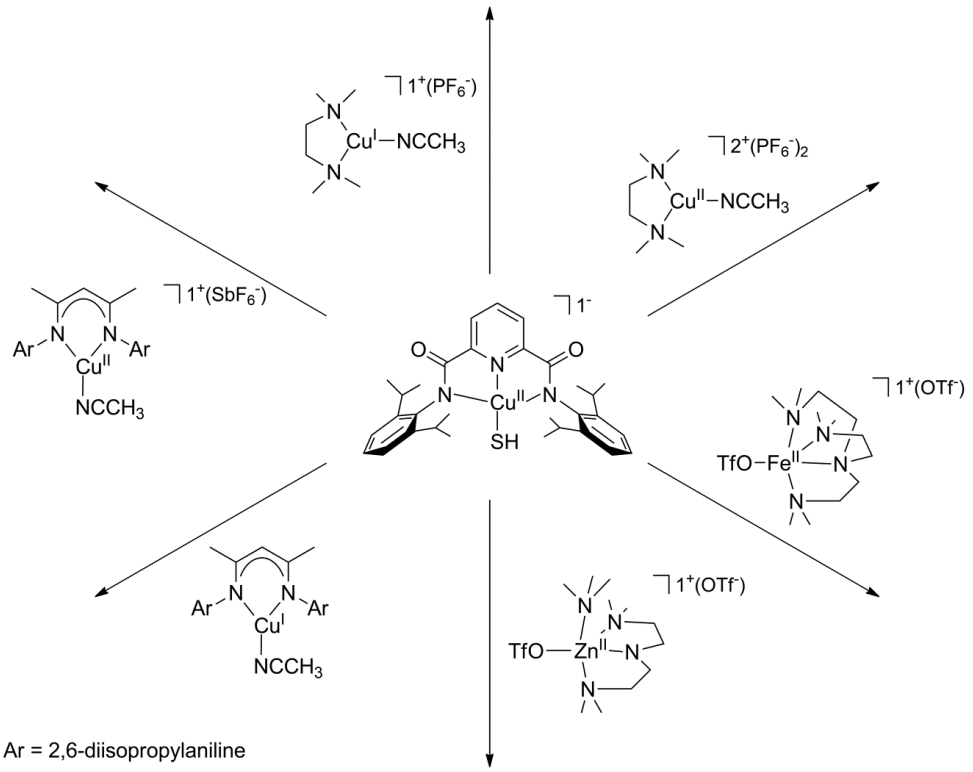

Scheme 2-15: Selected first row transition metal complexes that were added to (Bu_4N)**5** in attempt to make bimetallic complexes.

2.4 Perspectives and Future work

In order to model the Cu_Z site of nitrous oxide reductase, two strategies were employed to synthesize low coordinate and low nuclearity copper-sulfur complexes. The first strategy involved the use of dinucleating phenolate and xylene based ligands but was unsuccessful at isolating copper-sulfur complexes. The second strategy utilized an NNN-pincer ligand to successfully isolate two novel copper(II)-sulfur complexes: a copper(II)-$SSiPh_3$ complex ((Na)**4)** and a copper(II)-SH complex ((Bu_4N)**5**). The (Na)**4** complex has interesting spectroscopic properties similar to the blue and red copper proteins. The synthesis of (Bu_4N)**5** marks the first report of a copper(II)-hydrosulfide in the literature that has been fully characterized. It should be noted that initial attempts to obtain stretching frequencies for the copper-sulfur bond by resonance Raman spectroscopy did not give definitive results for either (Na)**4** or (Bu_4N)**5**; further studies should be performed.

Preliminary attempts to synthesize homo- and heterodinucelar complexes using (Bu_4N)**5** as a synthon with copper(I), copper(II), iron(II), and zinc(II) complexes were unsuccessful. Further studies should be pursued to form hetero-dinculear complex with (Bu_4N)**5** with other coordination complexes. In particular, the reaction of a molybdenum complex with (Bu_4N)**5** would be of interest, as this metal pair may provide a structural model of the Cu_M site of carbon monoxide dehydrogenase.[25] In addition, the use of $NaSSiPh_3$ and Bu_4NSH as sulfur transfer reagents to copper(II) and copper(I) complexes should be explored further, as these are convenient sulfur sources that lack a sulfur-sulfur bond.

2.5 Experimental

General Considerations. All solvents and reagents were obtained from commercial sources and used as received unless otherwise noted. The solvents diethyl ether and pentane were passed through solvent purification columns (Glass Contour, Laguna, California). Acetonitrile was passed through solvent purification columns and dried over CaH_2, degassed and distilled under vacuum. Tetrahydrofuran was dried over sodium/benzophenone, degassed and distilled under vacuum. $L^{iPr}Cu(CH_3CN)$ (**1**) was prepared according to the literature procedure.[122] $NaSSiPh_3$ and Bu_4NSH were prepared according to literature procedures.[259,260] The preparation of 4-methyl-2,6-diformylphenol (IPAH) was achieved by following a publish procedure.[261] All reactions metallation and sulfur reactions of phenol and xylene based ligands were performed in a glovebox. Reactions of $L^{iPr}Cu(CH_3CN)$ with Bu_4NSH and $NaSSiPh_3$ were performed in glovebox under a dry N_2 atmosphere. UV-Vis spectra were recorded on an HP8453 (190-1100 nm) diode-array spectrophotometer equipped with a Unisoky low-temperature crysostat. Electrospray ionization mass spectra (ESI-MS) were recorded on a Bruker BioTOF II instrument. Electron paramagnetic resonance (EPR) spectra were recorded a Bruker Continuous Wave EleXsys E500 spectrometer at 10 K. Elemental analyses were performed by Robertson Microlit Laboratory (Ledgewood, New Jersey). Graphical representations of protein structures were performed in Pymol. Graphical representations of single molecule X-ray crystal structures were performed in Crystal Maker. Data analysis and graphical representations were performed using the program Origin.

L^1-phen (2,6-bis(((2-dimethylamino)ethyl)(methyl)amino)methyl)-4-methylphenol): The ligand was prepared according to literature procedure[32b] to yield a pale yellow oil (10g,

93% yield). ^{1}H NMR (300 MHz, $CDCl_3$) δ ppm: 2.21 (s, 3H), 2.27 (s, 12H), 2.29 (s, 6H), 2.47 (m, 4H), 2.51 (m, 4H), 3.54 (s, 4H), 6.85 (s, 2H). ^{13}C NMR (300 MHz, $CDCl_3$): δ ppm 20.3, 42.1, 45.6, 54.9, 57.0, 58.2, 123.0, 127.0, 129.0, 153.6. ESI-MS: m/z 359 $[M+Na+H]^+$ (100%), 337 $[M+H]^+$ (50%). Deprotonation of L^1-phen (0.700 g, 2.03 mmol) was performed under inert conditions with a 1.1 molar excess of n-butyl lithium in THF to produce (Li)L^1-phen (0.522g, 74.3% yield).

$(Cu_2(L^1\text{-phen})(OH))(CF_3SO_3^-)_2$: To a 25 mL round bottom flask, (Li)L^1-phen (263.9 mg, 0.7710 mmol) was dissolved in ~15 mL THF to give a clear yellow solution. Copper(II) trifluoromethanesulfonate (545.8 mg, 1.509 mmol) was dissolved in ~10 mL THF to give a dark blue solution. The copper(II) triflate solution was added drop-wise to the L^1 solution and immediately a dark green solution was observed. The solution was allowed to stir for ~ 30 minutes and was then filtered. To the filtrate, ~ 10 mL of diethyl ether was added and the product was stored at −20 ºC overnight. Dark green crystals were collected by filtration (221.2 mg, yield: 28.51 %). ESI-MS: m/z 627 $[Cu(II)_2(L^1\text{-phen})(OH)(CF_3SO_3^-)]^+$. Anal. Calc. for $C_{21}H_{36}Cu_2F_6N_4O_8S_2$: %C, 32.24; %H, 4.48; %N, 6.96. Found: %C, 32.39; %H, 4.79; %H, 7.19.

(Na)($L^{iPr}CuSSiPh_3$) ((Na)**4).** A dark green solution of $L^{iPr}Cu(CH_3CN)$ (**1**) (41.9 mg, 0.0712 mmol) in THF (4 mL) was added drop-wise to a colorless solution of $NaSSiPh_3$ (26.2 mg, 0.0711 mmol) in THF (5mL) and a deep red solution formed within 1 min. The solution was stirred for ~ 5 minutes and volume reduced *in vacuo* to obtain a red oil. The oil was washed with ether (2 X 2 mL) to yield a red-brown powder (55.4 mg, 90.5 %). UV-Vis [λ_{max}, nm (ε, M^{-1} cm^{-1}) in THF]: 378 (4800), 480 (1200). Repeated attempts to obtain satisfactory elemental analysis were unsuccessful. X-ray quality crystals were

obtained by vapor diffusion of diethyl ether into a solution of **1** in THF at −20 °C after several days to yield deep red plates.

(Bu_4N)($L^{iPr}CuSH$) ((Bu_4N)5). $L^{iPr}Cu(CH_3CN)$ (**1**) (109.0 mg, 0.185 mmol) was dissolved in THF (~ 6 mL) to give a green solution. Bu_4NSH (56.9 mg, 0.206 mmol) was added to THF (~2mL) to give a yellow-green suspension. The slurry of Bu_4NSH was added drop-wise to the $L^{iPr}Cu(CH_3CN)$ solution to produce an inky purple solution. The reaction stirred for 30 minutes, was filtered and the solvent was removed *in vacuo*. The solid was washed with Et_2O (2 X 3 mL) to yield a purple-reddish solid (128.7 mg, 84.6 %). ESI-MS: 579 m/z. UV-Vis [λ_{max}, nm (ε, M^{-1} cm^{-1}) in THF]: 322 (5400), 400 (1100), 562 (500). Anal. Cald. for $C_{47}H_{74}CuN_4O_2S \cdot 1$ THF: C, 68.45; H, 9.24; N, 6.26; S, 3.58. Found: C, 66.94; H, 8.84; N, 6.48; S, 3.44. X-ray quality crystals were grown by vapor diffusion of diethyl ether into a solution of **5** in THF at −20 °C overnight to afford deep purple, block crystals.

Chapter 3: Exploring the Reactivity of a Copper(III)-OH Complex

This chapter presents an investigation of the influence of steric effects of a ligand on the reactivity of a copper(III)-hydroxide moiety towards weak C-H bonds. A *N,N'*-bis(2,6-dimethylphenyl)-2,6-pyridinedicarboxamide ligand was used to support a copper(III)-hydroxide complex (**7'**), which was compared to a previously described copper(III)-hydroxide complex (**2'**), supported by a more sterically encumbered ligand variant (*N,N'*-bis(2,6-diisopropylphenyl)-2,6-pyridinedicarboxamide). In the following, we compare the stability of the copper(III)-hydroxide complexes in solution as well as rates of C-H bond activation. In addition, preliminary studies aimed at assessing the bond dissociation free energy (BDFE) of the reactive copper(III)-hydroxide core are presented. Portions of this work have been published.[124]

3.1 Properties of Oxygen-Activating Monocopper Catalytic Sites

Copper containing proteins perform a variety of oxygen-activating reactions in biological systems (see section 1.1.1 for more details).[4,6,8] In particular, we are interested in modeling the active sites of mononuclear copper proteins and to assess their ability to use molecular oxygen to selectively activate C-H bonds. Key examples are peptidylglycine α-hydroxylating monoxygenase (PHM) and dopamine β-monooxygenase (DβM), monocopper containing proteins found in higher eukaryotes.[47] Both enzymes perform stereoselective hydroxylation of their respective substrates (**Figure 3-1**). DβM catalyzes the transformation of dopamine to norepinephrine, both of which are neurotransmitters that regulate blood pressure.[50,51] PHM, on the other hand, creates α-

hydroxylated products of C-terminal glycine-extended peptides, which are precursors for the synthesis of various hormones (oxytocin, vasopressin, calcitonin).[46]

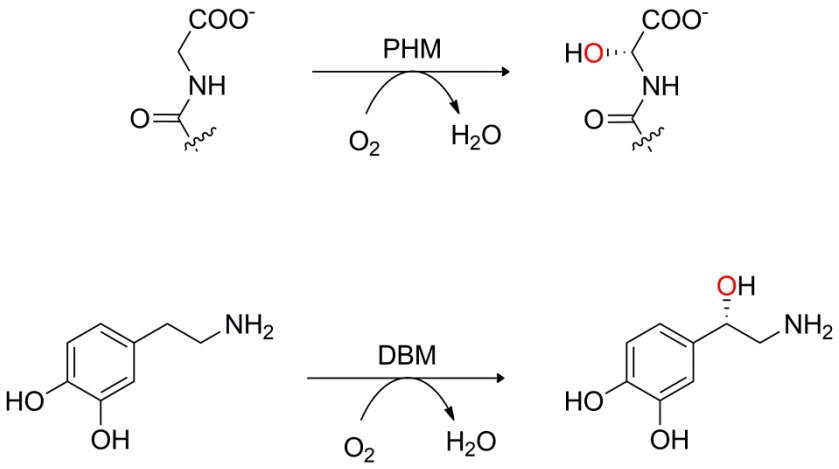

Figure 3-1: Stereoselective hydroxylation reactions catalyzed by PHM (top) and DβM (bottom).

While DβM and PHM are considered monocopper proteins, they actually contain two copper centers: a monocopper Cu_A (also referred to as Cu_H) site (for electron transfer) and a mononuclear Cu_B site (catalytic active site). DβM shows a 40% sequence homology to PHM, [49,262,263] and solutions state studies have indicated that they have indistinguishable mechanisms.[42,264] Due to difficulties in obtaining high expression levels of DβM, PHM has been studied more extensively. Numerous kinetic,[42–45,49] spectroscopic,[49,265–267] and X-ray crystallographic[268] studies have aimed to gain mechanistic information about the catalytic mechanism of PHM. The report of a high resolution crystal structure (1.85 Å) of PHM with molecular oxygen in the crystalline lattice revealed some interesting details about the reaction mechanism of both substrate and oxygen binding (**Figure 3-2** and **Figure 3-3**).

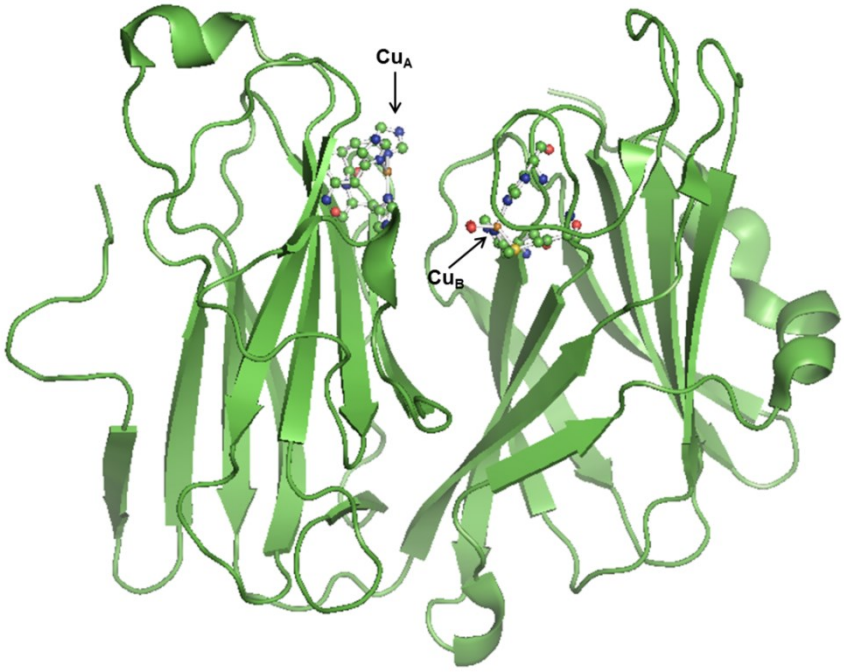

Figure 3-2: Cartoon representation of the crystal structure of the substrate bound PHM with the Cu_A and Cu_B sites drawn as ball and stick models. Resolution: 1.85 Å, PDB ID: ISDW.

By using a slow-reaction technique, a pre-catalytic complex was isolated in the crystal structure that revealed the Cu_B site in a tetrahedral environment: ligated by two histidine residues, a methionine residue and an end-on dioxygen species (**Figure 3-3**).

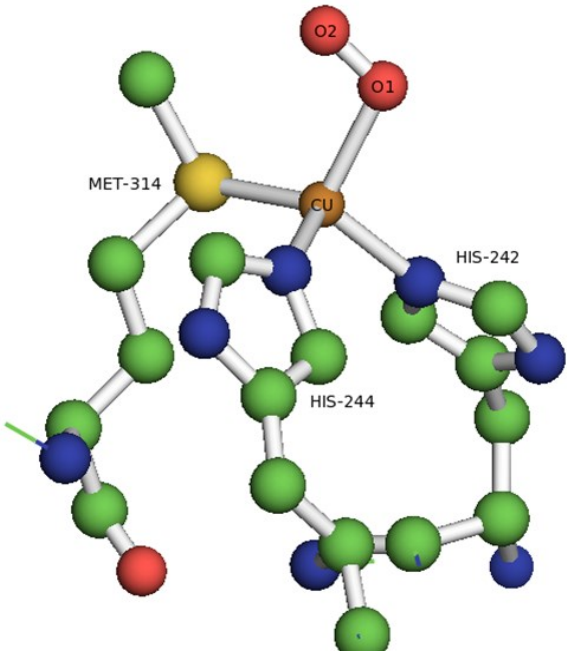

Figure 3-3: Representation of the X-ray crystal structure of PHM with a dioxygen species bound to the Cu_B site in an end-on fashion. PDB ID: ISDW.

The Cu_B site has Cu-O-O angle of 110° with the oxygen-oxygen bond distance refined to 1.23 Å. This bond length is consistent with a formulation of the moiety as either a dioxygen (O_2) or a superoxide (O_2^{1-}) species bound to the copper center. The formulation of the O_2 species as a peroxo species was discounted due to the longer oxygen-oxygen bond lengths (~1.4 Å) and a sharper Cu-O-O angle (~90°) typically observed for such species .[48,269] The Cu_B-η^1-O_2 structure is provocative, and provided a starting point for developing mechanistic hypotheses to explain the reactivity of PHM.

Klinman and coworkers suggest that the mechanism for PHM begins with O_2 binding to the Cu_B site in the fully reduced form of the enzyme (both Cu_A and Cu_B are in the +1 oxidation state), and with the substrate in close proximity (**Figure 3-4**).[47] The binding of O_2 to the $Cu(I)_B$ site causes electron transfer to O_2 to form a $Cu_B(II)$-superoxo species. The $Cu_B(II)$-superoxo species is thought to abstract a hydrogen atom from the

substrate in a step that includes a tunneling contribution as suggested by kinetic isotope studies.[47] The hydrogen atom abstraction step produces a $Cu(II)_B$-peroxo species and a substrate radical. Subsequently, electron transfer from the Cu_A site to the Cu_B site triggers a reductive cleavage event that releases water and creates a $Cu(II)_B$-oxyl species. A rapid radical recombination of the $Cu(II)_B$-oxyl species with the substrate-derived radical then gives the deprotonated hydroxylated product. Two reducing equivalents and a proton are needed to release product and return the enzyme to the resting form.

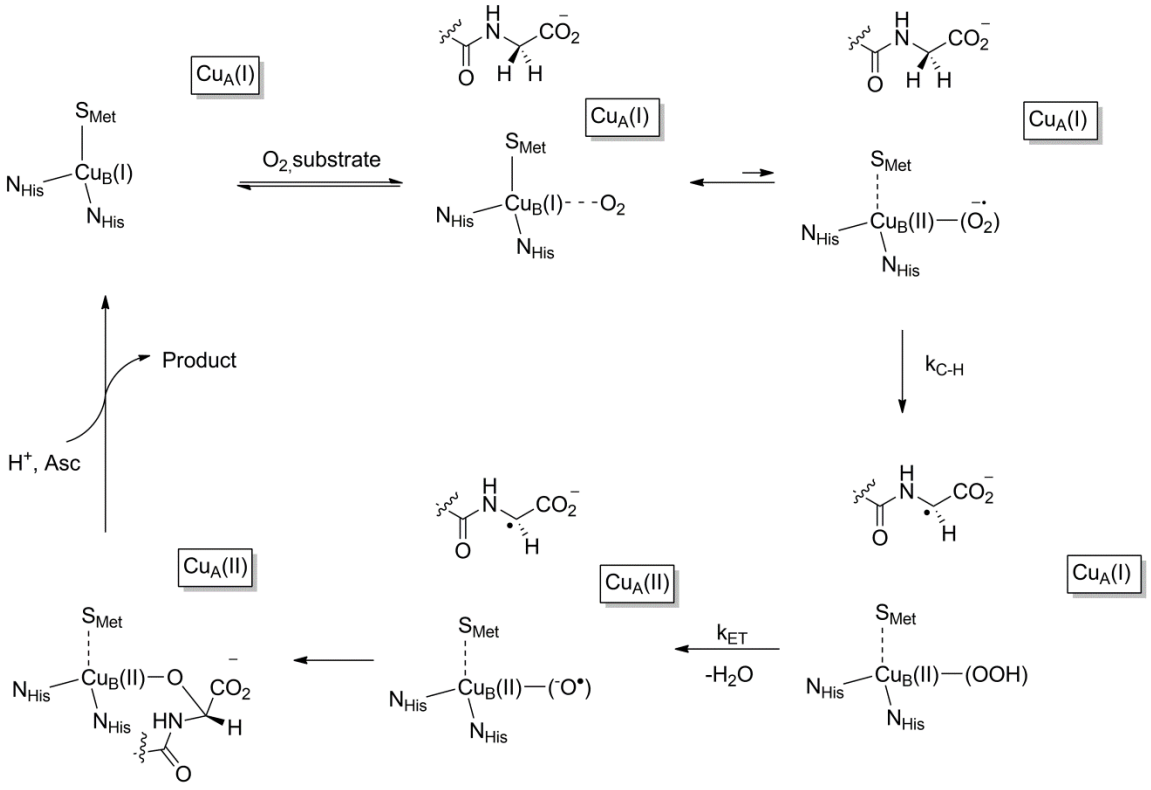

Figure 3-4: Proposed mechanism for the reaction of PHM with molecular oxygen to give the stereoselectively hydroxylated product. Figure adapted from ref.47.

Recent calculations by Yoshizawa and coworkers on the reaction pathway of DβM studied by the quantum mechanical/molecular modeling (QM/MM) method came to a different conclusion about the reactive copper-oxygen species.[52] Calculations using a

whole enzyme model based on the crystal structure reported for PHM suggests a copper(III)-oxo/copper(II)-oxyl species performs C-H bond activation in DβM. A significantly lower activation barrier for the copper(III)-oxo/copper(II)-oxyl species (5.4 kcal/mol) versus the copper(II)-superoxo species (23.1 kcal/mol) was calculated. The same trend was observed for the small-model calculations, where the copper(III)-oxo/copper(II)-oxyl pathway is energetically preferred over the copper(II)-superoxo pathway (**Figure 3-5**).

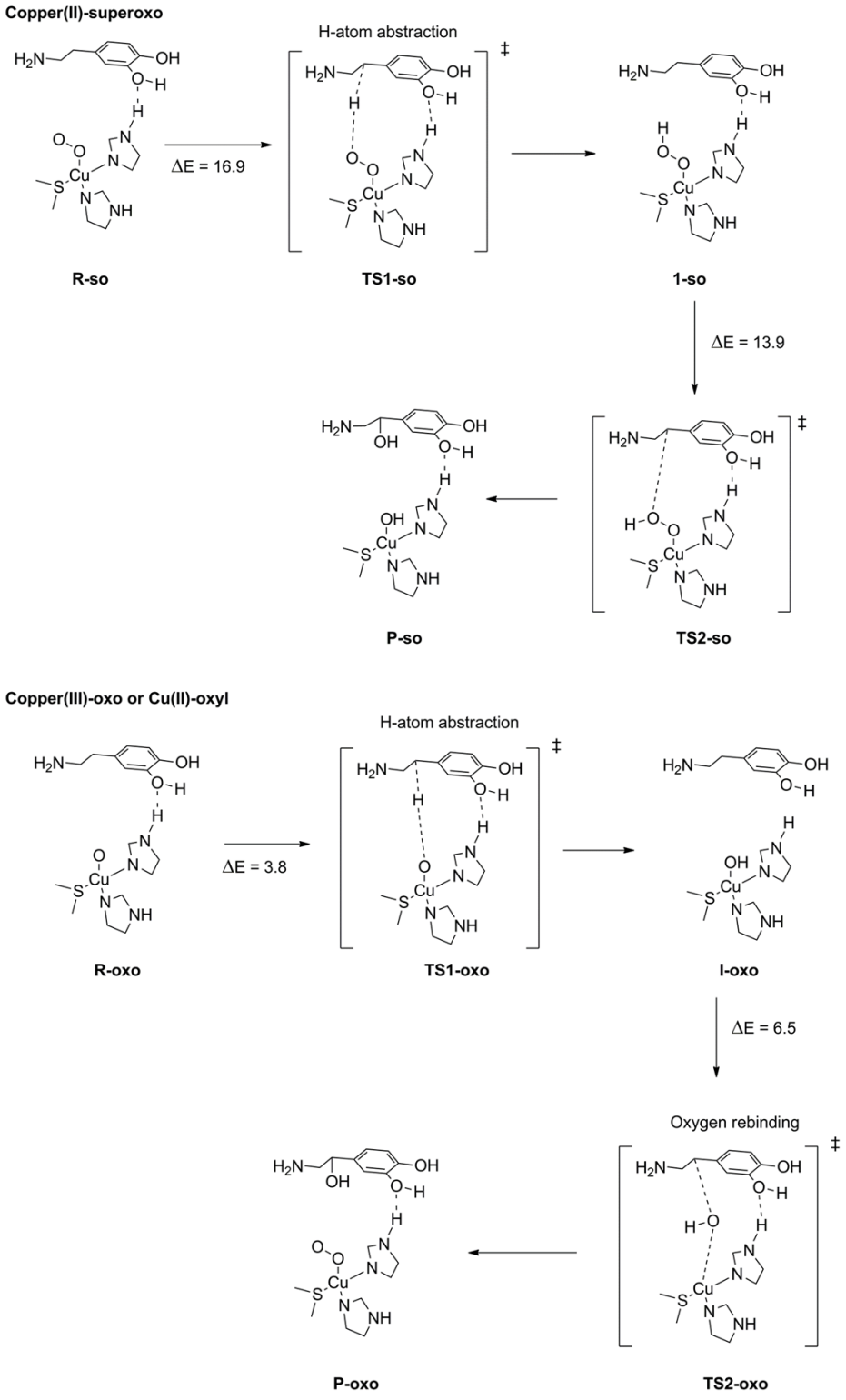

Figure 3-5: Proposed mechanism for DβM using a copper(II)-superoxo (top) or copper(III)-oxo/copper(II)-oxyl moiety as the active species. Energies are given in kcal/mol. R = reactants, TS = transition state, P = products. Figure adapted from ref.52.

These calculations suggest that a copper(III)-oxo/copper(II)-oxyl species is the reactive species that performs the selective C-H bond activation at the benzylic position of dopamine, which is in direct conflict with the proposal of an end-on copper(II)-superoxo species that is postulated as the C-H activating species in PHM.[47] As these two enzymes are believed, on the basis of kinetic data, to have identical mechanistic pathways, they should have the same reactive intermediate. The uncertainty about the identity of the copper-oxygen species that performs C-H bond activation makes obtaining a copper(III)-oxo/copper(II)-oxyl species an attractive synthetic target for synthetic model studies.

3.2 Review of Copper-Oxygen Modeling Efforts

To mimic the prevalence of histidine ligation of copper in the active sites of enzymes, a multitude of nitrogen-donor ligands have been used to support copper-oxygen complexes. Studies aimed at modeling the active sites of oxygen activating copper complexes have led to the characterization of several copper-oxygen motifs (**Figure 3-6**).[63,66,122,123,270–280] The vast majority of these complexes were created by the reaction of a copper(I) complex with molecular oxygen or an oxo-transfer reagent. The exception is the Cu(II)-OOH core, which is typically formed by the reaction of a copper(II) complex with a peroxide source.[281–287,287–289]

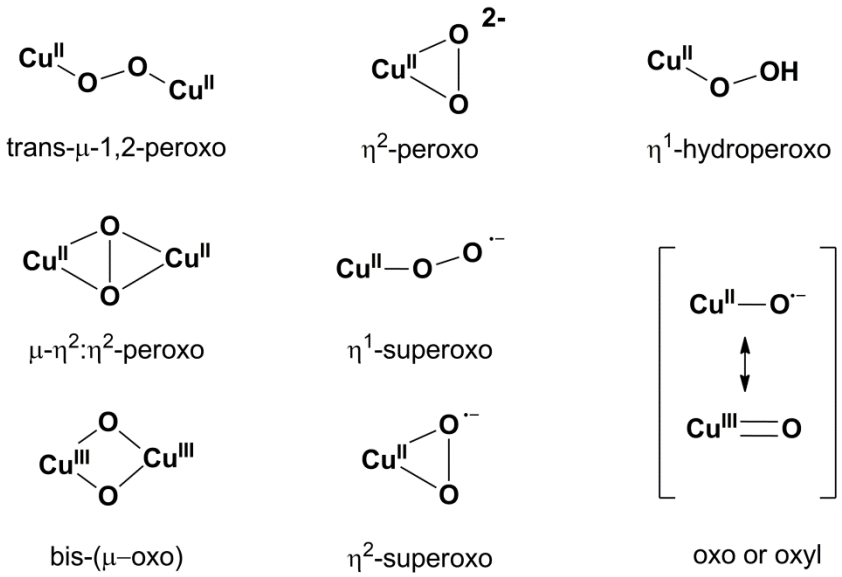

Figure 3-6: Representations of the various well-characterized synthetic copper-oxygen species. The copper-oxo/copper-oxyl species in brackets has only been observed in the gas phase.

These species exhibit very different reactivity profiles. For instance, a trigonal bipyramidal copper(II)-η^1-superoxo complex is able to attack phenols to form oxidized products,[274] while a tetrahedral copper(II)-η^1-superoxo complex undergoes intramolecular C-H bond activation.[276] The $Cu(II)_2$-*trans*-μ-1,2-peroxo species are nucleophilic in nature and have low levels of reactivity in oxidative processes.[270,273] The $Cu(II)_2$-μ-η^2: η^2-peroxo undergoes isomerization to the $Cu(III)_2$-bis-μ-oxo species and becomes more active at C-H bond activation (often via intramolecular attack on the supporting ligand).[40,63,66,271,272,275] Depending on the denticity and steric environment of the ligand, some of the copper-oxygen cores can convert to other copper-oxygen species (**Figure 3-7**).

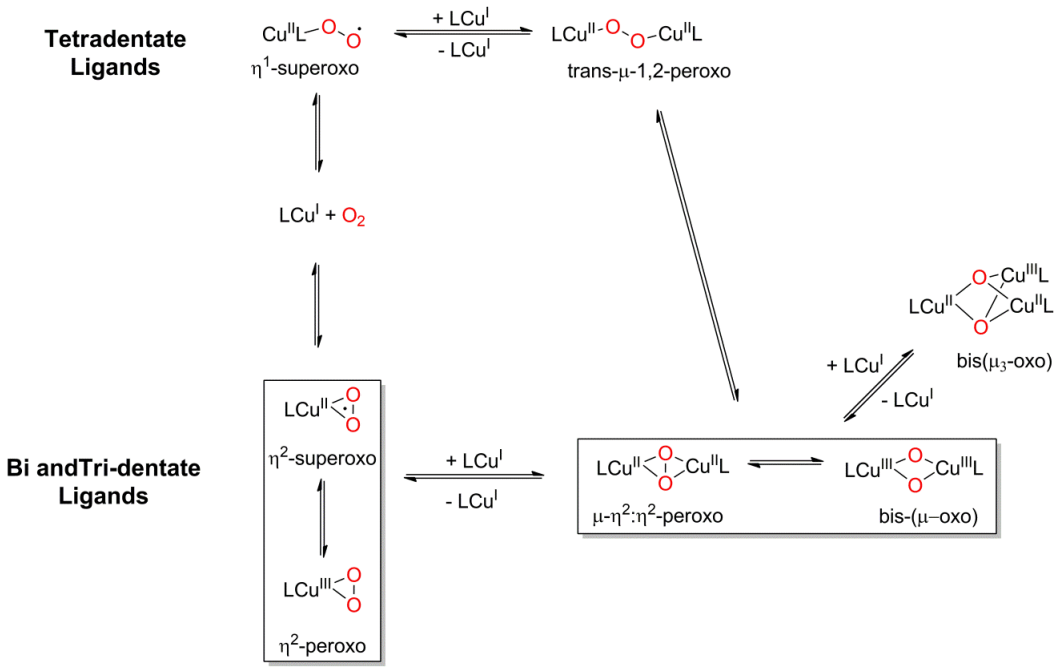

Figure 3-7: Summary of the well-characterized copper-oxygen complexes supported by bidentate, tridentate, and tetradentate ligands. Figure adapted from ref.8.

Several conclusions can be drawn from the wealth of complexes that have been synthesized, with respect to designing a good ligand for further studies to model copper-oxygen active sites. First, nitrogen donors are typically used in either neutral or mono-anionic ligands. Mono-anionic ligands tend to form more reducing copper(I) complexes that are more reactive towards O_2. Furthermore, sulfur and phosphorous donors should be avoided due to their propensity to form stable copper(I) complexes that are inert to O_2 reactivity. In addition, the ligand should have a coordination number between two and four, which allows an open coordination site for the substrate to interact with the copper center to form up to a 5-cooridinate species. Another vital aspect of ligand design is to strive for a 5-membered chelate ring, as 6-membered chelate rings show decreased reactivity due to their thermodynamic stability. In addition, it is prudent to work in

aprotic solvents and monitor reactions at low temperature in order to gain spectroscopic data on reactive intermediates.

Theoretical calculations also suggest that a mono-copper(III)-oxo $[CuO]^+$ (or copper(II)-oxyl species) is competent at C-H bond activation of methane.[290,291] The $[CuO]^+$ species has been implicated as a possible oxidant for several enzyme active sites[291–294] and synthetic copper complexes.[159,277,295,296] Studies performed on $[CuO]^+$ species generated in the gas phase, with a 1,10-phenanthroline supporting ligand, showed the oxidation of small alkanes, although methane was not oxidized.[297] When the bare $[CuO]^+$ species was generated in the gas phase by Dietl and coworkers, however, it was observed to activate methane.[298] Dietl and coworkers calculated that the $[CuO]^+$ species was in a high-spin triplet ground state that had significant radical density on the oxygen atom, which is believed to be critical to the H-atom abstraction ability of the $[CuO]^+$ moiety. The bonding picture of $[CuO]^+$ species has degenerate singly occupied π^* anti-bonding orbitals with significant $2p_\pi$ character from the oxygen orbitals, which creates a much larger spin density on the oxygen atom (1.68) versus the copper atom (0.32). Although the triplet ground state has lower energy than the singlet, the overall pathway for the triplet reaction is endothermic, making the triplet pathway energetically disfavored. The calculations suggest that when the $[CuO]^+$ species interacts with methane, σ-bonding interactions become more energetically favorable. This causes an intersystem crossing event to occur at the first transition state, where the triplet state crosses over to the singlet state, and the reaction continues along the singlet pathway (**Figure 3-8**).

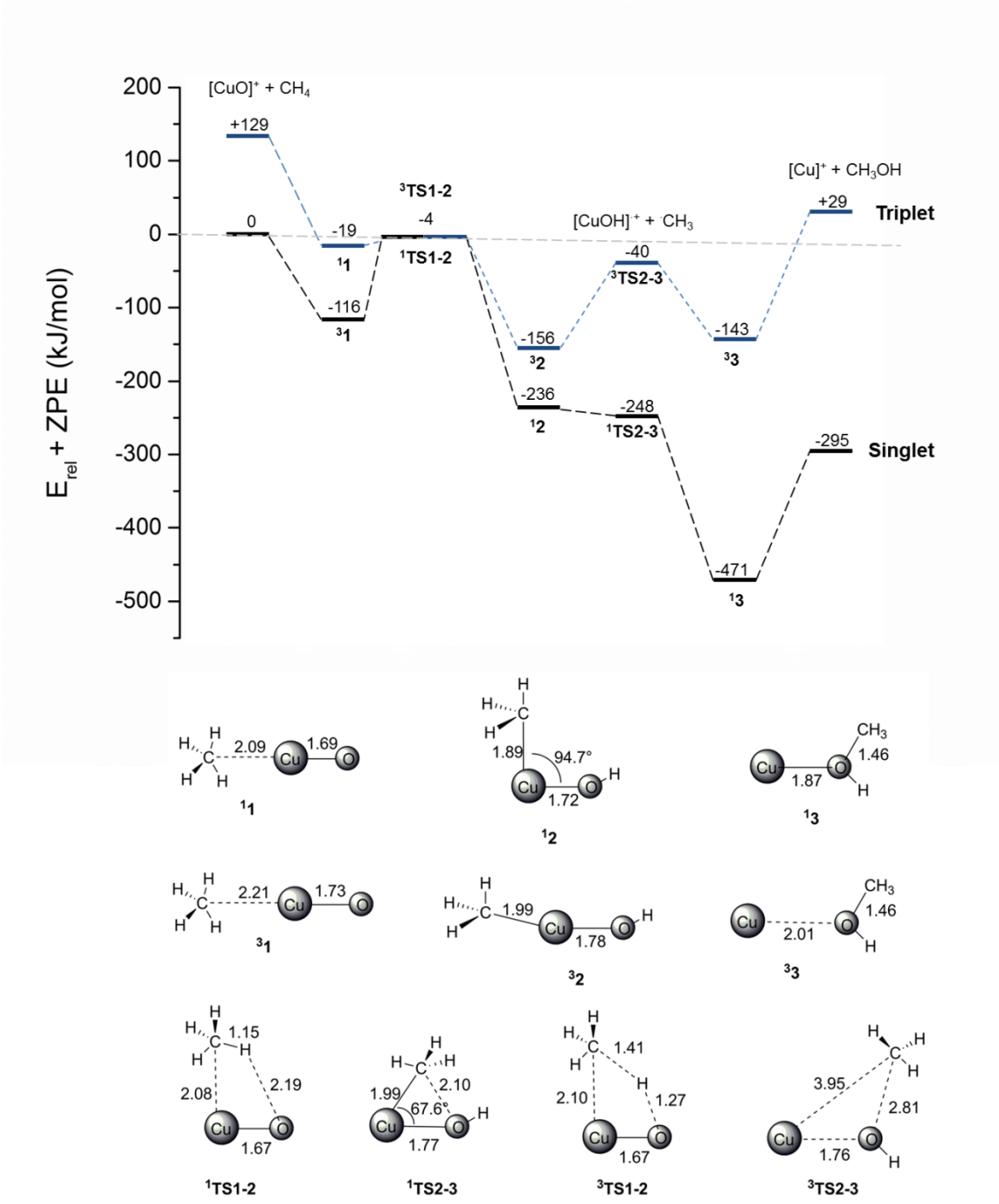

Figure 3-8: Potential-energy surface for the reaction of $[CuO]^+$ with methane for the triplet and singlet pathways with intermediates and transition state structures. Bond lengths are given in Å. Figure adapted from ref.298.

The work presented in this thesis aimed to use some of the ideas for ligand design from previous bioinorganic studies and gathered inspiration about reactive copper-oxygen species to take a new approach to making copper-oxygen complexes. We have begun to look at modeling copper proteins from a new perspective: instead of synthesizing a copper(I) complex and monitoring its reaction with molecular oxygen, we aim to create high-valent copper(III)-hydroxide complexes from copper(II) complexes. The copper(III)-hydroxide complexes can be synthesized by oxidation of a copper(II)-hydroxide complex, which would be created by the addition of a hydroxide source to a neutral copper(II) precursor. We feel this approach is akin to the strategy used for the synthesis of copper(II)-hydroperoxo complexes from copper(II) and peroxide sources[281–289] and may provide valuable insight into potential reactive intermediates relevant to enzyme active sites. With the goal of obtaining a synthetically accessible copper(III)-oxo/copper(II)-oxyl species, we developed an idealized synthetic scheme that could produce our desired complex in a stepwise fashion (**Scheme 3-1**). This strategy hinges on the isolation of a mononuclear copper(II)-hydroxide complex, which could then undergo further oxidation and ultimately, deprotonation in order to obtain the desired copper(III)-oxo or copper(II)-oxyl complex.

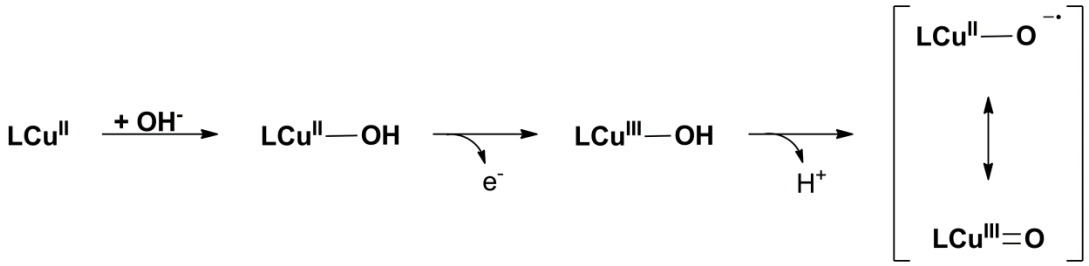

Scheme 3-1: Idealized synthetic route to obtain a copper-oxyl or copper-oxo species.

We were inspired by a recent report of a square planar nickel(II)-hydroxide complex supported by a *N,N′*-bis(2,6-dimethylphenyl)-2,6-pyridinedicarboxamide ligand from the Holm laboratory.[120] Both the square planar environment and the dianionic nature of the ligand are desirable attributes for stabilizing a copper(III) complex, which is critical for our idealized synthetic scheme. In seminal copper(III)-hydroxide work, from the Tolman laboratory, a sterically encumbered ligand, *N,N′*-bis(2,6-diisopropylphenyl)-2,6-pyridinedicarboxamide ligand was used to stabilize a copper(III)-hydroxide complex. Specifically, a copper(II)-hydroxide complex, (Bu_4N)**2**, was synthesized from a copper(II)-acetonitrile starting material, **1** (**Scheme 3-2**).[122,123]

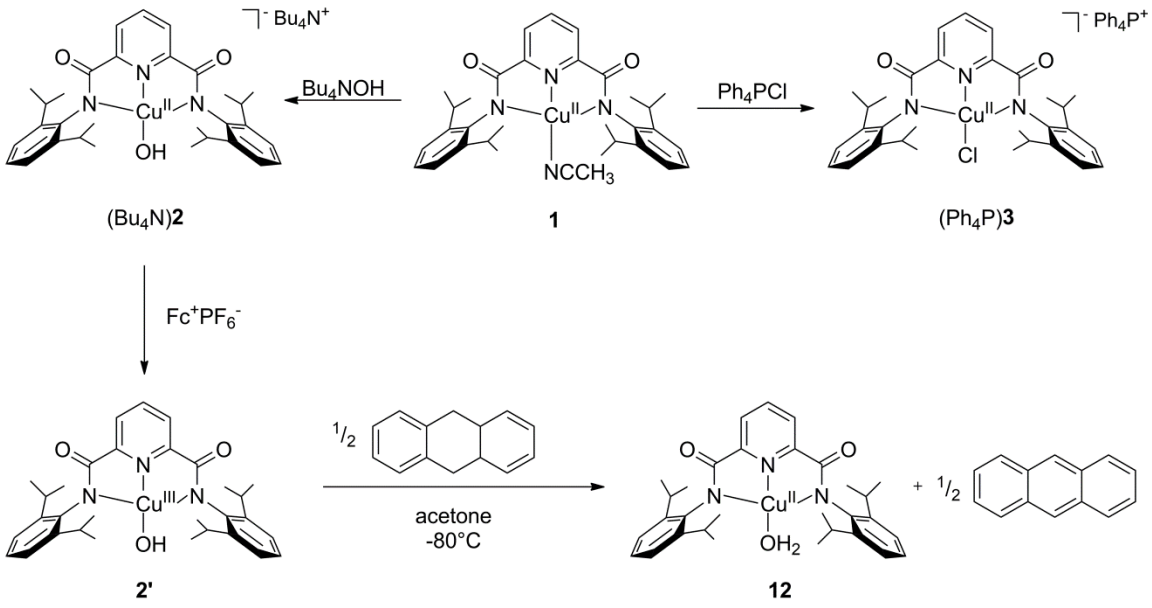

Scheme 3-2: Preparation of a copper(II)-hydroxide, (Bu_4N)**2**, that upon oxidation to **2'**, is competent at H-atom abstraction from 9,10-dihydroanthracene. In addition, the preparation of the copper(II)-Cl species, (Ph_4P)**3**, is displayed.

For crystallization purposes, the tetrabutylammonium cation of (Bu_4N)**2** was exchanged in a metathesis reaction with PPNCl. While this did aide in obtaining crystalline samples suitable for single crystal X-ray diffraction, it also led to various

levels of chloride ions displacing the hydroxide ligands throughout the crystalline lattice. This compositional disorder led to a longer than expected copper-hydroxide distance (1.947(2) Å) than predicted by DFT calculations (1.863 Å) (see Appendix A for more details).

Upon oxidation of (Bu_4N)**2** with $Fc^+PF_6^-$, an intense chromophore corresponding to the formation of a copper(III)-hydroxide, **2'**, was observed by UV-Vis spectroscopy. The formulation of **2'** as a copper(III) species was supported by TD-DFT calculations, which identified the transition as predominately based from a ligand orbital with π character to an orbital with predominately Cu d_{x2-y2} character. In addition, copper K-edge X-ray absorption spectroscopy (XAS) supported the formulation of the reactive species as a copper(III) complex, as indicated by contraction of the copper-ligand bonds and a 1.7eV shift in the pre-edge feature relative to the starting complex, (Bu_4N)**2**.[123] Rapid C-H bond activation of 9,10-dihydroanthracene by **2'** was observed (second-order $k \sim 1.1$ $M^{-1}s^{-1}$) at −80 °C in acetone (**Scheme 3-2**). Currently, this complex is among the most active synthetic complexes towards C-H bond activation, placing it on-par with high-valent iron and manganese complexes (**Figure 3-9**).

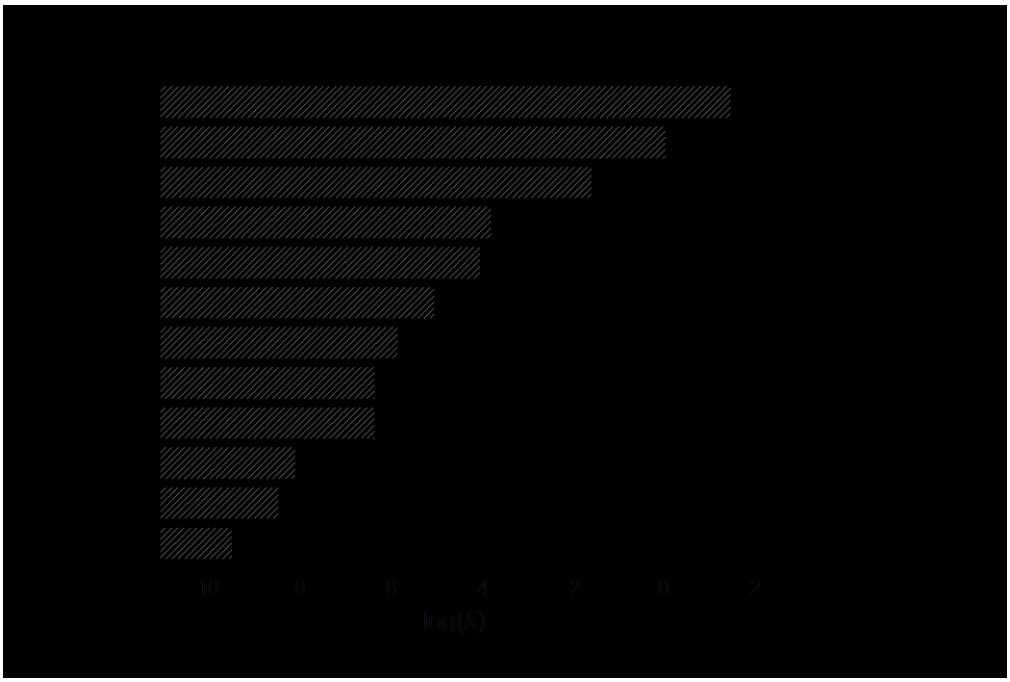

Figure 3-9: Comparison of the rate of H-atom abstraction from 9,10-dihydroanthracene by various transition metal complexes. References for the complexes are as follows: $[Fe^{III}(OH)(L')\text{-}(\mu\text{-}O)\text{-}Fe^{IV}(O)(L')]^{2+}$,[299] $L^{iPr}Cu^{III}OH$,[123] $Fe^{IV}(OH)(L')\text{-}(\mu\text{-}O)\text{-}Fe^{IV}(O)(L')]^{3+}$,[299] $Mn^{IV}(H_3buea)(O)]^{1-}$,[300] $[Fe^{IV}(L')\text{-}(\mu\text{-}O)\text{-}Fe^{IV}(L')]^{4+}$,[299] $[Fe^{III}(L')\text{-}(\mu\text{-}O)\text{-}Fe^{IV}(L')]^{3+}$,[299] $Mn^{III}(PY5)OH]^{2+}$,[301] $[Mn^{VI}O_4]^{1-}$,[302] $[Mn^{III}(H_3buea)(O)]^{2-}$,[300] $[Fe^{III}(PY5)OH]^{2+}$,[303] $[Fe^{III}(Hbim)(H_2bim)_2]^{2+}$,[304] $[Cu^{III}(Pre)]^{1+}$.[65] Where, L' = tris((4-methoxy-3,5-dimethylpyridin-2-yl)methyl)amine), H_3buea = tris[(N′-tert-butylureayl)-N-ethyl)]amine, PY5 = (2,6-bis(bis(2-pyridyl)methoxymethane)pyridine), H_2bim = 2,2'-bi-imidazoline, and Pre = 3,9-dimethyl-4,8-diazaundecane-2,10-dionedioximate. See **Figure 3-10** illustrations of the structures. Figure adapted from ref.123.

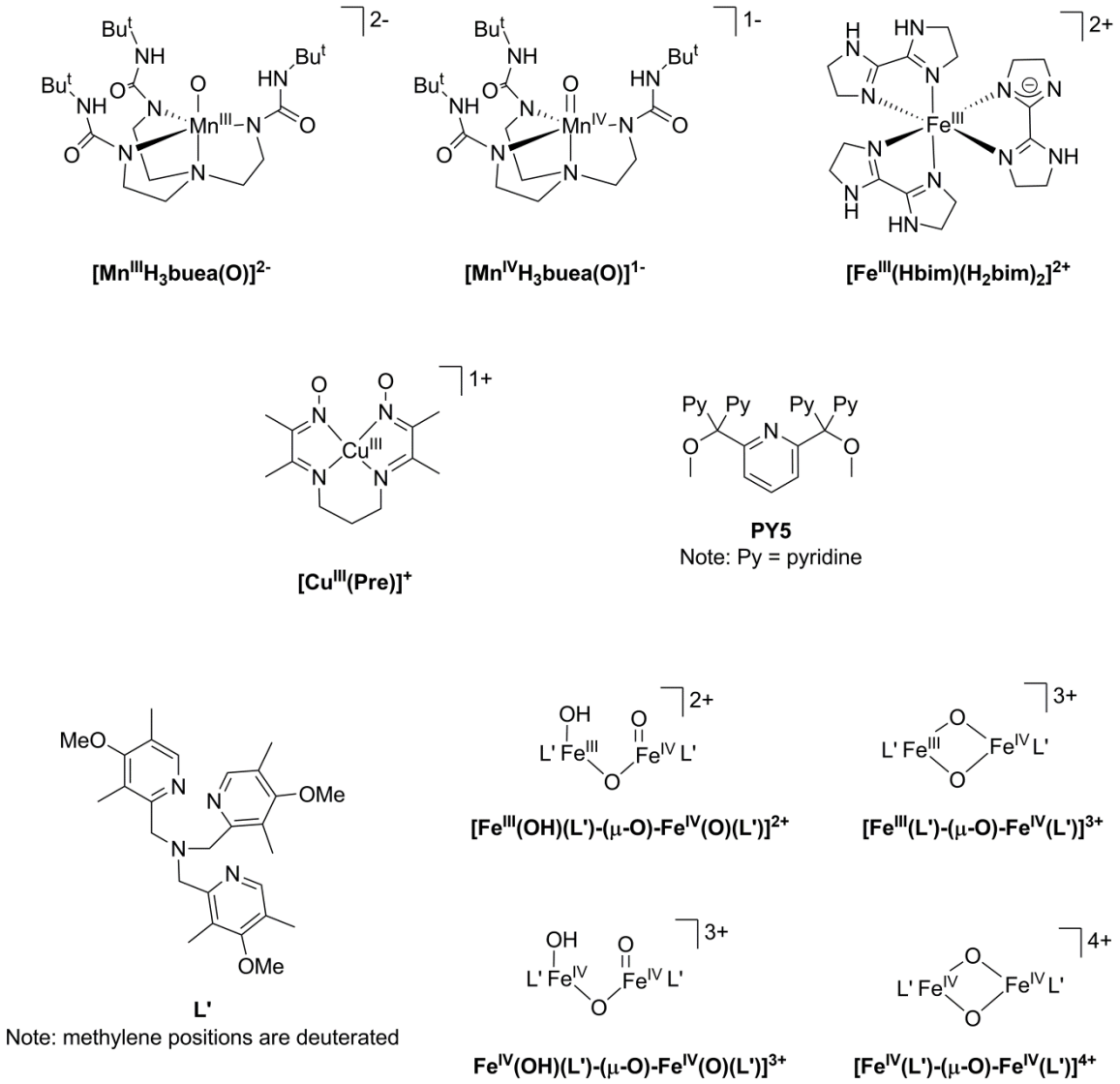

Figure 3-10: Representations of the metal complexes and ligands previously studied for H-atom abstraction from DHA.

The rapid C-H bond activation by a copper(III)-hydroxide complex, **2'**, was a surprising result that suggested this moiety may be considered as a strong C-H bond activating species in its own right, and not only as an intermediate species on the route to obtaining a copper(III)-oxo/copper(II)-oxyl complex.[123] This work has led us to pursue the synthesis of other copper(III)-hydroxide complexes in order to gain a deeper understanding of their spectroscopic properties and to perform reactivity studies in order

to garner mechanistic details about the C-H bond activating reactivity of these complexes. The following work presents results obtained when we reduced the steric protection around the copper center, which we suspected might allow for more facile attack on weak C-H bonds, and possibly lead to more rapid attack of substrates with more difficult C-H bonds.

3.3 Synthesis and Characterization of a Family of Copper(II) Complexes

Our previous work with a copper(II)-hydroxide complex, (Bu_4N)**2**, focused on the characterization of reactive copper(III)-hydroxide species, **2'**, capable of attacking weak C-H bonds.[122,123] We extended this work by reducing the steric bulk around the copper complex by using *N,N'*-bis(2,6-dimethylphenyl)-2,6-pyridinedicarboxamide, which is less bulky than the supporting ligand for (Bu_4N)**2**. We aimed to probe the impact of the steric environment around the copper center on the reactivity and stability of the corresponding copper(III)-hydroxide complex, **7'**. We found that this seemingly small change to the steric environment around the copper center had a profound impact on the stability of the corresponding copper(III)-hydroxide complex, **7'**.

3.3.1 Synthesis and Characterization of a Copper(II)-CH_3OH Complex

In order to synthesize our desired copper(II)-hydroxide, the ligand was prepared according to literature procedures,[120] and used to prepare the neutral copper(II)-CH_3OH (**6**) complex (**Scheme 3-3**). The product was obtained as a light green powder and was characterized by elemental analysis, ESI-MS, UV-Vis spectroscopy, and EPR spectroscopy. Repeated attempts to grow X-ray quality crystals were unsuccessful.

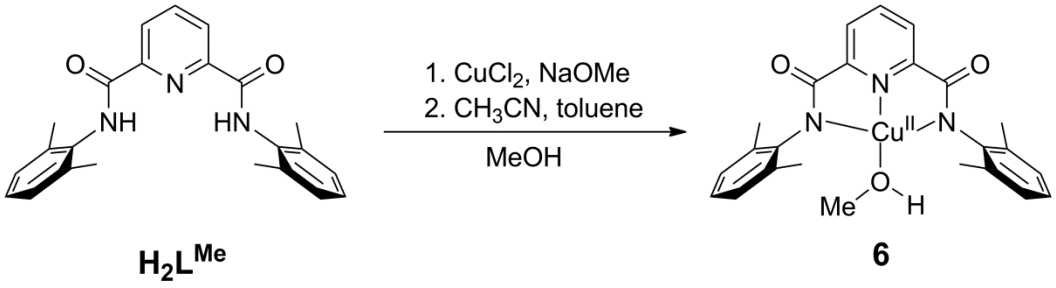

H_2L^{Me} **6**

Scheme 3-3: Synthetic route for the preparation of **6**.

The positive ESI-MS spectrum of **6** contains multiple features, including the parent ion peak $[Na+\mathbf{6}]^+$ (**Figure 3-11**).

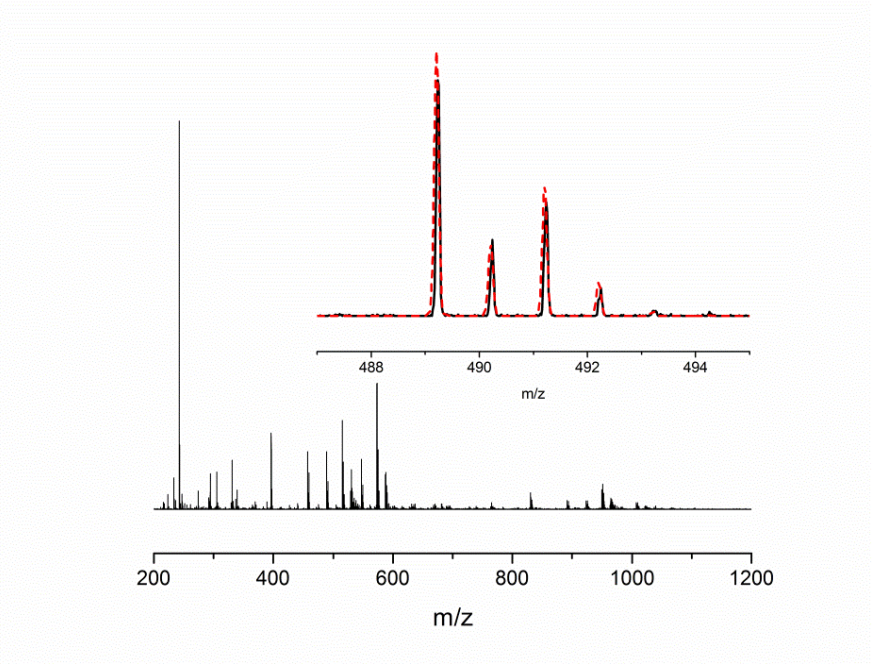

Figure 3-11: Positive mode ESI-MS spectrum of **6** collected in acetone/methanol. The inset indicates the parent peak, $[Na+\mathbf{6}]^+$, experimental spectrum (solid) and simulated spectrum (dashed).

Acetone was used as a weakly coordinating solvent to avoid displacement of the coordinated methanol in the experiment. The higher mass peaks correspond to various numbers of solvent molecules (methanol and acetone) associating with the parent ion, $[Na+\mathbf{6}]^+$ (**Table 3-1**).

Table 3-1: Description of the major peaks observed in the positive mode ESI-MS spectrum of **6**.

m/z	Description
457.20	$L^{2-} + Cu^{2+} + Na^{+}$
489.23	$L^{2-} + Cu^{2+} + Na^{+} + CH_3OH$
515.25	$L^{2-} + Cu^{2+} + Na^{+}$ + acetone
547.28	$L^{2-} + Cu^{2+} + Na^{+}$ + acetone + CH_3OH
573.30	$L^{2-} + Cu^{2+} + Na^{+}$ + 2(acetone)

The UV-Vis spectrum of **6** was measured in acetonitrile at room temperature and exhibited a charge transfer band at 397 nm ($\varepsilon \sim 1{,}400\ M^{-1}\ cm^{-1}$) and a d-d band at 545 nm ($\varepsilon \sim 720\ M^{-1}\ cm^{-1}$) (**Figure 3-12**). These bands are similar to the features observed for the neutral copper(II)-acetonitrile complex of the related isopropyl ligand, **1**, (**Scheme 3-2**) that was measured in acetonitrile 398 nm ($3{,}000\ M^{-1}\ cm^{-1}$) and 550 nm ($\varepsilon \sim 800\ M^{-1}\ cm^{-1}$).

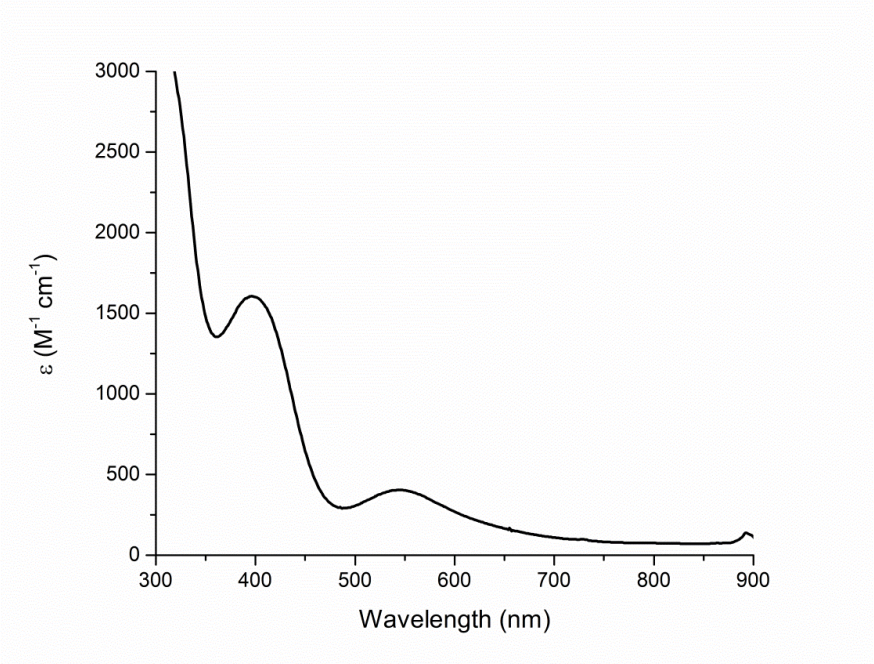

Figure 3-12: UV-Vis spectrum of 0.5mM **6** measured in acetonitrile at room temperature.

In addition to measurement of the electronic absorption spectra, the electronic environment of **6** was probed by EPR spectroscopy. The simulated EPR spectra of **6** is in good agreement with the measured spectrum (**Figure 3-13**). The spectrum is approximately axial ($g_x = 2.028$, $g_y = 2.055$, $g_z = 2.189$) with a large copper hyperfine coupling value ($A(Cu) = 193 \times 10^{-4}$ cm^{-1}) and distinct nitrogen super-hyperfine coupling ($A(N_{av}) = 15 \times 10^{-4}$ cm^{-1}). The EPR spectrum of **6** was simulated with an average nitrogen environment that included the pyridine nitrogen and the two amide nitrogen atoms. Simulations that split the nitrogen superhyperfine values into pyridine nitrogen (N_{py}) and amide nitrogen (N_{am}) did not improve the simulation. These values are similar to the values measures for **1** under identical conditions: $g_x = 2.027$, $g_y = 2.064$, $g_z = 2.190$, $A(Cu) = 199 \times 10^{-4}$ cm^{-1}, $A(N_{am}) = 18.8 \times 10^{-4}$ cm^{-1}, $A(N_{py}) = 14 \times 10^{-4}$ cm^{-1}. For reference, the average nitrogen superhyperfine value for **1**, $A(N_{av})$, was calculated to be 15.6×10^{-4}

cm^{-1}. The slight variations in g values and copper A values may be attributed to the identity of the solvent labile ligand for each complex, acetonitrile for **1** and methanol for **6**. The sharp nitrogen superhyperfine coupling observed in the EPR spectrum of **6** is consistent with the EPR spectra measured for other pyridine-dicarboxamide complexes, which do not possess hydrogen atoms in close proximity to the copper nucleus.[123,124] The lack of nearby hydrogen atoms to the spin center (copper) is thought to prevent spectral broadening that is often observed in other copper(II) complexes that have hydrogen atoms of the ligand near the copper nucleus.

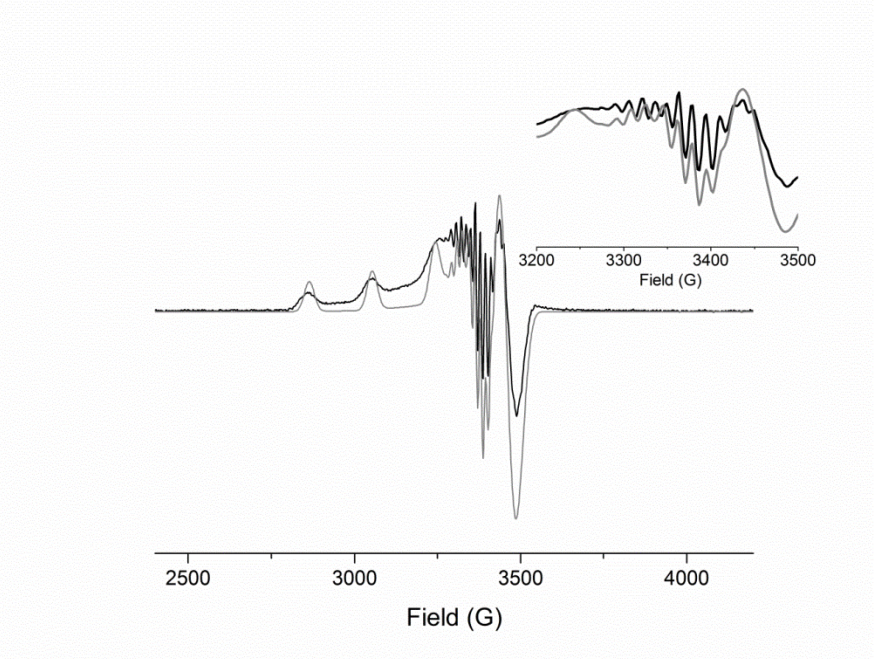

Figure 3-13: X-band EPR spectrum of **6** (black) and the simulated spectrum (grey). The sample was collected in 1:3::acetone:toluene at 10 K.

3.3.2 Synthesis and Characterization of a [Copper(II)-OH]$^{1-}$ Complex

The synthesis of our desired copper(II)-hydroxide, (Bu_4N)**7**, was achieved by using a procedure similar to the published procedure for the synthesis of (Bu_4N)**2**

(**Scheme 3-4**).[123] Briefly, a slurry of **6** was prepared in diethylether and one equivalent of tetrabutylammonium hydroxide (Bu_4NOH) was added, causing the instantaneous formation of an intense blue oil. The oil was triturated with diethyl ether and evaporated under vacuum to yield a dark blue powder.

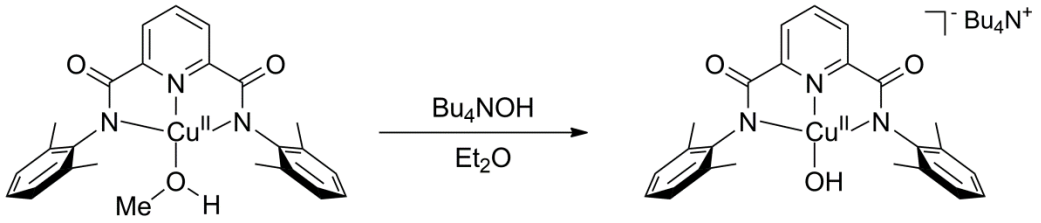

6 (Bu_4N)**7**

Scheme 3-4: Synthetic route for the preparation of (Bu_4N)**7** from **6**.

The dark blue powder obtained for (Bu_4N)**7** was fully characterized by elemental analysis, UV-Vis spectroscopy, ESI-MS, FT-IR spectroscopy, and EPR spectroscopy. Repeated attempts to grow X-ray quality crystals were unsuccessful, although a report of the (Et_4N)**7** appeared in the literature as this work was nearing completion and indicated a mononuclear copper complex.[213] The EPR spectrum of (Bu_4N)**7** displays rich nitrogen and copper hyperfine interactions (**Figure 3-14**).

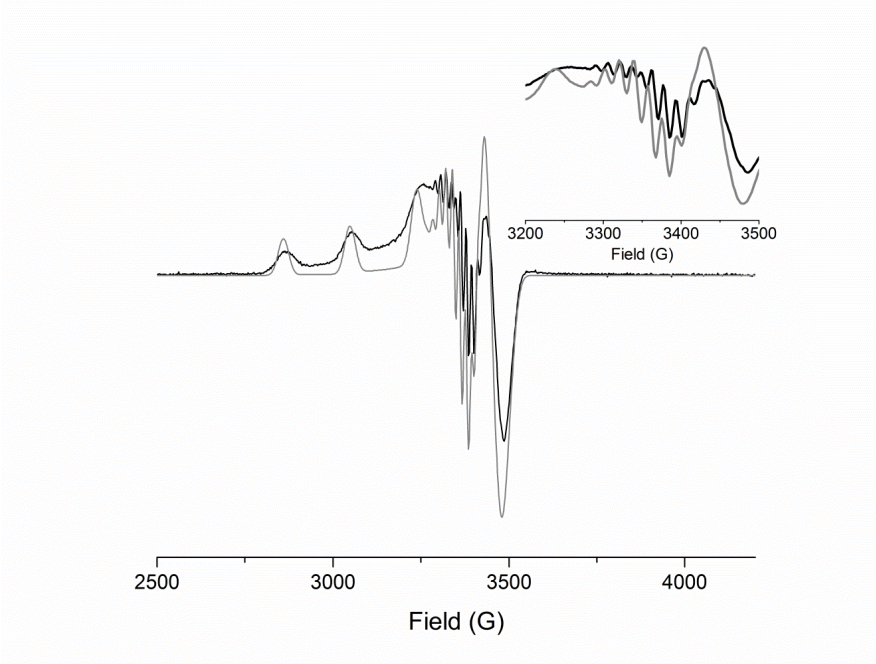

Figure 3-14: X-band EPR spectrum of the overlay of the experimental spectrum of (Bu_4N)**7** (black) and the simulated spectrum (grey) in 3:1::toluene:acetone at 10 K.

The simulated spectra for (Bu_4N)**7** is in good agreement with the measured spectrum (g_x = 2.033, g_y = 2.055, g_z = 2.19) with a large copper hyperfine coupling value (A(Cu) = 193 x10^{-4} cm^{-1}) and an average nitrogen superhyperfine coupling constant ($A(N_{av})$ = 16.7 x 10^{-4} cm^{-1}). The EPR spectrum of (Bu_4N)**7** was simulated with an average nitrogen environment that included the pyridine nitrogen and the two amide nitrogen atoms. Simulations that split the nitrogen superhyperfine values into pyridine nitrogen (N_{py}) and amide nitrogen (N_{am}) did not improve the simulation. These values are very similar to the values measured for (Bu_4N)**2**: g_x = 2.032, g_y = 2.055, g_z = 2.185, A(Cu) = 196 x10^{-4} cm^{-1}, $A(N_{am})$ = 17.7 x10^{-4} cm^{-1}, $A(N_{py})$ = 13.4 x10^{-4} cm^{-1}. For reference, $A(N_{av})$, was calculated to be 14.8 x10^{-4} cm^{-1}. It should be noted that the samples were measured in different solvents, which may account for some of the small changes in hyperfine coupling constants. The EPR spectrum of (Bu_4N)**7** is essentially superimposable on the EPR

spectrum measured for (Bu_4N)**2** (**Figure 3-15**). The observation that these spectra are essentially identical lends credence to our hypothesis that any difference observed in reactivity between (Bu_4N)**7** and (Bu_4N)**2** are due to steric effects, not electronic effects.

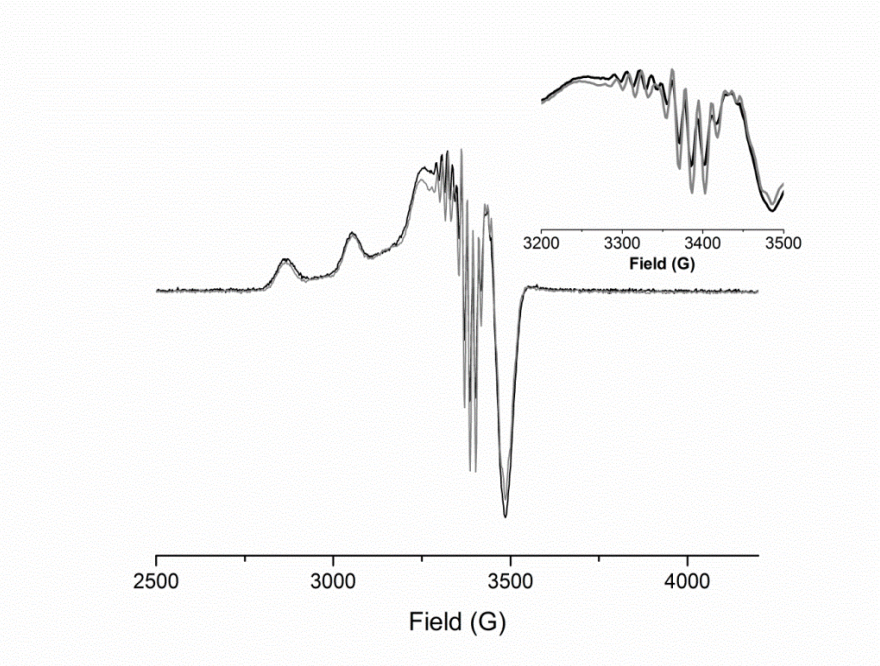

Figure 3-15: Overlay of the X-band EPR spectra of (Bu_4N)**7** (black) and (Bu_4N)**2** (grey).

The UV-Vis spectrum of (Bu_4N)**7** was measured in acetone at room temperature and exhibits a charge transfer band at 378 nm (ε ~1800 M^{-1} cm^{-1}) and a d-d band at 550 nm (ε ~ 230 M^{-1} cm^{-1}) (**Figure 3-16**). These values are slightly less intense than the UV-Vis features measured for (Bu_4N)**2**, which appeared at 378 nm (ε ~ 2400 M^{-1} cm^{-1}) and 550 nm (ε ~ 310 M^{-1} cm^{-1}).

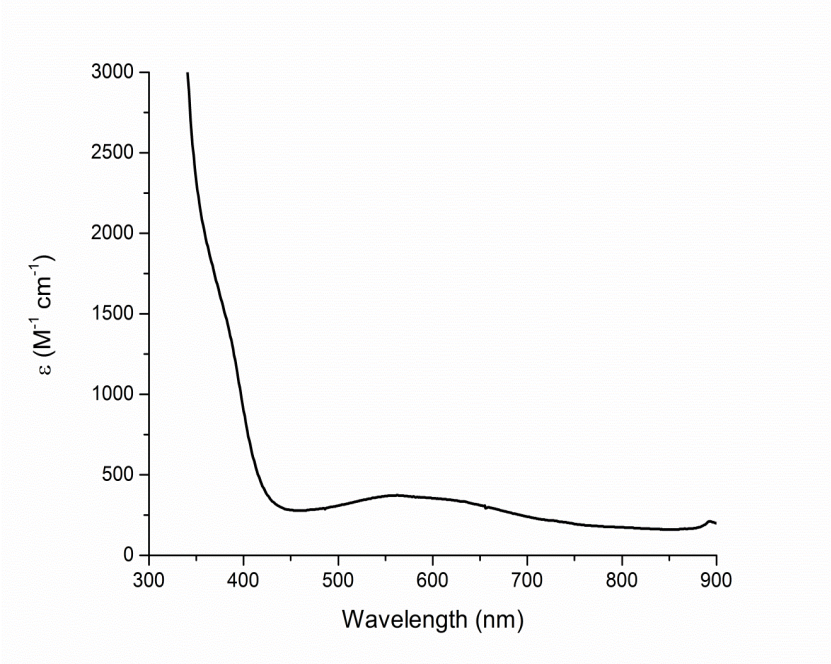

Figure 3-16: UV-Vis spectrum of 0.46 mM (Bu_4N)**7** in acetone measured at room temperature.

The FT-IR spectrum of (Bu_4N)**7** was measured in a Nujol mull in order to identify the hydroxide O-H stretching frequency (**Figure 3-17**). The spectrum exhibits a weak, yet sharp peak in the hydroxide stretching region at 3614 cm^{-1}, which is similar to the reported value for (Bu_4N)**2** (υ = 3628 cm^{-1}).[123] The sharpness of the O-H peak suggests that the hydroxide moiety is not engaged in hydrogen-bonding.

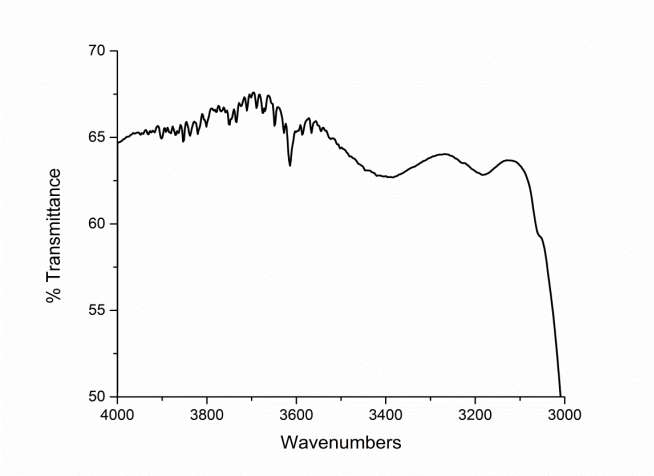

Figure 3-17: Enlarged high energy region of the FT-IR spectrum of (Bu_4N)**7** measured in a Nujol mull, where a sharp hydroxide peak ($\upsilon = 3614\ cm^{-1}$) is observed.

When electrochemical measurements (cyclic voltammetry) were performed on (Bu_4N)**7** in acetone, the voltammogram indicated the reduction was not completely reversible as evidenced by the reduced amplitude of the return wave (**Figure 3-18**). Neither altering the scan rate nor utilizing 1,2-difluorobenzene as a solvent improved the observed voltammograms. In contrast, (Bu_4N)**2** exhibits a reversible redox event when measured in acetone ($E_{1/2} = -0.076$ V vs Fc^+/Fc).[123]

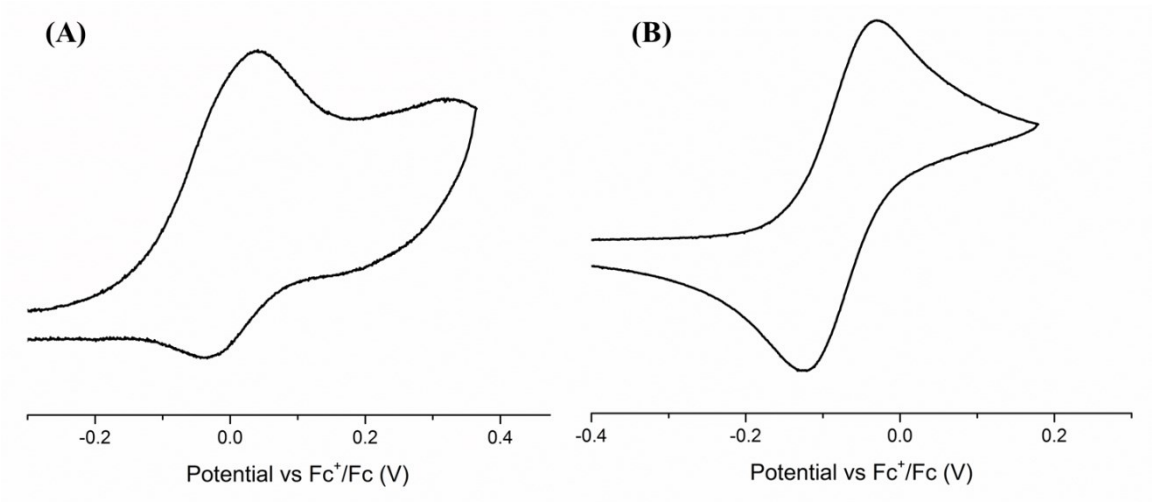

Figure 3-18: Cyclic voltammogram of (A) (Bu_4N)**7** in 0.2 M Bu_4NPF_6 in acetone, scan rate 200 mV/s and (B) (Bu_4N)**2** in 0.2 M Bu_4NPF_6 in acetone, scan rate 100 mV/s.

The E_{pa} values for (Bu_4N)**7** (E_{pa} ~ 0.037 V Vs Fc^+/Fc) and (Bu_4N)**2** (E_{pa} ~ 0.030 V Vs Fc^+/Fc) are similar, which is in agreement with the UV-Vis and EPR measurements that suggest that (Bu_4N)**2** and (Bu_4N)**7** are electronically similar. The reduced amplitude of the return wave for (Bu_4N)**7** suggests that the oxidized species (**7'**) is chemically reactive on the CV time scale. The observation of the less intense reduction wave of **7'** is consistent with less sterically protected copper center being more chemically reactive compared to the more sterically hindered **2'**.

3.3.3 Synthesis and Characterization of a [Copper(II)-Cl]$^{1-}$ Complex

Due to diminished steric protection around the copper center, there were concerns that dimerization may occur that may lead to the formation of bridged dicopper species. Owing to the difficulty in obtaining a crystal structure of **6** or (Bu_4N)**7**, the synthesis of (Ph_4P)**8** was carried out in order to obtain a solid state structure (**Scheme 3-5**). In addition, characterization of the chloride complex was prudent due to previous studies that indicated the metathesis of (Bu_4N)**2** with PPNCl led to chloride contamination in the crystalline lattice (see Appendix A for more details).[123]

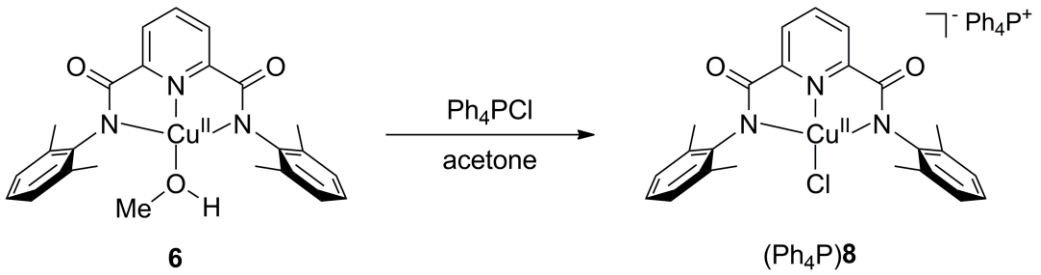

6 (Ph_4P)**8**

Scheme 3-5: Synthetic route for the preparation of (Ph_4P)**8** from **6**.

The resulting copper(II)-chloride complex (Ph_4P)**8** was isolated as a dark green powder and characterized by elemental analysis, ESI-MS, EPR spectroscopy, UV-Vis

spectroscopy, and single crystal X-ray spectroscopy. The crystal structure of (Ph_4P)**8** revealed a monocopper(II)-chloride complex with the copper atom in a square planar environment (**Figure 3-19**).

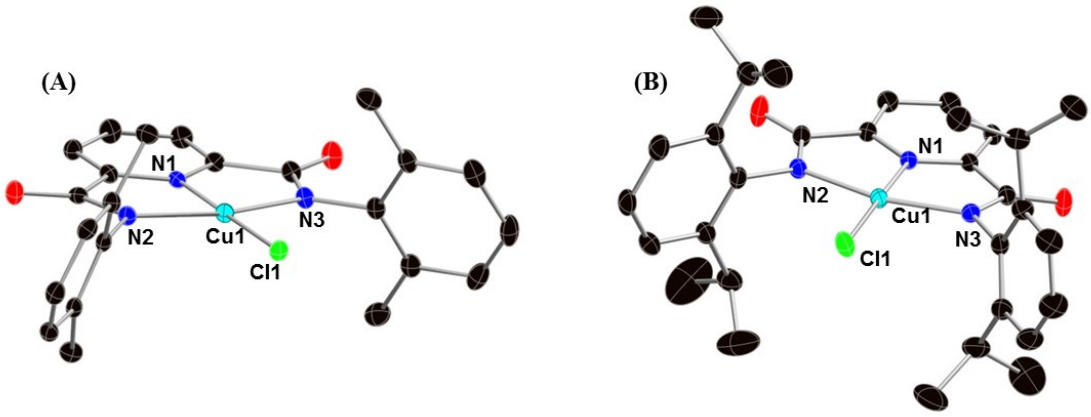

Figure 3-19: Representation of the cationic portion of the X-ray crystal structures of (A) (Ph_4P)**8** and (B) (Ph_4P)**3** with thermal ellipsoids drawn at 50% and hydrogen atoms omitted for clarity. For (Ph_4P)**8**: Space group: P-1, R1 = 0.0460, wR2 = 0.1147. For (Ph_4P)**3**: Space group: $P2_1/n$, R1 = 0.0626, wR2 = 0.2012.

The square planar structure of (Ph_4P)**8** and (Ph_4P)**3** are very similar: both structures exhibit a monocopper species in a square planar environment. Further evidence for their similarity is exhibited by the similar bond lengths and angles (**Table 3-2**). The (Ph_4P)**8** and (Ph_4P)**3** structures have copper(II)-amide bond distances (2.002(3) – 2.013(3) Å) that are within the range reported in the International Tables for Crystallography for bonds of this type (2.026 Å (σ = 0.056)) .[217] In addition, both structures have copper(II)-pyridine bonds (1.930(3) and 1.924(2) Å) that are much shorter than the range reported for four coordinate copper−pyridine complexes (2.023Å (σ = 0.019)), [217] although they are longer than the copper-pyridine distance reported for the neutral copper(II)-CH_3CN complex, (**1**), (1.912(3)Å). The lengthening of the copper-pyridine bond for (Ph_4P)**8** and (Ph_4P)**3** is expected relative to **1** due to the increase in negative charge of the copper-chloride

complexes. The copper-chloride bond distances (2.202(1) and 2.2035(9) Å) are only slightly shorter than the reported range for four-coordinated copper(II)-chloride bond distance (2.246Å (σ = 0.032)).[217]

Table 3-2: Selected bond distances (Å) and angles (°) for (Ph_4P)**8** and (Ph_4P)**3**

	(Ph_4P)8	**(Ph_4P)3**
Cu1-Cl1	2.202(1)	2.2035(9)
Cu1-N1	1.930(3)	1.924(2)
Cu1-N2	2.013(3)	2.002(3)
Cu1-N3	2.013(3)	2.006(3)
N1-Cu1-Cl1	179.64(8)	178.39(8)
N1-Cu1-N2	79.6(1)	80.3(1)
N1-Cu1-N3	80.6(1)	80.1(1)
N2-Cu1-N3	160.2(1)	160.4(1)
N2-Cu1-Cl1	100.57(8)	99.82(8)
N3-Cu1-Cl1	99.23(8)	99.81(8)

The ESI-MS of (Ph_4P)**8** is in agreement with the formulation of a monocopper(II)-chloride complex and the simulated isotope pattern is in good agreement with the experimental spectrum (**Figure 3-20**).

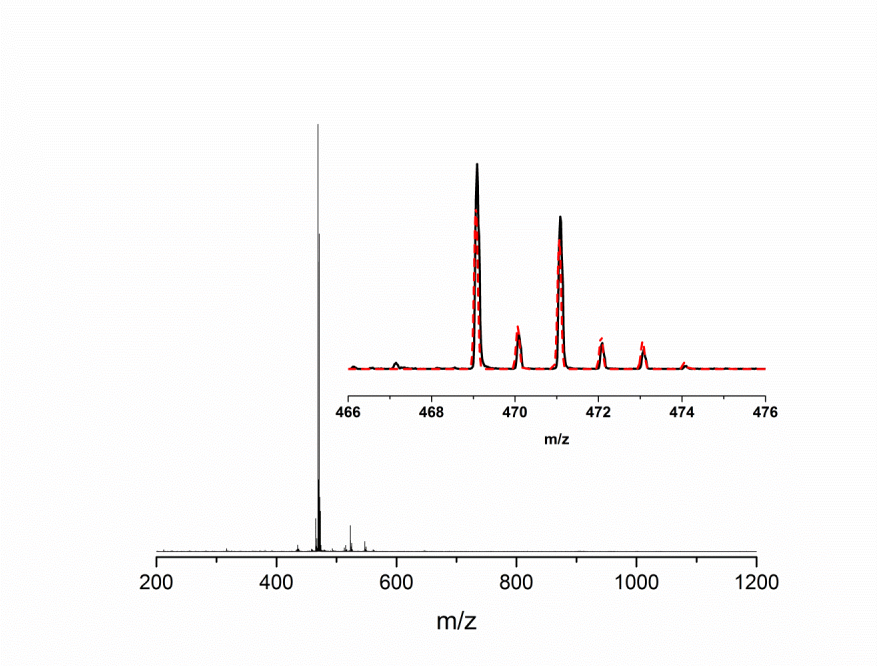

Figure 3-20: ESI-MS spectrum of (Ph_4P)**8** with the experimental spectrum of the parent ion (bold) and the simulated spectrum (dashed).

In addition, the EPR spectrum of (Ph_4P)**8** displays rich copper and nitrogen superhyperfine coupling and was satisfactorily simulated (**Figure 3-21**).

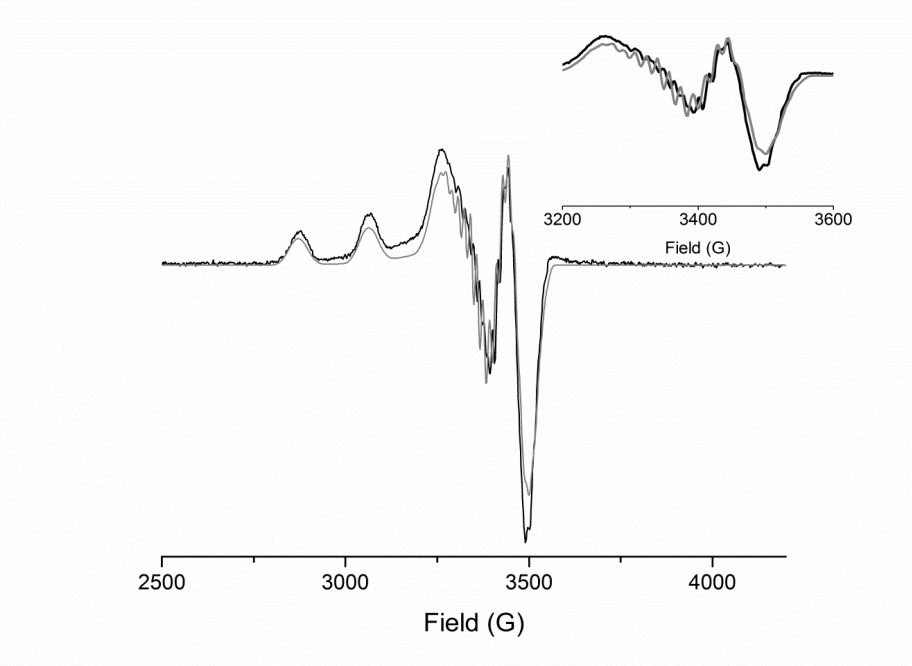

Figure 3-21: EPR spectrum of (Ph_4P)**8** in 3:1::toluene:acetone with the experimental spectrum (black) and simulated spectrum (grey).

The simulated spectrum for (Ph_4P)**3** is in good agreement with the measured spectrum (g_x = 2.026, g_y = 2.062, g_z = 2.182) with a large copper hyperfine coupling value (A(Cu) = 195 x10^{-4} cm^{-1}), and an average nitrogen superhyperfine coupling constant ($A(N\text{-}Cl_{av})$ = 15.3 x 10^{-4} cm^{-1}). The nitrogen superhyperfine was modeled as an average value an included the chloride as they have the same nuclear spin (I =1). Attempts to simulate with separated amide nitrogen, pyridine nitrogen, and chloride superhyperfine did not improve the simulation. These values are similar to the values measured for (Bu_4N)**3**: g_x = 2.016, g_y = 2.054, g_z = 2.177, A(Cu) = 195 x10^{-4} cm^{-1}, $A(N_{am})$ = 18.2 x10^{-4} cm^{-1}, $A(N_{py})$ = 15.3 x10^{-4} cm^{-1}, A(Cl) = 15.3 x10^{-4} cm^{-1}.[123] The average hyperfine coupling value for the nitrogen and chloride environments is 16.0 x10^{-4} cm^{-1}. It should be noted that the sample has different cations which may influence the spectra. The similarity of the two spectra is more obvious when the two spectra are overlaid (**Figure 3-22**). The nearly identical

features for (Ph_4P)**8** and (Bu_4N)**3** provides further evidence that the ligand modification has not significantly perturbed the electronic properties of the copper center.

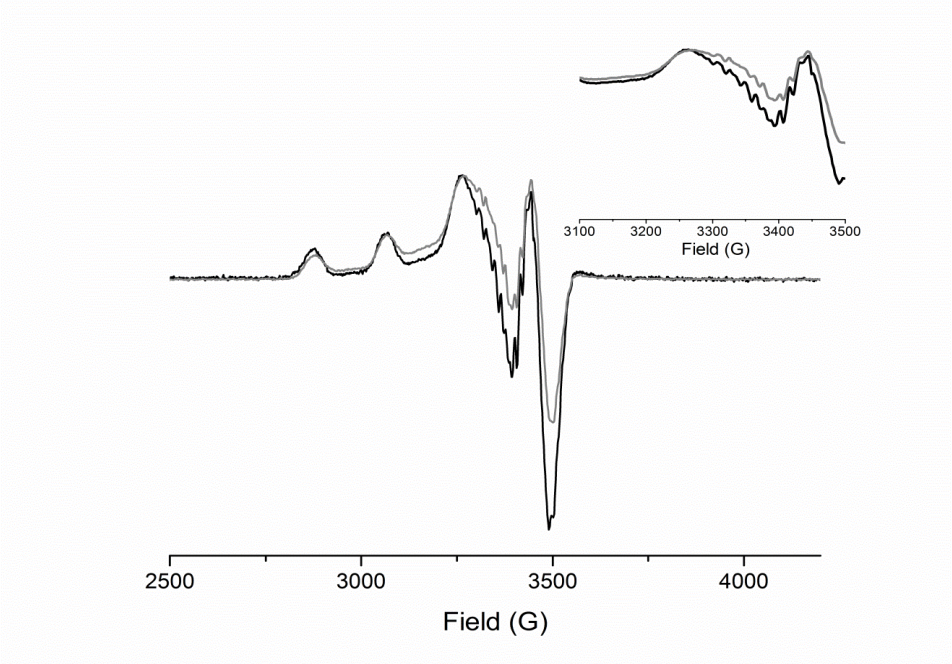

Figure 3-22: Overlay of the X-band EPR spectra of (Ph_4P)**8** (black) and (Bu_4N)**3** (grey). Both spectra were measure in 3:1::toluene:acetone at 10 K.

The UV-Vis spectrum of (Ph_4P)**8** was measured in acetonitrile and has a charge transfer band at 390 nm ($\varepsilon \sim 2{,}600\ M^{-1}cm^{-1}$) and a d-d band at 620 nm ($\varepsilon \sim 340\ M^{-1}cm^{-1}$) (**Figure 3-23**). This spectrum and the extinction coefficients are closely related the spectrum reported for (Bu_4N)**3**, with a band at 400 nm ($\varepsilon \sim 3{,}330\ M^{-1}\ cm^{-1}$) and 625 nm ($\varepsilon \sim 432\ M^{-1}cm^{-1}$) that was collected in acetone at −80 °C.[123]

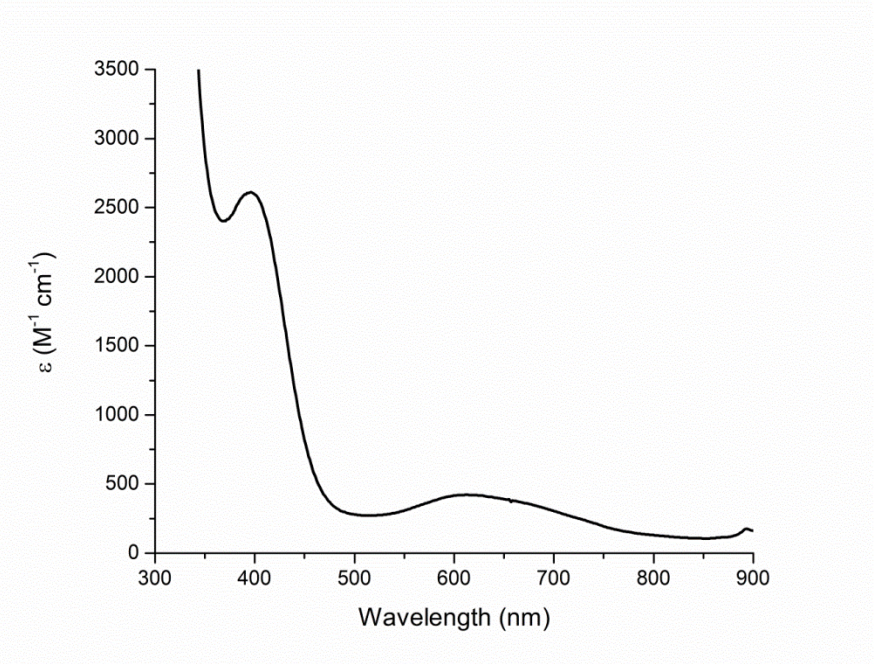

Figure 3-23: UV-Vis spectrum of 0.36 mM (Ph_4P)**8** in acetone measured at room temperature.

Reversible electrochemical oxidation of (Ph_4P)**8** was observed in cyclic voltammetry experiments (**Figure 3-24**). The oxidation potential ($E_{1/2}$ = 0.32 V vs Fc) of (P_h4P)**8** is at a much higher than the corresponding hydroxide complex, which can be oxidized by $Fc^+PF_6^-$. The potential is essentially identical to the previously reported copper(II)-chloride complex, (Bu_4N)**3** (($E_{1/2}$ = 0.30 V vs Fc).

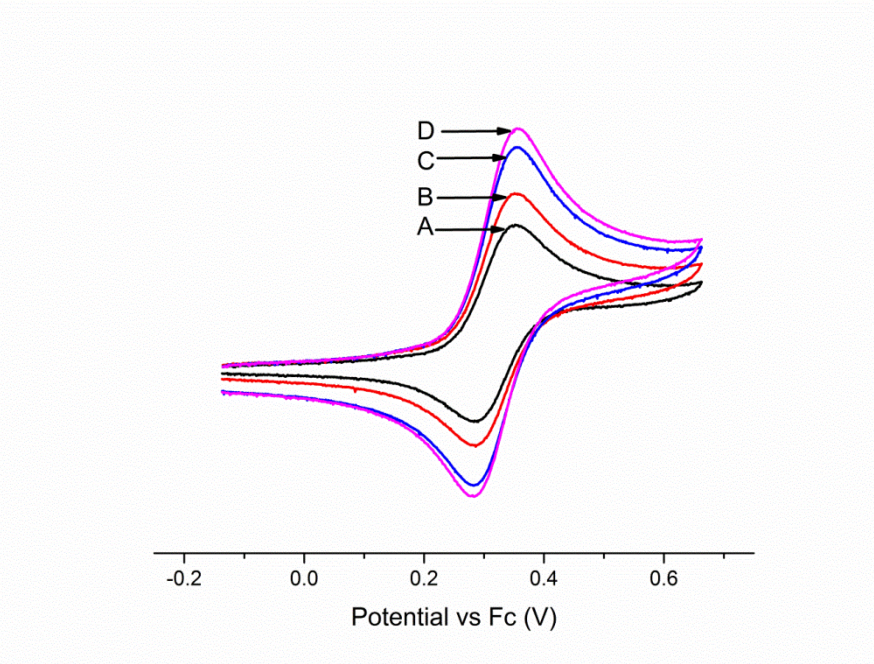

Figure 3-24: Cyclic voltammograms of 1mM (Ph_4P)**8** in 0.2 M Bu_4NPF_6 in acetone with varying scan rates. (A) 50 mV/s, (B) 75 mV/s, (C) 125 mV/s, (D) 150 mV/s.

3.3.4 Formation of a Copper(III)-OH Complex (7')

As the seminal copper(III)-hydroxide work with (Bu_4N)**2** was performed in acetone, (Bu_4N)**7** was oxidized by $Fc^+PF_6^-$ at −80 °C in acetone in an attempt to prepare the analogous copper(III)-hydroxide, **7'**. When the reaction was monitored by UV-Vis, the formation of an intense chromophore was observed (λ_{max} 560 nm, ε ~6,000 $M^{-1}cm^{-1}$), although with a lower extinction coefficient than the feature observed upon oxidation of (Bu_4N)**2** (λ_{max} 560 nm, ε ~10,000 $M^{-1}cm^{-1}$) (**Figure 3-25**).

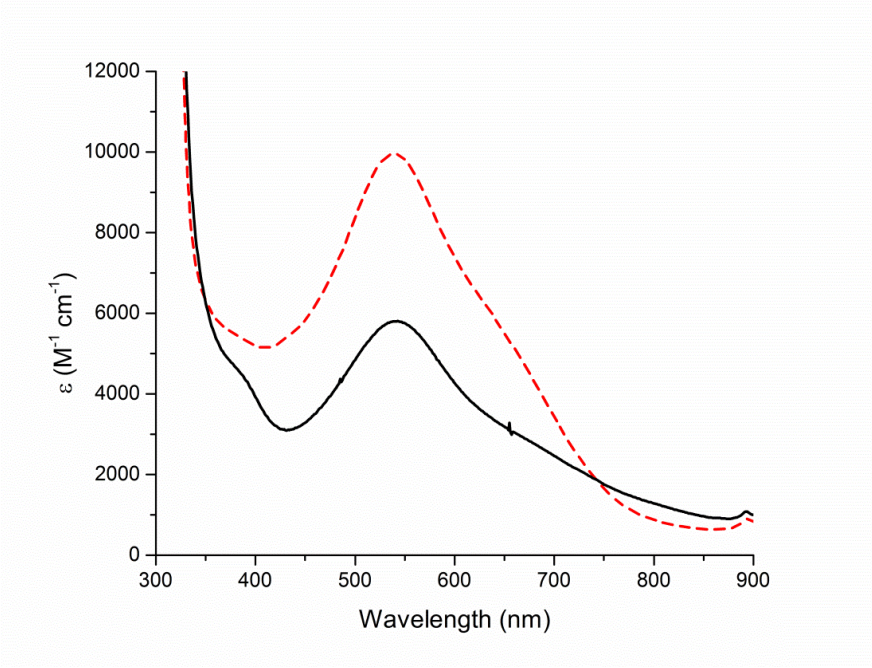

Figure 3-25: UV-Vis spectrum upon the addition of $Fc^{+}PF_6^{-}$ to 0.1 mM (Bu_4N)**7** (solid) and (Bu_4N)**2** (dashed) in acetone at −80 °C.

While the positions of the UV-Vis features of the oxidized species of (Bu_4N)**7** and (Bu_4N)**2**, **7'** and **2'** respectively, are similar, the marked decrease in intensity of **7'** compared to **2'** was unexpected. Due to the reduced steric protection of **7'**, we considered the possibility that the complex could be reacting with solvent (acetone). To investigate if the accessible C-H bonds in acetone were being attacked, the oxidations of (Bu_4N)**7** and (Bu_4N)**2** were carried out in acetone and d^6-acetone (**Figure 3-26**). The use of deuterated solvent did not significantly affect the formation of **2'**, yet a drastic increase in intensity was observed for the formation of **7'**. In addition, the observed yield for **7'** decreased with respect to the length of time since the distillation of the acetone, whereas no effect observed for the formation of **2'**. This suggests that **2'** is much more sensitive to solvent impurities, such as water formation due to the self-condensation reaction of acetone, than

7'. This sensitivity may be attributed to lack of steric protection around the copper center of **7'**, which increases the access of small molecules to the copper nucleus.

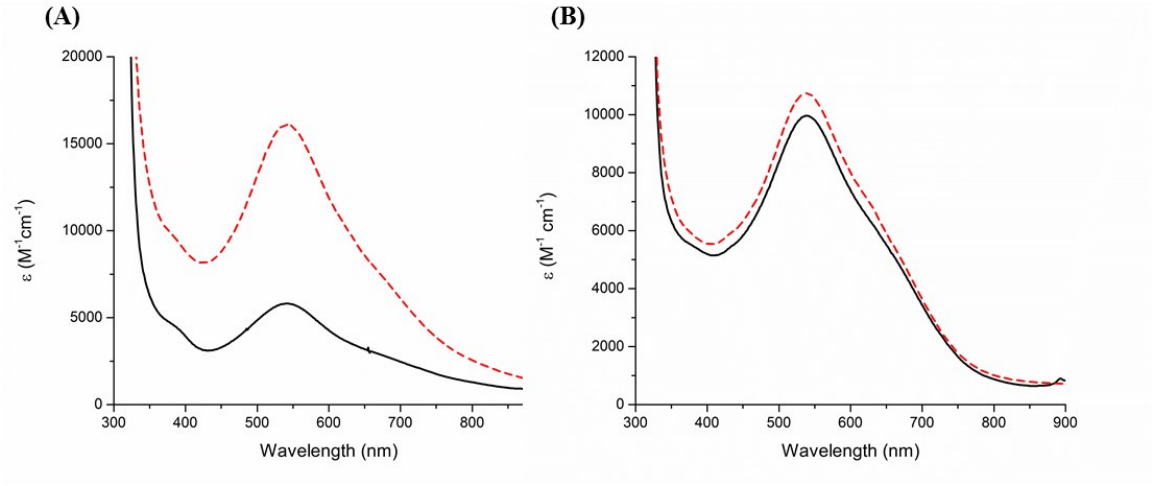

Figure 3-26: UV-Vis spectrum upon the addition of $Fc^{+}PF_6^{-}$ to 0.1 mM (A) (Bu_4N)**7** in acetone (solid) and d^6-acetone (dashed) at −80 °C; (B) (A) (Bu_4N)**2** in acetone (solid) and d^6-acetone (dashed) at −80 °C.

3.3.4.1 Self-decay of a Copper(III)-OH Complex

While the formation of **7'** was stunted by what appeared to be an interaction with acetone or impurities in the solvent, we investigated how the overall decay rate of **7'** compared with **2'**. All self-decay reactions were performed at −80 °C in acetone and were analyzed by following the loss of the chromophore at 560 nm, which corresponds to the copper(III)-hydroxide complex. Both reactions fit best to a first order decay process, although assessing the rate of self-decay for **7'** in acetone was difficult due to the rapid reaction rate (< 20 seconds) and difficulty obtaining reproducible rates of decay. It is unclear if **7'** is reacting with acetone, as acetone has a high bond dissociation enthalpy (BDE) of 98.3 kcal/mol (C-H bond at 298 K)[305,306] and a pK_a of ~19 (in water).[307]

The rapid self-decay of **7'** in acetone led us to seek a different polar solvent without any readily extractable C-H bonds. We chose to use 1,2-difluorobenzene due to its high polarity, lack of aliphatic C-H bonds, and a freezing point of −34 °C that allowed us to work at lower temperatures so that we could observe reactive intermediates. The oxidation of (Bu_4N)**2** and (Bu_4N)**7** by $Fc^+PF_6^-$ was achieved in 1,2-difluorobenzene, as formation of an intense chromophore (λ_{max} ~ 560 nm) was observed for both complexes (**Figure 3-27**). The two spectra are similar, although the spectrum of **2'** is more intense (ε ~ 12,000 $M^{-1}cm^{-1}$) than the spectrum of **7'** (ε ~ 7800 $M^{-1}cm^{-1}$).

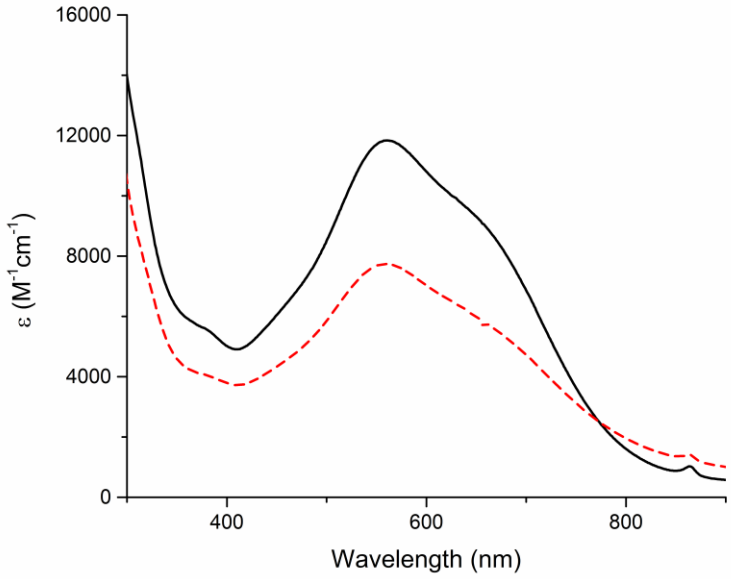

Figure 3-27: UV-Vis spectral overlay of the products arising from the oxidation of (Bu_4N)**2** (solid) and of (Bu_4N)**7** (dashed) with $Fc^+PF_6^-$ at −25 °C in 1,2-difluorobenzene.

The self-decay rates of **7'** and **2'** were assessed in 1,2-difluorobenzene at −25 °C. The self-decay of **7'** was rapid (< 2 min) in 1,2-difluorobenzene as evidenced by the complete decay of the intense chromophore at 540 nm (**Figure 3-28**). Although the self-decay of **7'** is rapid in 1,2-difluorobenzene, it is an order of magnitude less than the self-

decay rates measured in acetone at −80 °C. More importantly, the rates measured reproducible, unlike the measurements obtained in acetone.

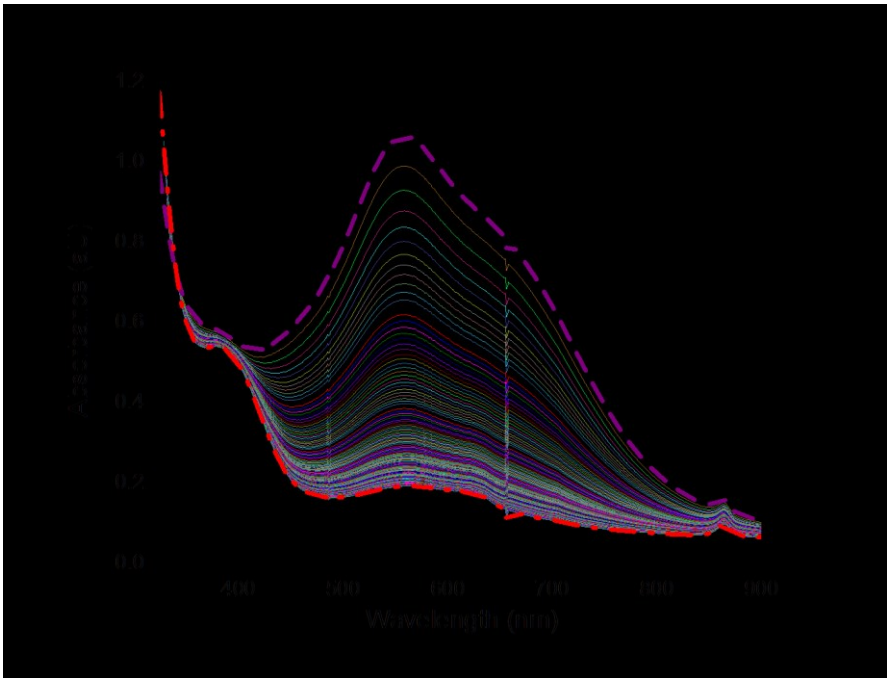

Figure 3-28: UV-Vis spectra of the formation of **7'** (bold dashed) upon addition of $Fc^{+}PF_6^{-}$ to (Bu_4N)**7** (bold solid) and subsequent decay to the product (bold dash-dot) at −25 °C. Intermediate spectra taken every second.

Due to the overlapping features of **7'** and the product, multi-wavelength analysis was used to deconvolute the spectra and extract kinetic information. The Olis GlobalWorks Software package was used to fit the data to multiple kinetic models, and the best fit was obtained for a first order process, $k = 3.6(2) \times 10^{-2}\ s^{-1}$. The first order model was selected based upon the similarity of calculated spectra to the experimentally obtained spectra and small residual error (**Figure 3-29**).

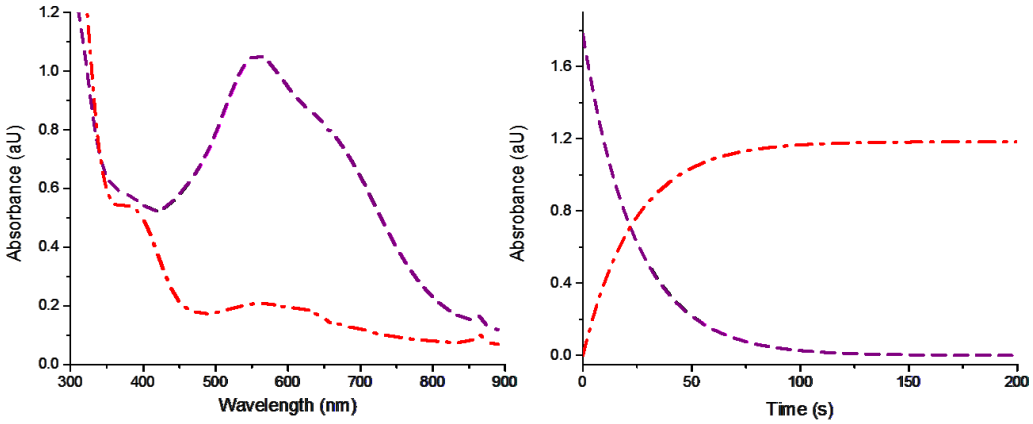

Figure 3-29: (Left) Calculated spectrum of the oxidized species, **7'** (dashed) and the product spectrum (dash-dot); (Right) Calculated reaction progress of the calculated spectra throughout the time course of the reaction, where the spectrum for **7'** is decaying (dashed) and the product spectrum in increasing (dash-dot).

To compare the stability of **7'** to the more sterically encumbered **2'**, the oxidation of (Bu_4N)**2** was performed under identical conditions (−25 °C in 1,2-difluorobenzene). The formation of intense chromophore at 540 nm was observed upon formation of **2'**, although the chromophore decayed significantly more slowly than **7'**(**Figure 3-30**).

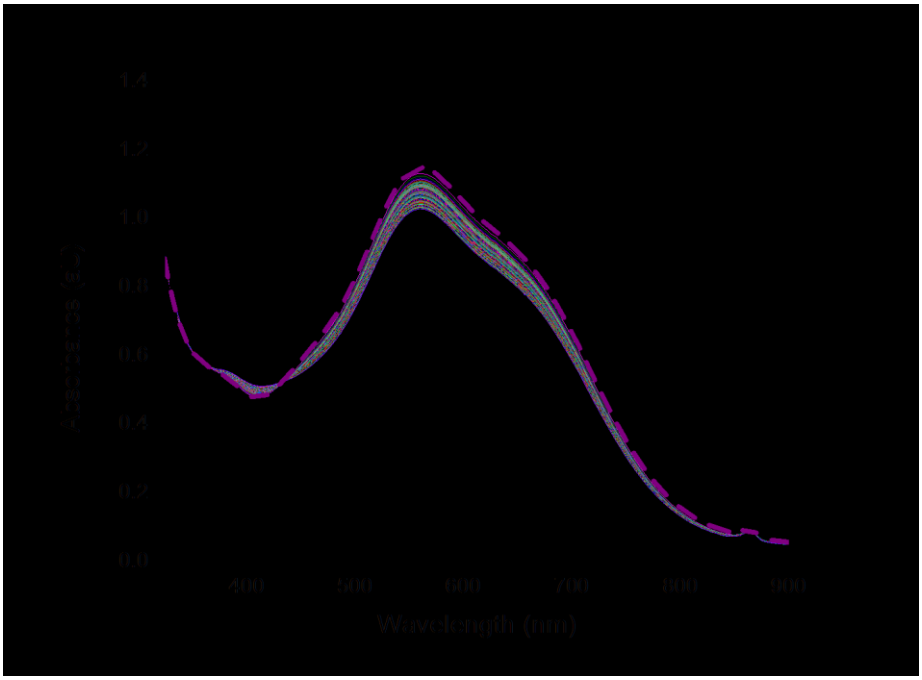

Figure 3-30: UV-Vis spectra of the formation of **2'** (bold dashed) upon addition of $Fc^{+}PF_6^{-}$ to (Bu_4N)**2** (bold solid) and subsequent decay to the product (bold dash-dot) at −25 °C. Intermediate spectra were taken in 30 seconds intervals.

The decay rate of **2'** in 1,2-difluorobenzene was prohibitively slow to measure the full decay of the species (~ 10% decay in 75 minutes) so the half-life was extrapolated from the initial decay measurement over the time span of 1.5 hours. The half-life (~ 2.1 $x10^6$ seconds) was then used to calculate the rate constant using the half-life equation for first order reactions ($t_{1/2} = \ln(2) / k$) to give, $k = 3.3 \times 10^{-7}$ s^{-1}. The self-decay rate constant for **2'** is five orders of magnitude less than the self-decay rate constant of **7'** in 1,2-difluorobenzene.

The self-decay pathway for **2'** leads to the formation of the corresponding copper(II)-aquo complex, as determined by the similar spectral features of the decay product of **2'** with the independently synthesized copper(II)-aquo complex, **12**.[123] The decay product of **7'** bears similar spectral features to that of **12**, suggesting **7'** and **2'** create the same decay product (**12**). In the absence of substrate, our current hypothesis is that the oxidized

species (**2'** or **7'**) attacks the tetrabutylammonium counterion, which has susceptible aliphatic C-H bonds. Precedence for this type of attack on tetrabutylammonium ion has recently been observed in aluminum-oxo chemistry.[308] The large difference in stability of **2'** and **7'** suggests that **7'** may be more readily accessible to substrate than **2'**, which led us to assess if this decreased stability might lead to enhanced reactivity with substrates containing weak C-H bonds.

3.3.4.2 **Reactivity towards Weak C-H Bonds**

Previously, **2'** has demonstrated the ability to perform rapid H-atom abstraction from 9,10-dihydroanthracene (DHA) at low temperatures in acetone.[123] We aimed to investigate if the decreased steric protection of **7'** would influence the rate of C-H bond activation from DHA. We elected to use 1,2-difluorobenzene as our solvent because the self-decay rate of **7'** is slower and more reproducible than reactions performed in acetone. By selecting 1,2-difluorobenzene as the solvent for these reactions, we extended the life-time of **7'** in order to give it an opportunity to react with the substrate (DHA) more rapidly than its self-decay pathway.

In order to compare the C-H bond activation rates of **2'** and **7**', their reactions must be measured in the same solvent. As acetone was not suitable for measurements with **7'**, the rates of reactions of **2'** and **7'** with DHA were monitored by UV-Vis in 1,2-difluorobenzene. The reaction of **2'** with DHA was monitored by UV-Vis spectroscopy under pseudo-first order conditions. In the experiment, (Bu_4N)**2** and 17 equivalents DHA were added to a cuvette and cooled to −25° C. Subsequent addition of one molar equivalent of Fc^+PF6^- resulted in the immediate formation of an intense chromophore, associated with the formation of **2'**, which began to decay rapidly while peaks

corresponding to the formation of anthracene (358 and 378 nm, marked with asterisks) began to increase in intensity (**Figure 3-31**). The reaction was monitored until no further spectral changes were observed (~100 seconds).

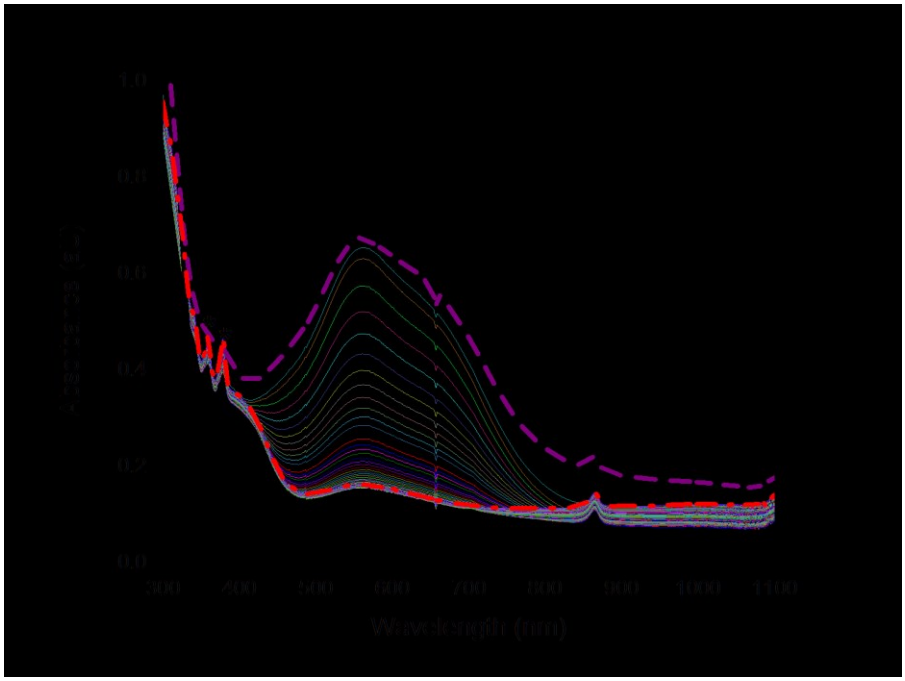

Figure 3-31: UV-Vis spectra of the formation of **2'** (bold dashed) upon addition of $Fc^{+}PF_6^{-}$ to (Bu_4N)**2** (bold solid) and subsequent decay to the product (bold dash-dot) at −25 °C. Intermediate spectra were taken every second. Note: asterisked peaks indicated the formation of anthracene.

Spectral deconvolution software was employed due to the overlapping features observed for **2'** and the product spectrum. The data were fit to many reaction types, although only a first order fit produced calculated UV-Vis spectra that were in good agreement with independently measured spectra (**Figure 3-34**). The reaction was rapid (k_{DHA} = 1.5 x10^2 M^{-1} s^{-1}) with a rate that was on-par with the rate of reaction of **2'** with DHA reported in acetone at the similar temperature of −30 °C (k_{DHA} = 2.4 x10^2 M^{-1} s^{-1}).

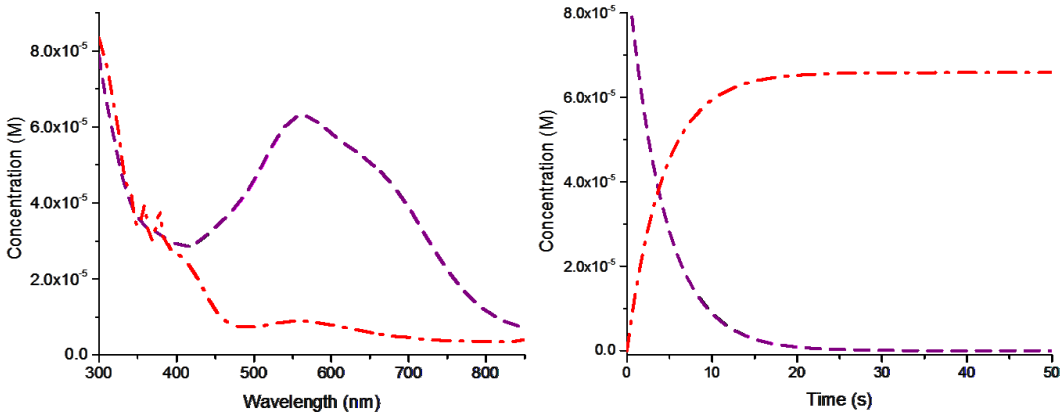

Figure 3-32: (Left) Calculated spectrum of the oxidized species, **2'** (dashed) and the product spectrum (dash-dot); (Right) Calculated reaction progress of the calculated spectra throughout the time course of the reaction, where the spectrum for **2'** is decaying (dashed) and the product spectrum in increasing (dash-dot).

The reaction of **7'** with DHA under pseudo-first order conditions was then monitored by UV-Vis spectroscopy under the same conditions as **2'** (17 equivalents of DHA, −25° C, 1,2-difluorobenzene). The chromophore associated with **7'** began to rapidly decay while two peaks (358 and 378 nm) corresponding to the formation of anthracene began to grow in intensity (**Figure 3-33**). The reaction was monitored in 0.5 second increments until no further spectral changes were observed (~100 seconds).

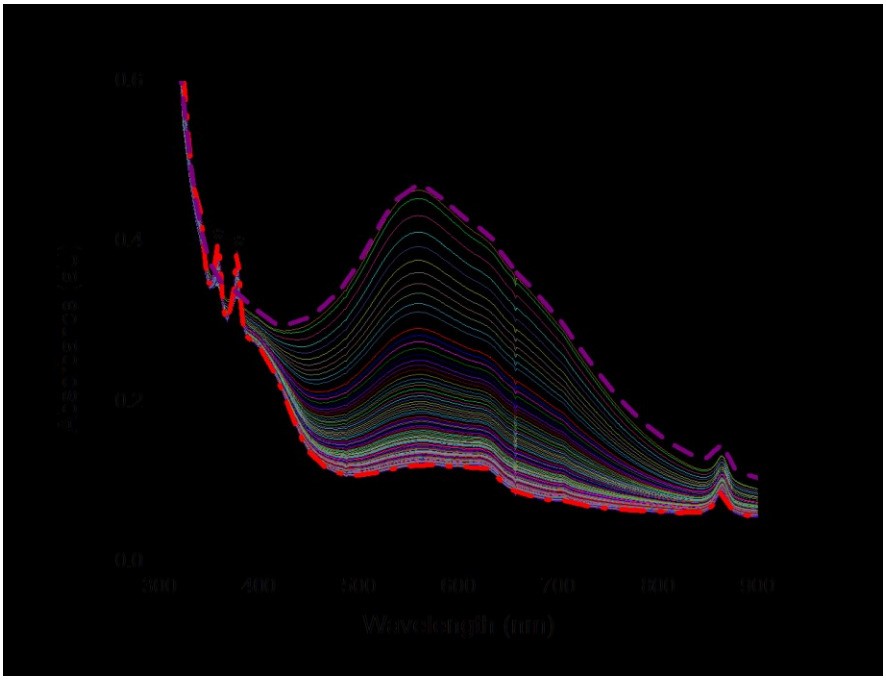

Figure 3-33: UV-Vis spectra of the formation of **7'** (bold dashed) upon addition of $Fc^{+}PF_6^{-}$ to (Bu_4N)**7** (bold solid) and subsequent decay to the product (bold dash-dot) at −20 °C. Intermediate spectra were taken every 0.5 seconds. Note: the asterisked peaks indicated the formation of anthracene.

In order to extract kinetic information from the reaction, the data was analyzed using a multi-wavelength spectral analysis. In this case, the data were fit to several kinetic models and it was determined that the observed rate was a composite of two first order processes: a self-decay reaction (k_{SD}) and a reaction with DHA (k_{DHA}). The rate constants for this reaction indicate that reaction of **7'** with DHA is more rapid (k_{DHA} = 1.3 x10^2 $M^{-1}s^{-1}$) than the self-decay of **7'** (k_{SD} = 0.039 s^{-1}), which is expected otherwise product (anthracene) formation would not be observed (**Figure 3-34**). In addition, the k_{SD} value matches the independently measured $k_{SD,}$ 0.036 s^{-1}, which provides further support for this kinetic model. In addition, the calculated spectra components are in good agreement with the independently measured spectral components.

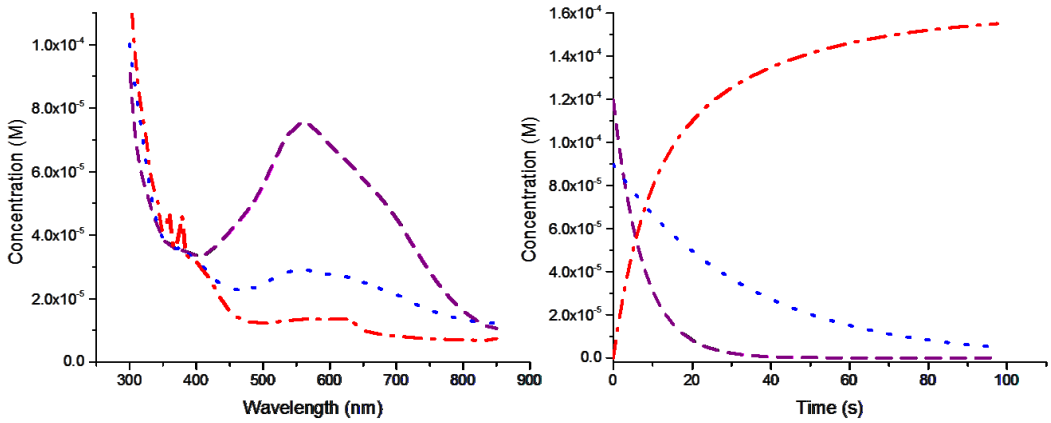

Figure 3-34: (Left) Calculated spectrum of the oxidized species, **7'** that reacts with DHA (dashed), spectrum of **7'** that performs the self-decay reaction (dotted), and the product spectrum (dash-dot); (Right) Calculated reaction progress of the calculated spectra throughout the time course of the reaction. The spectrum for the reaction of **7'** with DHA is decaying (dashed), the spectrum for the self-decay reaction of **7'** is decaying (dotted), and the product spectrum in increasing (dash-dot).

While the self-decay rates of **2'** and **7'** varied by five orders of magnitude, their rates of reactivity towards DHA are essentially identical (1.5 x10^2 $M^{-1}s^{-1}$ for **2'** and 1.3 x10^2 $M^{-1}s^{-1}$ for **7'**). This finding was surprising, as we initially believed the less sterically encumbered **7'** might react with DHA more rapidly than **2'**. What we discovered, however, is that the self-decay rate of **7'** is rapid enough to compete with rate of reaction with DHA. In order to investigate the C-H bond activating potential of **7'** towards substrates with stronger C-H bonds, it is critical to select a cation and solvent system combination that lacks accessible C-H bonds. If the self-decay pathway for **7'** can be shut down or significantly slowed, further studies can assess the reactivity of **7'** towards substrates with stronger C-H bonds.

3.3.5 Investigation of Cation Effects on the Stability of [Copper(III)-OH] Complexes

The self-decay reactions suggested that the reactive copper(III)-hydroxide may be attacking the tetrabutylammonium counterion. In order to investigate if attack on the counterion was occurring, we synthesized copper(II)-hydroxide complexes with a tetramethyl counterion (Me_4N), which does not contain any extractable methylene ($-CH_2$) bonds. Both (Me_4N)**7** and (Me_4N)**2** were synthesized in an analogous fashion to their tetrabutylammonium counterparts. Replacing the tetrabutylammonium with tetramethylammonium significantly decreased the solubility of the complexes in organic solvents, which limited our solvent choice to dimethylformamide (DMF). The oxidation of (Me_4N)**7** and (Bu_4N)**7** was monitored by UV-Vis spectroscopy and carried out under identical conditions (1 mM, −40 °C in DMF) (**Figure 3-35**). Unfortunately, there was no formation of an intermediate detected when the reaction was monitored for several minutes.

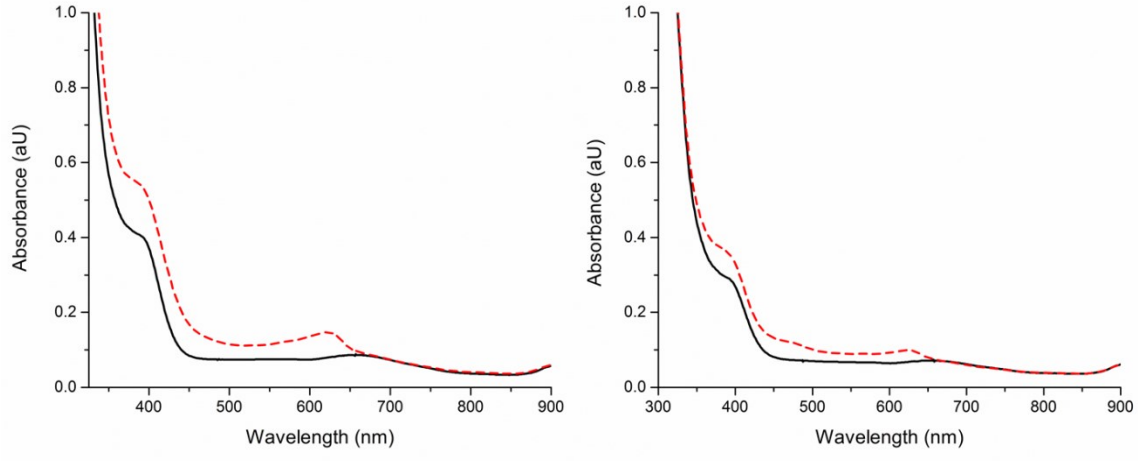

Figure 3-35: (Left): UV-Vis spectrum of (Bu_4N)**7** (solid) at −40 °C and the spectrum after addition of 1 equivalent of $Fc^+PF_6^-$ (dashed) in DMF. (Right): UV-Vis spectrum of (Me_4N)**7** (solid) at −40 °C and the spectrum after addition of 1 equivalent of $Fc^+PF_6^-$ (dashed) in DMF.

When the more sterically hindered (Bu_4N)**2** was assessed under identical conditions, a short-lived intermediate was observed (λ_{max} ~ 545 nm) (**Figure 3-36**). The species decayed rapidly (< 200 s) , which may be why no intermediate was observed with the less sterically hindered (Me_4N)**7** and (Bu_4N)**7**.

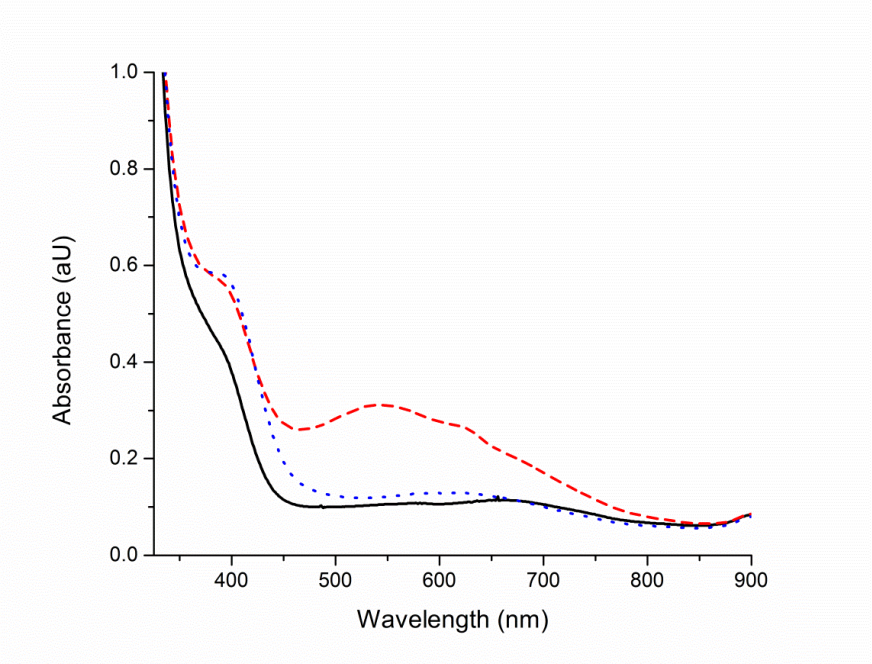

Figure 3-36: UV-Vis spectrum of (Bu_4N)**2** (solid) at −40 °C, the spectrum after addition of 1 equivalent of $Fc^+PF_6^-$ (dashed) and the resulting spectrum after decay of the intermediate (dotted) in DMF.

As no intermediate was observable for (Bu_4N)**7** in DMF, further studies should focus on the synthesis of cations that lack easily extractable C-H bonds, and will increase the solubility in non-coordinating polar organic solvents.

3.3.6 Determination of the pK_a of the Copper(II)-OH_2 Species

The rapid reaction of **2'** and **7'** with C-H bonds in DHA led us to investigate the thermodynamics of this reaction. Formally, this reaction is a hydrogen atom transfer (HAT) reaction, which can be viewed as occurring via a concerted or stepwise process

(**Scheme 3-6**). The large kinetic isotope effect (k_H/k_D ~29 at 25 °C) measured for the H-atom abstraction of DHA by **2'** suggests there is a tunneling contribution for this reaction, as this is beyond the semiclassical limit ($k_H/k_D < 7$). [123]

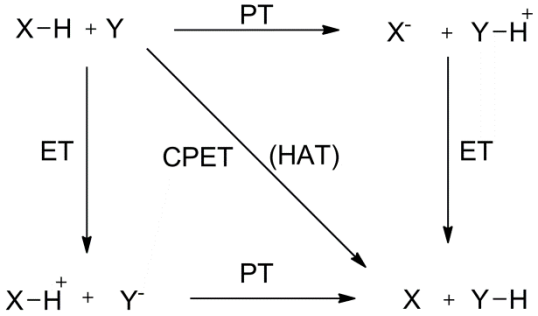

Scheme 3-6: Pathways for H-atom transfer (HAT) than include stepwise electron transfer and proton transfer pathways as well as the concerted proton/electron transfer (CPET) pathway. PT = proton transfer, ET = electron transfer.

We aimed to find the bond dissociation free energy (BDFE) for the reaction of the copper(II)-hydroxide to form the copper(II)-aquo species (**Figure 3-37**). Obtaining information about the BDFE of our complex would enable a more direct comparison to other complexes in the literature, without the compounding entropic effects associated with measuring BDEs (bond dissociation enthalpies).[309,310]

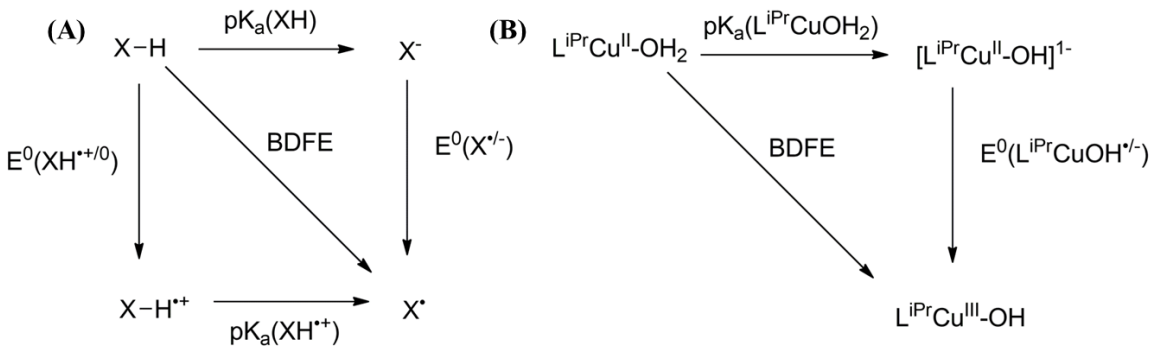

$$BDFE_{sol}(C-H) = 1.37pK_a + 23.06E^0 + C_{G,sol}$$

Figure 3-37: (A): General scheme for routes to determine the bond dissociation free energy (BDFE) of a reaction involving the dissociation of a C-H bond; (B): Specific route for the determination of the BDFE for the reaction of **2'** to form **12** ($L^{iPr}Cu\text{-}OH_2$). Figure adapted from [310].

We chose to focus on the determination of the pK_a of **12** because both **12** and (Bu_4N)**2** are synthetically accessible and have been well characterized. The BDFE can then be calculated according the formula presented in **Figure 3-37**, where the pK_a and E^0 (typically $E_{1/2}$ is used from CV) are experimentally determined for the desired compound and $C_{G,sol}$ is a solvent correction value that is equivalent to the H^+/H^- standard reduction potential in a given solvent.[310] As this correction value is solvent dependent, it is important that the electrochemical and pKa measurements are carried out in the same solvent. Unfortunately, only a handful of organic solvents have measured C_G values. The limited availability of C_G values limited our choice of solvent to either acetonitrile or tetrahydrofuran.

The next important step for establishing the conditions to use for pK_a determination was selecting a suitable strong base/weak acid pair that is non-coordinating and non-nucleophilic. Two routes can be envisioned for determining the pK_a of **12**: Route

A, deprotonating **12** with a strong base, or Route B, protonating (Bu_4N)**2** with a weak acid (**Scheme 3-7**).

Route A:

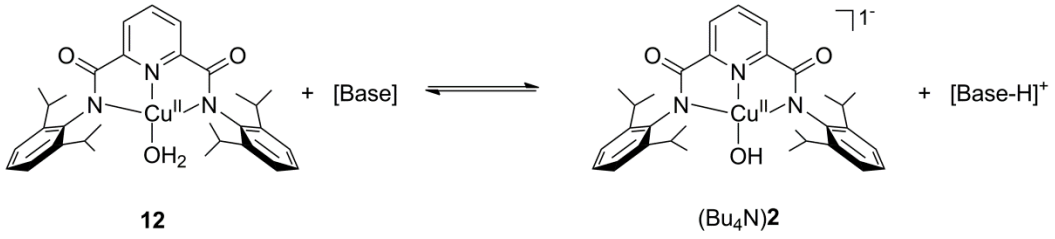

12 (Bu_4N)**2**

Route B:

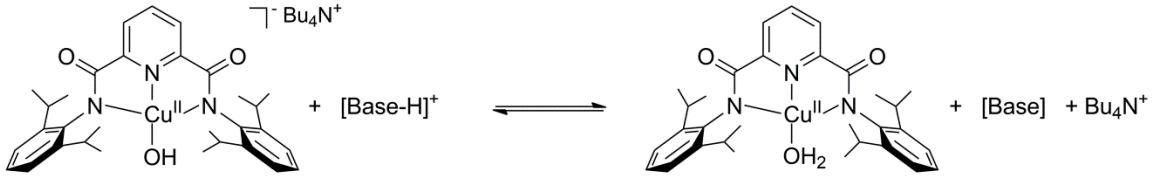

(Bu_4N)**2** **12**

Scheme 3-7: (Top): Route A: Strategy for determining the pK_a by adding a base to deprotonate **12** and generate $\mathbf{2}^-$ and the conjugate base. (Bottom): Route B: Protonation of (Bu_4N)**2** with a weak acid ($[Base\text{-}H]^+$) to generate **12** and the free base.

Either route should allow us to establish an equilibrium between all of the species in solution, which would enable us to calculate the pK_a of **12** using the equation presented in **Figure 3-38**. In order to calculate the pK_a of **12**, the pK_a(Reaction) is measured experimentally by determining the ratios of each species in solution, using the known pK_a (Base) in the given solvent. After consulting tables of established pKa values in acetonitrile and tetrahydrofuran, we selected triethylamine (Et_3N) and proton sponge (PS = 1,8-Bis(dimethylamino)naphthalene). Both have similar values in acetonitrile, 18.82 for Et_3N and 18.62 for PS, but are significantly different in tetrahydrofuran, 14.1 for Et_3N and 11.7 for PS.[311,312]

Route B:

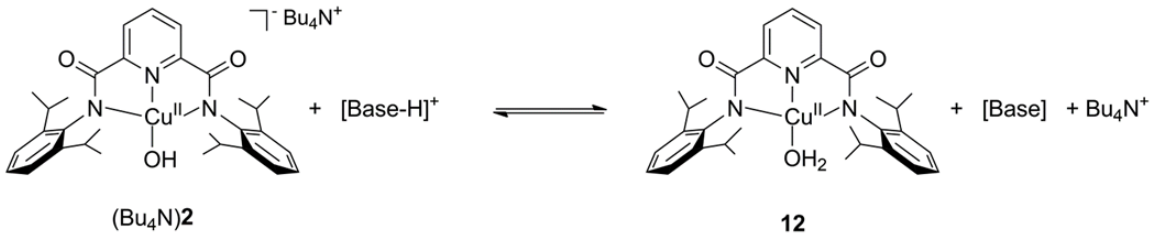

(Bu$_4$N)**2** **12**

$$\mathrm{K} = \frac{[LCuOH_2][Base]}{[LCuOH][Base-H]} = \frac{K_a(LCuOH_2)}{K_a(Base)}$$

$$pK_a(Reaction) = pK_a(LCuOH_2) - pK_a(Base)$$

Figure 3-38: Example of the equilibrium expression for Route B, and the resulting algebra that leads to the equation relating the pK_a values.

Due to the paramagnetic nature of copper(II), we could not monitor these reactions by NMR spectroscopy. Instead, we elected to monitor these reactions by UV-Vis spectroscopy. We first began investigating the pK_a of **12** in acetonitrile, by following Route B and protonating (Bu$_4$N)**2** with a weak acid, protonated proton sponge $(PSH)^+(OTf)^-$. This was achieved by adding 0.2 molar equivalents of $(PSH)^+(OTf)^-$ to a solution of 0.22 mM (Bu$_4$N)**2** in acetonitrile at 20 °C and allowing one minute to transpire for the system to equilibrate before each measurement. Each addition up to ~ 1.4 molar equivalents caused a shift in the d-d band region of the UV-spectrum (**Figure 3-39**).

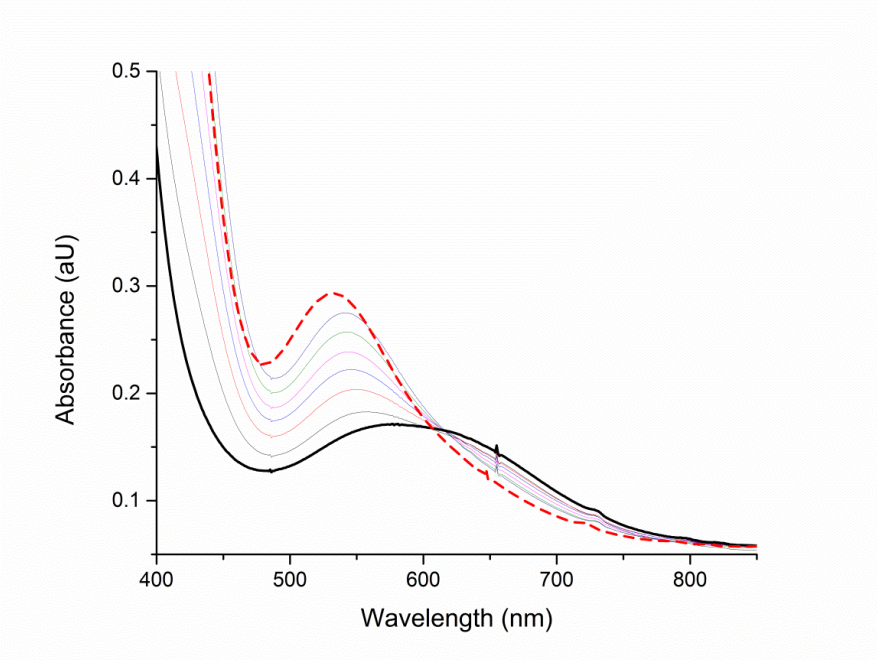

.

Figure 3-39: UV-Vis spectrum of (Bu_4N)**2** (bold solid) and the spectrum after addition of 1.4 equivalents of $(PSH)^+(OTf)^-$ (bold dashed). Intermediate spectra represent additions of 0.2 molar equivalence aliquots of $(PSH)^+(OTf)^-$.

While this result was initially encouraging, the final spectrum did not correlate with the intended product, **12**, but rather was identical to the spectrum of **1**. We interpret this finding to indicate that (Bu_4N)**2** is protonated by $(PSH)^+(OTf)^-$, but that the water ligand of **12** is readily displaced by the more strongly coordinating solvent, acetonitrile, to form **1** (**Scheme 3-8**).

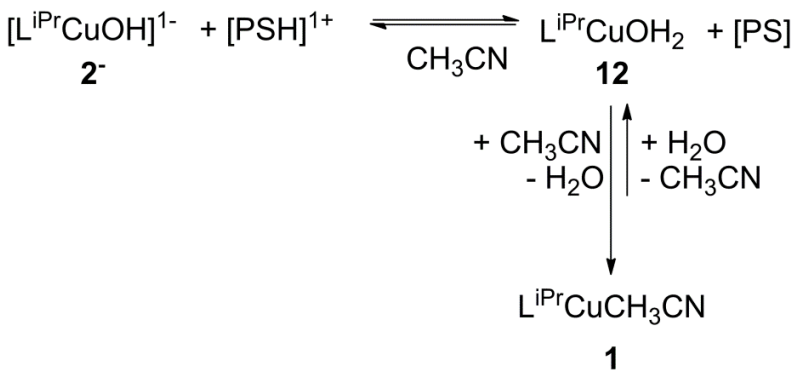

Scheme 3-8: Reaction scheme indicating the equilibrium between **2**$^-$ and **12** and the equilibrium between **12** and **1**.

Although an equilibrium arrow is drawn for the reaction of **12** with acetonitrile to form **1**, the reaction is essentially irreversible due to the concentration of acetonitrile being several orders of magnitude higher than water. This indicates we are no longer observing an equilibrium reaction and therefore cannot use this method to determine the pK_a of **12**. This experiment does provide us with a lower limit for the pK_a value of **12** in acetonitrile, as (Bu_4N)**2** was able to be protonated by $(PSH)^+(OTf)^-$.This indicates the pK_a value of **12** in acetonitrile must be less than the pK_a value of $(PSH)^+(OTf)^-$ in acetonitrile (18.62).

Due to the competing coordination of acetonitrile with our aquo ligand, we chose to use tetrahydrofuran as our solvent. Tetrahydrofuran is a much more weakly coordinating solvent when compared to acetonitrile and might not as readily displace our aquo ligand. We attempted the deprotonation of (Bu_4N)**2** in THF by adding sub-stoichiometric amounts of $(PSH)^+(OTf)^-$ and did not see the formation of any new species; only dilution of the (Bu_4N)**2** features was observed (**Figure 3-40**).

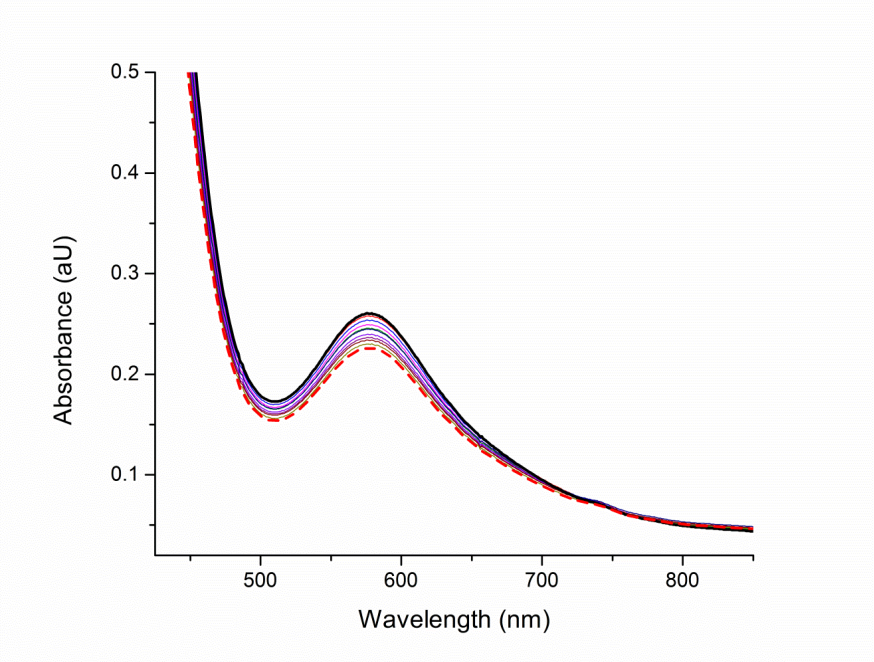

Figure 3-40: UV-Vis spectrum of 0.20 mM (Bu_4N)**2** (bold solid) and the spectrum upon 2.2 molar equivalents of $(PSH)^+(OTf)^-$ (bold dashed line). Intermediate spectra are 0.2 equivalents of $(PSH)^+(OTf)^-$.

As no new species were observed, this indicates that $(PSH)^+(OTf)^-$ is not a strong enough acid to protonate (Bu_4N)**2** in THF, so we cannot calculate a pK_a value for **12** based on these measurements. This experiment, however, does provide us with a lower limit for our pK_a of **12**, which must be greater than pK_a of PS in tetrahydrofuran (11.7). Further studies with stronger weak acids (protonated phosphazine-based compounds) are underway.

In order to calculate the BDFE for **12** we also need to identify the E^0 of (Bu_4N)**2** in the desired solvent. The E° value is often determined by the $E_{1/2}$ value obtained by cyclic voltammetry.[310] The cyclic voltammogram of (Bu_4N)**2** in tetrahydrofuran indicates irreversible redox events, although a reversible wave was obtained in 1,2-difluorobenzene (**Figure 3-41**).

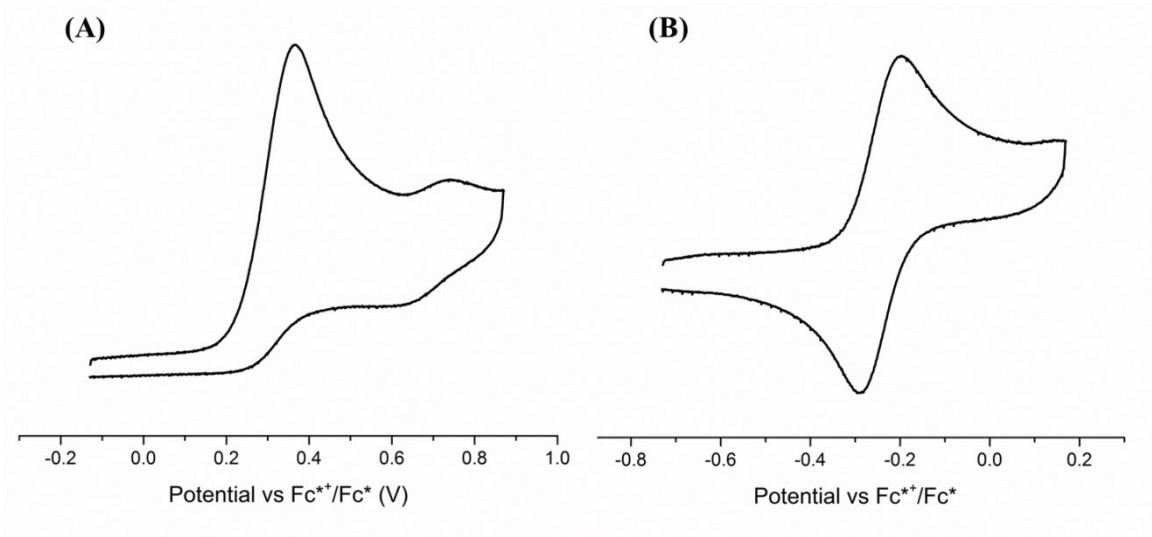

Figure 3-41: (A): Cyclic voltammogram of (Bu_4N)**2** in 0.3 M Bu_4NPF_6/ tetrahydrofuran with a scan rate of 100 mV/s, referenced to decamethylferrocene (Fc*). (B) Cyclic voltammogram of (Bu_4N)**2** in 0.3 M Bu_4NPF_6/ 1,2-difluorobenzene with a scan rate of 100 mV/s, referenced to decamethylferrocene (Fc*).

In tetrahydrofuran, the irreversible reduction of (Bu_4N)**2** led to estimation of the $E_{1/2}$ ~ 0.30 V vs Fc^{*+}/Fc (-0.145 V vs Fc^{+}/Fc). The $E_{1/2}$ was estimated by taking the mean of the anodic and catholic peaks. In contrast, when the cyclic voltammogram of (Bu_4N)**2** was measured in 1,2-difluorobenzene, a reversible wave was obtained $E_{1/2}$ ~ 0.42 Fc^{*+}/Fc (-0.025 V vs Fc^{+}/Fc). The $E_{1/2}$ value of (Bu_4N)**2** measured in acetone (-0.076 V vs Fc^{+}/Fc) is less than the potential measured in 1,2-difluorobenzene (-0.025 V vs Fc^{+}/Fc), which suggests that 1,2-difluorobenzene is more stabilizing of the copper(III) complex. While the $E_{1/2}$ of (Bu_4N)**2** measured in tetrahydrofuran (-0.145 V vs Fc^{+}/Fc) is also less than the potential measured in acetone, the irreversible wave obtained indicates that the copper(III) complex is less stable in tetrahydrofuran than in acetone.

3.4 Summary and Future Directions

The work described in this chapter has shown that small changes to the steric environment around a reactive copper(III)-hydroxide center can lead to differences in

stability. In particular, the self-decay rate of less sterically hindered (Bu_4N)**7** was found to be five orders of magnitude faster than the self-decay rate of (Bu_4N)**2**. On the other hand, the two complexes had nearly identical rates of reaction with 9,10-dihydroanthracene. Currently, the self-decay pathway is believed to involve attack of the copper(III)-hydroxide on the tetrabutylammonium counterion and is thought to be enhanced for (Bu_4N)**7** due to differences in steric protection. In order to extend the lifetime of the copper(III)-hydroxide in solution so that it may be able to attack more difficult C-H bonds, it would be prudent to select a different cation devoid of easily extractable C-H bonds and that has moderately soluble in common organic solvents. One can imagine bis(triphenylphosphoranylidene)ammonium hydroxide (PPNOH) could be a good candidate and could potentially be synthesized via a metathesis reaction with the corresponding chloride complex (PPNCl).

In addition, we have begun to explore the thermodynamics of the H-atom transfer to our copper(III)-hydroxide complex to form a copper(II)-aquo complex. With the goal of obtaining the bond dissociation free energy (BDFE) for this reaction, initial efforts focused on selecting the appropriate solvent system for these measurements. In order to calculate the BDFE, two experimental values must be determine: the pK_a of the copper(II)-aquo and copper(II)-hydroxide reaction, and the E° of the copper(II)-hydroxide/copper(III)-hydroxide redox event. The results from these efforts suggest tetrahydrofuran is the best candidate for measuring the pK_a value, although the use of stronger weak acid than the protonated-proton sponge is needed. The use of phosphazine bases may be fruitful for this endeavor as they are strong, non-nucleophilic bases.[311,313] The cyclic voltammetry measurements in tetrahydrofuran did not exhibit reversible

behavior, although the $E_{1/2}$ was estimated to be ~ -0.025 V vs Fc^+/Fc. These preliminary results suggest that the determination of the pK_a of the copper(II)-aquo complex is contingent on finding the appropriate base. Once this issue is resolved, calculation of the BDFE can be accomplished.

3.5 Experimental

General Considerations. All solvents and reagents were obtained from commercial sources and used as received unless otherwise noted. $L^{Me}H_2$ was prepared according to the literature procedure.[120] The solvents Et_2O and pentane were passed through purification columns (Glass Contour, Laguna, California) before use. Acetonitrile was dried over CaH_2, degassed, distilled under vacuum and stored over CaH_2 in a glovebox. Acetone was dried over 3Å molecular sieves, degassed, vacuum transferred and stored over 3Å molecular sieves in a glovebox. 1,2-Difluorobenzene was dried over CaH_2, degassed, distilled under vacuum and stored over 3Å molecular sieves in a glovebox. Anydrous DMF was stored over 3Å molecular sieves in a glovebox for 2 days and dried over a section portion of 3Å molecular sieves for an additional 2 days before use. All reactions of $LCu(CH_3OH)$ (**6**) were performed in glovebox under a dry N_2 atmosphere.

Physical Methods. NMR spectra were recorded on a 300 MHz Varian Inova spectrometer and cation resonances are omitted for clarity. UV-Vis spectra were recorded on an HP8453 (190-1100 nm) diode-array spectrophotometer equipped with a Unisoku low-temperature cryostat. Electrospray ionization mass spectra (ESI-MS) were recorded in negative ion mode on a Bruker BioTOF II instrument. Electron paramagnetic resonance (EPR) spectra were recorded a Bruker Continuous Wave EleXsys E500 spectrometer at 10 K. EPR simulations were achieved by using Bruker Simfonia

software. Infrared spectra were collected on a Nicolet Avatar 370FT-IR Elemental analyses were performed by Robertson Microlit Laboratory (Ledgewood, New Jersey) and Compete Analysis Laboratories Inc (Parsippany, New Jersey). X-ray crystallography data collection and structure solution were conducted using a SMART Apex II instrument and the current SHELXTL suite of programs. All graphical representations utilized the Origin software program. Representations of single molecule crystals were obtained using CrystalMaker software. Graphical representations of protein molecules were made using PyMOL.

$L^{Me}Cu(MeOH)$ (6). $L^{Me}H_2$ (1.015 g, 2.72 mmol), anhydrous $CuCl_2$ (0.367 g, 2.73 mmol) and MeOH (100 mL) were added to a 250 mL round bottom flask to give a light green solution. Addition of a solution of NaOMe in MeOH (0.5 M, 9.2 mL, 4.6 mmol) yielded a deep forest green solution, which was stirred for 30 min. The solvent was removed *in vacuo* to give a green oil. This oil was dissolved in CH_3CN (~ 20 mL) and toluene (100 mL) was added, after which a precipitate formed and the solution became mahogany in color. The mixture was filtered through a fine porosity frit and solvent was removed from the filtrate *in vacuo* to produce a bright green powder. Subsequent washings with acetonitrile (3 x 5 mL) and hexanes (3 x 5 mL) afforded the product as a bright green solid, which was dried in the vacuum oven at 40 °C overnight (0.75 g, 69%). ESI-MS (CH_3OH, *m*/*z*): calcd 465.11 $[M+Na]^{1-}$, found 457.20. UV-Vis [λ_{max}, nm (ε, M^{-1} cm^{-1}) in CH_3CN]: 397 (1400), 545 (720). Anal. Calcd. for $C_{24}H_{25}CuN_3O_3$: C, 61.72; H, 5.40; N, 9.00. Found: C, 61.83; H, 5.29; N, 8.93.

$(Bu_4N)(L^{Me}CuOH)$ ((Bu_4N)7). To **6** (147 mg, 0.314 mmol) was added Et_2O (~ 10mL) to give a green reaction mixture. Upon the addition of Bu_4NOH in MeOH (1.0 M, 0.31 mL,

0.31 mmol) a blue sticky precipitate formed. The reaction was stirred for ~5 min and the solvent was removed *in vacuo* to give a dark blue oil. The oil was washed with Et_2O (3 x 5 mL) to yield the product as a bright blue-purple solid (129 mg, 85%). UV-Vis [λ_{max}, nm (ε, M^{-1} cm^{-1}) in acetone]: 378 (1800), 550 (230). Anal. Calcd. for $C_{39}H_{58}CuN_4O_3$: C, 67.45 H, 8.42; N, 8.07. Found: C, 66.86; H, 8.15; N, 8.02. EPR (10 K): $g_x = 2.02$, $g_y = 2.06$, $g_z = 2.19$; A values (x 10^{-4} cm^{-1}): A(Cu) =192, A(N_{py}) =18.2, A (N_{am}) =13.5.

(Ph4P)(LCuCl) ((Ph$_4$P)8). A suspension of Ph4PCl (54.6 mg, 0.146 mmol) in acetone (4 mL) was added drop-wise to a mahogony solution of compound 5 (68.0 mg, 0.146 mmol) in acetone (10 mL). The resulting deep emerald green solution was stirred for ~10 minutes. The solvent was removed in vacuo to yield a dark green residue. The residue was triturated with Et2O (4 x 5 mL) until a fine green precipitate was observed. Residual solvent was removed in vacuo to give a bright green powder (87.6 mg, 75.8%). ESI-MS (CH3OH, m/z): calcd 469.06 $[M\text{-}Ph4P]^{1-}$, found 469.09. UV-Vis [λ_{max}, nm (ε, $M^{-1}cm^{-1}$) in CH_3CN]: 390 (2600), 620 (340). EPR(1:3-acetone:toluene, 10 K): $g_x = 2.026$, $g_y = 2.062$, $g_z = 2.182$; A values (x10^{-4} cm^{-1}): A (Cu) =195, A(N) =15.3. Anal. Cald. for $C_{47}H_{41}ClCuN_3O_2P$: C, 69.71; H, 5.10; N, 5.19; Cl, 4.38. Found: C, 68.88; H, 4.96; N, 5.11; Cl, 4.29.

General procedure for obtaining kinetic data by low temperature UV-Vis spectroscopy. All reactions were prepared in a nitrogen filled glovebox and cuvettes were sealed under inert atmosphere with a septum. Reactions were monitored by UV-Vis and performed following the general procedure described herein. To a cuvette, 0.10 mL of 3mM **2** or **7** in 1,2-difluorobenzene was added to 2.70 mL of 1,2-difluorobenzene. In reactions with DHA, 0.07 mL of a 3mM solution of **2** or **7** in 1,2-difluorobenzene and

0.14 mL of 30 mM DHA in 1,2-difluorobenze was added to 2.64 mL 1,2-difluorobenzene were added to the cuvette. The cuvette was cooled to −25 °C and 1.5 mM $FcPF_6$ (0.10 mL) was added to give rise to an intense chromophore (λ_{max} ~560) which was sampled at an appropriate rate for the reaction. The decay of the chromophore was monitored until no further spectral changes were observed. The data was then analyzed using the Olis Global Fitting software package using the single value decomposition (SVD) fitting protocol. The data was fit to several reaction order types using the SVD protocol until a suitable fit was achieved where the error was reduced and the spectral contributions calculated by the Olis software were in good agreement with experimentally observed spectra.

Procedure for self-decay rate constant of 2' (k_{SD}). The rate of the self-decay of **2'** was obtained in 1,2-difluorobenzne at −25 °C in duplicate at 1 mM. The decay of the chromophore (λ_{max} ~560 nm, ε ~ 10400 $M^{-1}cm^{-1}$) was monitored by taking spectra in 0.5 seconds. The slow decay of **2'** (10% decay in 75 min) was amenable to single wavelength analysis. The $t_{½}$ was estimated by monitoring the decay of the feature at 560 nm and scaled to give an approximate $t_{½}$ (where 50% decay would be observed). The $t_{½}$ was used in the half-life equation for first order reaction to give k_{SD}.

Procedure for obtaining self-decay rate constant of 7'(k_{SD}). The rate of the self-decay of **7'** was obtained as described above at 1.25 mM . The decay of the chromophore (λ_{max} ~560 nm, ε ~ 4200 $M^{-1}cm^{-1}$) was monitored by taking spectra in 0.5 second intervals until spectral changes were no longer observed. The data was analyzed as described above to give k_{SD}

Procedure for obtaining rate constant for the reaction of 2' with DHA (k_{DHA}). The rate of reaction of **2'** with DHA was obtained as described above at 1.25 mM. . The decay of the chromophore (λ_{max} ~560 nm, $\varepsilon \sim 4200\ M^{-1}cm^{-1}$) was monitored by taking spectra in 1 second intervals. The data was analyzed by using the Olis Global Fitting software and fit to two first order decay processes on a subset of data (300-850 nm). Spectral contributions of each component were calculated and are in good agreement with $[LCuOH]^{1-}$ and anthracene spectra. The observed rate constant (k_{obs}) was obtained and the reaction was determined to be first order in LCuOH. The rate constant for the reaction with DHA, k_{DHA}, was obtained using the equation $k_{DHA} = k_{obs}/[LCuOH]_0$.

Procedure for obtaining rate constant for the reaction of 7' with DHA. The rate of reaction of **7'** with DHA was obtained in 1,2-difluorobenzne at −25 °C in duplicate at a concentration of 1.25 mM. The decay of the chromophore (λ_{max} ~560 nm) was monitored by collecting spectra in 0.5 second intervals until no further spectral changes were observed. Due to the large k_{SD} the observed rate was determined to be a composite of the self-decay rate and the rate of the reaction with DHA (k_{DHA}). Using the Olis Global Fitting software, the data was fit to two first order decay processes applied to a subset of data (300-850 nm): 1^{st} order self-decay process (k_{SD}) and the reaction with DHA under pseudo first order conditions (k_{obs}). The rate constant for the reaction with DHA, k_{DHA}, was obtained using the equation $k_{DHA} = k_{obs}/[LCuOH]_0$. The calculated k_{SD} is in good agreement with the independently measured k_{SD} and the spectral contributions of each component were calculated and are in good agreement with $[LCuOH]^{1-}$ and anthracene spectra.

Chapter 4: Isolation and Reactivity of Novel [M(II)-CH_2CN]$^{1-}$ (M = Cu, Ni) Complexes

In a serendipitous finding, dissolution of a copper(II)-hydroxide complex ((Bu_4N)**7**) in acetonitrile led to the isolation of a novel copper(II)-cyanomethide species ((Bu_4N)**9**). The same behavior was exhibited when the analogous nickel(II)-hydroxide ((Bu_4N)**10**) was dissolved in acetonitrile to afford the corresponding nickel(II)-cyanomethide complex ((Bu_4N)**11**). The novelty of these reactions of metal(II)-hydroxide complexes with CH_3CN, in addition to the scarcity of metal cyanomethide complexes in the literature, led us to pursue mechanistic studies of these findings. This chapter first places these unusual metal-cyanomethide complexes into perspective by describing other known metal-cyanomethide complexes and surveying the typical pathways in which metal-hydroxide complexes react with nitriles. The cyanomethide complexes are placed in further perspective by describing the significance of species with copper(II/III)-carbon bonds. A description of the synthesis and characterization of (Bu_4N)**9** and (Bu_4N)**10** follows, including a discussion of mechanistic studies aimed at understanding how the cyanomethide complexes are formed. Preliminary reactivity studies of these compounds are also presented. Aspects of this work have been published.[124]

4.1.1 Previously Reported Metal-Cyanomethide Complexes

Reports of metal-cyanomethide complexes are rare in the literature and most examples contain 4d and 5d metals (Pt,[314–318] Pd,[319] Ir,[320–322] Rh,[320,323–325] Hg,[326] and Au[327]). A few 3d metal cyanomethide complexes have been reported, including: an unstable nickel complex,[328] a nickel complex appearing after this work was published,[329]

and an iron complex.[330] The following section includes a discussion of the synthetic strategies employed to create these metal-cyanomethide complexes, which include: photolysis, oxidative addition, and the use of a superbase.

4.1.1.1 Synthesis of Metal-Cyanomethide Complexes via Photolysis

One method that has been used to create metal-cyanomethide complexes is irradiation of a metal complex in acetonitrile. For example, irradiation of $Rh(Cp^*)(PMe_3)H_2$ in neat acetonitrile yields the C-H bond activated acetonitrile product, $Rh(Cp^*)(PMe_3)(CH_2CN)(H)$ (**Scheme 4-1**).[324] In order to gain further information about the mechanism of this reaction, photolysis experiments were also carried out at low temperature (−40 °C). Emphasis was placed on observing η^1- or η^2-nitrile species that are anticipated to be intermediates on the route to the C-H activated complex. However, no Rh(I) species were detected by ^{1}H NMR spectroscopy and only peaks corresponding to the product and starting material were observed. Changing one of the hydride ligands to a phenyl ligand gave the rhodium complex $Rh(Cp^*)(PMe_3)(Ph)(H)$. Subsequently irradiation of $Rh(Cp^*)(PMe_3)(Ph)(H)$ in acetonitrile yielded the same C-H activated product, $Rh(Cp^*)(PMe_3)(CH_2CN)(H)$, however, upon further heating, a rearrangement occurs and the C-C bond scission product ($Rh(Cp^*)(PMe_3)(CN)(CH_3)$) was observed (**Scheme 4-1**).[324]

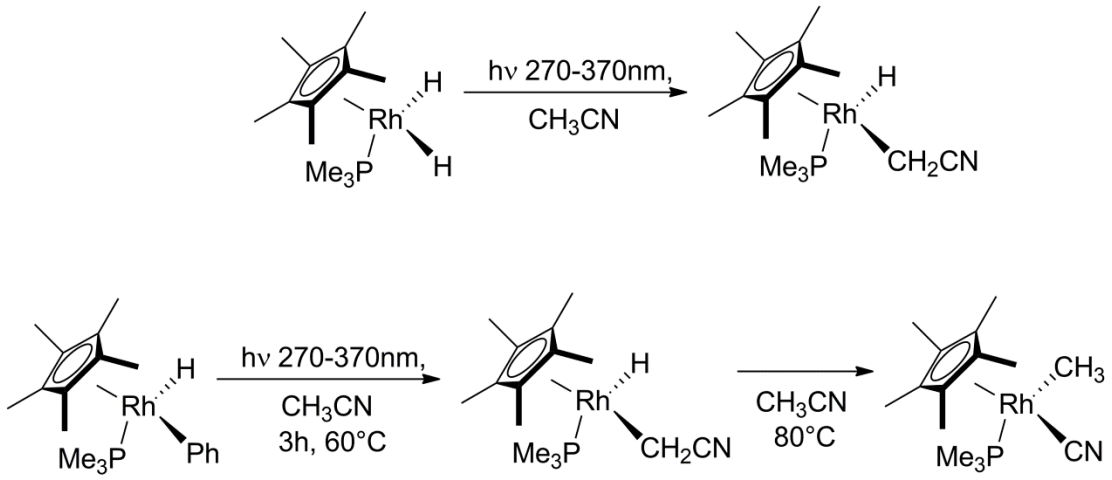

Scheme 4-1: (Top): Photolysis of Rh(Cp*)(PMe_3)H_2 to give the acetonitrile C-H bond activated product Rh(Cp*)(PMe_3)(CH_2CN)(H). (Bottom): Pathway for the photolysis reaction of Rh(Cp*)(Ph)(H) (left) with acetonitrile to give Rh(Cp*)(CH_2CN)(H) (middle). Additional heating gives the C-C bond scission product Rh(Cp*)(CN)(CH_3) (right).

The authors suggest that the Rh-(CH_2CN)(H) complex is the kinetic product of the reaction, whereas the Rh(Cp*)(PMe_3)(CN)(CH_3) complex is the thermodynamic product because it is only observed after further heating. DFT calculations were carried out to support the experimental observations and it was found that the activation energy for the C-H activated pathway is significantly lower (0.5 kcal/mol) relative to that for the C-C bond activated pathway (4.8 kcal/mol) under gas-phase conditions (**Figure 4-1**).

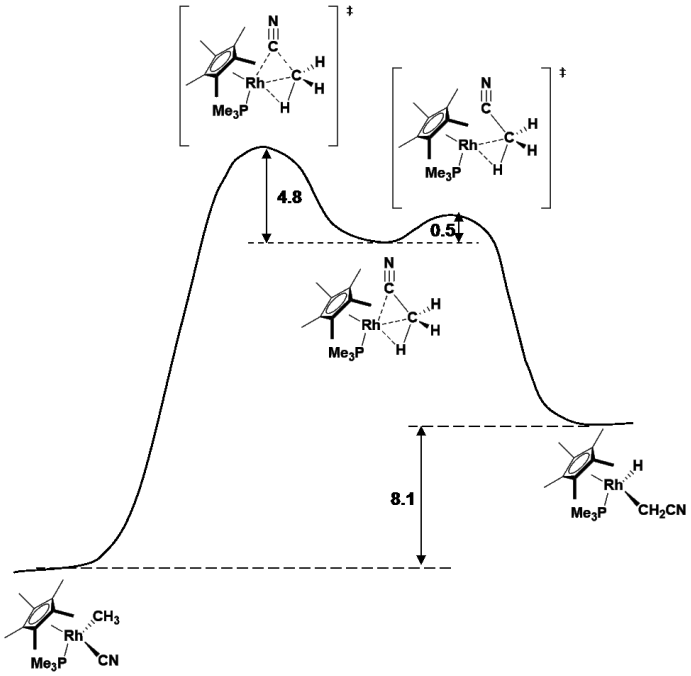

Figure 4-1: DFT calculated energetic pathways for C-H and C-C bond activation of acetonitrile by Rh(Cp*)(PMe_3) (free energies in kcal/mol at 298 K, gas phase). Energies are normalized to the Rh(Cp*)(CN)(CH_3) product.

Upon applying solvation corrections for the transition states, the C-H bond activation energy rose to 40.3 kcal/mol, whereas the C-C bond pathway only rose to 38.6 kcal/mol. These results would suggest that the C-C bond scission product is the kinetic product, which is not what was observed experimentally (the authors do not provide an explanation for this discrepancy). Interestingly, the homologous nickel complex (Ni(Cp*)(PMe_3)(CN)(CH_3)) generated the C-C activated product exclusively, although the C-H activated complex was observable at temperatures below −40 °C.[328] Similarly, when the complex Rh(Tp')(CNR)(carboimide) (Tp' = hydrotris(3,5-dimethylpyrazol-1-yl)borate) was irradiated in acetonitrile, the C-H bond activated product was observed exclusively even after heating for several days. When the related Rh(Tp')(PMe_3) complex was heated in acetonitrile, the C-H activated product (Rh(Tp')(PMe_3)(CH_2CN)(H)) was initially observed, but, upon further heating for several days, the C-C cleavage product

($Rh(Tp')(PMe_3)(CN)(CH_3)$) was obtained.[325] The authors attributed the stabilization of the C-C cleaved product to the π-accepting character of the isocyanide (CNR) ligand rather than to the σ-donation of the trimethylphosphine (PMe_3) to the rhodium center.

4.1.1.2 Synthesis of Metal-Cyanomethide Complexes via Oxidative Addition

Another method used for obtaining metal-cyanomethide complex is via oxidative addition of acetonitrile to a low valent metal center. For example, dissolution of $[Ir(PMe_3)_4]Cl$ in acetonitrile led to the isolation of $Ir(PMe_3)_4(H)(CH_2CN)$, which was characterized by X-ray crystallography and NMR spectroscopy (**Scheme 4-2**).[322]

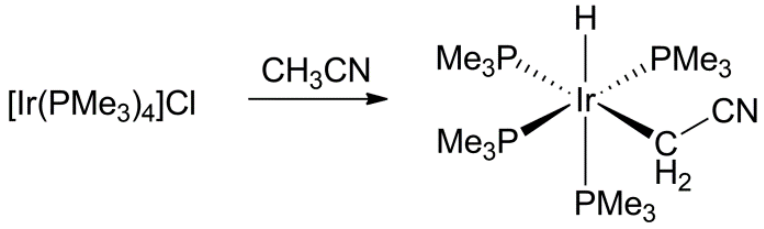

Scheme 4-2: Formation of a (Ir-(H)(CH_2CN)) complex via oxidative addition.

The $[Ir(PMe_3)_4]Cl$ complex had been shown previously to undergo oxidative addition with acetonitrile to give the cyanomethide complex, which forms carboxylated acetonitrile in the presence of carbon dioxide.[320] The authors observed rapid C-H and C-D (when using CD_3CN) activation of acetonitrile while monitoring the reaction by NMR spectroscopy, but were unable to observe coordination of the nitrile group to the metal center prior to observing product formation. In an attempt to trap an intermediate, various substituents on the para position of para-X-benzonitrile (X = CF_3, F, Me and OMe) were investigated for interactions with the iridium center by NMR spectroscopy, but no metal-acetonitrile interactions were observed.

A recent example of an iron(II)-cyanomethide complex, reported by the Nocera group, is believed to form via reaction of acetonitrile to a high valent iron(IV) center .[330] In this report, an iron(II) species reacts with an oxo-transfer reagent to generate a high spin iron(IV) intermediate, which attacks acetonitrile instantaneously at −40 °C to produce an iron(III)-cyanomethide and an iron(III)-hydroxide complex (**Scheme 4-3**). The authors suggest that a high spin Fe(IV)-oxo species is responsible for attacking acetonitrile, but spectroscopic data in support of this hypothesis was not obtained. Of particular interest is the observation that the iron(III)-hydroxide complex can be synthesized independently and is non-reactive towards acetonitrile, which is in direct contrast to the observed reactivity of our copper(II)-hydroxide and nickel(II)-hydroxide complexes (see sections 4.2 and 4.3).

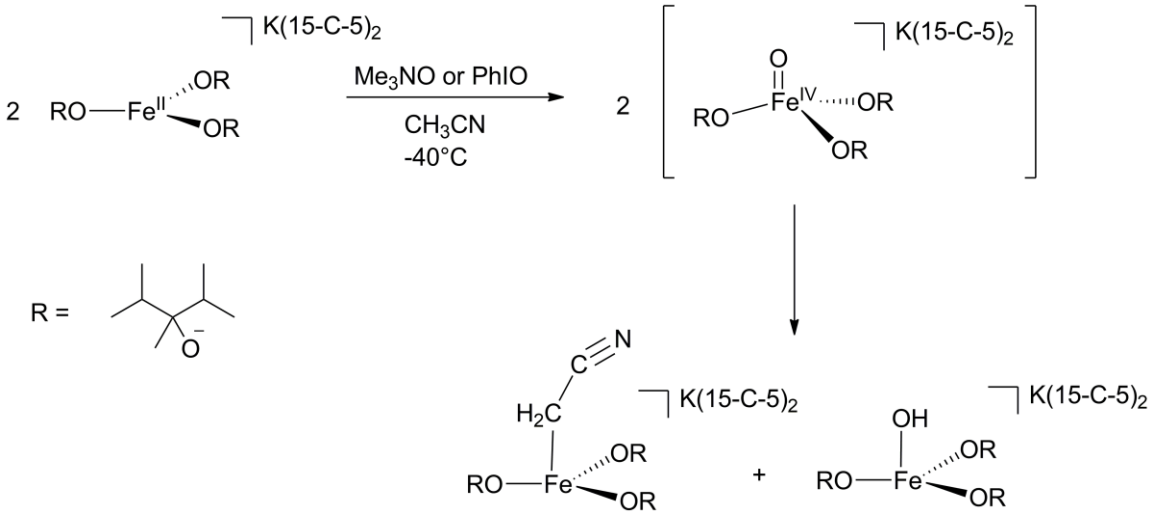

Scheme 4-3: Reaction of $(K(15\text{-}C\text{-}5)_2)(Fe(ditox)_3)$ with oxidant (Me_3NO or PhIO) to give a high valent iron species that undergoes an immediate reaction with acetonitrile at −40 °C to give $(K(15\text{-}C\text{-}5)_2)(Fe(ditox)_3(CH_2CN))$ and $(K(15\text{-}C\text{-}5)_2)(Fe(ditox)_3(OH))$.

4.1.1.3 Synthesis of Metal-Cyanomethide Complexes Using a Superbase

Metal-cyanomethide complexes have also been prepared by using a superbase to deprotonate acetonitrile and generate a cyanomethide ion in solution that is then able to

coordinate to a metal center. For example, a gold-cyanomethide complex ($Au(CH_2CN)(PPh_3)$) was isolated via crystallization after refluxing $Au(Cl)(PPh_3)$) in the presence of 1,2,4,5-tetrakis(*N,N′*-dimethylethyleneguanidino)benzene) (tdemgb) in acetonitrile (**Scheme 4-4**).[327] The pK_a of the tdemgb ligand was experimentally determined to be ~23.8 in acetonitrile, which is slightly less than the pK_a of acetonitrile (~25). Several experiments indicated that deprotonation of acetonitrile by the superbasic ligand to form the cyanomethide ion, which would then ligate to the gold center, is an unlikely mechanism for this reaction. Attempts to identify the formation of the cyanomethide ion by NMR spectroscopy were unsuccessful. Furthermore, when a stronger guanidine-based ligand was used under the same reaction conditions, no formation of an Au-CH_2CN complex was observed.

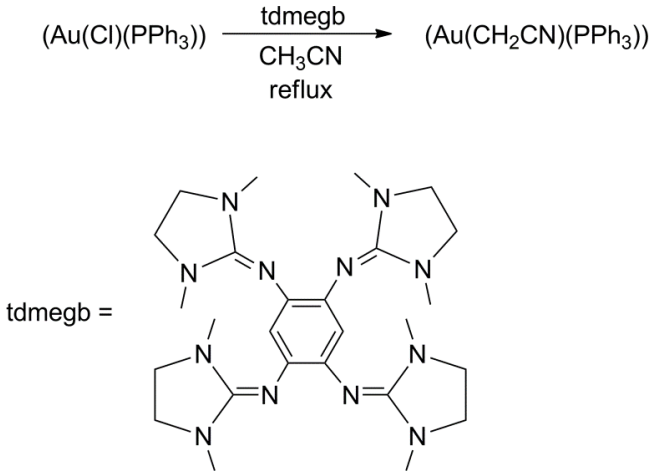

Scheme 4-4: Reaction of $(Au(Cl)(PPh_3))$ with acetonitrile in the presence of a super basic ligand (tdemgb) to give $(Au(CH_2CN)(PPh_3))$.

The authors suggest that C-H activation of acetonitrile involves a gold(I) complex, where the tdmegb ligand stabilizes the transition state proposed in **Figure 4-2**. The authors do not provide any computational calculation to support this proposed transition state, but

note that it is similar to a transition state suggested for a gold promoted arene-H activation pathway.[331]

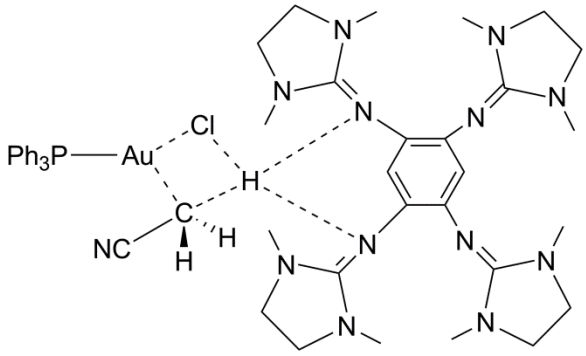

Figure 4-2: Proposed transition state for the gold-mediated deprotonation of acetonitrile and stabilization of the cyanomethide ion.

An alternative method for preparing cyanomethide complexes is to use a strong base such as n-butyl lithium, potassium *tert*-butoxide, or $LiN(SiMe_3)_2$ to deprotonate acetonitrile in the presence of a metal or by adding the alkali metal salt to the solution of the desired transition metal.[329,332–335] Addition of potassium *tert*-butoxide (KO^tBu) to a Ni-$NCCH_3$ complex supported by an N-heterocylic carbene (NHC) and a cyclopentadienyl (Cp) ligand produced the corresponding $((Mes)_2NHC)(Cp)Ni\text{-}CH_2CN$ complex (**Scheme 4-5**).[333] The mechanism proposed by DFT calculations favors deprotonation of the N-bound acetonitrile complex by KO^tBu , followed by rearrangement of the cyanomethide ligand to form the C-bound nickel(II)-cyanomethide.

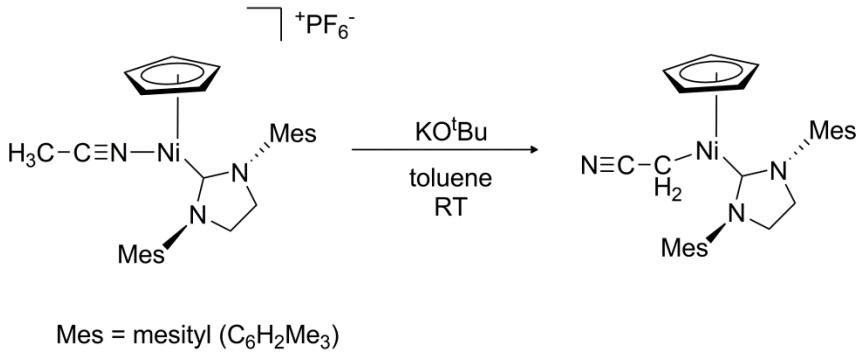

Scheme 4-5: Reaction of $[((Mes)_2NHC)(Cp)Ni\text{-}CH_3CN]^{1-}$ with potassium tert-butoxide to give $((Mes)_2NHC)(Cp)Ni\text{-}(CH_2CN)$.

After this work was completed and published, a neutral nickel(II)-cyanomethide complex was reported, $(POCOP)Ni(CH_2CN)$ (POCOP = 2,6-$(i Pr_2PO)_2C_6H_3$). Addition of $LiCH_2CN$ to a (POCOP)Ni-Cl complex supported by a bis(phosphinite)-based pincer ligand resulted in the isolation of the neutral nickel(II)-cyanomethide complex (**Scheme 4-6**)[329].

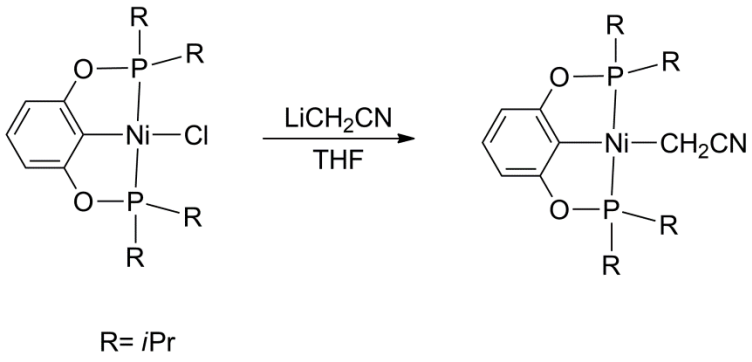

Scheme 4-6: Synthetic route for the preparation of a neutral nickel(II)-cyanomethide complex supported by a phosphinite based pincer ligand. $(POCOP)Ni(CH_2CN)$ (POCOP = 2,6-$(i Pr_2PO)_2C_6H_3$)

The air and water stable nickel-cyanomethide complex was successfully used for the catalytic cyanomethylation of aldehydes with a large turnover number (up to 82,000) without the use of exogenous base when acetonitrile was used as the solvent. Mechanistic

studies led the authors to propose a catalytic cycle for the cyanomethylation of benzaldehyde (PhCHO), which involves a reversible insertion of the aldehyde to generate a nickel-alkoxide complex (**Scheme 4-7**). The nickel-alkoxide is proposed to deprotonate acetonitrile to give the cyanomethylated product and regenerate the nickel(II)-cyanomethide. The authors indicate that the alkoxide is not basic enough to deprotonate acetonitrile outright, and instead attribute this reactivity of the nickel center to dπ-pπ repulsion between the nickel and oxygen nuclei.

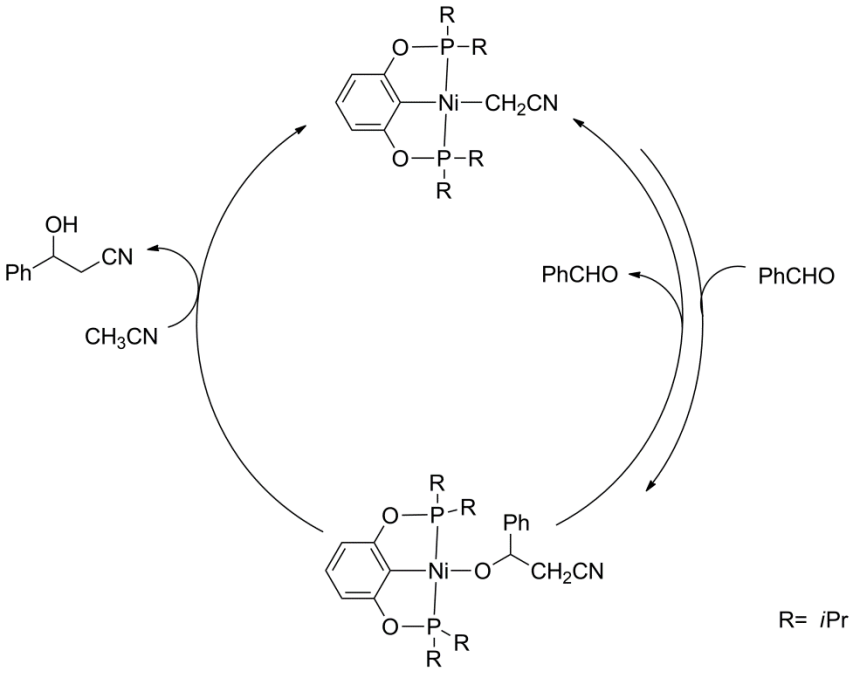

Scheme 4-7: Proposed catalytic cycle for the cyanomethylation of aldehydes by a nickel(II)-CH_2CN complex.

4.1.2 Reactivity of Metal-hydroxides with Nitriles

The reaction we observed of metal(II)-hydroxides with acetonitrile to form a cyanomethide is unique in the literature. In general, metal-hydroxide complexes are instead proposed as intermediates in the metal promoted hydrolysis of nitriles.[336,336–347] The predominant mechanism for hydrolysis is believed to involve nucleophilic attack of

the metal bound hydroxide at the nitrile carbon. For example, copper-hydroxide complexes often react with nitriles to form carboxamides.[340,348] While amides are typically poor ligands for transition metals, the carboxamides formed by hydrolysis of nitriles can undergo carboxamide-iminol tautomerization. Binding of the metal center can then be envisioned as a carbonyl binding if the carboxamide resonance form is predominate or binding of a hydroxide to the metal if the iminol resonance form is more favored (**Figure 4-3**).[340]

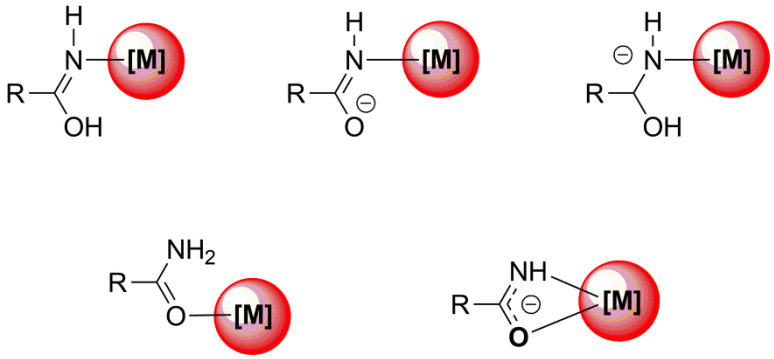

Figure 4-3: Possible binding modes of the carboxamide ligand displaying the amide-iminol tautomerization. [M] denotes a metal complex. Figure adapted from ref.340.

The two primary mechanisms for the metal-mediated hydrolysis of nitriles are: (1) a metal-hydroxide species forms and attacks a nitrile and (2) exogenous hydroxide attack of the nitrile creates a negatively charged amide which is stabilized by the Lewis acid metal. Both mechanisms are typically found to be first order in both regents.[340] There are many examples of metal-hydroxide promoted hydrolyses of nitriles in the literature, involving a variety of 3d, 4d, and 5d transition metals.[336–339,341–347,349–354] A representative study on first row transition metals containing complexes of copper, zinc, and nickel supported by 2-cyano-1,10-phenathroline was examined for hydrolysis of the nitrile group of the ligand and formed a carboxamide.[355] Kinetic studies of the nickel-catalyzed

reaction were performed, as the copper catalyzed reaction was too rapid ($t_{1/2}$ < 10 sec) to study via the available techniques. The kinetic studies indicated that the hydration of the nitrile was first order in hydroxide which is consistent with two possible mechanisms: attack of an external hydroxide to Ni-bound ligand (Pathway A), or coordination of hydroxide to nickel followed by intramolecular attack of the nitrile ligand (Pathway B) (**Figure 4-4**).

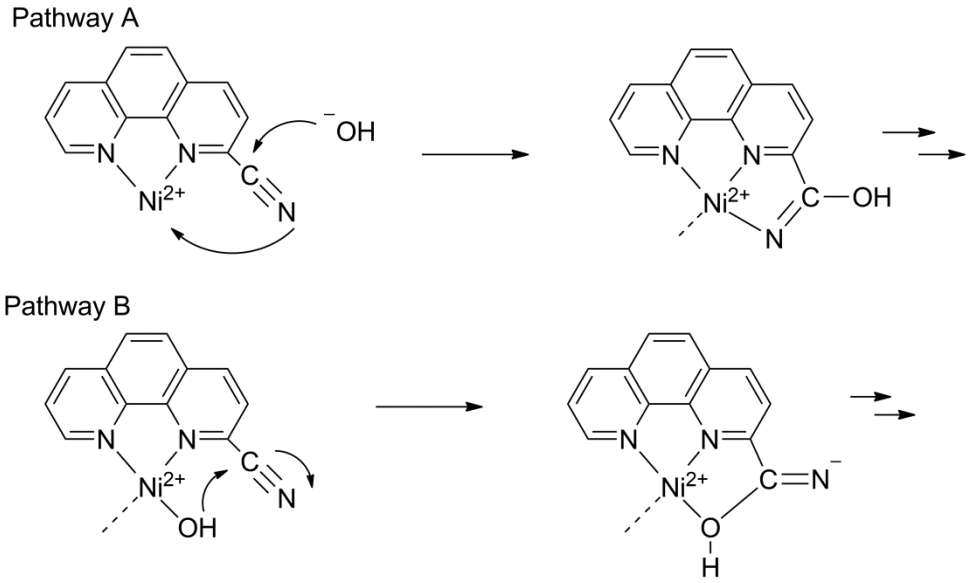

Figure 4-4: Two possible pathways for the hydrolysis of the nitrile group of the ligand scaffold. (Pathway A) Exogenous attack of a hydroxide; (Pathway B) coordination of the hydroxide to the nickel followed by intramolecular nucleophilic attack of the nitrile group.

In Pathway A, the hydrolysis of the nitrile is metal-mediated, where the metal acts as a Lewis acid to stabilize the negative charge, which results after nucleophilic attack by the hydroxide. Pathway B involves the formation of the hydroxide followed by intramolecular attack of the nitrile to generate the O-bound amide. Experiments carried out in 50% aqueous ethanol showed enhanced rates versus the rates measured using purely aqueous solutions, which was expected as ethanol is more basic than water and

should enhance the rate of a simple nucleophilic reaction.[356] The authors suggest that the observed rate enhancement favors Pathway A because the coordination of ethanol to the nickel center would compete with water and lead to a slower observed rate.

In contrast to the bidentate ligand case previously discussed, when a tetradentate macrocycle is employed, a different mechanism of metal-mediated nitrile attack is observed. When copper(II) complexes of N-functionalized tetraaza macrocycles with appended nitrile side chains were dissolved in water, a copper(II)-hydroxide formed that underwent intramolecular attack of the nitrile side chain of the ligand while producinga carboxamide product (**Scheme 4-8**).[357]

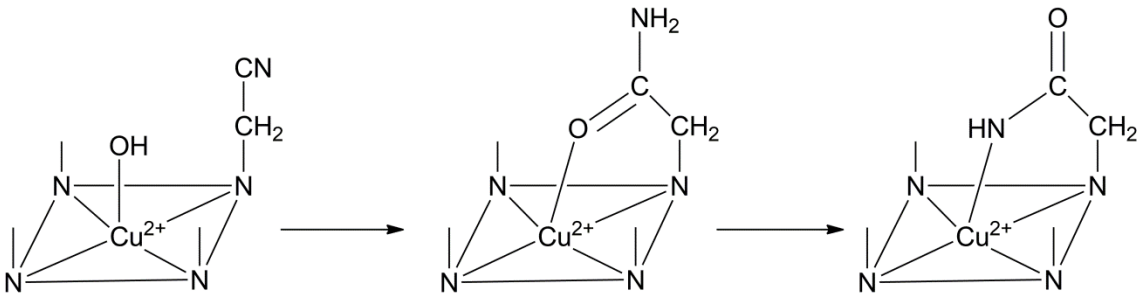

Scheme 4-8: Proposed mechanism for the attack of a copper-hydroxide to the intramolecular nitrile group causing formation of an O-bound carboximide followed by deprotonation under slightly basic conditions to give the N-bound carboxamide.

Mechanistic experiments were carried out under differing concentrations of aqueous sodium hydroxide to assess if ligand hydrolysis could be occurring due to exogenous hydroxide attack instead of from the copper(II)-hydroxide moiety. Previous reports have shown a mixture of products is observed when ligand hydrolysis occurs in the absence of a metal. [358] Addition of sodium hydroxide to the copper(II)-hydroxide complex showed exclusive formation of the amide product, which suggest that the copper(II)-hydroxide is the active species, not free hydroxide. The O-bound amide was isolated under acidic

conditions, and upon the addition of base, deprotonation of the amide caused rearrangement to give the N-coordinate amide. Further mechanistic studies using SCN- as an inhibitor for hydroxide binding showed that this anion shut down the pathway for nitrile hydrolysis. These results suggest the copper(II)-hydroxide complex is an essential moiety on the pathway to nitrile hydrolysis.

Currently, the only report of a copper complex characterized to activate the C-H or C-C bond of acetonitrile is an air stable dinuclear copper(II) cryptate that activates acetonitrile to give the C-C bond cleaved product and a stable cyano-bridged dicopper(II) complex (**Figure 4-5**).[359]

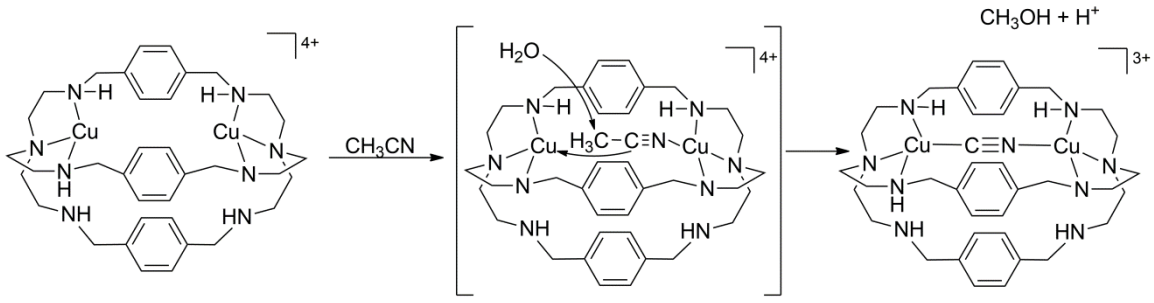

Figure 4-5: Proposed mechanism for the C-C bond activation of acetonitrile by a dicopper(II) complex to afford a cyano-bridged dicopper(II) complex. Figure adapted from ref.359.

The presence of methanol was also detected as a product, and kinetic studies indicated the reaction was first order in water. The authors proposed a mechanism for C-C bond cleavage of methanol that begins with N-coordination of acetonitrile to one copper center. This coordination event is thought to allow the other copper(II) atom to interact with the π-orbital of the sp-carbon atom of acetonitrile, which is thought to increase the electrophilicity of the methyl carbon . The more electrophilic carbon atom enables cleavage of the C-C bond by a water molecule to produce methanol, the cyanide bridged

complex, and a proton. While details concerning the reaction mechanism are unclear, the driving force for this reaction is believed to be the formation of the stable copper(II)cyano-bridged complex.

The hydrolysis of nitriles by metal-hydroxide complexes is well established in the literature, although different mechanisms may be at play depending on the denticity of the ligand and the identity of the transition metal. These numerous examples place our observations of a copper(II)-hydroxide attacking acetonitrile to form a copper(II)-cyanomethide complex into uncharted territory.

4.1.3 Copper Catalyzed C-C Bond Forming Reactions

The reaction of a copper(II)-hydroxide complex that activates the C-H bond in acetonitrile to give a copper(II)-cyanomethide complex raises many interesting questions, including ones centered on the potential utility of the copper(II)-cyanomethide as a cyanomethylating reagent. The copper(II)-cyanomethide complex ((Bu_4N)**9**) is a well characterized example of a copper-alkyl complex, which bares significance to the development of copper catalysts that are capable of forming carbon-carbon bonds. A copper-alkyl complex is particularly relevant for reaction mechanisms that involved a copper-alkyl intermediate. The area of copper-catalyzed carbon-carbon bond forming reactions has garnered much attention for over half of a century and continues to be an active area of research.[360–374] Many copper-catalyzed organic reactions have been studied over the past 60 years, including: ones using the Gilman reagent,[79] the Ullman reaction,[360,361] and Castro-Stevens cross-coupling reactions. [362,363] Another example of a bimetallic carbon-carbon coupling reaction is the Sonogashira coupling reaction that

utilizes both palladium(0) and copper(I) to couple terminal alkylenes with aryl or vinyl halides (**Scheme 4-9**).[365,375]

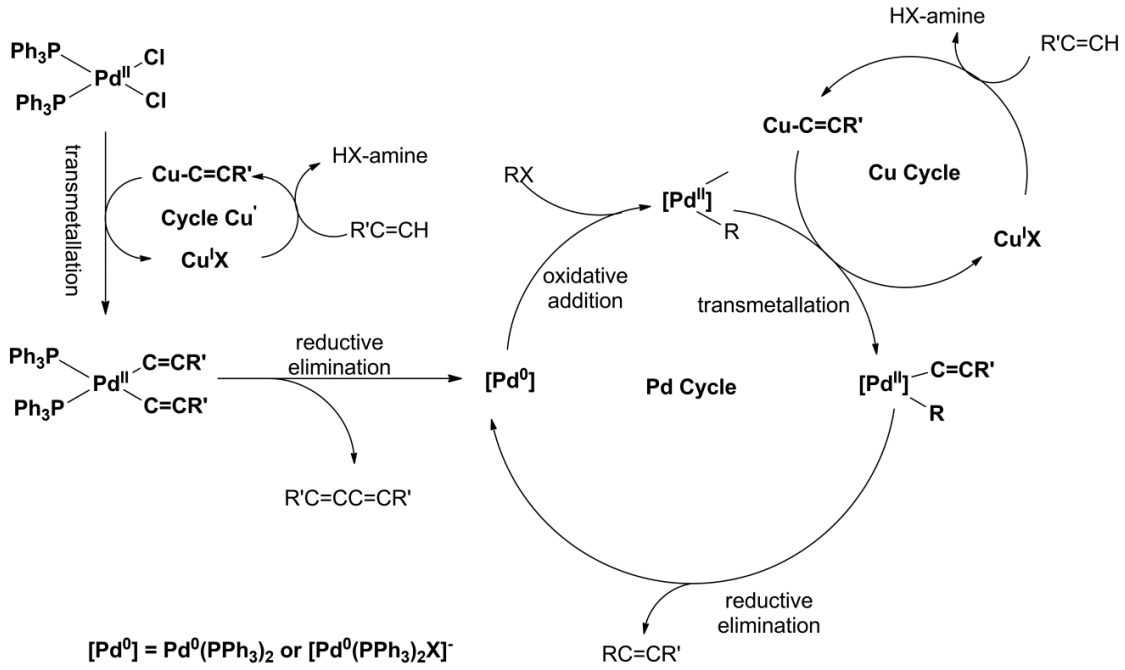

Scheme 4-9: Reaction scheme for the Sonogahira coupling of palladium and copper catalyzed coupling of sp^2-carbon-halides with terminal acetylenes. Figure adapted from ref.365.

In addition, copper-free reaction conditions may be used.[376,377] The exact role that copper(I) plays in the mechanism remains unclear, although it is generally thought to form a copper-alkyl species that undergoes transmetallation with a palladium species, which is responsible for carbon-carbon coupling.[365] Palladium is often used for carbon-carbon formation, although the cost and low natural abundance of palladium has led researchers to look for less expensive and more abundant metals to replace palladium in catalytic reactions. Developing a copper based system capable of achieving carbon-carbon coupling would be highly desirable as it has the potential to be a more cost effective catalyst. In order to develop a copper catalyst to be competent in such carbon-

carbon bond formation reactions, it necessary to gain a fundamental understanding of the nature of the copper-alkyl species that are proposed as intermediates in such reactions.

4.1.3.1 Copper-alkyls as Important Reactive Intermediates

There are many reports of low valent, copper(I)-alkyl species in the literature that bear great significance in many important organometallic transformations.[81,118,378–385] This section includes a brief overview of some relevant copper(I) catalyzed carbon-carbon (C-C) bond forming reactions followed by a discussion of rare copper(II)-alkyl complexes.

The original Ullman reaction couples aryl halides using stoichiometric metallic copper to make biaryls, although it requires the use of harsh reaction conditions (> 200 °C) and is notoriously difficult to reproduce.[360,361] The Ullman reaction has been improved by using copper(I) catalysts,[366] but despite multiple efforts to clarify the mechanism of the reaction, it is still unclear what oxidation state the copper adopts in the active species. The active species of these reactions is unclear, as some favor the formation of an organocopper(I) species as the acting catalyst, [368] while other mechanisms suggest the copper(I) starting complexes generate a reactive copper(III) species.[68,69,99]

Other leading copper catalyzed carbon-carbon bond coupling reactions are the Castro-Stevens cross coupling reactions,[362,363] where a copper(I)-acetylide and an aryl halide react to give an alkyne and a copper(I) halide (**Scheme 4-10**). These reactions are generally high yielding, but they are limited in scope to the production of biaryl products.

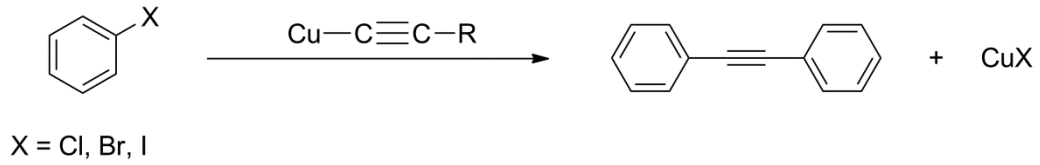

Scheme 4-10: Castro-Stevens cross coupling of an aryl halide with a copper(I)-acetylide to give an alkyne and a copper halide.

While much progress has been made in carbon-carbon formation reactions using a copper catalyst, many questions about the mechanism of these reactions remain.[379,381,383,384,386] Reports of an in-situ generated copper(I)-cyanomethide complex, created by mixing copper(I) iodide with cyanomethyllithium, show that the complex attacks allylic halides to generate γ,δ-unsaturated nitriles, but does not attack alkyl haldies or benzyl bromide.[260] In contrast, a cyanomethylcopper(I) species generated by the decarboxylation of copper(I) and copper(II)-cyanoacetates was able to successfully cyanomethylate allyl bromide and aromatic halides.[387]

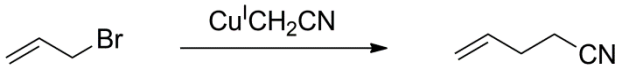

Scheme 4-11: Reaction of allylbromide with in-situ generated copper(I)-cyanomethide to yield 4-pentenenitrile.

Both of the previously discussed examples use a copper(I)-alkyl species to perform C-C coupling and are believed to go through a copper(III) intermediate (see section 1.2.2 for more details). Briefly, the mechanism involves transmetallation of the copper(I) salt with the main-group organometallic reagent (R-M), followed by nucleophilic attack on the copper by an electrophile (E), which generates the formally copper(III)-intermediate (**Figure 4-6Figure 4-6**).[69] Reductive elimination yields the desired carbon-carbon coupled product (R-E) and regenerates the starting copper(I) complex to complete the catalytic cycle.

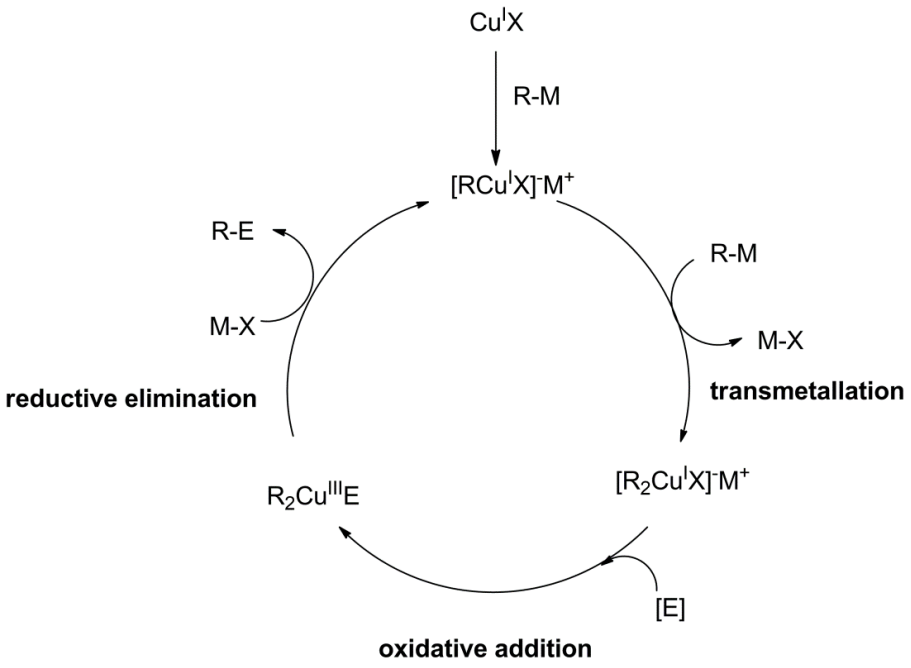

Figure 4-6: Proposed catalytic cycle for the reaction of copper(I)-alkyl complexes with a main-group organometallic reagent (M-X) and an electrophile (E) to give a copper(III) intermediate, followed by reductive elimination to form the desired carbon-carbon coupled product (R-E). Adapted from [69].

Many copper(I)-alkyl and copper(III)-alkyl species have been extensively studied throughout the years;[68,69,80,81,81–87,94,99–108,110,371,382,386,388–397] however, there remains a dearth of copper(II)-alkyl complexes. While there are several examples of copper(II)-C(sp^2) complexes,[109,110,112,116,388] few examples of copper(II)-C(sp^3) species are reported in the literature.[155,398,399] Both *N*-confused porphyrin and pyrrole-appended *O*-confused oxaporphyrin ligands have been used to stabilize both copper(II)- C(sp^2) and copper(III)-C(sp^2) complexes.[110,114,116] The few reported copper(II)-C(sp^3) species in the literature are stabilized due to forming intramolecular bonds to carbon atoms in a macrocyclic[399,109,116] or tripodal[155,400,398] ligand (**Figure 4-7**).

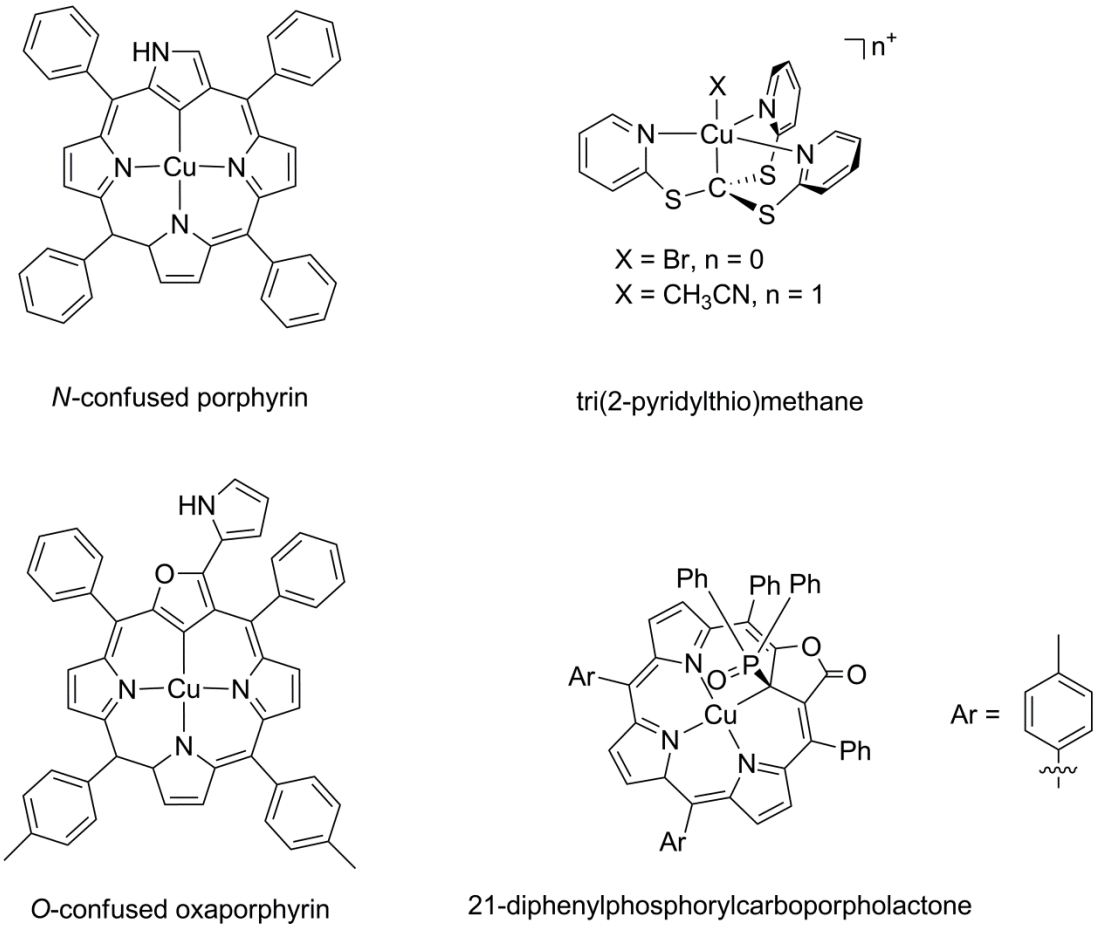

Figure 4-7: Selected examples of copper(II) complexes with bonds to sp^2 (left column) and sp^3 (right column) hybridized carbon atoms.

Kinoshita et al. reported a tripodal pyridine thiolate ligand with a copper(II)-C(sp^3) distance of 2.004(3) Å in 2003, although the sp^3-hybridized carbon atom is bound directly to thiolates.[155] The first report of an alkyl copper(II)-C(sp^3) bond appeared later that year from Latos-Grażyński and coworkers, where a 21-diphenylphosphoryl-carbaporpholactone ligand with a pendant arm was used to form a macrocyclic complex with a copper-C(sp^3) bond that was measured to be 2.232(2) Å by X-ray crystallography. While neither of these complexes was reported to undergo reactions to form C-C bonds, they provide a useful basis for comparison to future synthesized complexes with copper(II)-C(sp^3) bonds.

4.2 Isolation of a [Copper(II)-CH_2CN]$^{1-}$ Complex

Our previous work with a copper(II)-hydroxide complex, (Bu_4N)**2**,[122,123] focused on the characterization of reactive copper-oxygen species capable of attacking weak C-H bonds.[122,123] We extended this work by reducing the steric bulk around the copper center by using a *N,N'*-bis(2,6-diisopropylphenyl)-2,6-pyridinedicarboxamide ligand and synthesizing a copper(II)-hydroxide, (Bu_4N)**7**. This seemingly small change to the steric environment around the copper center had a profound impact on the stability of the corresponding copper(III)-hydroxide, **7'** (see Chapter 3). This chapter includes a discussion of the rapid reaction of (Bu_4N)**7** with acetonitrile that was not observed with the corresponding sterically hindered complex, (Bu_4N)**2**.

Dissolution of (Bu_4N)**7** in acetonitrile caused an immediate color change from blue to red-purple. Removal of the solvent led to the isolation of a deep purple-red solid that was determined to be copper(II)-cyanomethide complex, (Bu_4N)**9** (**Scheme 4-12**).

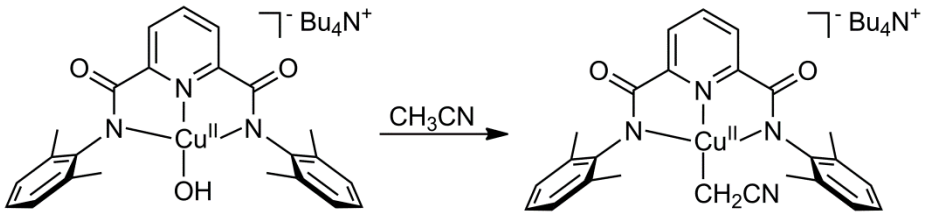

(Bu$_4$N)7 **(Bu$_4$N)9**

Scheme 4-12: Synthetic route for the preparation of (Bu_4N)**9** from (Bu_4N)**7**.

The complex (Bu_4N)**9** is the first reported example of a copper-cyanomethide complex. The formulation of (Bu_4N)**9** was confirmed by several techniques, including: ESI-MS, elemental analysis, single crystal X-ray crystallography, FT-IR spectroscopy, and EPR spectroscopy. The X-ray structure confirmed the copper(II)-cyanomethide formulation as

shown in (**Figure 4-8**); selected bond distance and angles of interest are presented in **Table 4-1**.

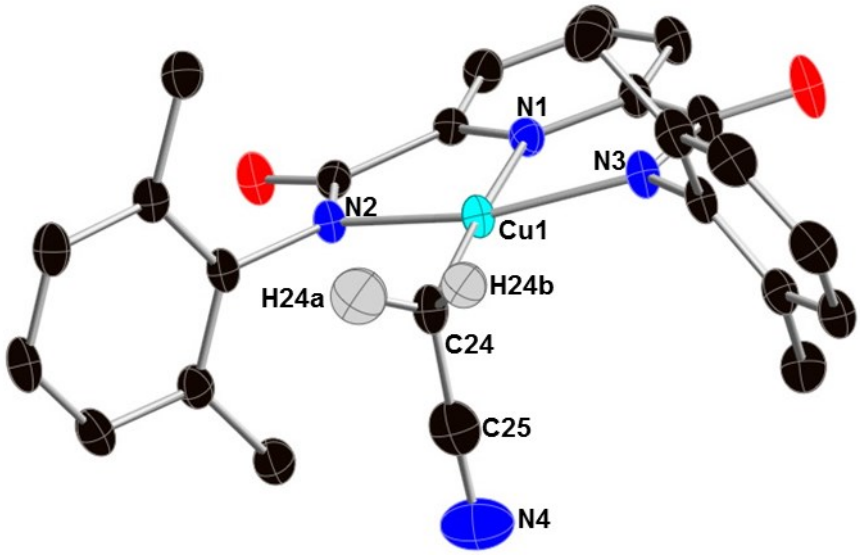

Figure 4-8: X-ray crystal structure of (Bu_4N)**9** with all hydrogen atoms omitted for clarity except for the hydrogen atoms on the cyanomethide ligand. The cation, (Bu_4N), and a molecule of acetonitrile in the unit cell are omitted for clarity. Space group: $P2_1/c$, R1 = 0.0510, wR2 = 0.1526.

The structure of (Bu_4N)**9** reveals a single cyanomethide ligand bound to the square planar copper ion, where the hydrogen atoms of the cyanomethide were placed using the difference Fourier map. The copper-nitrogen distances (2.011-2.015 Å) are within the range expected for copper(II)-amide bonds (2.026 Å ($\sigma = 0.056$)) according to the International Tables for Crystallography. [217] The copper-carbon bond distance is 1.986(3) Å, indicating a single bond between the two atoms. For reference, copper(II) complexes with a terminal isocyanide ligand have a median copper-carbon bond distance of 1.895 ($\sigma = 0.009$) Å and copper(II) complexes with terminal cyano ligands have a median copper-carbon distance of 1.975($\sigma = 0.1$).[217] The methide-carbon (C24) to the nitrile-carbon (C25) bond distance is 1.411 Å, and is contracted relative to the bond in free acetonitrile

(1.46 Å). The nitrile C-N distance of 1.1696(5) Å is elongated relative to the 1.158 Å in free acetonitrile, indicating a weakening of the nitrile bond.[401] Both the carbon-carbon bond contraction and the elongation of the nitrile bond are observed in the reported nickel-cyanomethide complexes (see section 4.3 for further details).[329,333]

Table 4-1: Selected bond distances (Å) and angles (°) for (Bu_4N)**9**.

	Bond distance		**Bond angle**
Cu1-C24	1.986(3)	N2-Cu1-N3	158.96(9)
Cu1-N1	1.945(2)	N1-Cu1-C24	175.4(1)
Cu1-N2	2.015(2)	N2-Cu1-C24	101.1(1)
Cu1-N3	2.011(2)	N3-Cu1-C24	100.0(1)
C24-C25	1.411(5)	C24-C25-N4	176.7(4)
C25-N4	1.166(5)		

The electronic structure of (Bu_4N)**9** was studied by UV-Vis and EPR spectroscopy. The UV-Vis spectrum of (Bu_4N)**9** has spectral features that are typical for copper(II) complexes with a ligand to metal charge transfer band (LMCT) at $\lambda_{max} = 315$ ($\varepsilon \sim 3800\ M^{-1}\ cm^{-1}$) and a d → d transition at $\lambda_{max} = 476$ ($\varepsilon \sim 380\ M^{-1}\ cm^{-1}$).[402]

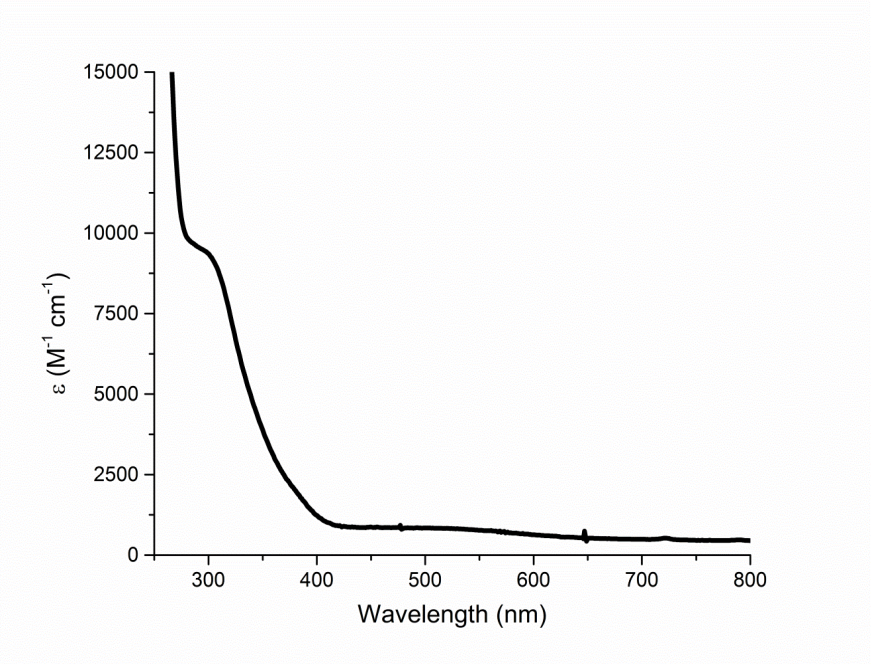

Figure 4-9: UV-Vis spectrum of (Bu_4N)**9** in acetonitrile.

The EPR spectrum of (Bu_4N)**9** in equal parts acetonitrile and toluene displayed a very broad axial signal with broad copper hyperfine visible (see (A) in **Figure 4-10**). In contrast, The EPR spectra of the related copper(II)-methanol, copper(II)-hydroxide, and copper(II)-chloride complexes exhibit hyperfine coupling to copper as well as the nitrogen atoms (see **Figure 4-10**).

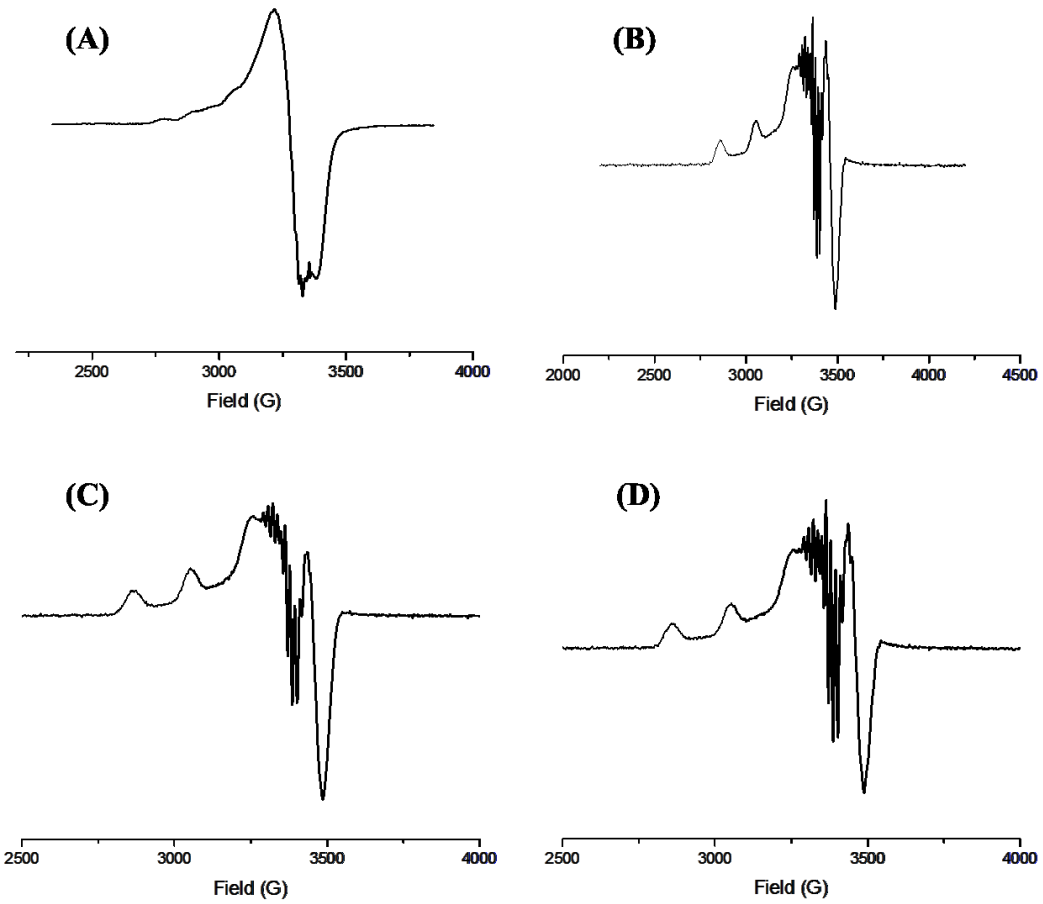

Figure 4-10: X-band perpendicular mode EPR spectrum at 10 K of (A) (Bu_4N)**9** in 1:1::acetonitrile:toluene mixture; (B) (Ph_4P)**8** in 1:1::acetone:toluene; (C) (Bu_4N)**7** in 1:1::acetone:toluene; and (D) **6** in 1:1::acetone:toluene.

To further corroborate the formulation of (Bu_4N)**9** in solution, ESI-MS spectrometry was employed. The negative mode ESI-MS of (Bu_4N)**9** in acetonitrile (Figure 4-10) showed a mass envelope with an isotopic pattern that aligned well with the anion $\mathbf{9}^-$. Similarly, (Bu_4N)**9D** was examined in d_3-acetonitirile and the mass envelope for the deuterated anion $\mathbf{9D}^-$ was observed. There was no evidence for the protio anion($\mathbf{9}^-$) under these experimental conditions.

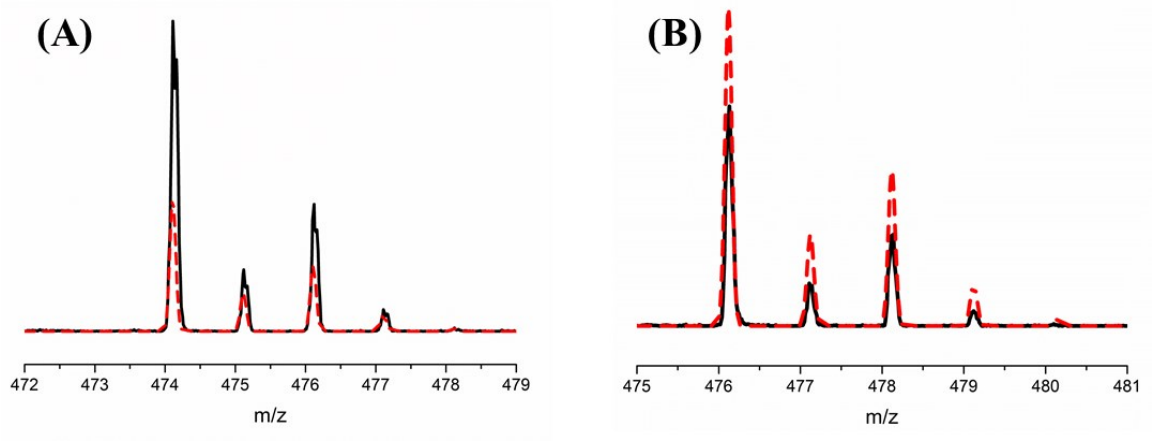

Figure 4-11: (A): Overlay of ESI-MS spectrum of(Bu_4N)**9** in acetonitrile and methanol (solid) and the simulated spectrum (dashed); (B): Overlay of ESI-MS mass spectrum of (Bu_4N)**9D** in d^3-acetonitrile and methanol (solid) and the simulated spectrum (dashed).

When the ESI-MS spectrum of (Bu_4N)**9D** was taken in protio solvent, however, a combination of the protio and deuterated anions, $\mathbf{9}^-$ and $\mathbf{9D}^-$, was observed (**Figure 4-12**). Satisfactory simulation of the experimental spectrum of (Bu_4N)**9D** was achieved by combining the simulations of the protio and deuteron isotopic patterns. This result indicates ligand exchange of the cyanomethide ion occurs under these experimental conditions. It is unclear if this exchange is due to kinetic lability of the cyanomethide ion at room temperature or if this exchange occurs only under the experimental conditions used for ESI-MS (high temperature and ionization radiation).

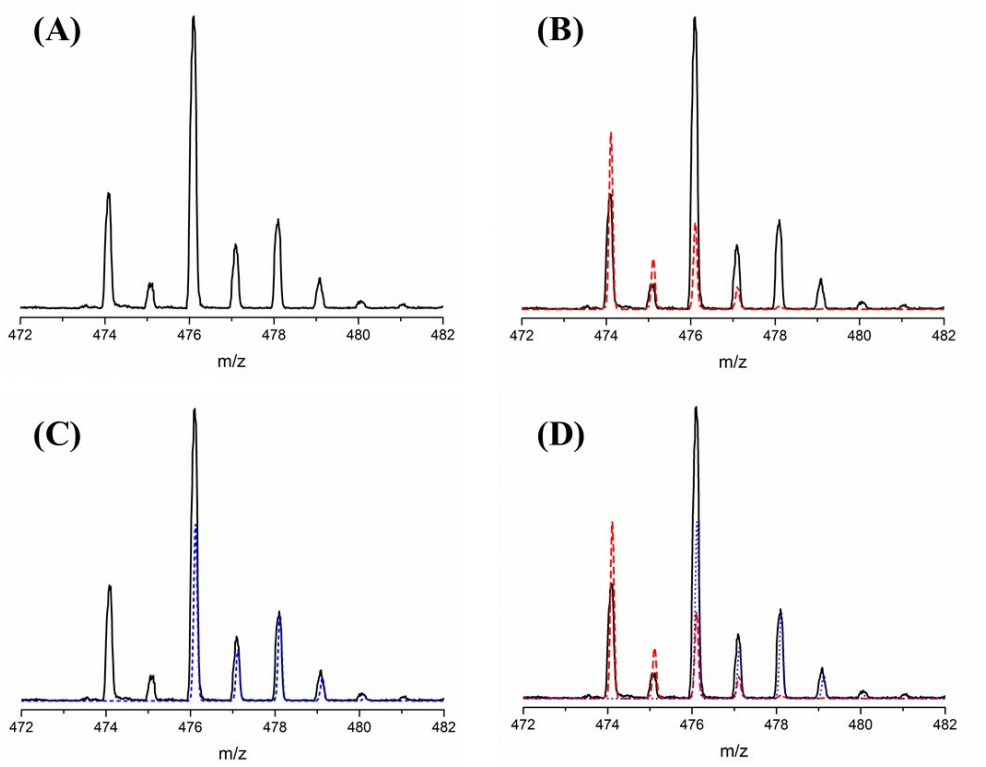

Figure 4-12: (A): ESI-MS spectrum of (Bu_4N)**9D** in acetonitrile and methanol; (B): Overlay of experimental spectrum (solid) and simulated (Bu_4N)**9** spectrum (dashed); (C): Overlay of experimental spectrum (solid) and simulated (Bu_4N)**9D** spectrum (dotted);); (D): Overlay of experimental spectrum (solid) with simulated (Bu_4N)**9** spectrum (dashed) and simulated (Bu_4N)**9D** spectrum (dotted).

Interestingly, the FT-IR spectrum of (Bu_4N)**9D** displays two peaks for the nitrile stretch, 2162 and 2192 cm^{-1}, as opposed to the single peak observed in the protio complex, (Bu_4N)**9**, at 2173 cm^{-1} (**Figure 4-13**). The protio stretch is slightly lower than the range of other reported transition metal-cyanomethide complexes (range from 2176-2201 cm^{-1}), but is well removed from free acetonitrile (2204 cm^{-1}).[327,329,335,403]

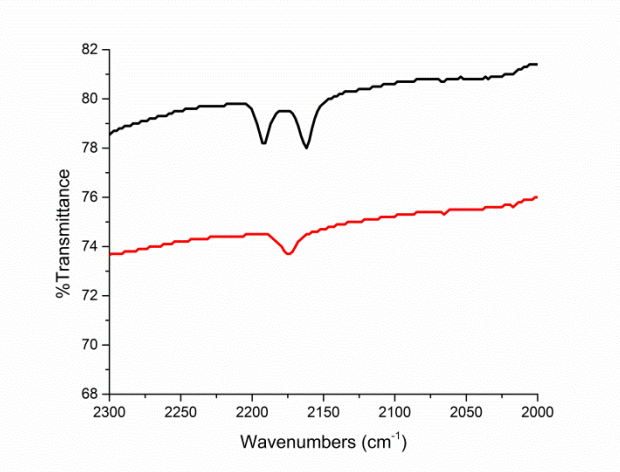

Figure 4-13: (Left): ESI-MS spectrum of the experimental spectrum of (Bu_4N)**9D** (solid) and simulated spectrum of (Bu_4N)**9D** (dashed). (Right): FT-IR spectra of the nitrile region of (Bu_4N)**9D (**top) and (Bu_4N)**9** (bottom) in a nujol mull.

The observed doublet can be attributed to a Fermi doublet arising from the coupling of the symmetric and anti-symmetric C-D bond stretches to the nitrile stretch. Fermi doublets occur when quantum mechanical mixing occurs due to coincidentally similar energies of the two stretching modes.[404] These experimental observations were corroborated by DFT calculations (**Table 4-2**). While all of the DFT stretching frequencies are slightly higher in energy than the experimental values, they show a high level of agreement as the scaling factor for experimental to the calculated value is greater than 0.96. In addition, the experimental values all scale proportionally to the calculated values, indicating good agreement between experiment and theory.

Table 4-2: DFT calculated nitrile vibration for (Bu_4N)**9** and (Bu_4N)**9D** reported in cm^{-1}. The ν_{Exp} / ν_{DFT} is a scaling factor that indicates a high level of agreement between the experimental measurements and DFT calculated value.

	νDFT	**νExp**	**νExp / νDFT**
(Bu_4N)**9**			
Nitrile vibration	2247	2173	0.967
(Bu_4N)**9D**			
Nitrile/C-D coupled vibration	2216	2192	0.989
Nitrile/C-D coupled vibration	2253	2162	0.960

4.2.1 Kinetic Investigation of the Conversion of [Copper(II)-OH]$^{1-}$ to a [Copper(II)CH_2CN]$^{1-}$ Complex

In order to gain information about possible mechanistic pathways of the conversion of (Bu_4N)**7** to (Bu_4N)**9** under ambient conditions, we carried out kinetic studies. In the kinetic experiments, a range of concentrations of (Bu_4N)**7** (0.13-2.89 mM) was used with a large excess of CH_3CN (14.9-18.3 M, 5200-16,000 equiv) in 1,2-difluorobenzene. The conversion was monitored by UV-Vis spectroscopy with illustrative data shown in **Figure 4-14**.

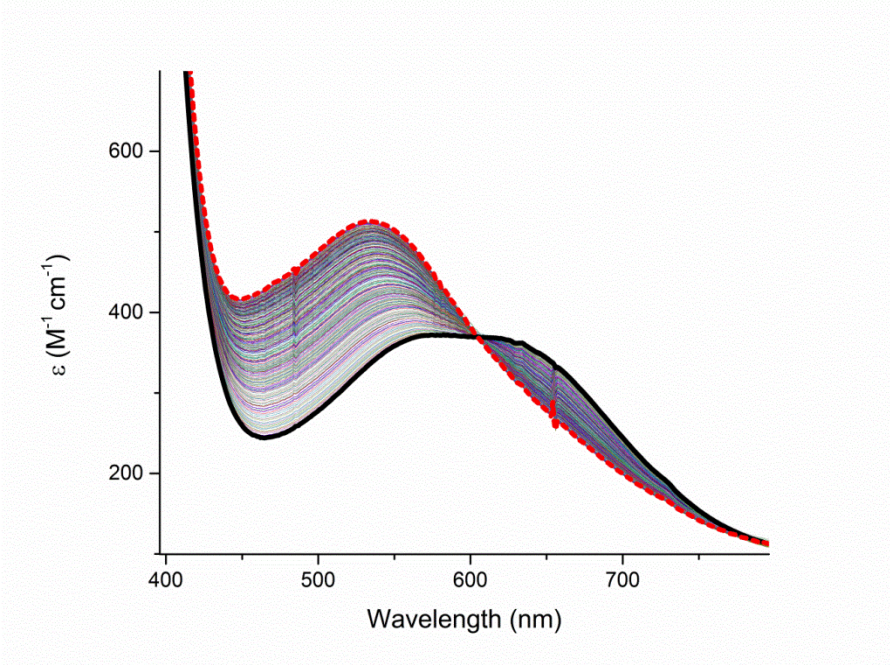

Figure 4-14: Conversion of 15mM of (Bu_4N)**7** (bold solid line) to (Bu_4N)**9** (bold dashed line) over a period of 2h; intermediate spectra taken at 60 second intervals.

The data were analyzed using a multi-wavelength decomposition software package, Olis Global Works, where the single-value decomposition fitting protocol was used and the reaction time courses were fit to first or second order reactions. Only the first order fits produced calculated UV-Vis spectra that were in good agreement with experimental

spectra of (Bu_4N)**7** and (Bu_4N)**9** (see **Figure 4-15**). The reaction followed pseudo-first order kinetics with k_{obs} = 4(1) x 10^{-4} s^{-1} (20 °C).

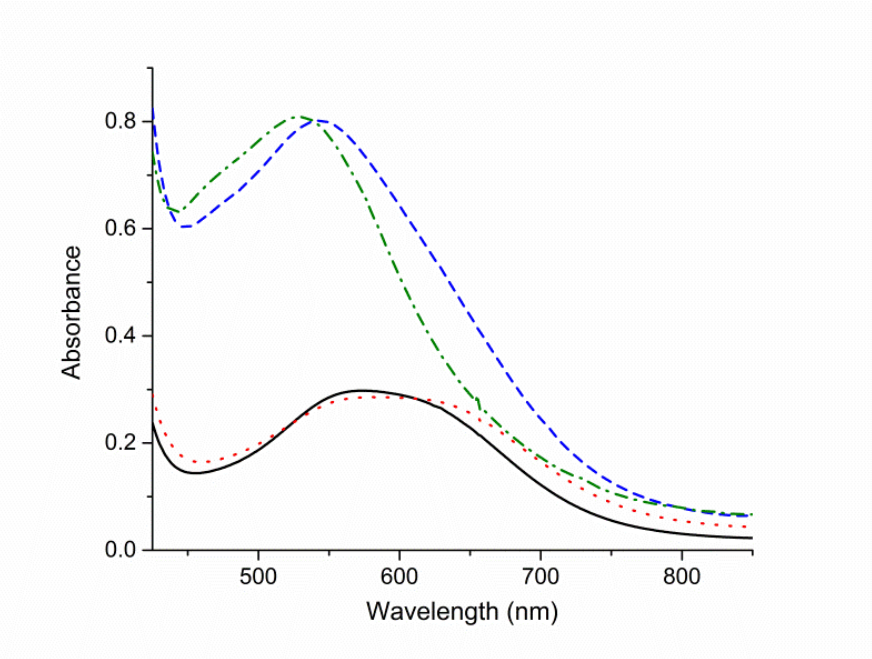

Figure 4-15: Overlay of the spectra of (solid) experimental (Bu_4N)**7** ; (dotted) calculated (Bu_4N)**7**; (dashed) experimental (Bu_4N)**9**; (dash-dot**)** calculated (Bu_4N)**9**.

We found that k_{obs} remains relatively invariant over the concentration range of acetonitrile used for the kinetic measurements(14.7-18.4 M) (see **Figure 4-16**).

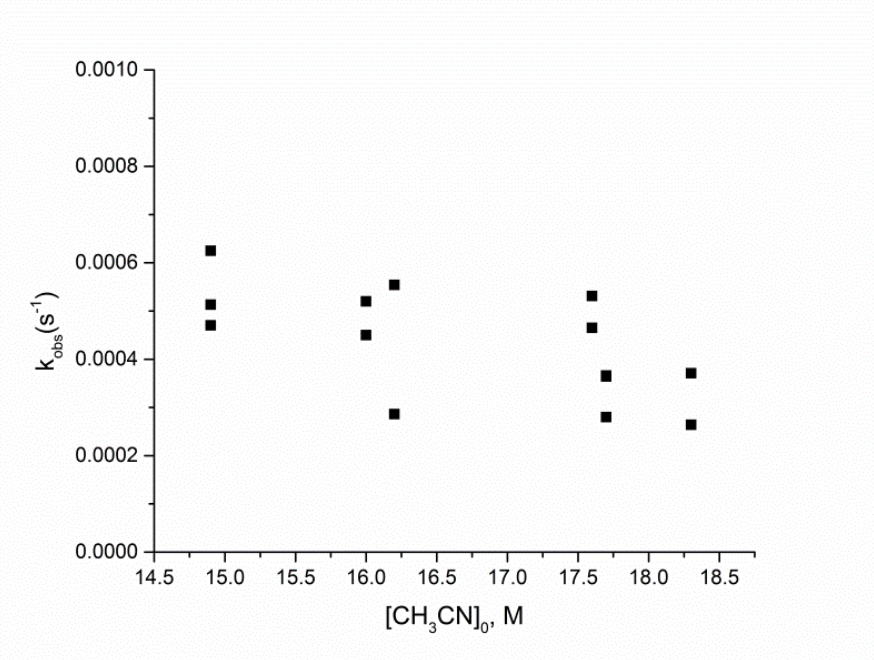

Figure 4-16: Plot of triplicate measurements of k_{obs} versus the initial concentration of CH_3CN for the reaction of (Bu_4N)**7** with CH_3CN to give (Bu_4N)**9**. The nearly invariant k_{obs} values observed over the concentration range suggest the reaction is zeroth order under these conditions.

In experiments aimed at further evaluating the order of the reaction in acetonitrile, reactions were formed with less of a gross excess of acetonitrile. The initial concentration of (Bu_4N)**7** was increased (15 mM in 1,2-difluorobenzene) and an aliquot of acetonitrile was added (100 equiv) in a short path UV cell in order to monitor the d-d band at higher concentrations. Under these conditions, the reaction was too slow to monitor accurately, as no change was observed over several days. When a slightly larger excess of acetonitrile was used (600 equiv) under similar conditions, a slow conversion was observed (**Figure 4-17**) over the course of 12 hours.

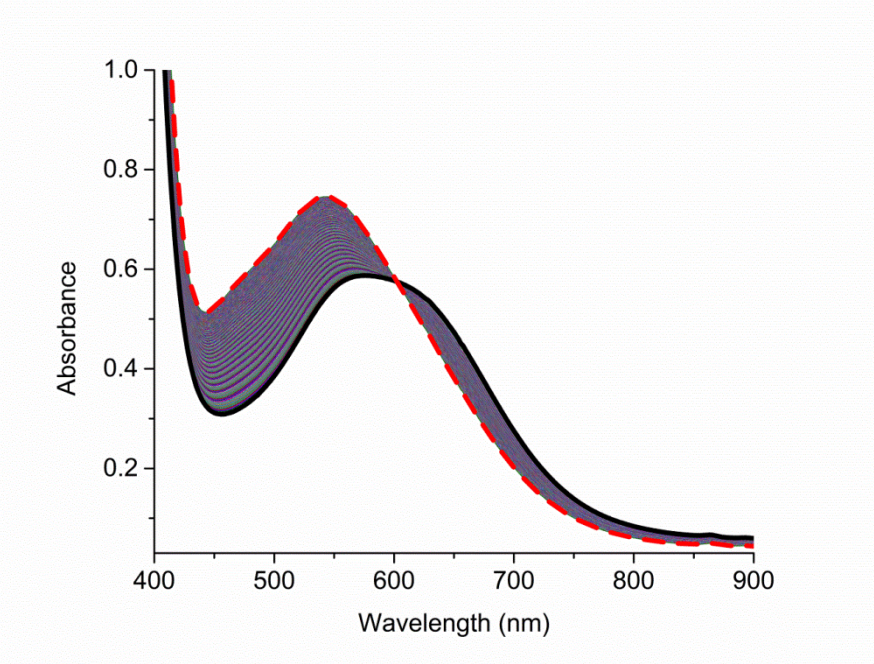

Figure 4-17: UV-Vis spectra of the conversion of 1.05 mM (Bu_4N)**7** in 1,2-difluorobenzene (solid bold line) to (Bu_4N)**9** (dashed bold line) upon the addition of 600 equiv. of acetonitrile at 20 °C over the course of 12 hours. Intermediate spectra taken in 1 minute intervals.

Spectral deconvolution of the reaction using the Olis Global Works software package led to similar k_{obs} values for a first and second order fit. When the calculated spectra of the components identified by the global fitting software were compared to experimental spectra, both first and second order fits provided accurate spectra for the starting complex (Bu_4N)**7**. The first order fit, however, provided a more accurate UV-Vis spectrum of the product, (Bu_4N)**9**, when compared to the second order fit as seen in (**Figure 4-18**).

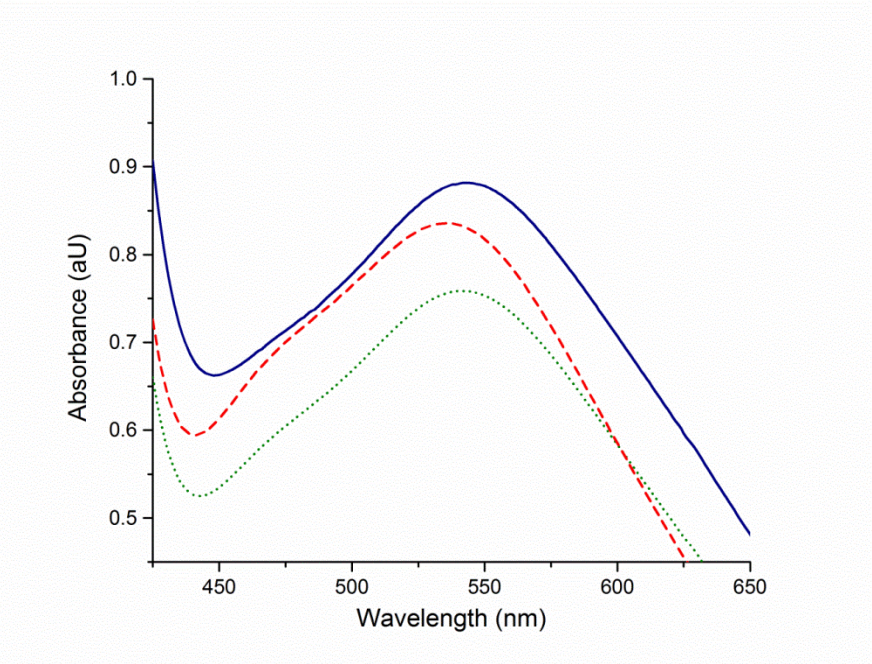

Figure 4-18: UV-Vis spectra of (**solid**): (Bu_4N)**9** in 1,2-difluorobenzene; (dashed): calculated product spectrum obtained from the second order fit; (dotted): calculated product spectrum obtained from the first order fit.

In order to truly assess the order in acetonitrile, further experiments are needed in order to compare the observed rate of conversion to (Bu_4N)**9** to the initial concentration of acetonitrile. Future experiments should aim to use at least 600 molar equivalents of acetonitrile, so that the reaction time is within a reasonable range. In addition, these reactions should use less than 5000 equivalents of acetonitrile as saturation was observed at higher concentrations (**Figure 4-16**).

In order to gain further information about the mechanism of this reaction, the kinetic isotope effect (KIE) for the reaction was measured by performing the reaction of (Bu_4N)**7** with acetonitrile and d^3-acetonitrile under identical conditions ($[(Bu_4N)\mathbf{7}]_0$ =1.11mM, 20 °C) in triplicate. A large KIE (k_H/k_D) of 4.1(1) was observed and suggests some degree of C-H bond breaking occurs during the rate limiting step. The deuterium

incorporated product, (Bu_4N)**9D**, was independently synthesized and its identity confirmed by ESI-MS spectrometry and FT-IR spectroscopy (see **Figure 4-13**).

4.2.2 Proposed Mechanism for Formation of [Copper(II)-CH_2CN]$^{1-}$ Complex

The kinetic experiments of the conversion of (Bu_4N)**7** to (Bu_4N)**9** elucidated the order of the reaction in (Bu_4N)**7**; however, due to the slow rate of reaction when acetonitrile is not in large excess, we were unable to determine the order in acetonitrile. Given that the reaction is first order in (Bu_4N)**7**, several possible mechanisms can be envisioned, as illustrated in **Scheme 4-13**.

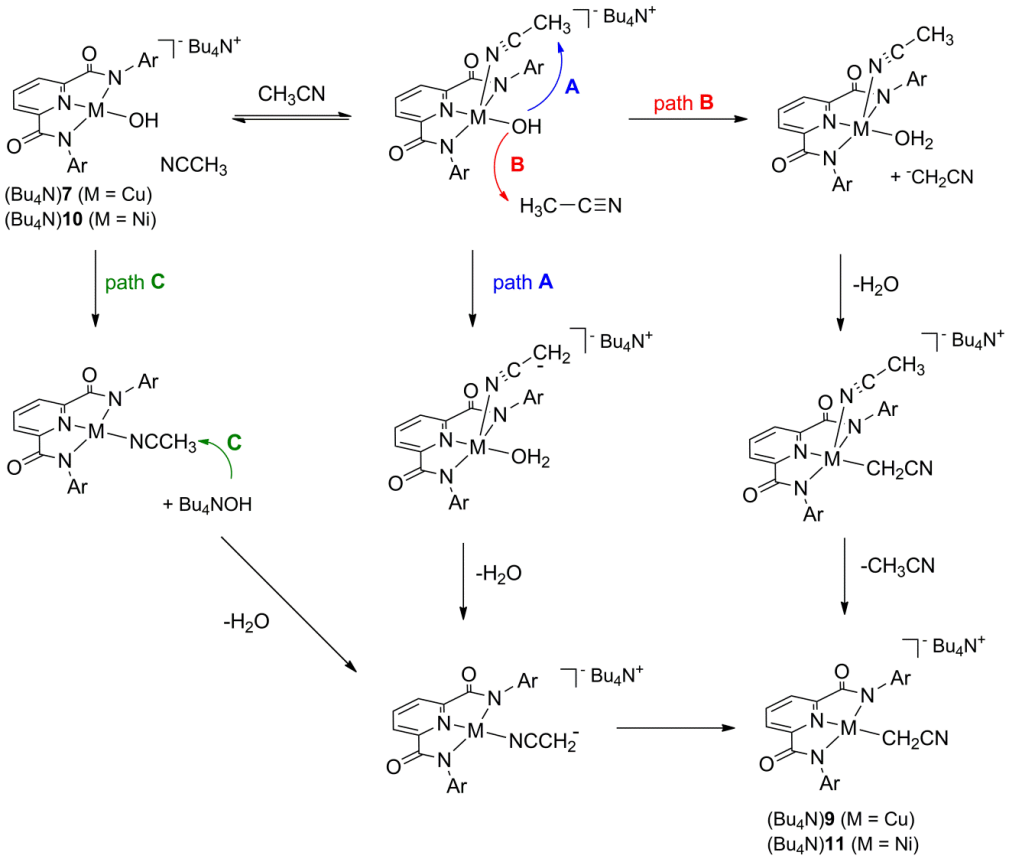

Scheme 4-13: Three proposed mechanisms for the conversion of (Bu_4N)**7** and (Bu_4N)**10** to (Bu_4N)**9** and (Bu_4N)**11** respectively in acetonitrile at room temperature, where Ar = 2,6-dimethylphenyl.

Pathway **A** involves an equilibrium between the four coordinate (Bu_4N)**7** and the five coordinate (Bu_4N)**7**-CH_3CN complex. From the (Bu_4N)**7**-CH_3CN, intramolecular attack of the hydroxide to deprotonate the axially bound acetonitrile generates a 5-coordinate (Bu_4N)($Cu(OH_2)(NCCH_2)^-$) complex. The dissociation of water and migration of the cyanomethide ligand to the equatorial position is then followed by rearrangement to give the C-bound cyanomethide complex, (Bu_4N)**9**. The dissociation of water and the rearrangement of the cyanomethide from N-bound to C-bound can also be envisioned as a concerted process. Similarly, Pathway **B** begins with an equilibrium between the 4- and 5-coordinate (Bu_4N)**7** species. From the 5-coordinate species, attack of the hydroxide moiety on an exogenous acetonitrile molecule generates the neutral ($Cu(NCCH_3)(OH_2)$) species and a free cyanomethide ion. Subsequent ligand exchange of the cyanomethide for the aqua ligand yields the 5-coordinate (Bu_4N)**9**-CH_3CN complex, which upon dissociation of the axial acetonitrile gives (Bu_4N)**9**. For pathway **C**, the hydroxide ligand is replaced by an acetonitrile molecule to give the 4-coordinate neutral N-bound ($Cu)(NCCH_3$) complex. Deprotonation of the bound acetonitrile by the exogenous hydroxide generates the (Bu_4N)($L^{Me}CuNCCH_2^-$), which upon rearrangement to the C-bound cyanomethide gives (Bu_4N)**9**.

Without the order of the reaction in acetonitrile, we are unable to distinguish between pathway **A** and **B** in the proposed mechanisms in **Scheme 4-13**. Pathway **A** is attractive considering the metal complex maintains a -1 charge throughout the process, whereas Pathway **B** and **C** both invoke neutral intermediates. Pathway **C**, seems less likely as complex (Bu_4N)**2** complex is obtained by the reaction of the copper(II)-

acetonitrile complex, **1**, with Bu_4NOH,[123] albeit in diethyl ether and not in excess acetonitrile.

4.2.3 Oxidation of [Copper(II)-CH_2CN]$^{1-}$ to Generate a Copper(III)-CH_2CN Complex

Electrochemical studies (cyclic voltammetry) were performed on (Bu_4N)**9** to probe its electronic properties. When(Bu_4N)**9** was generated in-situ by the addition of (Bu_4N)**7** to 0.1 M Bu_4NPF_6 in acetonitrile at room temperature under inert conditions, a pseudo-reversible wave is observed at $E_{1/2}$= -0.345 V vs Fc/Fc^+ and ΔE_p = 105 mV (scan rate 200 mV/s) (**Figure 4-19**).

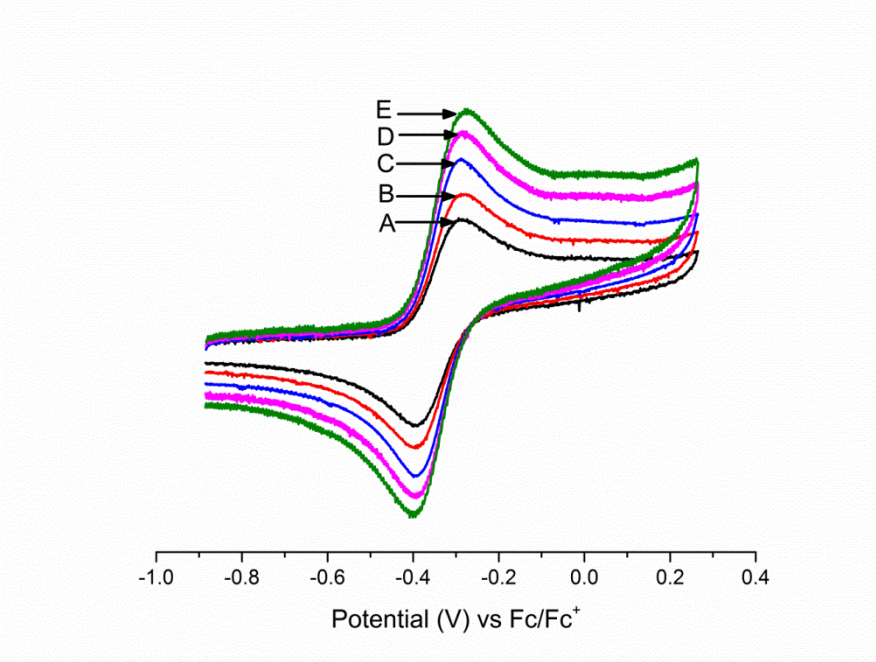

Figure 4-19: Cyclic voltammograms of 1 mM (Bu_4N)**9**in 0.1 M [Bu_4N][PF_6] in acetonitrile referenced to Fc/Fc^+ with varying scan rates (A) 100 mV/s; (B) 150 mV/s; (C) 200 mV/s; (D) 300 mV/s; (E) 400 mV/s.

The oxidation of (Bu_4N)**9** was further investigated by UV-Vis spectroscopy due to the desire to generate a copper(III)-alkyl species that bears relevance to intermediates proposed in many reactions important in organic transformations (see section 4.1.2).

Chemical oxidation of (Bu_4N)**9** was readily achieved by oxidation with $FcPF_6$ at −30 °C in acetonitrile to generate an intense orange chromophore, **9'**(λ_{max} ~ 465 nm, ε ~ 7700 M^{-1} cm^{-1}). The spectrum of **9'** has markedly different spectral features from those of the oxidation product of (Bu_4N)**7** (**Figure 4-20**).

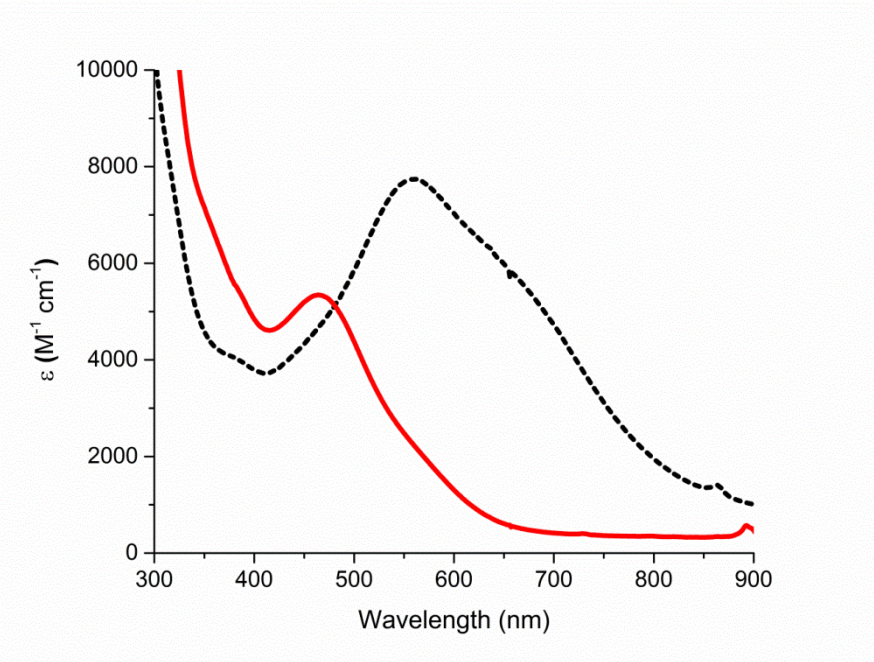

Figure 4-20: UV-Vis spectral overlay of **(**solid) oxidation product of (Bu_4N)**9** in acetonitrile at −30 °C (dashed) oxidation product of (Bu_4N)**2** in 1,2-difluorobenzene at −25 °C.

The stability of **9'** at −30 °C is in stark contrast to other neutral copper(III)-species, such as η^1-copper(III) σ-allyl complexes and η^3-copper(III) π-allyl complexes, which were only recently observed by Rapid Injection NMR (RI-NMR) spectroscopy at −100 °C.[82,100,101] While the stability of the complexes varied at −100 °C depending on the nature of the ligands, the complexes decomposed at temperatures higher than −80 °C. It should be noted that in contrast, some copper(III)-aryl complexes are stable at room temperature.[405]

The pseudo-reversible electrochemical oxidation observed for (Bu_4N)**9** led us to investigate if the complex was chemically reversible. Upon addition of 1 molar equivalent of $Fc^+PF_6^-$ to (Bu_4N)**9** at −30 °C in acetonitrile, an immediate color change from red-purple to intense orange solution was observed. Addition of 1 molar equivalent of decamethylferrocene (Cp^*_2Fc) to the solution led to an immediate color change back to a red-purple solution. The formation of ferrocene was also observed upon growth of the diagnostic feature at ~790 nm. A second course of sequential oxidation (addition of 1 molar equivalent of $Fc^+PF_6^-$) and reduction (addition of 1 molar equivalent of Cp^*_2Fc) led to the same spectral features, indicating that oxidation of (Bu_4N)**9** is chemically reversible (**Figure 4-21**).

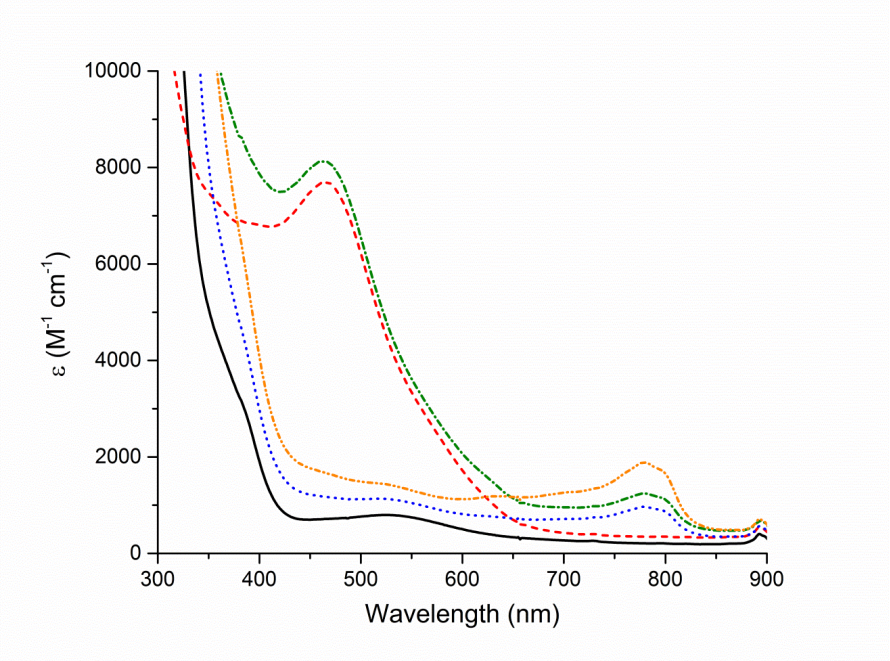

Figure 4-21: UV-spectra indicating the reversible oxidation of (Bu_4N)**9** (0.19 mM) in CH_3CN at −30°C. (solid): (Bu_4N)**9**; (dashed) after addition of 1 (equiv. $Fc^+PF_6^-$; (dotted) after addition of 1 equiv. of Cp^*_2Fc; (dash-dot) after addition of a second 1 equiv. aliquot of $Fc^+PF_6^-$; (dash-dot-dot) after addition of a second 1 equiv. of $Cp^*_{2;\,R}Fc$. Note: The feature at ~790 nm corresponds to the formation of ferrocene.

4.2.3.1 Computational Studies on Copper(III)-CH_2CN

Time dependent density functional calculations (TD-DFT) on the electronic structure of **9'** indicates the singlet configuration of a copper(III) complex is favored over the triplet configuration of acopper(II)-radical species by 22 kcal/mol. The TD-DFT electronic calculations indicate a strong correlation of the singlet structure with the experimental data as indicated in **Figure 4-22**. The triplet state formulation includes strong transitions at low energy (1171 nm, 844 nm, and 758 nm) that are not observed in the experimental spectrum. Additionally, the calculations suggest the singlet bond distances contract by 0.1 Å, whereas the triplet expands. This contraction of the bond distances of the singlet state was also observed for the oxidation of the (Bu_4N)**2** to **2'**.[406]

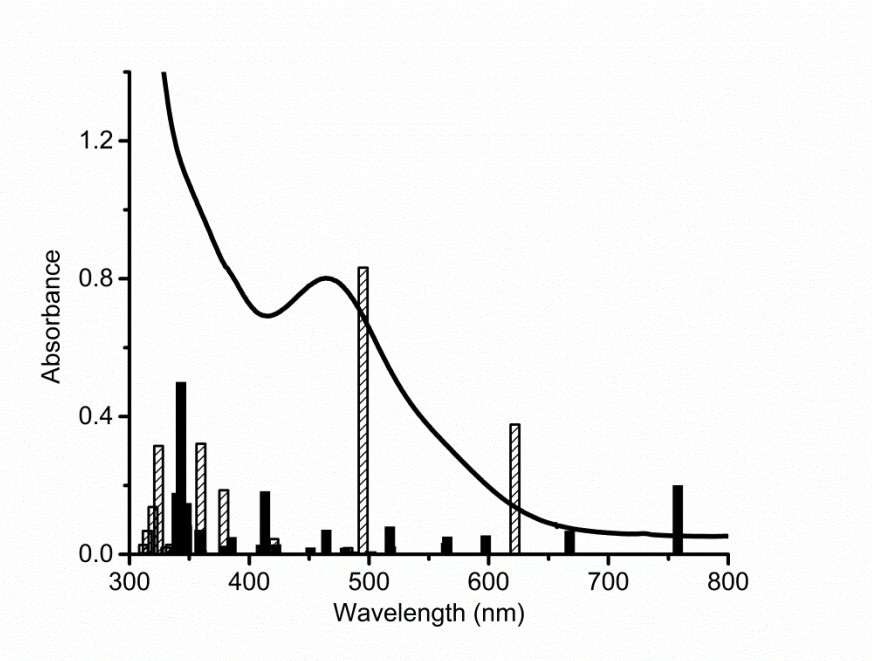

Figure 4-22: Overlay comparing the electronic features of (black line). The experimental UV-Vis spectrum of (Bu_4N)**9** to the DFT calculated (B98) electronic transition for the restricted singlet (dashed bars) and triplet structures (solid bars).

The singlet state spectrum has two major ligand-metal charge transfer (LMCT) bands at 495 and 622 nm. The 495 nm transition results from an excitation that is a combination of three different ligand orbitals: two amide(π) based and one aryl(π) based orbitals that are excited into the Cu(dx^2-y^2) anti-bonding orbital (orbitals A, B, C, and D respectively in **Figure 4-23**).

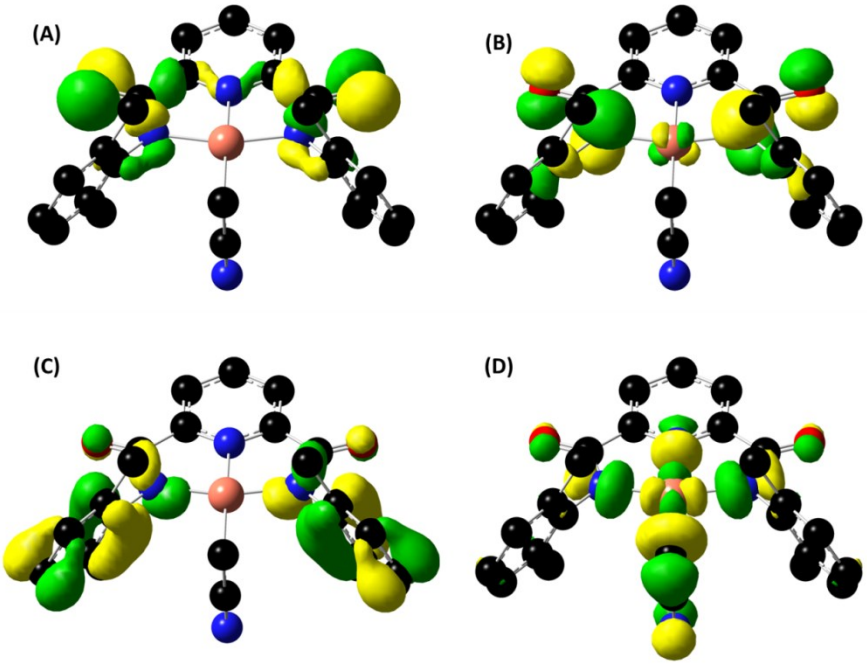

Figure 4-23: DFT calculated orbitals involved in the electronic transitions observed upon oxidation of (Bu_4N)**9** (A) amide(π); (B) amide(π); (C) aryl(π); (D) Cu(dx^2-y^2).

The major contribution for the 495 nm feature is excitation of an amide(π) based orbital (A) into the Cu(dx^2-y^2) anti-bonding orbital (D). The 622 nm feature contains contributions of an amide(π) orbital (B) and an aryl(π) orbital (C) exciting into the Cu(dx^2-y^2) anti-bonding orbital with the major contribution coming from the excitation from (C) to (D) excitation.

4.2.4 Reactivity of a Copper(III)-CH_2CN Complex

Due to the nucleophilic nature of carbanions, the reactivity of **9'** was investigated with *trans*-chalcone.

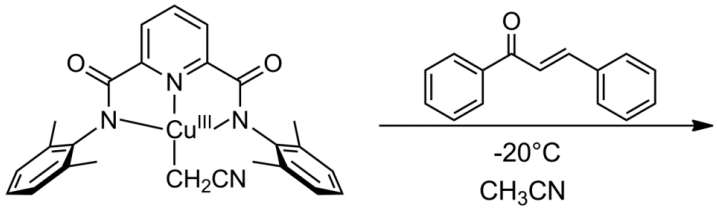

Scheme 4-14: Reaction of **9'**with *trans*-chalcone.

The UV-Vis spectra of the reaction of **9'**with 10 eq of *trans*-chalcone at −30 °C did not show any appreciable change in the decay rate of **9'(Figure 4-24)** or the formation of any new species. Similarly, GC-MS analysis of the reaction mixture, after acidic work-up and extraction with organic solvent, displayed starting material. This indicates that **9'** is not reactive towards activating internal alkenes, particularly α,β-unsaturated ketones.

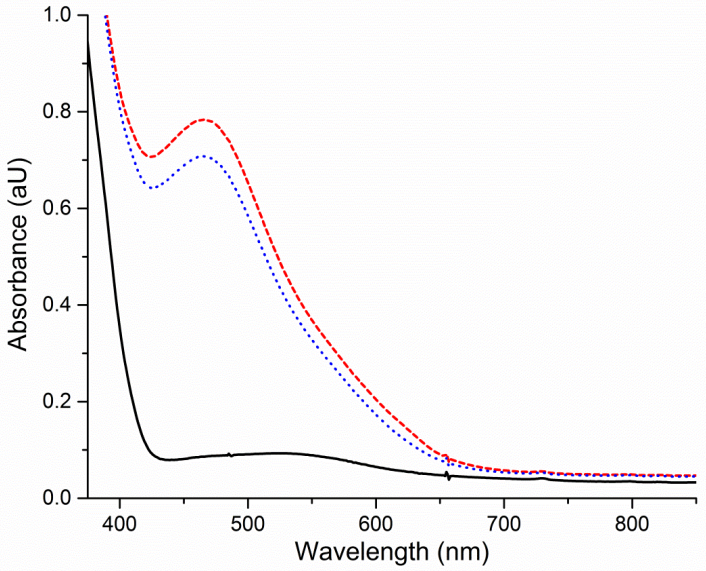

Figure 4-24: UV-Vis spectra of (solid) (Bu_4N)**9** in the presence of 10 equiv. of *trans*-chalcone; (dashed) (Bu_4N)**9** upon addition of 1 equiv. of FcPF6 to give **9'** (dotted) spectrum after 80 minutes in acetonitrile at −30 °C.

The potential for utilizing **9'** as a hydrogen atom abstractor was also surveyed, as the corresponding hydroxide complex (**7'**) proved very effective at hydrogen atom abstraction from dihydroanthracene (DHA) (see Chapter 3). The reaction of **9'** with 10-100 equivalents of DHA ranging from −20 °C to 10 °C was monitored by UV-Vis spectroscopy. The reactions did not show enhanced rate of decay of **9'** or formation of anthracene, which would be expected upon reaction with DHA. Analysis of the reaction mixture after acidic workup and organic extraction did not indicate the formation of anthracene. These studies indicate **9'** does not rapidly attack weak C-H bonds, unlike the corresponding hydroxide complex, **7'**.

4.3 Isolation of a [Nickel(II)-CH_2CN]$^{1-}$ Complex

The synthesis of (Bu_4N)**11** was carried out in an analogous fashion to the copper chemistry (see section 4.2), and it was characterized by ESI-MS spectrometry, FT-IR spectroscopy, NMR spectroscopy, and X-ray crystallography. The solid state structure of (Bu_4N)**11** was determined by single crystal X-ray crystallography and reveals a square planar nickel center coordinated by the dicarboxamide ligand and a cyanomethide ligand (**Figure 4-25**). Important bond distances and angles of (Bu_4N)**11** are presented in **Table 4-3**.

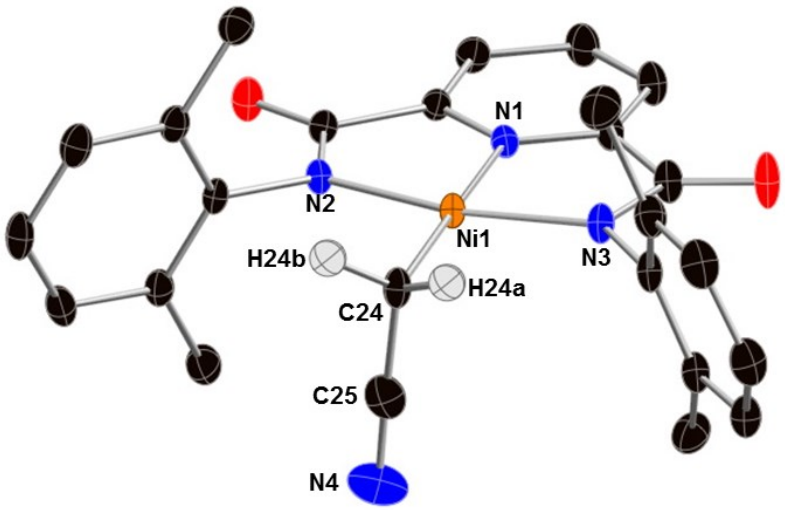

Figure 4-25: X-ray crystallographic representation of the anionic portion of (Bu_4N)**11** with thermal ellipsoids drawn a 50%. The hydrogen atoms of the ligand, the cation, and a solvent molecule are omitted for clarity. Space group: $P2_1/c$, R1 = 0.0398, wR2 = 0.1133.

The solid state structures of (Bu_4N)**11** and (Bu_4N)**9** both crystalize in the same space group ($P2_1/c$) and are homologous, with metal to ligand bond distances differing due to the size of the metallic ion (**Figure 4-26**).

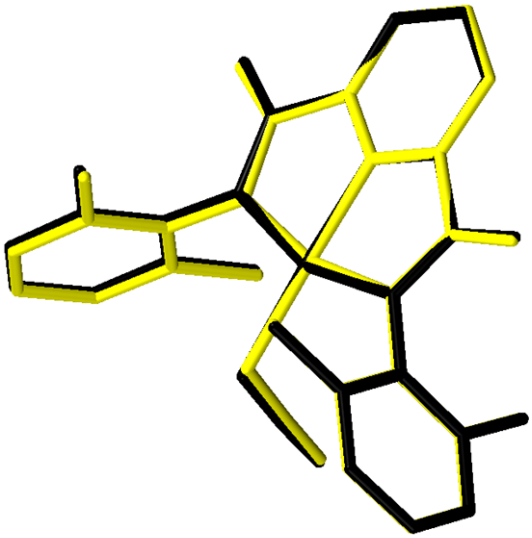

Figure 4-26: Overlay of the anion portions of (Bu_4N)**9** (black) and (Bu_4N)**11** (grey), indicating a high degree of structural similarity. RMS (root mean square) ~ 0.07.

A nickel-carbon bond distance measure in (Bu_4N)**11** is 1.921(2) Å, which indicates a single bond between the two atoms and is the shortest nickel-cyanomethide distance in the literature. The recent report of Guan and coworkers' square planar (POCOP)Ni(CH_2CN) (POCOP = 2,6-($iPr_2PO)_2C_6H_3$) complex has a nickel-CH_2CN distance of 2.0123(9) Å , which is longer than the nickel-CH_2CN distance observed in (Bu_4N)**11**. [329] Guan and coworkers attribute the longer nickel-carbon bond to a strong *trans* influence arising from the aromatic ring of the pincer ligand. Similarly, Jones and coworkers report a complex (Ni(dippe)(CH_2CN)Cl) (dippe= 1,2-bis(diisopropylphosphino)ethane) with nickel-CH_2CN distance of 2.0135 Å.[328] A three-coordinate (($Mes)_2$NHC)(Cp*)Ni(CH_2CN) (Mes = mesityl) complex has a shorter nickel-cyanomethide bond of 1.961(2) Å.[333] The geometry about the nickel center is trigonal, unlike the square planar geometry of the other complexes, making direct comparison of bond distances difficult. The Guan and Jones complexes are both neutral complexes,

which may be a factor in why both structures exhibit longer nickel to carbon bond distances than (Bu_4N)**11**. The methide-carbon (C24) to the nitrile-carbon (C25) bond is 1.436 Å and is contracted relative to the bond in free acetonitrile (1.4521 Å), which is to be expected upon deprotonation of the methyl group. This contraction is observed for the Guan and Jones complexes, which have distances of 1.438(3) Å and 1.445(2) Å respectively. The nitrile bond measures 1.159(3) Å, which is within error of the nitrile bond distance 1.158 Å in free acetonitrile.[401] This finding is in contrast to the copper(II)-CH_2CN complex that displayed a slight elongation of the nitrile bond. Both the Guan and Jones complexes display an elongation of the nitrile bond with distances of 1.149(3) Å and 1.153(2) Å observed.

Table 4-3: Selected bond distances (Å) and angles (°) for (Bu_4N)**11.**

Bond Distance			**Bond angle**
Ni1-C24	1.941(2)	N2-Ni1-N3	164.67(6)
Ni1-N1	1.850(2)	N3-Ni1-C24	97.64(7)
Ni1-N2	1.918(1)	N2-Ni1-C24	97.69(7)
Ni1-N3	1.913(1)	N1-Ni1-C24	177.90(7)
C24-C25	1.436(3)	C24-C25-N4	178.0(2)
C25-N4	1.159(3)	Ni1-C24-C25	107.2(1)

Further evidence for the solid state structure was provided by FT-IR, where a sharp stretch (ν = 2190 cm^{-1}) was observed in the nitrile region and was shifted significantly from free acetonitrile (ν = 2204 cm^{-1}). The formulation of (Bu_4N)**11** was also suggested to be preserved in solution , as evidence by the observation of the $\mathbf{11}^-$ species by ESI-MS (**Figure 4-27**). Preparation of the deuterated cyanomethide complex, (Bu_4N)**11D**, was

also confirmed by ESI-MS spectrometry and ligand exchange was observed as described with related copper complex (Bu_4N)**9**.

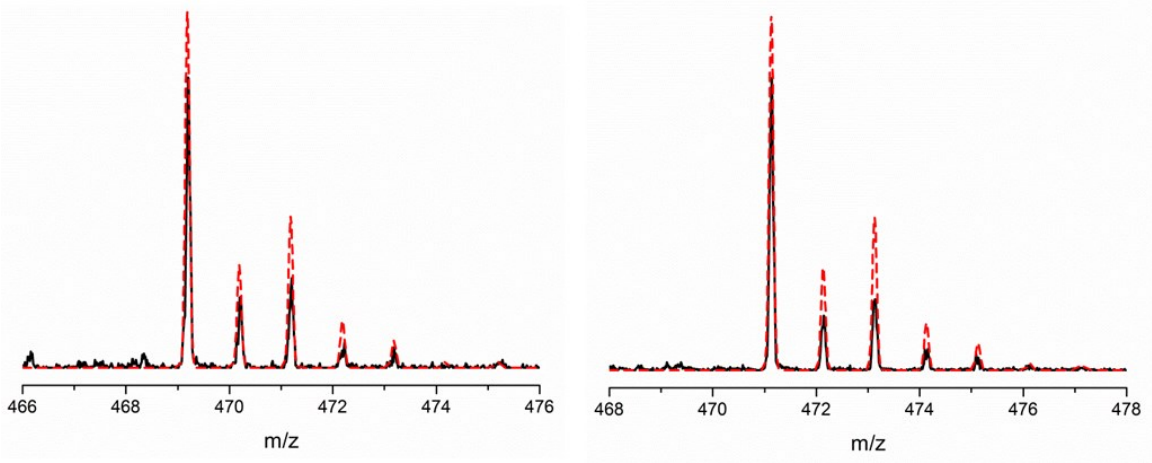

Figure 4-27: (Left): ESI-MS spectrum of (Bu_4N)**11 (solid)** experimental spectrum; (dashed) simulated spectrum. (Right): ESI-MS spectrum of (Bu_4N)**11D (solid)** experimental spectrum; (dashed) simulated spectrum.

The diamagnetic nature of (Bu_4N)**11** allowed for collection of ^{1}H-NMR spectra, which indicated the two cyanomethide protons were equivalent and shifted upfield δ = -.089 (s, 2H). This value suggests the nickel(II)-cyanomethide moiety remains intact in solution. In addition, UV-Vis spectroscopy of (Bu_4N)**11** displays similar spectral features and intensities to those of the related hydroxide and bicarbonate complexes[121] (**Figure 4-28**).

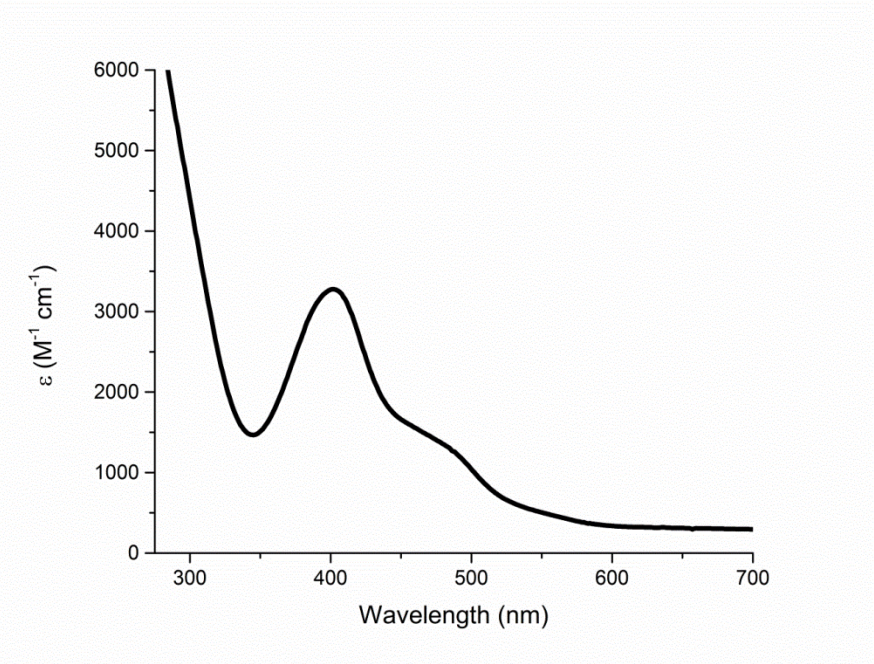

Figure 4-28: UV-Vis spectrum of (Bu_4N)**11** in acetonitrile at room temperature.

4.4 Attempts to Use [M(II)-CH_2CN]$^{1-}$Complexex as –CH_2CN Transfer Agents (M = Cu, Ni)

The utility of the copper(II)-CH_2CN, (Bu_4N)**9**, and nickel(II)-CH_2CN, (Bu_4N)**11**, complexes as cyanomethyating reagents was tested by allowing each metal complex to react at room temperature for 6 hours with 100 equivalents of either allyl bromide, benzyl bromide, or benzaldehyde in acetonitrile. Allyl bromide and benzyl bromide were chosen because previous work with copper(I) systems have shown that allyl bromide is readily cyanomethylated under most conditions, whereas benzyl bromide is only cyanomethylated with particular copper catalyst systems (see section 4.1.3.1 for more details). Inspired by the current report of cyanomethylation of aldehydes by a nickel(II)-CH_2CN complex, we investigated the reactivity of our metal(II)-CH_2CN complexes towards benzaldehyde.[329] All reactions were analyzed by GC-MS and ^{1}H-NMR

spectroscopy after acidification of the reaction mixture and extraction with organic solvent. Analysis of the organic reaction mixture revealed only starting material, and no features corresponding to product formation were observed by GC-MS or ^{1}H-NMR spectroscopy. Future work should examine the reactivity of the metal(III)-cyanomethide species, **9'** and **11'** respectively, for their utility as cyanomethylating reagents, as they may be more reactive than their metal(II) counterparts.

4.5 Perspectives and Future Work

A novel copper(II)-cyanomethide ((Bu_4N)**9**) and a rare nickel(II)-cyanomethide ((Bu_4N)**11**) complex were synthesized via reaction of their corresponding hydroxide complexes with acetonitrile. Both complexes were characterized using ESI-MS, X-ray crystallography, FT-IR and UV-Vis spectroscopy. The reactivity of these metal-hydroxides with nitriles is unprecedented, as nitriles are typically hydrolyzed under such conditions. Kinetic studies on the copper(II)-hydroxide complex indicate that the reaction is first order with respect to copper. The order of the reaction for acetonitrile has been more difficult to assess due to the need to use excess acetonitrile to observe reasonable reaction rates.

Initial efforts to utilize the copper(II)-cyanomethide and nickel(II)-cyanomethide complex as cyanomethylating reagents towards aldehydes and alkyl halides were unsuccessful. Further studies should aim to investigate the ability of the oxidized metal-cyanomethide complexes to act as a cyanomethylating reagent.

4.6 Experimental

General Considerations. All solvents and reagents were obtained from commercial sources and used as received unless otherwise noted. $L^{Me}H_2$ was prepared according to the literature procedure.[120] The solvents Et_2O and pentane were passed through purification columns (Glass Contour, Laguna, California) before use. Acetonitrile was dried over CaH_2, degassed, distilled under vacuum and stored over CaH_2 in a glovebox. Acetone was dried over 3Å molecular sieves, degassed, vacuum transferred and stored over 3Å molecular sieves in a glovebox. 1,2-Difluorobenzene was dried over CaH_2, degassed, distilled under vacuum and stored over 3 Å molecular sieves in a glovebox. Anydrous DMF was stored over 3Å molecular sieves in a glovebox for 2 days and dried over a section portion of 3Å molecular sieves for an additional 2 days before use. All reactions of $LCu(CH_3OH)$ (**6**) were performed in glovebox under a dry N_2 atmosphere.

Physical Methods. NMR spectra were recorded on a 300 MHz Varian Inova spectrometer and cation resonances are omitted for clarity. UV-Vis spectra were recorded on an HP8453 (190-1100 nm) diode-array spectrophotometer equipped with a Unisoku low-temperature cryostat. Electrospray ionization mass spectra (ESI-MS) were recorded in negative ion mode on a Bruker BioTOF II instrument. Electron paramagnetic resonance (EPR) spectra were recorded a Bruker Continuous Wave EleXsys E500 spectrometer at 10 K. EPR simulations were achieved by using Bruker Simfonia software. Infrared spectra were collected on a Nicolet Avatar 370FT-IR Elemental analyses were performed by Robertson Microlit Laboratory (Ledgewood, New Jersey) and Compete Analysis Laboratories Inc (Parsippany, New Jersey). X-ray crystallography

data collection and structure solution were conducted using a SMART Apex II instrument and the current SHELXTL suite of programs.[407]

$L^{Me}Cu(MeOH)$ (6). $L^{Me}H_2$ (1.015 g, 2.72 mmol), anhydrous $CuCl_2$ (0.367 g, 2.73 mmol) and MeOH (100 mL) were added to a 250 mL round bottom flask to give a light green solution. Addition of a solution of NaOMe in MeOH (0.5 M, 9.2 mL, 4.6 mmol) yielded a deep forest green solution, which was stirred for 30 min. The solvent was removed *in vacuo* to give a green oil. This oil was dissolved in CH_3CN (~ 20 mL) and toluene (100 mL) was added, after which a precipitate formed and the solution became mahogany in color. The mixture was filtered through a fine porosity frit and solvent was removed from the filtrate *in vacuo* to produce a bright green powder. Subsequent washings with acetonitrile (3 x 5 mL) and hexanes (3 x 5 mL) afforded the product as a bright green solid, which was dried in the vacuum oven at 40 °C overnight (0.75 g, 69%). ESI-MS (CH_3OH, *m*/*z*): calcd 465.11 $[M-H]^{1-}$, found 465.16. UV-Vis [λ_{max}, nm (ε, M^{-1} cm^{-1}) in CH_3CN]: 397 (1400), 545 (720). Anal. Calcd. for $C_{24}H_{25}CuN_3O_3$: C, 61.72; H, 5.40; N, 9.00. Found: C, 61.83; H, 5.29; N, 8.93.

$(Bu_4N)(L^{Me}CuOH)$ (7). To **6** (147 mg, 0.314 mmol) was added Et_2O (~ 10mL) to give a green reaction mixture. Upon the addition of Bu_4NOH in MeOH (1.0 M, 0.31 mL, 0.31 mmol) a blue sticky precipitate formed. The reaction was stirred for ~5 min and the solvent was removed *in vacuo* to give a dark blue oil. The oil was washed with Et_2O (3 x 5 mL) to yield the product as a bright blue-purple solid (129 mg, 85%). UV-Vis [λ_{max}, nm (ε, M^{-1} cm^{-1}) in acetone]: 378 (1800), 550 (230). Anal. Calcd. for $C_{39}H_{58}CuN_4O_3$: C, 67.45 H, 8.42; N, 8.07. Found: C, 66.86; H, 8.15; N, 8.02. EPR (10 K): $g_x = 2.02$, $g_y = 2.06$, $g_z = 2.19$; A values (x 10^{-4} cm^{-1}): A(Cu) =192, A(N_{py}) =18.2, A (N_{am}) =13.5.

[Bu_4N][$L^{Me}Cu(CH_2CN)$] (9). Compound **7** (109 mg, 0.185 mmol) was added to CH_3CN (~ 10 mL) to give a dark blue solution, which became red-purple (< 2min). The reaction was stirred for 30 min and the solvent was removed *in vacuo*. The resulting solid was washed with Et_2O (2 x 3 mL) to yield the product as a deep purple solid (129 mg, 85%). Negative ion ESI-MS (CH_3OH, *m*/*z*): calcd 474.11 $[M\text{-}Bu_4N]^{1-}$, found 473.96. UV-Vis [λ_{max}, nm (ε, M^{-1} cm^{-1}) in CH_3CN]: 315 (3800), 476 (380). FT-IR(Nujol mull): 2173 cm^{-1}. Anal. Cald. for $C_{41}H_{59}CuN5O_2$: C,68.63; H,8.29; N,9.76. Found: C, 68.58; H, 8.22; N, 9.66.

(Bu_4N)($L^{Me}Cu(CD_2CN)$) (9D). This compound was prepared according to the same procedure used to prepare **9**, except using CD_3CN (99.8%) on a 52.5mg (0.0756 mmol) scale, to give **5** as a deep purple solid (54.4 mg, 73.2 %). ESI-MS (CH_3OH, *m*/*z*): calcd 476.12 $[M\text{-}Bu_4N]^{1-}$, found 476.09. IR (Nujol mull): 2162, 2192 cm^{-1}.

(Bu_4N)($L^{Me}NiOH$) (10). The synthesis of **10** was carried out in an analogous fashion to the previously reported[120](Et_4N)($L^{Me}NiOH$) complex and similar UV-VIS and ^{1}H-NMR spectroscopic features were obtained.

(Bu_4N)($L^{Me}Ni(CH_2CN)$) (11). The synthesis of **11** was analogous to the procedure used for **6.** Briefly, **4** (115 mg, 0.167 mmol) was added to CH_3CN (~ 10 mL) to give a yellow orange solution which became red-orange upon stirring overnight. The solvent was removed *in vacuo* to give a sticky red solid to which 5 mL of Et_2O was added and stirred for 3 hrs. ESI-MS (CH_3OH, *m*/*z*): calcd 469.12 $[M\text{-}Bu_4N]^{1-}$, found 469.20. UV-Vis [λ_{max}, nm (ε, M^{-1} cm^{-1}) in CH_3CN]: 400 (4500),478 (sh, 1500). FT-IR(Nujol mull): 2190 cm^{-1}. ^{1}H NMR (CD_2Cl_2): δ -0.89 (s, 1), 2.29 (s, 12), 6.84 (m, 6), 7.58 (d, 2), 7.88 (t, 1).

(Bu_4N)([L^{Me}Ni(CD_2CN)) (11D). The synthesis of **11D** was analogous to the procedure used for **7.** Briefly, **4** (119.3 mg, 0.167 mmol) was added to CD_3CN (~ 5 mL) to give an orange solution hich became red-orange upon stirring overnight. The solvent was removed *in vacuo* and washed with Et_2O (2 X 5 mL) to give a sticky orange solid to which Et_2O (10 mL) was added and stirred for 3 hours. The solvent was removed *in vacuo* to give a red orange powder that was filtered onto a fine porosity frit and washed with Et_2O (5 mL). The red orange powder was dried under vacuum for 2 hours (80.8 mg, 67.7 %). ESI-MS (CH_3OH, *m*/*z*): calcd 471.13 $[M\text{-}Bu_4N]^{1-}$, found 471.20. FT-IR(Nujol mull): 2182 cm^{-1}.

General procedure for obtaining kinetic data by low temperature UV-Vis spectroscopy. All reactions were prepared in a nitrogen filled glovebox and cuvettes were sealed under inert atmosphere with a septum. Reactions were monitored by UV-Vis and performed following the general procedure described herein. The data was then analyzed using the Olis Global Fitting software package using the single value decomposition (SVD) fitting protocol. The data was fit to several reaction order types using the SVD protocol until a suitable fit was achieved where the error was reduced and the spectral contributions calculated by the Olis software were in good agreement with experimentally observed spectra.

Procedure for the conversion of (Bu_4N)7 to (Bu_4N) 9. To a cuvette of 2.2 mL of CH_3CN was added 0.1 mL of 15 mM of **7** in 1,2-difluorobenzene at 20 °C. UV-Vis spectra were taken every 30 seconds and the reaction was performed in triplicate. The data was fit to a first order process using the Olis Global Works Software package as described above on a subset of data (400-890 nm) from which the UV-Vis spectra of the

two components were calculated and the rate of the reaction (k_{obs}) were given. The calculated spectra were in good agreement with the independently measured $[LCuOH]^{1-}$ and$[LCuCH_2CN]^{1-}$ spectra. The second order rate constant, k_{CH2CN}, was obtained using the equation $k_{CH2CN} = k_{obs}/[LCuOH]_0$. Fitting to a second order process gave a poor error model and unreasonable calculated spectra with negative absorption values.

Procedure for the oxidation of (Bu_4N) 9 to 9'. To a cuvette, 0.15 mL of a 3mM solution of **6** in acetonitrile was added to 2.50 mL of acetonitrile. The cuvette was cooled to −30 °C and 0.30 mL of a 1.5mM solution of $FcPF_6$ was added to give rise to an intense chromophore ($\lambda_{max} \sim 465$ nm, $\varepsilon \sim 5500$ M^{-1} cm^{-1}).

Bibliography:

(1) Bertini, I. *Bioinorganic chemistry*; University Science Books: Mill Valley, Calif., 1994.

(2) Zumft, W. G.; Matsubara, T. *FEBS Lett.* **1982**, *148*, 107–112.

(3) Amundsen, A. R.; Whelan, J.; Bosnich, B. *J. Am. Chem. Soc.* **1977**, *99*, 6730–9.

(4) Gray, H. B.; Solomon, E. I. *Copper proteins* **1981**, 1–39.

(5) Coyle, C. L.; Zumft, W. G.; Kroneck, P. M. H.; Körner, H.; Jakob, W. *European Journal of Biochemistry* **1985**, *153*, 459–467.

(6) Lindley, P. F. *Handbook on metalloproteins* **2001**, 763–811.

(7) Arciero, D. M.; Pierce, B. S.; Hendrich, M. P.; Hooper, A. B. *Biochemistry* **2002**, *41*, 1703–1709.

(8) Mirica, L. M.; Ottenwaelder, X.; Stack, T. D. P. *Chem. Rev. (Washington, DC, U. S.)* **2004**, *104*, 1013–1045.

(9) Solomon, E. I.; Baldwin, M. J.; Lowery, M. D. *Chem. Rev. (Washington, DC, U. S.)* **1992**, *92*, 521–542.

(10) Solomon, E. I.; Sundaram, U. M.; Machonkin, T. E. *Chem. Rev. (Washington, DC, U. S.)* **1996**, *96*, 2563–2606.

(11) Adman, E. T. *Adv. Protein Chem.* **1991**, *42*, 145–197.

(12) Steiner, R. A.; Kalk, K. H.; Dijkstra, B. W. *PNAS* **2002**, *99*, 16625–16630.

(13) Klinman, J. P. *Chem. Rev. (Washington, DC, U. S.)* **1996**, *96*, 2541–2562.

(14) Prigge, S. T.; Kolhekar, A. S.; Eipper, B. A.; Mains, R. E.; Amzel, L. M. *Nat Struct Mol Biol* **1999**, *6*, 976–983.

(15) Prigge, S. T.; Mains, R. E.; Eipper, B. A.; Amzel, L. M. *Cell. Mol. Life Sci.* **2000**, *57*, 1236–1259.

(16) Wang, S. X.; Mure, M.; Medzihradszky, K. F.; Burlingame, A. L.; Brown, D. E.; Dooley, D. M.; Smith, A. J.; Kagan, H. M.; Klinman, J. P. *Science* **1996**, *273*, 1078–1084.

(17) Whittaker, M. M.; Kersten, P. J.; Cullen, D.; Whittaker, J. W. *J. Biol. Chem.* **1999**, *274*, 36226–36232.

(18) Wilmot, C. M.; Hajdu, J.; McPherson, M. J.; Knowles, P. F.; Phillips, S. E. V. *Science* **1999**, *286*, 1724–1728.

(19) Whittaker, J. W. *Chem. Rev. (Washington, DC, U. S.)* **2003**, *103*, 2347–2364.

(20) Rogers, M. S.; Dooley, D. M. *Current Opinion in Chemical Biology* **2003**, *7*, 189–196.

(21) Csiszar, K. In *Progress in Nucleic Acid Research and Molecular Biology*; Academic Press, 2001; Vol. Volume 70, pp. 1–32.

(22) Harrenga, A.; Michel, H. *J. Biol. Chem.* **1999**, *274*, 33296–33299.

(23) Pomowski, A.; Zumft, W. G.; Kroneck, P. M. H.; Einsle, O. *Nature* **2011**, *477*, 234–237.

(24) Tainer, J. A.; Getzoff, E. D.; Beem, K. M.; Richardson, J. S.; Richardson, D. C. *Journal of Molecular Biology* **1982**, *160*, 181–217.

(25) Resch, M.; Dobbek, H.; Meyer, O. *J Biol Inorg Chem* **2005**, *10*, 518–528.

(26) Brader, M. L.; Borchardt, D.; Dunn, M. F. *J. Am. Chem. Soc.* **1992**, *114*, 4480–6.

(27) Gazdag, E. M.; Cirstea, I. C.; Breitling, R.; Lukes, J.; Blankenfeldt, W.; Alexandrov, K. *Acta Crystallographica Section F* **2010**, *66*, 871–877.

(28) Blackburn, N. J.; Barr, M. E.; Woodruff, W. H.; van der Ooost, J.; de Vries, S. *Biochemistry* **1994**, *33*, 10401–10407.

(29) Blackburn, N. J.; de Vries, S.; Barr, M. E.; Houser, R. P.; Tolman, W. B.; Sanders, D.; Fee, J. A. *J. Am. Chem. Soc.* **1997**, *119*, 6135–6143.

(30) Gamelin, D. R.; Williams, K. R.; LaCroix, L. B.; Houser, R. P.; Tolman, W. B.; Mulder, T. C.; de Vries, S.; Hedman, B.; Hodgson, K. O.; Solomon, E. I. *J. Am. Chem. Soc.* **1997**, *119*, 613–614.

(31) Richardson, D. J.; Watmough, N. J. *Curr. Opin. Chem. Biol.* **1999**, *3*, 207–219.

(32) Jolly, W. L. *The inorganic chemistry of nitrogen.*; New York, WABenjamin, 1964.

(33) Alvarez, M. L.; Ai, J.; Zumft, W.; Sanders-Loehr, J.; Dooley, D. M. *J. Am. Chem. Soc.* **2001**, *123*, 576–587.

(34) Anderson, B.; Bartlett, K.; Frolking, S.; Hayhoe, K.; Jenkins, J.; Salas, W. *Methane and Nitrous Oxide Emissions From Natural Sources*; EPA 430-R-10-001; United States Environmental Protection Agency, Office of Atmospheric Programs (6207J): Washington, DC, 2010.

(35) York, J. T.; Bar-Nahum, I.; Tolman, W. B. *Inorg. Chem.* **2007**, *46*, 8105–8107.

(36) Bar-Nahum, I.; York, J. T.; Young, V. G.; Tolman, W. B. *Angew. Chem., Int. Ed.* **2008**, *47*, 533–536.

(37) Brown, E. C.; Bar-Nahum, I.; York, J. T.; Aboelella, N. W.; Tolman, W. B. *Inorg. Chem.* **2007**, *46*, 486–496.

(38) Tolman, W. B. *J Biol Inorg Chem* **2006**, *11*, 261–271.

(39) Bar-Nahum, I.; Gupta, A. K.; Huber, S. M.; Ertem, M. Z.; Cramer, C. J.; Tolman, W. B. *J. Am. Chem. Soc.* **2009**, *131*, 2812–2814.

(40) Lewis, E. A.; Tolman, W. B. *Chem. Rev. (Washington, DC, U. S.)* **2004**, *104*, 1047–1076.

(41) Kim, E.; Chufán, E. E.; Kamaraj, K.; Karlin, K. D. *Chem. Rev. (Washington, DC, U. S.)* **2004**, *104*, 1077–1134.

(42) Francisco, W. A.; Merkler, D. J.; Blackburn, N. J.; Klinman, J. P. *Biochemistry* **1998**, *37*, 8244–8252.

(43) Francisco, W. A.; Knapp, M. J.; Blackburn, N. J.; Klinman, J. P. *J. Am. Chem. Soc.* **2002**, *124*, 8194–8195.

(44) Bell, J.; El Meskini, R.; D'Amato, D.; Mains, R. E.; Eipper, B. A. *Biochemistry* **2003**, *42*, 7133–7142.

(45) Francisco, W. A.; Blackburn, N. J.; Klinman, J. P. *Biochemistry* **2003**, *42*, 1813–1819.

(46) Owen, T. C.; Merkler, D. J. *Medical Hypotheses* **2004**, *62*, 392–400.

(47) Klinman, J. P. *J. Biol. Chem.* **2006**, *281*, 3013–3016.

(48) Gorsky, L. D.; Koop, D. R.; Coon, M. J. *J. Biol. Chem.* **1984**, *259*, 6812–6817.

(49) Eipper, B. A.; Quon, A. S. W.; Mains, R. E.; Boswell, J. S.; Blackburn, N. J. *Biochemistry* **1995**, *34*, 2857–2865.

(50) Kruse, L. I.; DeWolf, W. E.; Chambers, P. A.; Goodhart, P. J. *Biochemistry* **1986**, *25*, 7271–7278.

(51) Li, B.; Tsing, S.; Kosaka, A. H.; Nguyen, B.; Osen, E. G.; Bach, C.; Chan, H.; Barnett, J. *Biochem. J.* **1996**, *313*, 57–64.

(52) Yoshizawa, K.; Kihara, N.; Kamachi, T.; Shiota, Y. *Inorg. Chem.* **2006**, *45*, 3034–3041.

(53) Steggerda, J. J.; Bour, J. J.; Birker, P. J. M. W. L. *Inorg. Chem.* **1971**, *10*, 1202–1205.

(54) Keyes, W. E.; Dunn, J. B. R.; Loehr, T. M. *J. Am. Chem. Soc.* **1977**, *99*, 4527–4529.

(55) Kirksey, S. T.; Neubecker, T. A.; Margerum, D. W. *J. Am. Chem. Soc.* **1979**, *101*, 1631–1633.

(56) Rybka, J. S.; Kurtz, J. L.; Neubecker, T. A.; Margerum, D. W. *Inorg. Chem.* **1980**, *19*, 2791–2796.

(57) Diaddario, L. L.; Robinson, W. R.; Margerum, D. W. *Inorg. Chem.* **1983**, *22*, 1021–1025.

(58) Sulfab, Y.; Al-Shatti, N. I. *Inorganica Chimica Acta* **1984**, *87*, L23–L24.

(59) Corey, E. J.; Boaz, N. W. *Tetrahedron Letters* **1985**, *26*, 6015–6018.

(60) Anson, F. C.; Collins, T. J.; Richmond, T. G.; Santarsiero, B. D.; Toth, J. E.; Treco, B. G. R. T. *J. Am. Chem. Soc.* **1987**, *109*, 2974–2979.

(61) Caira, M. R.; Koch, K. R.; Sacht, C. *Acta Crystallographica Section C Crystal Structure Communications* **1991**, *47*, 26–29.

(62) Ruiz, R.; Surville-Barland, C.; Aukauloo, A.; Anxolabehere-Mallart, E.; Journaux, Y.; Cano, J.; Muñoz, M. C. *J. Chem. Soc., Dalton Trans.* **1997**, 745–752.

(63) Itoh, S.; Nakao, H.; Berreau, L. M.; Kondo, T.; Komatsu, M.; Fukuzumi, S. *J. Am. Chem. Soc.* **1998**, *120*, 2890–2899.

(64) Hanss, J.; Beckmann, A.; Krüger, H.-J. *European Journal of Inorganic Chemistry* **1999**, *1999*, 163–172.

(65) Lockwood, M. A.; Blubaugh, T. J.; Collier, A. M.; Lovell, S.; Mayer, J. M. *Angewandte Chemie International Edition* **1999**, *38*, 225–227.

(66) Itoh, S.; Taki, M.; Nakao, H.; Holland, P. L.; Tolman, W. B.; Que, Jr., L.; Fukuzumi, S. *Angewandte Chemie International Edition* **2000**, *39*, 398–400.

(67) Fritsky, I. O.; Kozłowski, H.; Kanderal, O. M.; Haukka, M.; Świątek-Kozłowska, J.; Gumienna-Kontecka, E.; Meyer, F. *Chem. Commun.* **2006**, 4125–4127.

(68) Rousseaux, S.; Vrancken, E.; Campagne, J.-M. *Angewandte Chemie International Edition* **2012**, *51*, 10934–10935.

(69) Casitas, A.; Ribas, X. *Chem. Sci.* **2013**, *4*, 2301–2318.

(70) Serr, B. R.; Headford, C. E. L.; Elliott, C. M.; Anderson, O. P. *Acta Crystallographica Section C Crystal Structure Communications* **1990**, *46*, 500–502.

(71) Yao, T. M.; You, X. Z.; Li, C.; Li, L. F.; Yang, Q. C. *Acta Crystallographica Section C Crystal Structure Communications* **1994**, *50*, 67–69.

(72) Bossu, F. P.; Chellappa, K. L.; Margerum, D. W. *J. Am. Chem. Soc.* **1977**, *99*, 2195–2203.

(73) Margerum, D. W.; Chellappa, K. L.; Bossu, F. P.; Burce, G. L. *J. Am. Chem. Soc.* **1975**, *97*, 6894–6896.

(74) Birker, P. J. M. W. L. *Inorg. Chem.* **1977**, *16*, 2478–2482.

(75) Soto, J.; Martínez-Máñez, R.; Payá, J.; Lloret, F.; Julve, M. *Transition Met Chem* **1993**, *18*, 69–72.

(76) Trott, T.; Henwood, R. W.; Langford, C. H. *Environ. Sci. Technol.* **1972**, *6*, 367–368.

(77) Natarajan, P.; Endicott, J. F. *J. Phys. Chem.* **1973**, *77*, 2049–2054.

(78) Balzani, V.; Carassiti, V.; Moggi, L.; Sabbatini, N. *Inorg. Chem.* **1965**, *4*, 1247–1250.

(79) Gilman, H.; Jones, R. G.; Woods, L. A. *The Journal of Organic Chemistry* **1952**, *17*, 1630–1634.

(80) Taylor, R. J. K. *Organocopper reagents : a practical approach*; Oxford University Press: Oxford ; New York, 1994.

(81) Bertz, S. H.; Cope, S.; Dorton, D.; Murphy, M.; Ogle, C. A. *Angewandte Chemie International Edition* **2007**, *46*, 7082–7085.

(82) Bartholomew, E. R.; Bertz, S. H.; Cope, S. K.; Murphy, M. D.; Ogle, C. A.; Thomas, A. A. *Chemical Communications* **2010**, *46*, 1253 – 1254.

(83) Kochi, J. K. *Journal of Organometallic Chemistry* **2002**, *653*, 11–19.

(84) Whitesides, G. M.; Fischer, W. F.; San Filippo, J.; Bashe, R. W.; House, H. O. *J. Am. Chem. Soc.* **1969**, *91*, 4871–4882.

(85) Corey, E. J.; Posner, G. H. *J. Am. Chem. Soc.* **1968**, *90*, 5615–5616.

(86) Corey, E. J.; Posner, G. H. *J. Am. Chem. Soc.* **1967**, *89*, 3911–3912.

(87) Beletskaya, I. P.; Cheprakov, A. V. *Coordination Chemistry Reviews* **2004**, *248*, 2337–2364.

(88) Krauss, S. R.; Smith, S. G. *J. Am. Chem. Soc.* **1981**, *103*, 141–148.

(89) Goering, H. L.; Kantner, S. S.; Tseng, C. C. *J. Org. Chem.* **1983**, *48*, 715–721.

(90) Bertz, S. H.; Dabbagh, G.; Cook, J. M.; Honkan, V. *J. Org. Chem.* **1984**, *49*, 1739–1743.

(91) Murphy, M. D.; Ogle, C. A.; Bertz, S. H. *Chem. Commun.* **2005**, 854–856.

(92) Johnson, C. R.; Dutra, G. A. *J. Am. Chem. Soc.* **1973**, *95*, 7783–7788.

(93) Hu, H.; Snyder, J. P. *J. Am. Chem. Soc.* **2007**, *129*, 7210–7211.

(94) Snyder, J. P. *J. Am. Chem. Soc.* **1995**, *117*, 11025–11026.

(95) Snyder, J. P. *Angewandte Chemie* **1995**, *107*, 112–113.

(96) Dorigo, A. E.; Wanner, J.; von Ragué Schleyer, P. *Angewandte Chemie International Edition in English* **1995**, *34*, 476–478.

(97) Dorigo, A. E.; Wanner, J.; Schleyer, P. von R. *Angewandte Chemie* **1995**, *107*, 492–494.

(98) Mori, S.; Nakamura, E.; Morokuma, K. *J. Am. Chem. Soc.* **2000**, *122*, 7294–7307.

(99) Phipps, R. J.; Gaunt, M. J. *Science* **2009**, *323*, 1593–1597.

(100) Bartholomew, E. R.; Bertz, S. H.; Cope, S.; Dorton, D. C.; Murphy, M.; Ogle, C. A. *Chem. Commun. (Cambridge, U. K.)* **2008**, 1176 – 1177.

(101) Bartholomew, E. R.; Bertz, S. H.; Cope, S.; Murphy, M.; Ogle, C. A. *J. Am. Chem. Soc.* **2008**, *130*, 11244 – 11245.

(102) Barton, D. H. R.; Finet, J.-P.; Khamsi, J. *Tetrahedron Letters* **1988**, *29*, 1115–1118.

(103) Phipps, R. J.; Grimster, N. P.; Gaunt, M. J. *J. Am. Chem. Soc.* **2008**, *130*, 8172–8174.

(104) Chen, B.; Hou, X.-L.; Li, Y.-X.; Wu, Y.-D. *J. Am. Chem. Soc.* **2011**, *133*, 7668–7671.

(105) Harvey, J. S.; Simonovich, S. P.; Jamison, C. R.; MacMillan, D. W. C. *J. Am. Chem. Soc.* **2011**, *133*, 13782–13785.

(106) Xu, J.; Fu, Y.; Luo, D.-F.; Jiang, Y.-Y.; Xiao, B.; Liu, Z.-J.; Gong, T.-J.; Liu, L. *J. Am. Chem. Soc.* **2011**, *133*, 15300–15303.

(107) Cho, S. H.; Yoon, J.; Chang, S. *J. Am. Chem. Soc.* **2011**, *133*, 5996–6005.

(108) Duong, H. A.; Gilligan, R. E.; Cooke, M. L.; Phipps, R. J.; Gaunt, M. J. *Angewandte Chemie International Edition* **2011**, *50*, 463–466.

(109) Chmielewski, P. J.; Latos-Grażyński, L.; Schmidt, I. *Inorg. Chem.* **2000**, *39*, 5475–5482.

(110) Furuta, H.; Maeda, H.; Osuka, A. *J. Am. Chem. Soc.* **2000**, *122*, 803 – 807.

(111) Araki, K.; Winnischofer, H.; Toma, H. E.; Maeda, H.; Osuka, A.; Furuta, H. *Inorg. Chem.* **2001**, *40*, 2020 – 2025.

(112) Araki, K.; Engelmann, F. M.; Mayer, I.; Toma, H. E.; Baptista, M. S.; et al. *Chemistry Letters* **2003**, 244 – 245.

(113) Maeda, H.; Ishikawa, Y.; Matsuda, T.; Osuka, A.; Furuta, H. *J. Am. Chem. Soc.* **2003**, *125*, 11822 – 11823.

(114) Maeda, H.; Osuka, A.; Furuta, H. *J. Am. Chem. Soc.* **2003**, *125*, 15690 – 15691.

(115) Maeda, H.; Osuka, A.; Ishikawa, Y.; Aritome, I.; Hisaeda, Y.; Furuta, H. *Org. Lett.* **2003**, *5*, 1293–1296.

(116) Pawlicki, M.; Kanska, I.; Latos-Grazynski, L. *Inorg. Chem.* **2007**, *46*, 6575 – 6584.

(117) Ribas, X.; Calle, C.; Poater, A.; Casitas, A.; Gómez, L.; Xifra, R.; Parella, T.; Benet-Buchholz, J.; Schweiger, A.; Mitrikas, G.; Solà, M.; Llobet, A.; Stack, T. D. P. *J. Am. Chem. Soc.* **2010**, *132*, 12299–12306.

(118) King, A. E.; Huffman, L. M.; Casitas, A.; Costas, M.; Ribas, X.; Stahl, S. S. *J. Am. Chem. Soc.* **2010**, *132*, 12068–12073.

(119) Casitas, A.; King, A. E.; Parella, T.; Costas, M.; Stahl, S. S.; Ribas, X. *Chem. Sci.* **2010**, *1*, 326–330.

(120) Huang, D.; Holm, R. H. *J. Am. Chem. Soc.* **2010**, *132*, 4693–4701.

(121) Huang, D.; Makhlynets, O. V.; Tan, L. L.; Lee, S. C.; Rybak-Akimova, E. V.; Holm, R. H. *Inorg. Chem.* **2011**, *50*, 10070–10081.

(122) Donoghue, P. J.; Gupta, A. K.; Boyce, D. W.; Cramer, C. J.; Tolman, W. B. *J. Am. Chem. Soc.* **2010**, *132*, 15869–15871.

(123) Donoghue, P. J.; Tehranchi, J.; Cramer, C. J.; Sarangi, R.; Solomon, E. I.; Tolman, W. B. *J. Am. Chem. Soc.* **2011**, *133*, 17602–17605.

(124) Tehranchi, J.; Donoghue, P. J.; Cramer, C. J.; Tolman, W. B. *European Journal of Inorganic Chemistry* **2013**, *2013*, 4077–4084.

(125) Richard, J. P. *Biochemistry* **2013**, *52*, 2009–2011.

(126) Kroneck, P. M. H.; Antholine, W. A.; Riester, J.; Zumft, W. G. *FEBS Lett.* **1988**, *242*, 70–74.

(127) Kroneck, P. M. H.; Antholine, W. A.; Riester, J.; Zumft, W. G. *FEBS Lett.* **1989**, *248*, 212–213.

(128) Riester, J.; Zumft, W. G.; Kroneck, P. M. H. *European Journal of Biochemistry* **1989**, *178*, 751–762.

(129) Chen, P.; Cabrito, I.; Moura, J. J. G.; Moura, I.; Solomon, E. I. *J. Am. Chem. Soc.* **2002**, *124*, 10497–10507.

(130) Bottomley, F.; Lin, I. J. B.; Mukaida, M. *J. Am. Chem. Soc.* **1980**, *102*, 5238–42.

(131) Piro, N. A.; Lichterman, M. F.; Harman, W. H.; Chang, C. J. *J. Am. Chem. Soc.* **2011**, *133*, 2108–2111.

(132) Zumft, W. G. *Microbiology and Molecular Biology Reviews* **1997**, *61*, 533–616.

(133) Chen, P.; Gorelsky, S. I.; Ghosh, S.; Solomon, E. I. *Angew. Chem., Int. Ed.* **2004**, *43*, 4132–4140.

(134) *Inventory of U.S. Greenhouse Gas Emissions and Sinks: 1990-2011*; EPA 430-R-13-001; Environmental Protection Agency: Washington, DC, 2013; pp. 1–505.

(135) Ravishankara, A. R.; Daniel, J. S.; Portmann, R. W. *Science* **2009**, 1176985.

(136) Lashof, D. A.; Ahuja, D. R. *Nature* **1990**, *344*, 529–531.

(137) Brown, K.; Djinovic-Carugo, K.; Haltia, T.; Cabrito, I.; Saraste, M.; Moura, J. J. G.; Moura, I.; Tegoni, M.; Cambillau, C. *J. Biol. Chem.* **2000**, *275*, 41133–41136.

(138) Brown, K.; Tegoni, M.; Prudencio, M.; Pereira, A. S.; Besson, S.; Moura, J. J.; Moura, I.; Cambillau, C. *Nature Structural Biology* **2000**, *7*, 191–195.

(139) Rasmussen, T.; Berks, B. C.; Butt, J. N.; Thomson, A. J. *Biochemical Journal* **2002**, *364*, 807–815.

(140) Scott, R. A.; Zumft, W. G.; Coyle, C. L.; Dooley, D. M. *PNAS* **1989**, *86*, 4082–4086.

(141) SooHoo, C. K.; Hollocher, T. C.; Kolodziej, A. F.; Orme-Johnson, W. H.; Bunker, G. *J. Biol. Chem.* **1991**, *266*, 2210–2218.

(142) Charnock, J. M.; Dreusch, A.; Körner, H.; Neese, F.; Nelson, J.; Kannt, A.; Michel, H.; Garner, C. D.; Kroneck, P. M. H.; Zumft, W. G. *European Journal of Biochemistry* **2000**, *267*, 1368–1381.

(143) Savelieff, M. G.; Lu, Y. *J Biol Inorg Chem* **2010**, *15*, 461–483.

(144) Prudencio, M.; Pereira, A. S.; Tavares, P.; Besson, S.; Cabrito, I.; Brown, K.; Samyn, B.; Devreese, B.; Van Beeumen, J.; Rusnak, F.; Fauque, G.; Moura, J. J. G.; Tegoni, M.; Cambillau, C.; Moura, I. *Biochemistry* **2000**, *39*, 3899–3907.

(145) Ghosh, S.; Gorelsky, S. I.; Chen, P.; Cabrito, I.; Moura; MouraMoura, I.; Solomon, E. I. *J. Am. Chem. Soc.* **2003**, *125*, 15708–15709.

(146) Dell'Acqua, S.; Pauleta, S. R.; Sousa, P. M. P. de; Monzani, E.; Casella, L.; Moura, J. J. G.; Moura, I. *J Biol Inorg Chem* **2010**, *15*, 967–976.

(147) Dell'Acqua, S.; Pauleta, S. R.; Moura, I.; Moura, J. J. G. *J Biol Inorg Chem* **2011**, *16*, 183–194.

(148) Rasmussen, T.; Berks, B. C.; Sanders-Loehr, J.; Dooley, D. M.; Zumft, W. G.; Thomson, A. J. *Biochemistry* **2000**, *39*, 12753–12756.

(149) Fujita, K.; Chan, J. M.; Bollinger, J. A.; Alvarez, M. L.; Dooley, D. M. *Journal of Inorganic Biochemistry* **2007**, *101*, 1836–1844.

(150) Zumft, W. G.; Kroneck, P. M. H. In *Advances in Microbial Physiology*; Robert K. Poole, Ed.; Academic Press, 2006; Vol. Volume 52, pp. 107–227.

(151) Paraskevopoulos, K.; Antonyuk, S. V.; Sawers, R. G.; Eady, R. R.; Hasnain, S. S. *Journal of Molecular Biology* **2006**, *362*, 55–65.

(152) Fujisawa, K.; Moro-oka, Y.; Kitajima, N. *Journal of the Chemical Society, Chemical Communications* **1994**, 623–624.

(153) Sletten, J.; Grove, H. *Acta Chemica Scandinavica* **1997**, *51*, 822–831.

(154) Helton, M. E.; Chen, P.; Paul, P. P.; Tyeklar, Z.; Sommer, R. D.; Zakharov, L. N.; Rheingold, A. L.; Solomon, E. I.; Karlin, K. D. *Journal of the American Chemical Society* **2003**, *125*, 1160–1161.

(155) Kinoshita, I.; James Wright, L.; Kubo, S.; Kimura, K.; Sakata, A.; Yano, T.; Miyamoto, R.; Nishioka, T.; Isobe, K. *Dalton Trans.* **2003**, 1993–2003.

(156) Brown, E. C.; Aboelella, N. W.; Reynolds, A. M.; Aullon, G.; Alvarez, S.; Tolman, W. B. *Inorg. Chem.* **2004**, *43*, 3335–3337.

(157) Brown, E. C.; York, J. T.; Antholine, W. E.; Ruiz, E.; Alvarez, S.; Tolman, W. B. *J. Am. Chem. Soc.* **2005**, *127*, 13752–13753.

(158) York, J. T.; Brown, E. C.; Tolman, W. B. *Angew. Chem., Int. Ed.* **2005**, *44*, 7745–7748.

(159) Helton, M. E.; Maiti, D.; Zakharov, L. N.; Rheingold, A. L.; Porco, J. A.; Karlin, K. D. *Angewandte Chemie, International Edition* **2006**, *45*, 1138–1141.

(160) Lee, D.-H.; Hatcher, L. Q.; Vance, M. A.; Sarangi, R.; Milligan, A. E.; Narducci Sarjeant, A. A.; Incarvito, C. D.; Rheingold, A. L.; Hodgson, K. O.; Hedman, B.; Solomon, E. I.; Karlin, K. D. *Inorganic Chemistry (Washington, DC, United States)* **2007**, *46*, 6056–6068.

(161) Maiti, D.; Woertink, J. S.; Vance, M. A.; Milligan, A. E.; Narducci Sarjeant, A. A.; Solomon, E. I.; Karlin, K. D. *J. Am. Chem. Soc.* **2007**, *129*, 8882–8892.

(162) York, J. T.; Bar-Nahum, I.; Tolman, W. B. *Inorg. Chim. Acta* **2008**, *361*, 885–893.

(163) York, J. T.; Llobet, A.; Cramer, C. J.; Tolman, W. B. *J. Am. Chem. Soc.* **2007**, *129*, 7990–7999.

(164) Thompson, J. S.; Marks, T. J.; Ibers, J. A. *J. Am. Chem. Soc.* **1979**, *101*, 4180–4192.

(165) Kitajima, N.; Fujisawa, K.; Morooka, Y. *J. Am. Chem. Soc.* **1990**, *112*, 3210–3212.

(166) Kitajima, N.; Fujisawa, K.; Tanaka, M.; Morooka, Y. *J. Am. Chem. Soc.* **1992**, *114*, 9232–9233.

(167) Qiu, D.; Kilpatrick, L.; Kitajima, N.; Spiro, T. G. *J. Am. Chem. Soc.* **1994**, *116*, 2585–2590.

(168) Holland, P. L.; Tolman, W. B. *J. Am. Chem. Soc.* **2000**, *122*, 6331–6332.

(169) Matsunaga, Y.; Fujisawa, K.; Ibi, N.; Miyashita, Y.; Okamoto, K. *Inorg. Chem.* **2005**, *44*, 325–335.

(170) Sarangi, R.; York, J. T.; Helton, M. E.; Fujisawa, K.; Karlin, K. D.; Tolman, W. B.; Hodgson, K. O.; Hedman, B.; Solomon, E. I. *J. Am. Chem. Soc.* **2008**, *130*, 676–686.

(171) Sarangi, R.; Yang, L.; Winikoff, S. G.; Gagliardi, L.; Cramer, C. J.; Tolman, W. B.; Solomon, E. I. *J. Am. Chem. Soc.* **2011**, *133*, 17180–17191.

(172) Ponec, R.; Ramos-Cordoba, E.; Salvador, P. *J. Phys. Chem. A* **2013**, *117*, 1975–1982.

(173) Mealli, C.; Ienco, A.; Poduska, A.; Hoffmann, R. *Angewandte Chemie* **2008**, *120*, 2906–2910.

(174) Carrasco, R.; Aullón, G.; Alvarez, S. *Chemistry – A European Journal* **2009**, *15*, 536–546.

(175) Alvarez, S.; Hoffmann, R.; Meallim, C. *Chemistry - A European Journal* **2009**, *15*, 8358–8373.

(176) Berry, J. F. *Chemistry – A European Journal* **2010**, *16*, 2719–2724.

(177) Root, D. E.; Henson, M. J.; Machonkin, T.; Mukherjee, P.; Stack, T. D. P.; Solomon, E. I. *J. Am. Chem. Soc.* **1998**, *120*, 4982–4990.

(178) Cole, A. P.; Root, D. E.; Mukherjee, P.; Solomon, E. I.; Stack, T. D. P. *Science* **1996**, *273*, 1848–1850.

(179) Machonkin, T. E.; Mukherjee, P.; Henson, M. J.; Stack, T. D. P.; Solomon, E. I. *Inorganica Chimica Acta* **2002**, *341*, 39–44.

(180) Yang, L.; Tehranchi, J.; Tolman, W. B. *Inorg. Chem.* **2011**, *50*, 2606–2612.

(181) King, M. G.; McQuillan, G. P. *J. Chem. Soc. A* **1967**, 898–901.

(182) Hieber, W.; John, P. *Chem. Ber.* **1970**, *103*, 2161–77.

(183) Kuhn, N.; Schumann, H. *Journal of Organometallic Chemistry* **1986**, *304*, 181–193.

(184) Robson, R. *Australian Journal of Chemistry* **1970**, *23*, 2217–24.

(185) Dickson, I. E.; Robson, R. *Inorg. Chem.* **1974**, *13*, 1301–6.

(186) Harris, C. M.; McKenzie, E. D. *Nature* **1962**, *196*, 670–1.

(187) Harris, C. M.; Kokot, E. V.; Lenzer, S. L. *Nature* **1962**, *196*, 471–2.

(188) Hodgkin, J. H. *Australian Journal of Chemistry* **1984**, *37*, 2371–8.

(189) Iliopoulos, P.; Murray, K. S.; Robson, R.; Wilson, J.; Williams, G. A. *Journal of the Chemical Society, Dalton Transactions: Inorganic Chemistry (1972-1999)* **1987**, 1585–91.

(190) McFadyen, W. D.; Robson, R.; Schaap, H. *Inorg. Chem.* **1972**, *11*, 1777–85.

(191) Pilkington, N. H.; Robson, R. *Australian Journal of Chemistry* **1970**, *23*, 2225–36.

(192) Eduok, E. E.; O'Connor, C. J. *Inorganica Chimica Acta* **1984**, *88*, 229–33.

(193) Grzybowski, J. J.; Merrell, P. H.; Urbach, F. L. *Inorg. Chem.* **1978**, *17*, 3078–82.

(194) Loroesch, J.; Haase, W. *Inorganica Chimica Acta* **1985**, *108*, 35–40.

(195) Anekwe, J.; Hammerschmidt, A.; Rompel, A.; Krebs, B. *Zeitschrift fuer Anorganische und Allgemeine Chemie* **2006**, *632*, 1057–1066.

(196) Banerjee, A.; Sarkar, S.; Chopra, D.; Colacio, E.; Rajak, K. K. *Inorg. Chem.* **2008**, *47*, 4023–4031.

(197) Bharathi, K. S.; Sreedaran, S.; Rahiman, A. K.; Rajesh, K.; Narayanan, V. *Polyhedron* **2007**, *26*, 3993–4002.

(198) Kannappan, R.; Mahalakshmy, R.; Rajendiran, T. M.; Venkatesan, R.; Rao, P. S. *Proceedings - Indian Academy of Sciences, Chemical Sciences* **2003**, *115*, 1–14.

(199) Iryna, A. K.; Daniel, P.; Arno, F. S.; Patrick, G.; Bernt, K.; Jan, R. *European Journal of Inorganic Chemistry* **2003**, *2003*, 1669–1674.

(200) Kaminskaia, N. V.; Spingler, B.; Lippard, S. J. *J. Am. Chem. Soc.* **2000**, *122*, 6411–6422.

(201) Knight, P. D.; White, A. J. P.; Williams, C. K. *Inorg. Chem.* **2008**, *47*, 11711–11719.

(202) Casella, L.; Gullotti, M.; Bartosek, M.; Pallanza, G.; Laurenti, E. *Journal of the Chemical Society, Chemical Communications* **1991**, 1235–7.

(203) Foxon, S. P.; Utz, D.; Astner, J.; Schindler, S.; Thaler, F.; Heinemann, F. W.; Liehr, G.; Mukherjee, J.; Balamurugan, V.; Ghosh, D.; Mukherjee, R. *Dalton Transactions* **2004**, 2321–2328.

(204) Breyfogle, L. E.; Williams, C. K.; Young, V. G.; Hillmyer, M. A.; Tolman, W. B. *Dalton Transactions* **2006**, 928–936.

(205) Higuchi, C.; Sakiyama, H.; Okawa, H.; Fenton, D. E. *J. Chem. Soc., Dalton Trans.* **1995**, 4015–20.

(206) Ghosh, D.; Mukherjee, R. *Inorg. Chem.* **1998**, *37*, 6597–6605.

(207) Crane, J. D.; Fenton, D. E.; Latour, J. M.; Smith, A. J. *Journal of the Chemical Society, Dalton Transactions: Inorganic Chemistry (1972-1999)* **1991**, 2979–87.

(208) Drago, R. S. *Physical methods for chemists*; 2nd ed.; Saunders College Pub.: Ft. Worth, 1992.

(209) Menif, R.; Martell, A. E. *J. Chem. Soc., Chem. Commun.* **1989**, 1521–1523.

(210) Menif, R.; Martell, A. E.; Squattrito, P. J.; Clearfield, A. *Inorg. Chem.* **1990**, *29*, 4723–4729.

(211) Menif, R.; Martell, A. E. *Journal of the Chemical Society, Chemical Communications* **1989**, 1521–3.

(212) Mandal, S.; Das, G.; Singh, R.; Shukla, R.; Bharadwaj, P. K. *Coordination Chemistry Reviews* **1997**, *160*, 191–235.

(213) Zhang, X.; Huang, D.; Chen, Y.-S.; Holm, R. H. *Inorg. Chem.* **2012**, *51*, 11017–11029.

(214) Sreekanth, A.; Prathapachandra, K. M. R. *Polyhedron* **2003**, *22*, 3321–3332.

(215) Schaumann, E.; Wriede, U.; Ehlers, J. *Synthesis* **1980**, 907–8.

(216) Pawlenko, S. *Methods of Organic Chemistry, Vol. 13: Organometallic Compounds, Pt. 5: Organosilicon Compounds. 4th Ed*; Thieme, 1980.

(217) Orpen, A. G.; Brammer, L.; Allen, F. H.; Watson, D. G.; Taylor, R. In *International Tables for Crystallography Volume C: Mathematical, physical and chemical tables*; Prince, E., Ed.; International Tables for Crystallography; Springer Netherlands, 2004; Vol. C, pp. 812–896.

(218) Giolando, D. M.; Rauchfuss, T. B.; Clark, G. M. *Inorg. Chem.* **1987**, *26*, 3080–3082.

(219) Albertsen, J.; Steudel, R. *Journal of Organometallic Chemistry* **1992**, *424*, 153–158.

(220) Becker, B.; Radacki, K.; Wojnowski, W.; Konitz, A. *Zeitschrift für anorganische und allgemeine Chemie* **1995**, *621*, 904–908.

(221) Sweeney, Z. K.; Polse, J. L.; Andersen, R. A.; Bergman, R. G.; Kubinec, M. G. *J. Am. Chem. Soc.* **1997**, *119*, 4543–4544.

(222) Kovacs, I.; Pearson, C.; Shaver, A. *Journal of Organometallic Chemistry* **2000**, *596*, 193–203.

(223) Becker, B.; Zalewska, A.; Konitz, A.; Wojnowski, W. *Zeitschrift für anorganische und allgemeine Chemie* **2001**, *627*, 271–279.

(224) Komuro, T.; Kawaguchi, H.; Tatsumi, K. *Inorg. Chem.* **2002**, *41*, 5083–5090.

(225) Kovács, I.; Bélanger-Gariépy, F.; Shaver, A. *Inorg. Chem.* **2003**, *42*, 2988–2991.

(226) Sydora, O. L.; Wolczanski, P. T.; Lobkovsky, E. B. *Angewandte Chemie International Edition* **2003**, *42*, 2685–2687.

(227) Zhou, H.-C.; Holm, R. H. *Inorg. Chem.* **2003**, *42*, 11–21.

(228) Komuro, T.; Matsuo, T.; Kawaguchi, H.; Tatsumi, K. *Dalton Trans.* **2004**, 1618–1625.

(229) Vela, J.; Smith, J. M.; Yu, Y.; Ketterer, N. A.; Flaschenriem, C. J.; Lachicotte, R. J.; Holland, P. L. *J. Am. Chem. Soc.* **2005**, *127*, 7857–7870.

(230) Sydora, O. L.; Henry, T. P.; Wolczanski, P. T.; Lobkovsky, E. B.; Rumberger, E.; Hendrickson, D. N. *Inorg. Chem.* **2006**, *45*, 609–626.

(231) Smith, C. A.; Tuna, F.; Bodensteiner, M.; Helliwell, M.; Collison, D.; Layfield, R. A. *Dalton Trans.* **2012**, *42*, 71–74.

(232) Tuna, F.; Smith, C. A.; Bodensteiner, M.; Ungur, L.; Chibotaru, L. F.; McInnes, E. J. L.; Winpenny, R. E. P.; Collison, D.; Layfield, R. A. *Angewandte Chemie International Edition* **2012**, *51*, 6976–6980.

(233) Bauer, A.; Schneider, W.; Angermaier, K.; Schier, A.; Schmidbaur, H. *Inorganica Chimica Acta* **1996**, *251*, 249–253.

(234) Griffiths, T. R.; Scarrow, R. K. *Trans. Faraday Soc.* **1969**, *65*, 1727–1733.

(235) Scaife, D. E.; Wood, K. P. *Inorg. Chem.* **1967**, *6*, 358–365.

(236) El-Ayaan, U.; Murata, F.; Fukuda, Y. *Monatshefte fuer Chemie* **2001**, *132*, 1279–1294.

(237) Wei, X.; Yu, L.; Wang, D.; Jin, X.; Chen, G. Z. *Green Chem.* **2008**, *10*, 296–305.

(238) Solomon, E. I.; Hodgson, K. O.; American Chemical Society. Division of Inorganic Chemistry; American Chemical Society. Meeting (213th : 1997 : San Francisco, C.) *Spectroscopic methods in bioinorganic chemistry*; American Chemical Society ; New York: Washington, DC, 1998.

(239) Lieberman, R. L.; Arciero, D. M.; Hooper, A. B.; Rosenzweig, A. C. *Biochemistry* **2001**, *40*, 5674–5681.

(240) Basumallick, L.; Sarangi, R.; DeBeer George, S.; Elmore, B.; Hooper, A. B.; Hedman, B.; Hodgson, K. O.; Solomon, E. I. *J. Am. Chem. Soc.* **2005**, *127*, 3531–3544.

(241) Farver, O.; Pecht, I. *Copper proteins* **1981**, 151–192.

(242) Gray, H. B.; Malmström, B. G.; Williams, R. J. P. *J. Biol. Inorg. Chem.* **2000**, *5*, 551–559.

(243) Solomon, E. I.; Randall, D. W.; Glaser, T. *Coordination Chemistry Reviews* **2000**, *200*, 595–632.

(244) Kroneck, P. M. *Handbook of Metalloproteins* **2001**.

(245) Solomon, E. I.; Szilagyi, R. K.; DeBeer George, S.; Basumallick, L. *Chem. Rev. (Washington, DC, U. S.)* **2004**, *104*, 419–458.

(246) Solomon, E. I. *Inorg. Chem.* **2006**, *45*, 8012–8025.

(247) Han, J.; Loehr, T. M.; Lu, Y.; Valentine, J. S.; Averill, B. A.; Sanders-Loehr, J. *J. Am. Chem. Soc.* **1993**, *115*, 4256–4263.

(248) Den Blaauwen, T.; Hoitink, C. W. G.; Canters, G. W.; Han, J.; Loehr, T. M.; Sanders-Loehr, J. *Biochemistry* **1993**, *32*, 12455–12464.

(249) Malmström, B. G. *European Journal of Biochemistry* **1994**, *223*, 711–718.

(250) Pierloot, K.; De Kerpel, J. O. A.; Ryde, U.; Roos, B. O. *J. Am. Chem. Soc.* **1997**, *119*, 218–226.

(251) Holland, P. L.; Tolman, W. B. *J. Am. Chem. Soc.* **1999**, *121*, 7270–7271.

(252) Yang, L.; Tolman, W. B. *Journal of Biological Inorganic Chemistry* **2012**, *17*, 285–291.

(253) Connelly, N. G.; Geiger, W. E. *Chem. Rev. (Washington, DC, U. S.)* **1996**, *96*, 877–910.

(254) Ainscough, E. W.; Bingham, A. G.; Brodie, A. M.; Ellis, W. R.; Gray, H. B.; Loehr, T. M.; Plowman, J. E.; Norris, G. E.; Baker, E. N. *Biochemistry* **1987**, *26*, 71–82.

(255) Peisach, J.; Levine, W. G.; Blumberg, W. E. *J. Biol. Chem.* **1967**, *242*, 2847–2858.

(256) Randall, D. W.; DeBeer, G. S.; Holland, P. L.; Hedman, B.; Hodgson, K. O.; Tolman, W. B.; Solomon, E. I. *J. Am. Chem. Soc.* **2000**, *122*, 11632–11648.

(257) Nersissian, A. M.; Valentine, J. S.; Immoos, C.; Hill, M. G.; Hart, P. J.; Williams, G.; Herrmann, R. G. *Protein Science* **1998**, *7*, 1915–1929.

(258) Han, L.; Shi, L.-X.; Zhang, L.-Y.; Chen, Z.-N.; Hong, M.-C. *Inorganic Chemistry Communications* **2003**, *6*, 281–283.

(259) Cotton, J. D.; Waddington, T. C. *J. Chem. Soc. A* **1966**, 785–789.

(260) Corey, E. J.; Kuwajima, I. *Tetrahedron Letters* **1972**, *13*, 487–489.

(261) Huang, W.; Gou, S.; Hu, D.; Meng, Q. *Synthetic Communications* **2000**, *30*, 1555–1561.

(262) Lamouroux, A.; Vigny, A.; Faucon Biguet, N.; Darmon, M. C.; Franck, R.; Henry, J. P.; Mallet, J. *EMBO J.* **1987**, *6*, 3931–3937.

(263) Southan, C.; Kruse, L. I. *FEBS Lett.* **1989**, *255*, 116–120.

(264) Tian, G.; Berry, J. A.; Klinman, J. P. *Biochemistry* **1994**, *33*, 226–234.

(265) Boswell, J. S.; Reedy, B. J.; Kulathila, R.; Merkler, D.; Blackburn, N. J. *Biochemistry* **1996**, *35*, 12241–12250.

(266) Jaron, S.; Blackburn, N. J. *Biochemistry* **2001**, *40*, 6867–6875.

(267) Blackburn, N. J.; Rhames, F. C.; Ralle, M.; Jaron, S. *J. Biol. Inorg. Chem.* **2000**, *5*, 341–353.

(268) Prigge, S. T.; Eipper, B. A.; Mains, R. E.; Amzel, L. M. *Science* **2004**, *304*, 864–867.

(269) Solomon, E. I.; Brunold, T. C.; Davis, M. I.; Kemsley, J. N.; Lee, S.-K.; Lehnert, N.; Neese, F.; Skulan, A. J.; Yang, Y.-S.; Zhou, J. *Chem. Rev. (Washington, DC, U. S.)* **2000**, *100*, 235–350.

(270) Paul, P. P.; Tyeklar, Z.; Jacobson, R. R.; Karlin, K. D. *J. Am. Chem. Soc.* **1991**, *113*, 5322–5332.

(271) Cramer, C. J.; Pak, Y. *Theor Chem Acc* **2001**, *105*, 477–480.

(272) Taki, M.; Teramae, S.; Nagatomo, S.; Tachi, Y.; Kitagawa, T.; Itoh, S.; Fukuzumi, S. *J. Am. Chem. Soc.* **2002**, *124*, 6367–6377.

(273) Hatcher, L. Q.; Karlin, K. D. *J Biol Inorg Chem* **2004**, *9*, 669–683.

(274) Maiti, D.; Fry, H. C.; Woertink, J. S.; Vance, M. A.; Solomon, E. I.; Karlin, K. D. *J. Am. Chem. Soc.* **2007**, *129*, 264–265.

(275) Gherman, B. F.; Cramer, C. J. *Coordination Chemistry Reviews* **2009**, *253*, 723–753.

(276) Kunishita, A.; Kubo, M.; Sugimoto, H.; Ogura, T.; Sato, K.; Takui, T.; Itoh, S. *J. Am. Chem. Soc.* **2009**, *131*, 2788–2789.

(277) Hong, S.; Huber, S. M.; Gagliardi, L.; Cramer, C. C.; Tolman, W. B. *J. Am. Chem. Soc.* **2007**, *129*, 14190–14192.

(278) Hong, S.; Gupta, A. K.; Tolman, W. B. *Inorg. Chem.* **2009**, *48*, 6323–6325.

(279) Hong, S.; Hill, L. M. R.; Gupta, A. K.; Naab, B. D.; Gilroy, J. B.; Hicks, R. G.; Cramer, C. J.; Tolman, W. B. *Inorg. Chem.* **2009**, *48*, 4514–4523.

(280) Gupta, A. K.; Tolman, W. B. *Inorg. Chem.* **2012**, *51*, 1881–1888.

(281) Wada, A.; Harata, M.; Hasegawa, K.; Jitsukawa, K.; Masuda, H.; Mukai, M.; Kitagawa, T.; Einaga, H. *Angewandte Chemie International Edition* **1998**, *37*, 798–799.

(282) Chen, P.; Fujisawa, K.; Solomon, E. I. *J. Am. Chem. Soc.* **2000**, *122*, 10177–10193.

(283) Ohta, T.; Tachiyama, T.; Yoshizawa, K.; Yamabe, T. *Tetrahedron Letters* **2000**, *41*, 2581–2585.

(284) Ohta, T.; Tachiyama, T.; Yoshizawa, K.; Yamabe, T.; Uchida, T.; Kitagawa, T. *Inorg. Chem.* **2000**, *39*, 4358–4369.

(285) Ohtsu, H.; Itoh, S.; Nagatomo, S.; Kitagawa, T.; Ogo, S.; Watanabe, Y.; Fukuzumi, S. *Chem. Commun.* **2000**, 1051–1052.

(286) Kodera, M.; Kita, T.; Miura, I.; Nakayama, N.; Kawata, T.; Kano, K.; Hirota, S. *J. Am. Chem. Soc.* **2001**, *123*, 7715–7716.

(287) Ohtsu, H.; Itoh, S.; Nagatomo, S.; Kitagawa, T.; Ogo, S.; Watanabe, Y.; Fukuzumi, S. *Inorg. Chem.* **2001**, *40*, 3200–3207.

(288) Chen, P.; Solomon, E. I. *Journal of Inorganic Biochemistry* **2002**, *88*, 368–374.

(289) Osako, T.; Nagatomo, S.; Tachi, Y.; Kitagawa, T.; Itoh, S. *Angewandte Chemie International Edition* **2002**, *41*, 4325–4328.

(290) Gherman, B. F.; Tolman, W. B.; Cramer, C. J. *Journal of Computational Chemistry* **2006**, *27*, 1950–1961.

(291) Yoshizawa, K.; Shiota, Y. *J. Am. Chem. Soc.* **2006**, *128*, 9873–9881.

(292) Crespo, A.; Marti, M. A.; Roitberg, A. E.; Amzel, L. M.; Estrin, D. A. *J. Am. Chem. Soc.* **2006**, *128*, 12817–12828.

(293) Chen, P.; Solomon, E. I. *J. Am. Chem. Soc.* **2004**, *126*, 4991–5000.

(294) Kamachi, T.; Kihara, N.; Shiota, Y.; Yoshizawa, K. *Inorg. Chem.* **2005**, *44*, 4226–4236.

(295) Maiti, D.; Narducci Sarjeant, A. A.; Karlin, K. D. *Inorg. Chem.* **2008**, *47*, 8736–8747.

(296) Réglier, M.; Amadeï, E.; Tadayoni, R.; Waegell, B. *J. Chem. Soc., Chem. Commun.* **1989**, 447–450.

(297) Schröder, D.; Holthausen, M. C.; Schwarz, H. *J. Phys. Chem. B* **2004**, *108*, 14407–14416.

(298) Dietl, N.; Linde, C. van der; Schlangen, M.; Beyer, M. K.; Schwarz, H. *Angewandte Chemie, International Edition* **2011**, *50*, 4966 – 4969.

(299) Xue, G.; De Hont, R.; Münck, E.; Jr, L. Q. *Nat Chem* **2010**, *2*, 400–405.

(300) Parsell, T. H.; Yang, M.-Y.; Borovik, A. S. *J. Am. Chem. Soc.* **2009**, *131*, 2762–2763.

(301) Goldsmith, C. R.; Cole, A. P.; Stack, T. D. P. *J. Am. Chem. Soc.* **2005**, *127*, 9904–9912.

(302) Gardner, K. A.; Kuehnert, L. L.; Mayer, J. M. *Inorg. Chem.* **1997**, *36*, 2069–2078.

(303) Goldsmith, C. R.; Stack, T. D. P. *Inorg. Chem.* **2006**, *45*, 6048–6055.

(304) Roth, J. P.; Mayer, J. M. *Inorg. Chem.* **1999**, *38*, 2760–2761.

(305) McKean, D. C.; Duncan, J. L.; Batt, L. *Spectrochimica Acta Part A: Molecular Spectroscopy* **1973**, *29*, 1037–1049.

(306) McKean, D. C. *Spectrochimica Acta Part A: Molecular Spectroscopy* **1975**, *31*, 861–870.

(307) Guthrie, J. P.; Cossar, J.; Klym, A. *J. Am. Chem. Soc.* **1982**, *104*, 895–896.

(308) Myers, T. W.; Berben, L. A. *J. Am. Chem. Soc.* **2011**, *133*, 11865–11867.

(309) Mader, E. A.; Manner, V. W.; Markle, T. F.; Wu, A.; Franz, J. A.; Mayer, J. M. *J. Am. Chem. Soc.* **2009**, *131*, 4335–4345.

(310) Warren, J. J.; Tronic, T. A.; Mayer, J. M. *Chem. Rev.* **2010**, *110*, 6961–7001.

(311) Rodima, T.; Kaljurand, I.; Pihl, A.; Mäemets, V.; Leito, I.; Koppel, I. A. *J. Org. Chem.* **2002**, *67*, 1873–1881.

(312) Kaljurand, I.; Kütt, A.; Sooväli, L.; Rodima, T.; Mäemets, V.; Leito, I.; Koppel, I. A. *J. Org. Chem.* **2005**, *70*, 1019–1028.

(313) Kaljurand, I.; Rodima, T.; Leito, I.; Koppel, I. A.; Schwesinger, R. *J. Org. Chem.* **2000**, *65*, 6202–6208.

(314) Suzuki, K.; Yamamoto, H.; Kanie, S. *Journal of Organometallic Chemistry* **1974**, *73*, 131–6.

(315) Ros, R.; Michelin, R. A.; Bataillard, R.; Roulet, R. *Journal of Organometallic Chemistry* **1977**, *139*, 355–9.

(316) Pra, A. D.; Zanotti, G.; Bombieri, G.; Ros, R. *Inorganica Chimica Acta* **1979**, *36*, 121–5.

(317) Pregosin, P. S.; Favez, R.; Roulet, R.; Boschi, T.; Michelin, R. A.; Ros, R. *Inorganica Chimica Acta* **1980**, *45*, L7–L9.

(318) Henderson, W.; Oliver, A. G. *Acta Crystallogr., Sect. C: Cryst. Struct. Commun.* **1999**, *C55*, 1406–1408.

(319) McCrindle, R.; Ferguson, G.; McAlees, A. J.; Parvez, M.; Roberts, P. J. *Journal of the Chemical Society, Dalton Transactions* **1982**, 1699–708.

(320) English, A. D.; Herskovitz, T. *J. Am. Chem. Soc.* **1977**, *99*, 1648–9.

(321) Milstein, D.; Calabrese, J. C.; Williams, I. D. *J. Am. Chem. Soc.* **1986**, *108*, 6387–6389.

(322) Crestani, M. G.; Steffen, A.; Kenwright, A. M.; Batsanov, A. S.; Howard, J. A. K.; Marder, T. B. *Organometallics* **2009**, *28*, 2904–2914.

(323) Evans, M. E.; Li, T.; Vetter, A. J.; Rieth, R. D.; Jones, W. D. *Journal of Organic Chemistry* **2009**, *74*, 6907–6914.

(324) Evans, M. E.; Li, T.; Jones, W. D. *J. Am. Chem. Soc.* **2010**, *132*, 16278–16284.

(325) Tanabe, T.; Evans, M. E.; Brennessel, W. W.; Jones, W. D. *Organometallics* **2011**, *30*, 834–843.

(326) Liu, Q.-X.; Li, S.-J.; Zhao, X.-J.; Zang, Y.; Song, H.; Guo, J.-H.; Wang, X.-G. *European Journal of Inorganic Chemistry* **2010**, *2010*, 983–988.

(327) Emeljanenko, D.; Peters, A.; Vitske, V.; Kaifer, E.; Himmel, H.-J. *European Journal of Inorganic Chemistry* **2010**, *2010*, 4783–4789.

(328) Ateşin, T. A.; Li, T.; Lachaize, S.; Brennessel, W. W.; García, J. J.; Jones, W. D. *J. Am. Chem. Soc.* **2007**, *129*, 7562–7569.

(329) Chakraborty, S.; Patel, Y. J.; Krause, J. A.; Guan, H. *Angewandte Chemie International Edition* **2013**, *52*, 7523–7526.

(330) Chambers, M. B.; Groysman, S.; Villagrán, D.; Nocera, D. G. *Inorg. Chem.* **2013**, *52*, 3159–3169.

(331) Lu, P.; Boorman, T. C.; Slawin, A. M. Z.; Larrosa, I. *J. Am. Chem. Soc.* **2010**, *132*, 5580–5581.

(332) Fan, L.; Ozerov, O. V. *Chem. Commun.* **2005**, 4450–4452.

(333) Oertel, A. M.; Ritleng, V.; Chetcuti, M. J.; Veiros, L. F. *J. Am. Chem. Soc.* **2010**, *132*, 13588–13589.

(334) Davidson, J. G.; Barefield, E. K.; Van Derveer, D. G. *Organometallics* **1985**, *4*, 1178–1184.

(335) Alburquerque, P. R.; Pinhas, A. R.; Krause Bauer, J. A. *Inorganica Chimica Acta* **2000**, *298*, 239–244.

(336) Eglin, J. L. *Comments on Inorganic Chemistry* **2002**, *23*, 23–43.

(337) Tyler, L. A.; Noveron, J. C.; Olmstead, M. M.; Mascharak, P. K. *Inorg. Chem.* **2003**, *42*, 5751–5761.

(338) Siegfried, L.; Comparone, A.; Neuburger, M.; Kaden, T. A. *Dalton Trans* **2005**, 30–36.

(339) Zhang, Z.; He, Y.; Zhao, Q.; Xu, W.; Li, Y.-Z.; Wang, Z.-L. *Inorganic Chemistry Communications* **2006**, *9*, 269–272.

(340) Kukushkin, V. Y.; Pombeiro, A. J. L. *Inorganica Chimica Acta* **2005**, *358*, 1–21.

(341) Kopylovich, M. N.; Kukushkin, V. Y.; Guedes, da S.; Haukka, M.; Frausto, da S.; Pombeiro, A. J. L. *J. Chem. Soc., Perkin Trans. 1* **2001**, 1569–1573.

(342) da, R.; Chiericato, G.; Tfouni, E. *Adv. Chem. Ser.* **1997**, *253*, 297–313.

(343) Kukushkin, V. Y.; Zenkevich, I. G.; Bel'skii, V. K.; Konovalov, V. E.; Moiseev, A. I.; Sidorov, E. O. *Inorg. Chim. Acta* **1989**, *166*, 79–84.

(344) Corain, B.; Basato, M.; Veronese, A. C. *J. Mol. Catal.* **1993**, *81*, 133–55.

(345) Ghaffar, T.; Parkins, A. W. *J. Mol. Catal. A: Chem.* **2000**, *160*, 249–261.

(346) Dequeant, M.; Eglin, J. L.; Graves-Brook, M. K.; Smith, L. T. *Inorg. Chim. Acta* **2003**, *351*, 141–149.

(347) Kopylovich, M. N.; Kukushkin, V. Y.; Haukka, M.; Frausto, da S.; Pombeiro, A. J. L. *Inorg. Chem.* **2002**, *41*, 4798–4804.

(348) Murthy, N. N.; Mahroof-Tahir, M.; Karlin, K. D. *J. Am. Chem. Soc.* **1993**, *115*, 10404–10405.

(349) Greene, J. L.; Clark, R. E. Conversion of nitriles to amides in the presence of alkaline catalysts., August 22, 1972.

(350) Goretta, L. A.; Seale, V. L. Mixed catalyst for the hydrolysis of nitriles to amides., February 10, 1981.

(351) Cechi, de M.; Marques, R. M. F. Preparation of copper-chromium catalysts for production of amides from nitriles via hydrolysis., August 7, 1990.

(352) Fairlie, D. P.; Woon, T. C.; Wickramasinghe, W. A.; Willis, A. C. *Inorg. Chem.* **1994**, *33*, 6425–6428.

(353) Chin, C. S.; Chong, D.; Lee, S.; Park, Y. J. *Organometallics* **2000**, *19*, 4043–4050.

(354) Tyler, L. A.; Noveron, J. C.; Olmstead, M. M.; Mascharak, P. K. *Inorg Chem* **2003**, *42*, 5751–61.

(355) Breslow, R.; Fairweather, R.; Keana, J. *J. Am. Chem. Soc.* **1967**, *89*, 2135–2138.

(356) Jencks, W. P.; Gilchrist, M. *J. Am. Chem. Soc.* **1962**, *84*, 2910–2913.

(357) Schibler, W.; Kaden, T. A. *J. Chem. Soc., Chem. Commun.* **1981**, 603–604.

(358) Wainwright, K. P. *J. Chem. Soc., Dalton Trans.* **1980**, 2117–2120.

(359) Lu, T.; Zhuang, X.; Li, Y.; Chen, S. *J. Am. Chem. Soc.* **2004**, *126*, 4760–4761.

(360) Ullmann, F.; Bielecki, J. *Berichte der deutschen chemischen Gesellschaft* **1901**, *34*, 2174–2185.

(361) Ullmann, F. *Justus Liebigs Annalen der Chemie* **1904**, *332*, 38–81.

(362) Stephens, R. D.; Castro, C. E. *J. Org. Chem.* **1963**, *28*, 3313–3315.

(363) Owsley, D. C.; Castro, C. E. *Org. Syn.* **1972**, *52*, 128–31.

(364) Dieck, H. A.; Heck, F. R. *Journal of Organometallic Chemistry* **1975**, *93*, 259–263.

(365) Sonogashira, K. *Journal of Organometallic Chemistry* **2002**, *653*, 46–49.

(366) Wang, Z.; Bao, W.; Jiang, Y. *Chem. Commun.* **2005**, 2849–2851.

(367) Yoshida, H.; Morishita, T.; Nakata, H.; Ohshita, J. *Org. Lett.* **2009**, *11*, 373–376.

(368) Sperotto, E.; Klink, G. P. M. van; Koten, G. van; Vries, J. G. de *Dalton Trans.* **2010**, *39*, 10338–10351.

(369) Audisio, D.; Messaoudi, S.; Peyrat, J.-F.; Brion, J.-D.; Alami, M. *J. Org. Chem.* **2011**, *76*, 4995–5005.

(370) Dong, Y.; Wang, M.; Liu, J.; Ma, W.; Liu, Q. *Chem. Commun. (Cambridge, U. K.)* **2011**, *47*, 7380–7382.

(371) Stollenz, M.; Meyer, F. *Organometallics* **2012**, *31*, 7708–7727.

(372) Huang, F.; Quach, T. D.; Batey, R. A. *Org. Lett.* **2013**, *15*, 3150–3153.

(373) Shirakawa, E.; Nishikawa, R.; Uchiyama, N.; Hata, I.; Hayashi, T. *Chem. Lett.* **2013**, *42*, 269–271.

(374) Sun, L.-L.; Hu, B.-L.; Tang, R.-Y.; Deng, C.-L.; Zhang, X.-G. *Adv. Synth. Catal.* **2013**, *355*, 377–382.

(375) Sonogashira, K.; Tohda, Y.; Hagihara, N. *Tetrahedron Letters* **1975**, *16*, 4467–4470.

(376) Böhm, V. P. W.; Herrmann, W. A. *European Journal of Organic Chemistry* **2000**, *2000*, 3679–3681.

(377) Méry, D.; Heuzé, K.; Astruc, D. *Chem. Commun.* **2003**, 1934–1935.

(378) Baeckvall, J. E.; Sellen, M.; Grant, B. *J. Am. Chem. Soc.* **1990**, *112*, 6615–6621.

(379) Himo, F.; Lovell, T.; Hilgraf, R.; Rostovtsev, V. V.; Noodleman, L.; et al. *J. Am. Chem. Soc.* **2005**, *127*, 210 – 216.

(380) Li, Z.; Li, C.-J. *J. Am. Chem. Soc.* **2005**, *127*, 3672–3673.

(381) Zhang, S.-L.; Liu, L.; Fu, Y.; Guo, Q.-X. *Organometallics* **2007**, *26*, 4546 – 4554.

(382) Poater, A.; Cavallo, L. *Inorg. Chem.* **2009**, *48*, 2340 – 2342.

(383) Zhang, S.; Ding, Y. *Organometallics* **2011**, *30*, 633 – 641.

(384) Wang, Z.-L.; Zhao, L.; Wang, M.-X. *Organic Letters* **2012**, *14*, 1472–1475.

(385) Kubota, K.; Yamamoto, E.; Ito, H. *J. Am. Chem. Soc.* **2013**, *135*, 2635–2640.

(386) Casitas, A.; Ioannidis, N.; Mitrikas, G.; Costas, M.; Ribas, X. *Dalton Trans.* **2011**, *40*, 8796 – 8799.

(387) Tsuda, T.; Nakatsuka, T.; Hirayama, T.; Saegusa, T. *J. Chem. Soc., Chem. Commun.* **1974**, 557–558.

(388) Ribas, X.; Jackson, D. A.; Donnadieu, B.; Mahia, J.; Parella, T.; et al. *Angewandte Chemie, International Edition* **2002**, *41*, 2991 – 2994.

(389) Hu, X.; Castro-Rodriguez, I.; Meyer, K. *J. Am. Chem. Soc.* **2003**, *125*, 12237–12245.

(390) Xifra, R.; Ribas, X.; Llobet, A.; Poater, A.; Duran, M.; Solà, M.; Stack, T. D. P.; Benet-Buchholz, J.; Donnadieu, B.; Mahía, J.; Parella, T. *Chemistry – A European Journal* **2005**, *11*, 5146–5156.

(391) Santo, R.; Miyamoto, R.; Tanaka, R.; Nishioka, T.; Sato, K.; et al. *Angewandte Chemie, International Edition* **2006**, *45*, 7611 – 7614.

(392) Huffman, L. M.; Stahl, S. S. *J. Am. Chem. Soc.* **2008**, *130*, 9196 – 9197.

(393) Garcia-Lopez, J.; Yannez-Rodriguez, V.; Roces, L.; Garcia-Granda, S.; Martinez, A.; et al. *J. Am. Chem. Soc.* **2010**, *132*, 10665 – 10667.

(394) Meng, Q.; Wang, F.; Li, M. *Canadian Journal of Chemistry* **2010**, *88*, 981 – 990.

(395) Baskaran, S.; Venuvanalingam, P.; Sivasankar, C. *Journal of Organometallic Chemistry* **2011**, *696*, 2627 – 2634.

(396) Casitas, A.; Canta, M.; Sola, M.; Costas, M.; Ribas, X. *J. Am. Chem. Soc.* **2011**, *133*, 19386 – 19392.

(397) Bertz, S. H.; Hardin, R. A.; Murphy, M. D.; Ogle, C. A.; Richter, J. D.; Thomas, A. A. *J. Am. Chem. Soc.* **2012**, *134*, 9557–9560.

(398) Miyamoto, R.; Santo, R.; Matsushita, T.; Nishioka, T.; Ichimura, A.; Teki, Y.; Kinoshita, I. *Dalton Trans.* **2005**, *0*, 3179–3186.

(399) Grzegorzek, N.; Pawlicki, M.; Szterenberg, L.; Latos-Grazynski, L. *J. Am. Chem. Soc.* **2009**, *131*, 7224–7225.

(400) Miyamoto, R.; Hamazawa, R. T.; Hirotsu, M.; Nishioka, T.; Kinoshita, I.; Wright, L. J. *Chem. Commun. (Cambridge, U. K.)* **2005**, 4047–4049.

(401) Kessler, M.; Ring, H.; Trambarulo, R.; Gordy, W. *Phys. Rev.* **1950**, *79*, 54–6.

(402) Cotton, F. A. *Advanced inorganic chemistry : a comprehensive text*; Wiley: New York, 1988.

(403) Oertel, A. M.; Freudenreich, J.; Gein, J.; Ritleng, V.; Veiros, L. F.; Chetcuti, M. J. *Organometallics* **2011**, *30*, 3400–3411.

(404) Harris, D. C.; Bertolucci, M. D. *Symmetry and Spectroscopy: An Introduction to Vibrational and Electronic Spectroscopy*; Courier Dover Publications, 1978.

(405) Yao, B.; Wang, D.-X.; Huang, Z.-T.; Wang, M.-X. *Chem. Commun. (Cambridge, U. K.)* **2009**, 2899 – 2901.

(406) Donoghue, P. J.; Tehranchi, J.; Cramer, C. J.; Sarangi, R.; Solomon, E. I.; Tolman, W. B. *Journal of the American Chemical Society* **2011**, *133*, 17602–17605.

(407) Blessing, R. *SHELXTL*; Bruker Analytical X-Ray Systems: Madison, WI, 2000.

(408) Cole, H. *Journal of Applied Crystallography* **1970**, *3*, 405–406.

Appendix A:

Attempts to grow X-ray quality crystal of the copper(II)-hydroxide complex, (Bu_4N)**2**, supported by a *N,N'*-bis(2,6-diisopropylphenyl)-2,6-pyridinedicarboxamide ligand was synthesize by a postdoctoral associate, Dr. Patrick J. Donoghue. Repeated attempts to crystallized (Bu_4N)**2** were unsuccessful. In order to exchange the tetrabutylammonium cation for a more crystalline cation, a metathesis reaction of (Bu_4N)**2** was performed with bis(triphenylphosphine)iminium chloride (PPN) in tetrahydrofuran.[123] X-ray quality crystals were obtained by vapor diffusion of hexanes into the sample at −30 °C. Determining the crystal structure of (PPN)**2** was difficult due the contamination of chloride ions displacing hydroxide ions in the crystalline lattice (**Figure 4-29**). Three crystal structures were collected from different samples of the metathesis reaction, which contained various amounts of chloride contamination, as evidenced by their color and copper-X bond distance (X = Cl^- or OH^-)(**Table 4-4**). In addition, a sample of the pure copper(II)-chloride complex, (PPN)**3**, was prepared by the reaction of the copper(II)-CH_3CN complex with PPNCl in tetrahydrofuran. X-ray quality crystals were grown by vapor diffusion into hexanes at −30 °C.

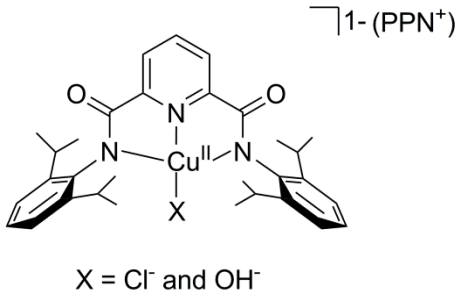

Figure 4-29: Representation of (PPN)**2** (X = OH^-) and (PPN)**3** (X = Cl^-), which are present in different ratios in the crystal structures of (PPN)

Table 4-4: Crystallographic parameters for the collection of (PPN)2 and (PPN)3 and intermediate structures.

Crystal code	**10129, (PPN)2**	**10133**	**10138**	**10173, (PPN)3**
Crystal color	blue	red	green	green
Cu…X (Cl or OH)(Å)	1.946(2) (OH)	2.1481(10) (Cl)	2.140(10) (Cl)	2.1843(9) (Cl)
Cu…N1(Å)	1.920(2)	1.923(2)	1.9448(2)	1.9236(2)
Cu…N2(Å)	1.996(2)	2.0155(2)	2.0076(2)	1.992(2)
Cu…N3(Å)	2.010(2)	2.0174(2)	2.0130(2)	1.993(2)
a (Å)	15.0268(3)	15.1248(13)	15.1401(2)	15.0982(16)
b (Å)	17.8103(3)	17.8566(16)	17.8870(3)	17.8967(19)
c (Å)	30.4807(5)	30.4402(3)	30.4340(4)	30.5305(3)
α (°)	90.0000	90.0000	90.0000	90.0000
β (°)	90.0000	90.0000	90.0000	90.0000
γ (°)	90.0000	90.0000	90.0000	90.0000
Volume ($Å^3$)	8156(3)	8221.2(13)	8241.2(2)	8249.6(15)
Temperature (°C)	-100	-150	-100	-100
R_{int}	0.0623	0.0556	0.0469	0.0638
R (%)	0.0542	0.0443	0.0475	0.0483
wR^2(%)	0.1255	0.1167	0.1270	0.1215
Goodness of Fit	0.956	1.049	1.023	0.966
Completeness to theta	98.3%	100.0%	98.5%	99.7%

All structures crystallized in an orthorhombic setting and in the $P2_12_12_1$ space group. The PPN cation created large solvent accessible channels that contained ~4 disordered THF molecules in all of the crystal structures, for which the program Platon SQUEEZE was used to remove the electron-density from the refinement of the structure. The 10129 structure of (Bu_4N)**2** exhibited a longer than expected copper-hydroxide bond distance (1.946(2) Å) than predicted by DFT calculations (1.863 Å) and the oxygen ellipsoid of the hydroxide moiety was elongated in the plane perpendicular to the copper-ligand plane.[123]

These factors led us to believe constitutional disorder may be occurring in the structure, despite its intense blue color.. It should also be noted, that due to the bulky isopropyl groups of the ligand, the hydroxide moiety is not bound to any hydrogen bonding acceptor. A search for interactions within a 5 Å radius of the oxygen atom of the hydroxide moiety did not reveal any suitable atoms for hydrogen bonding or Van deer Waal interactions. The absence of these interactions does not constrain the hydroxide moiety to a tightly defined region and thus enables the wavering in the direction perpendicular the bond. The deep green (PPN)**3** structure exhibited copper-chloride bond distance of 2.1843(9) Å, which is near the expected range for copper(II)-chloride complexes (2.246Å (σ = 0.032)).[217] The two other samples of (Bu_4N)**2** (10133 and 10138) contained intermediate levels of chloride contamination, leading to copper-X distances of 2.1481(10) and 2.140(10) Å. In these intermediate structures, peaks

corresponding to the copper-chloride and copper-hydroxide species could be observed, but they were not able to be refined independently. This is due to the difference in the bond distance between the copper-chloride and copper-hydroxide bond is quite small (0.32 Å), which is below the resolution limit of the instrument used to collect the structures. The resolution limit is determined by Bragg's Law ($d = ½(\lambda/\sin\theta)$), which in this case where Mo K_α radiation was used (0.71073 Å), places the resolution limit at ~0.366 Å.[408]